STRATIGRAPHY AND PALAEOENVIRONMENTS OF THE CARBONIFEROUS-JURASSIC KAROO SUPERGROUP IN THE LEBOMBO-TSHIPISE BASIN

Katherine E. Clayton

A dissertation presented to the Faculty of Science, University of the Witwatersrand, in partial fulfillment of the requirements for the degree of Master of Science.

August, 2017

Declaration

I declare that this thesis is my own, unaided work. It is being submitted for the degree of Master of Science at the University of the Witwatersrand, Johannesburg. It has not been submitted before for any other degree or examination in any other university.

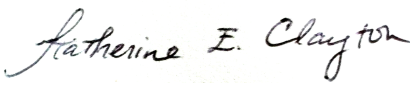

Katherine E. Clayton

On this 14th day of August 2017

ABSTRACT

The Karoo Supergroup represents a highly complete sedimentary succession that was deposited in several basins throughout southern Africa during the late Palaeozoic and Mesozoic (Carboniferous-Jurassic). While research in the Lebombo-Tshipise Basin of southern Africa has largely focused on lithological description of Karoo sediments or structural features of the basin, little effort has been made to describe the palaeoenvironments recorded in the sediments, or the basin fill's response to major tectonic or climatic events.

To address palaeoenvironmental reconstruction, lithostratigraphic analysis resulted in defining 11 facies associations from the Tshidize, Madzaringwe, Mikembeni, Fripp, Solitude, Elliot and Clarens Formations in the Pafuri sub-basin of the Lebombo-Tshipise Basin. Twenty boreholes drilled in Kruger National Park by the Council for Geoscience in 1979 record largely stable and consistent deposition of the Tshidize, Madzaringwe and Mikembeni Formations during the Permian. The Mikembeni Formation thins dramatically southwards, whereas the overlying Triassic successions tend to wedge out to the east. Late Triassic and Jurassic sediments directly overlie Precambrian basement in the southernmost boreholes. Significant thickness differences between the western and eastern boreholes indicate a large fault, which likely represents a rift shoulder.

The palaeoenvironments in this basin are similar to those of the Main Karoo Basin, but quantitative analyses suggest a more humid environment in the Late Triassic Elliot Formation. Sauropodomorph fossils validate assignment of formerly mapped Solitude Formation as actually being the Elliot Formation. Palaeosols in the Elliot are consistent with either Oxisols or Argillisols. Wet desert conditions, evidenced by burrows produced by invertebrate communities, and tectonic activity, suggested by seismites, persist into the Early Jurassic Clarens Formation.

ACKNOWLEDGEMENTS

I would like to gratefully acknowledge the DSF-Centre of Excellence in Palaeosciences and to the University of the Witwatersrand for financial support during the course of this research. This project would not have been possible without the generous assistance of the Evolutionary Study Institute staff and faculty, especially the supervisorship and help of Prof. Jonah Choiniere. Kind thanks to the lab personnel in the department of Geosciences Earth Labs, and special thanks to Susan Lutz for assistance in data production.

I would especially like to thank Dr. Zubair Jinnah, who in addition to being an exceptional supervisor, is a hoot in the field, and a kind, delightful friend. This adventure would have never been possible without your cutting insights into bureaucracy, willingness to drive, and tolerance of couch-crashing. You are indeed a gentleman and a scholar.

Studying in South Africa is an experience I will always be grateful for because of the incredible people I've had the fortune of befriending. I especially want to thank Cameron, Pia, and Blair for considerable help in various text reviews and for being generally fantastic human beings. I also am forever indebted to Kathleen's generosity of spirit and willingness to help with the submission of this manuscript. A true friend is indeed a queue friend.

I especially want to thank Casey and Cory for being the kind of friends that believe in adventure, feeding me, and the healing power of a good show. Thanks for being a pal and coming all the way to Johannesburg, Cory; I miss getting to hang out and eat all your good cookings.

Thanks also my family who have always encouraged me to explore life and take every opportunity. Even though we are often on the other side of the world from each other, it never feels like we're far apart. I especially want to thank Martin for being the most supportive partner, constant friend and confidant. Without your love and willingness to help, this could have never happened.

CONTENTS

LIST OF FIGURES

LIST OF TABLES

Chapter 1: Introduction

The assembly of Pangaea in the Late Carboniferous (~300 Ma) marked the formation of the last of numerous supercontinents in Earth's history (Rogers & Santosh, 2003). Long established compressive tectonic regimes in the south of the supercontinent caused by shallow-angle subduction of the palaeo-Pacific plate produced the early Late Palaeozoic, 6000km-long, Gondwanide Orogeny (Torsvik & Cocks, 2011). Several large basins, including the Main Karoo Basin of South Africa, the Paraná Basin of South America, the Bowen Basin of Australia, and the Beacon Basin of Antarctica, were formed during this orogenic event (Catuneanu et al., 1998).

The Main Karoo Basin, exposed in the Free State, Mpumalanga, KwaZulu Natal, Western, Eastern and Northern Cape provinces of South Africa, hosts the Karoo Supergroup, a Late Carboniferous-Early Jurassic (~305-180 Ma) sedimentary sequence (Johnson, 1996; Catuneanu, 1998; 2005; Tankard et al. 2009). The presence of economically valuable resources (i.e. coal, uranium, etc.) and a rich biostratigraphic record, including a diverse synapsid fauna, early dinosaurs, and crocodyliformes, have motivated numerous studies over decades, establishing the Karoo as one of the best studied basins in the world (Owen, 1854; Crompton & Charig, 1962; Crompton & Jenkins, 1968; Raath, 1969; Turner, 1977; Kitching, 1979; Kitching & Raath, 1984; LeRoux & Hambleton-Jones, 1991; Cadle et al., 1993; Johnson et al., 1996; Galton et al., 1998; 2005; Gow, 2000; Yates, 2003; Yates & Kitching, 2003; Oesterlen, 2005; Raath and Yates, 2005; Rubidge, 2005; Reisz et al., 2005; Yates et al., 2004; Yates, 2005;2007; Yates, 2008; Yates et al., 2010; Yates et al., 2011; Smith et al., 2012; McPhee et al., 2014).

Understanding palaeoenvironment is integral to palaeobiology and economic resource studies, as climate directly affects development of natural resources (e.g. coal) and has been tied to patterns in biodiversity

(Erwin, 2009). Palaeoenvironmental change over the Triassic-Jurassic boundary is of special interest to many researchers, as this is a pivotal time in the Mesozoic, defined by one of the five largest extinction events in earth's history. The subsequent faunal turnover in Gondwana produced dinosaurian and crocodylomorph radiation events and the emergence of true mammalians like *Megazostrodon rudnerae* from their cynodont ancestors (Crompton & Jenkins, 1968). New specimens and revision of early sauropods, theropods, and ornithischians from the Main Karoo Basin are elucidating the distribution and palaeobiology of basal dinosaurs (Crompton & Charig, 1962; Kitching, 1979; Galton et al., 1998; 2005; Gow, 2000; Yates, 2003; Yates & Kitching, 2003; Barrett, 2004, 2009; Raath & Yates, 2005; Reisz et al., 2005; Butler et al., 2007; Yates, 2007; Yates, 2008; Yates et al., 2010; Porro et al., 2011; Yates et al., 2011; McPhee et al., 2014).

Many penecontemporaneously formed basins across southern and central Africa (see Figure 1), including the Lebombo-Tshipise Basin in north-east South Africa, contain Karoo equivalent formations and analogous fauna, flora, and economic deposits (Raath, 1969; Bordy 2000; Durand 1996, 2001); yet these have received less overall attention than the Main Karoo, with most research directed at recording lithostratigraphy (McCourt & Brandl, 1980; Johnson, 1996; Brandl, 2002; Durand, 2012; Eriksson & Bordy, 2015). Over the past two decades, researchers have begun assessing palaeoenvironmental and palaeoclimactic conditions in these subsidiary basins (Bordy 2000; Bordy & Catuneanu, 2002; Bordy & Prevec, 2008; Bordy, 2008; Bordy et al., 2010a,b; Malaza et al. 2015). One of the difficulties in these studies is assigning stratigraphic patterns a climactic or tectonic cause (Jordan et al., 1988; Leeder et al., 1998; Bordy et al., 2004).

The similar sedimentary sequences found in these basins were theorized to have been deposited through comparable genetic mechanisms

(Johnson 1996); however, as ideas of tectonic controls on sedimentation in southern Africa have evolved, interpretations of the tectonic drivers of deposition in these basins and the Main Karoo Basin have dramatically changed over the past few decades (Catuneanu et al., 1998; 2005; Turner, 1999; Bordy et al., 2004; Tankard 2009).

This project aims to characterize the palaeoenvironments of the Lebombo-Tshipise Basin in north-eastern South Africa, and compare these results to the Main Karoo Basin. Facies descriptions of the entire Karoo Supergroup, in addition to previous work published from the Madzaringwe Formation (Malaza et al., 2015), and interpretation of stacking patterns preserved in twenty-one boreholes will allow for discussion of the allocyclic controls on stratigraphy within this endorheic basin. Quantitative analysis of the Elliot Formation is also compared to recently published work on the same formation in the Main Karoo Basin (Scisicio & Bordy, 2016).

1.1 Formation and Break-up of Pangaea: Basin formation in Southern Africa

Early workers initially regarded all southern African basins containing Karoo Supergroup rocks to have been filled by a contiguous set of depositional environments with differences caused by variable rates of sedimentation and subsidence across southern Africa (Rust, 1959; 1962; 1975; Turner, 1975; Cole, 1992). Numerous explanations have been invoked by subsequent authors to account for these two variables which largely indicate an inversion of tectonic regimes from compressive during the Carboniferous and Permian to extensional in the Triassic and Jurassic.

Turner (1999) envisioned a polyphase basin history for the earlier Cape and Karoo basins with extensional regimes returning in the Late Triassic-Early Jurassic due to a thermal anomaly or hot spot activity linked to a mantle plume, in the same vein as research produced by Burke & Dewey (1973), Cox (1989), White & McKenzie (1989), and Hawkesworth et al.

(1999). Tankard et al. (2009) attribute varying stratigraphy to fault controlled subsidence of the rigid crustal blocks underlying the basin. The most common explanation, however, is that the Main Karoo Basin is a retroarc foreland basin, with accommodation driven by compression from the Cape Orogeny (Lock, 1978, 1980; Winter, 1984; de Wit et al. 1988; Johnson, 1991; de Wit & Ransom 1992; Tankard et al. 1992; Smith, 1993; SOEKOR, 1996; Catuneanu et al., 1998; 2005; Bordy et al., 2004; Johnson et al., 2006). This interpretation is not without contention: position of the inferred magmatic arc is lacking in geophysical evidence (Tankard et al., 2009); subsidence and forward modelling curves produced by Cloeting et al. (1992) and Pysklywec and Mitrovica (1999) are atypical for foreland basins; and the earliest dated deformation event in the Cape Orogeny is late Permian (261 ± 3–276 ± 5 Ma) from $^{40}Ar/^{39}Ar$ ages of muscovite in Cape Fold Belt shear zones (Hansma et al., 2016). Additional factors of foreland modelling have been invoked to explain changes in sedimentation including tectonic loading (e.g., Smellie, 1981, Johnson, 1991; Mpodozis and Kay, 1992; Veevers et al., 1994; Catuneanu et al., 1997; Catuneanu et al., 1998; Pysklywec & Mitrovica, 1999; Catuneanu & Elango, 2001), flexure of the lithosphere and a migrating stratigraphic hingeline (Catuneanu et al., 1998; 2005; Bordy et al., 2004), and dynamic loading of the overriding plate during subduction (Catuneanu et al., 2005), or a combination of these factors. Additionally, the role of weaknesses in the basement as a corollary to foreland modelling (Catuneanu, 2004) and as the sole control of basin formation (Tankard et al., 2009) have been suggested and explored.

Regardless, most authors now recognize a combination of southern convergent and northern divergent tectonic stresses along Gondwanan margins generated accommodation space in southern Africa, resulting in synchronous but partitioned basin formation (Wopfner, 1991; 1994; 2002; Bordy & Catuneanu, 2001; Bordy, 2002 a,b,c; Catuneanu, 2004a,b; Catuneanu et al., 2005; Hancox & Götz, 2014). This tensional stress

propagated gradually south during the Late Carboniferous, while Karoo sediments were deposited in resultant graben and rift structures; therefore, extensional structures in the south are inferred as younger than central and northern structures (Bordy & Catuneanu 2002c). Catuneanu et al. (2005) has assigned southern African basins to three genetic zones: retroarc flexural foreland-related basins formed proximal to the Cape Fold Belt and extending to the south of the Kalahari basin; eastern rift/extensional basins in the Mid-Zambezi and north east to the Tanzania (Wopfner, 2002); and western sag basins in the Huab (Namibia), Angola and Democratic Republic of the Congo. However, accommodation in the fault-bounded basins at the northern margins of the foreland basin zone is thought to have been controlled by flexural subsidence during the Carboniferous and Permian (Catuneanu et al., 2005), and southward-migrating extensional regimes subsequent to the Triassic (Hancox & Götz, 2014).

The Lebombo-Tshipise Basin is a combination of two basins: the east-west trending Tshipise-Pafuri Basin, a fault-controlled depository approximately 300 km long and 100 km wide (Malaza et al., 2015), which is posited to have been connected to the Tuli Basin in the past; and the Lebombo Basin, a 600 km long north-south trending basin (Brandl, 2002). The Tshipise basin is thus situated on the Archean Limpopo Belt, between the Kaapval Craton to the south and the Zimbabwe Craton to the north (Watkeys, 1979; van Reenen et al., 1992; Bordy, 2000). The underlying Limpopo mobile belt has had a tumultuous tectonic history, and an extended period of quiescence and erosion persisted before the onset of Karoo sedimentation (Cox et al., 1965). This varied topography has resulted in irregular thicknesses of Karoo Supergroup outcrop throughout the basin (Cox et al., 1965; Bordy, 2000).

Accommodation in this region was originally imputed to extensional tectonism from a failed western arm of a triple junction rift (Vail et al.,

1969; Burke & Dewey, 1973), however, the genesis of rifting events is linked to Gondwanan breakup during the Middle Jurassic near the termination of Karoo basin development, and is a dubious driver for sedimentation and basin formation in this area (Catuneanu, 2005). Bordy and Catuneanu (2001), and Catuneau et al. (2005) contend that accommodation in the Limpopo area was primarily driven by flexural subsidence of the back bulge province of the Karoo foreland system during the deposition of Carboniferous and Permian strata. Evidence of extensional tectonism in the upper strata of the neighboring Tuli Basin implicates a change in tectonic regime as initial flexural pressure inverted to extensional during deposition of Beaufort strata (early-mid Triassic) due to southwards migrating extensional regimes generated by the Tethyan spreading (Catuneau, 1999; Bordy & Catuneanu, 2001; 2002 a; b; c; Catuneanu, 2004a; b; Catuneanu et al., 2005). Palynological data from the Karoo Supergroup also support complex, cryptic tectonism through evidence of hiatuses in deposition or erosion in parts of the basin (MacRae, 1988; Bordy, 2000).

The basin fill has been described as horst and graben structures formed by extensional normal faulting, as the result of either rift or intracratonic thermal sag processes (Watkeys and Sweeny, 1988; Groenwald et al., 1991; Johnson et al., 1996; Malaza et al., 2015). Thus, the drivers of the basins' deposition and overall history remain difficult to synthesize and interpret.

1.2 Palaeoenvironments and deposition of the Karoo Supergroup

The Karoo Supergroup, a nearly continuous and remarkably complete sedimentary megasequence, is divided into the Carboniferous-Permian "Dwyka Group" (300-291 Ma), Permian "Ecca Group" (291-255 Ma), Late Permian-Early Triassic "Beaufort Group" (255-243 Ma), and the Late Triassic-Early Jurassic informally named "Stormberg Group" (230-180 Ma) (Catuneanu, 2004; Rubidge, 2005). This sequence is capped by the

Drakensberg basalts in west and central southern Africa, and the Lebombo Group basalts and overlying rhyolites over eastern and northern South Africa (Duncan and Marsh, 2006), which together mark the end of Karoo sedimentation around 180 Ma (Aldiss et al. 1984; Allsopp et al., 1984; Fitch & Miller 1984; Hooper et al., 1993). In the Main Karoo Basin this megasequence unconformably overlies the Cape Supergroup, and Proterozoic and Archaen strata, while in the Lebombo-Tshipise Basin it directly overlies Precambrian crystalline basement (Tankard et al., 1992).

The Dwyka Group of the Main Karoo Basin is comprised of mudrocks, gritty, pebbly sandstones, conglomerates and diamictites, which are divided into continental inlet valley facies associations formed on dissected uplands, and marine platform facies associations formed in the southern, submerged portion of the basin (Visser, 1986; Smith et al., 1993, Catuneanu et al., 2005). Extensive glaciation occurred in Late Carboniferous, and evidence of glaciers exists in the presence of NW-SE trending incised valleys in the Main Karoo basin's northern margins (Visser and Kingsley, 1982) and deposition of dropstones, diamictites, sandy proglacial outwash fans, kame and esker deposits, and fluvially reworked subglacial tills (Smith et al., 1993; Catuneanu et al., 2005). Clast-poor diamictites, sandstones and laminated mudrocks representing glacial advances and retreats are interpreted to have formed subaqueously (Visser, 1986).

The Tshidize Formation, the Dwyka representative in the Lebombo-Tshipise Basin is a poorly sorted diamictite with argillacous and sandy matrix, with clasts from the underlying Nzhelele Formation of the Soutpansberg Group (McCourt & Brandl 1980). McCourt and Brandl (1980) interpreted this formation as fluvio-glacial in origin. Rocks from the nearby Tuli and Ellisras basins are interpreted as colluvial and glacial outwash alluvial and fluvial facies (Faure et al., 1996; Bordy & Catuneanu, 2002c), derived from glacial lakes and rivers (Catuneanu et al., 2005).

The “Ecca Group” of the Main Karoo Basin is composed of mudrocks, siltstones, coal, sandstones and minor conglomerates (SACS, 1980; Cairncross 1987; Johnson et al. 1996; Johnson et al. 1997; Catuneanu et al., 2005) formed in a variety of continental and marine settings during a cool and wet climate (Smith et al., 1993; Catuneanu et al., 2005). The economically valuable coal deposits in these rocks are interpreted as the remains of peat marshes formed on sandy outwash braidplains and lobate deltas (Smith et al., 1993).

The Madzaringwe and Mikembeni Formations (“Ecca Group” representatives) are composed of feldspathic and micaceous conglomerate and sandstone, siltstone, shale and coal deposited in fluvial, swamp, and lacustrine settings (McCourt & Brandl, 1980; Catuneanu et al., 2005; Durand, 2012; Malaza et al., 2013). The coal seams are mostly found in the Madzaringwe Formation and attain a maximum thickness of 2-3 meters (McCourt & Brandl, 1980; Malaza et al., 2013).

The Beaufort Group in the Main Karoo Basin includes a wide range of red to purple mudrocks and sandstones interpreted to have been deposited by fluvial processes during the Permo-Triassic (Smith et al., 1993; Catuneanu et al., 2005). The presence of desiccation cracks and pedogenic nodules suggest that these rocks were deposited during a semi-arid climate with seasonal rainfall on large alluvial plains (Smith, 1990; Smith et al., 1993). The spectacular synapsid fauna and abundant palynological and palaeobotanical studies make this group the best studied in terms of palaeoenvironment and palaeobiology (Rubidge et al., 1995; Van der Walt et al., 2010; Day et al., 2015; Gastaldo et al., 2005; Bamford, 1999; 2004; Tohver et al., 2015).

The Beaufort-equivalent Fripp and Solitude formations in the Lebombo-Tshipise basin are composed primarily of coarse-grained, feldspathic and

micaceous sandstones and associated floodplain and levee siltstones and mudrocks, and minor shale and coal (McCourt & Brandl, 1980; Brandl, 2002).

The Stormberg Group is composed of terrestrial mudrocks, siltstones and sandstones that comprise a fluvial-aeolian clastic succession (Eriksson, 1979; Visser, 1984; Catuneanu et al., 1998, 2005; Bordy et al., 2004). The basal-most Molteno Formation is very coarse-grained and represents three, thick sedimentary wedges (Smith et al., 1993), marking renewed tectonic activity in the basin (Catuneanu et al., 2005). These braided river systems were eventually replaced by meandering fluvial environments of the lower Elliot Formation (Smith et al., 1993; Bordy, 2004b and c). Throughout deposition of the overlying Elliot Formation, perennial meandering fluvial environments disappeared as the environment became more arid; relatively stable river channels were replaced with wide, ephemeral rivers subject to flash floods, and development of calcrete-rich soil profiles (Bordy, 2004). In turn, this environment was drowned by erg dunes of the Clarens Formation, with ephemeral rivers and playa lakes occupying interdune areas (Smith, 1993; Johnson, 1996; Bordy, 2004b, 2005). These palaeohabitats hosted early dinosaurs, including *Massospondylus* (Owen, 1854; Yates & Barrett, 2010), *Coelophysis rhodesiensis* (formerly *Syntarusus;* Raath, 1969, 1977), and *Heterodontosaurus* (Crompton & Charig, 1962), as well as the earliest mammals (Crompton & Jenkins, 1968; Kitching & Raath, 1984), and the earliest crocodylomorphs (Whetstone & Whybrow, 1983; Gow, 2000).

In the Lebombo-Tshipise Basin, the “Stormberg Group” formations were originally named the Klopperfontein Sandstone, Bosbokpoort/Nyoka formations and the Clarens Formation (de Jager, 1983a; Brandl, 2002); however, Bordy and Eriksson (2015) recently subsumed the Bosbokpoort and Nyoka formations into the Elliot Formation (Table 1-1). These

mudrocks, siltstones and sandstones are interpreted to have formed from fluvial, overbank, and aeolian processes (Brandl, 2002; Durand, 2012).

Table 1-1: Stratigraphic correlation of Karoo Supergroup formations and units in the present study

Period	Karoo "Groups"	Main Karoo Basin (Johnson et al., 1996)	Lebombo-Tshipise Basin (McCourt & Brandl, 1980)	KNP Boreholes Core Logs
Jurassic	"Stormberg"	Clarens Formation	Clarens Formation Tshipise Sandstone Member Red Rocks Member	Cave Sandstone Red Beds
		Elliot Formation	Bosbokpoort Formation (Elliot Formation; Bordy & Eriksson, 2015)	
Triassic		Molteno Formation	Klopperfontein Sandstone	
Permian	"Beaufort"		Solitude Formation	
	"Ecca"		Fripp Sandstone Mikembeni Formation Madzaringwe Formation	
	"Dwyka"		Tshidize Formation	
Carboniferous				

1.3 Climate Change: Desertification during the Triassic and Jurassic

The nearly complete Karoo Supergroup sequence in the Main Karoo Basin provides an ideal record to study climate change over approximately 120 million years. Climate is an important parameter in a number of studies; Catuneanu et al. (2005) rank it as the second most important allogenic control on sedimentation in Southern Africa after tectonism, and attribute the similarities of sequences within penecontemporaneous basins to climate, while other researchers have invoked climate to explain faunal diversity patterns in the upper "Stormberg Group" (Kitching & Raath, 1984; Tucker & Benton, 1982). The general trend of aridification from wet and cool climates recorded in Late Carboniferous Dwyka to increasingly arid and hot climates of the Triassic and Jurassic Elliot and Clarens Formations has been noted by many authors (Smith et al., 1993; Du Toit, 1954; Visser

& Botha, 1980; Eriksson, 1983; Keyser, 1966; Johnson, 1976; Visser & Dukas, 1979; Stavrakis, 1980; Tankard et al., 1982; Visser, 1991a,b).

During the Mesozoic, this trend is understood to be primarily driven by the continent's northward drift towards the tropics, as evidenced by palaeomagnetic data (Parrish, 1990; Scotese et al., 1999; Bordy et al., 2004c; Catuneanu et al., 2005). At the end of the Triassic (200 million years ago), Southern Africa was positioned within the 60th southern parallel circle, but drifted nearly 10 degrees north by the end of the Early Jurassic (180 million years ago) (Reeves et al., 2004). This is reflected in the increasing prevalence of aoelian influences in deposition of the uppermost Elliot Formation (e.g., Botha, 1968; Le Roux, 1974; Visser & Botha, 1980; Eriksson, 1983, 1985; Smith & Kitching 1997; Bordy et al., 2004c)

While climate change is a major control on erosion and sedimentation, it is but one of many factors in basin histories and its effect on stratigraphy is often difficult to differentiate from tectonism. Research published by Bordy et al. (2004b) found that changes in palaeocurrent directions and sediment sources in the Elliot Formation of the Main Karoo Basin implicated that tectonism heavily impacted facies distributions and stratigraphic patterns along with climate change.

Quantitative palaeoclimate reconstructions are one solution to teasing out tectonic vs. climatic origins of changes in stratigraphy. Palaeosols are the ideal candidate from which to collect this data, as they record the weathering conditions present at Earth's surface at the time of formation (Sheldon & Tabor, 2009). Qualitative assignment of palaeosols to a palaeoenvironment (e.g., mollisol, entisol, etc.) and examination of authigenic clay, and other quantitative proxies (major element analysis, Chemical Indices of Alteration, etc.) can illuminate climatic conditions more directly than stratigraphic studies alone (Sheldon & Tabor, 2009).

1.4 Aims

The foremost aim of this project is to produce the first lithofacies description and palaeoenvironmental analysis of the entire suite of Karoo equivalent rocks in the Lebombo-Tshipise Basin. Malaza et al. (2015) provided a lithostratigraphic overview of the Permian-aged Madzaringwe Formation from outcrop in the Tshipise sub-basin (middle of the Tshipise Basin), whereas outcrop from this project is located in the eastern-most Parfuri sub-basin (Hancox & Götz, 2014). These lithofacies are compared and correlated with those of the Main Karoo Basin.

Palaeoenvironmental reconstruction is crucial to analyzing the past regional climate and interpreting climatic changes reflected in the landscape across southern Africa and through time. While a comprehensive qualitative study of all the palaeoenvironments present in the Karoo Supergroup of the Lebombo-Tshipise Basin would be ideal, we have focused on the Elliot Formation from the Stormberg Group to address climate change during the Triassic/Jurassic. The Elliot and Clarens Formations record an increasingly arid environment from the latest Triassic to the Early Jurassic (Eriksson, 1979; Smith et al., 1993) within the Main Karoo Basin. Of key interest in this study is whether these basins preserve similar palaeoenvironments, and if evidence of climate change is present in Lebombo-Tshipise Basin, and, if so, how it compares in terms of timing and extent to that of the Main Karoo. Quantitative analysis and qualitative assessment of clay minerals from palaeosol samples are compared to preliminary quantitative palaeoclimate data from the Elliot Formation of the Main Karoo Basin (Sciscio & Bordy, 2016).

Recovery and examination of previously discovered sauropodomorph materials in the Lebombo-Tshipise basin (Durand, 1996; 2001) allows us to comment on different preservational biases of the Elliot Formation in the Lebombo-Tshipise and Main Karoo Basins and briefly discuss

palaeogeographic distribution and faunal trends. Newly discovered trace fossils from our field area are described and compared to published finds from the Main Karoo, Tuli, and the Lebombo-Tshipise basins (Bordy, 2008).

Using a combination of palaeoenvironmental models, sediment provenance analysis, stratigraphy and geological mapping, the Lebombo-Tshipise Basin’s development is modelled and interpreted.

Chapter 2: Materials & Methods

2.1 Stratigraphic Sections:

Standard field techniques were employed to measure stratigraphic units, strike and dip, and sedimentary structures, including the use of a Jacob's staff, measuring tape, brunton compass, and laser view-finder. Stratigraphic sections were measured and samples from the Lebombo-Tshipise Basin were collected from two field areas: Red Rocks (KRR samples) and Makanya Hill (KDC and KDS samples), mapped in Figure 2-1. Red Rocks is an historical stop on the Red Rocks Loop (S52 road), north of Shingwedzi camp that is accessible to park visitors. Makanya Hill is a more remote field site, accessible to visitors by guided hike from Nyalaland Trail camp in Kruger Park. The Lower Makanya Hill area is composed of discontinuous outcrops of the Karoo Supergroup in a dry wash, marked as the 'Matsaringwe' (Messina 1:250,000 Map, 1981), which exposes approximately 300-400 m of section across 12 km, though the heavy vegetation obscures the majority of potential outcrop.

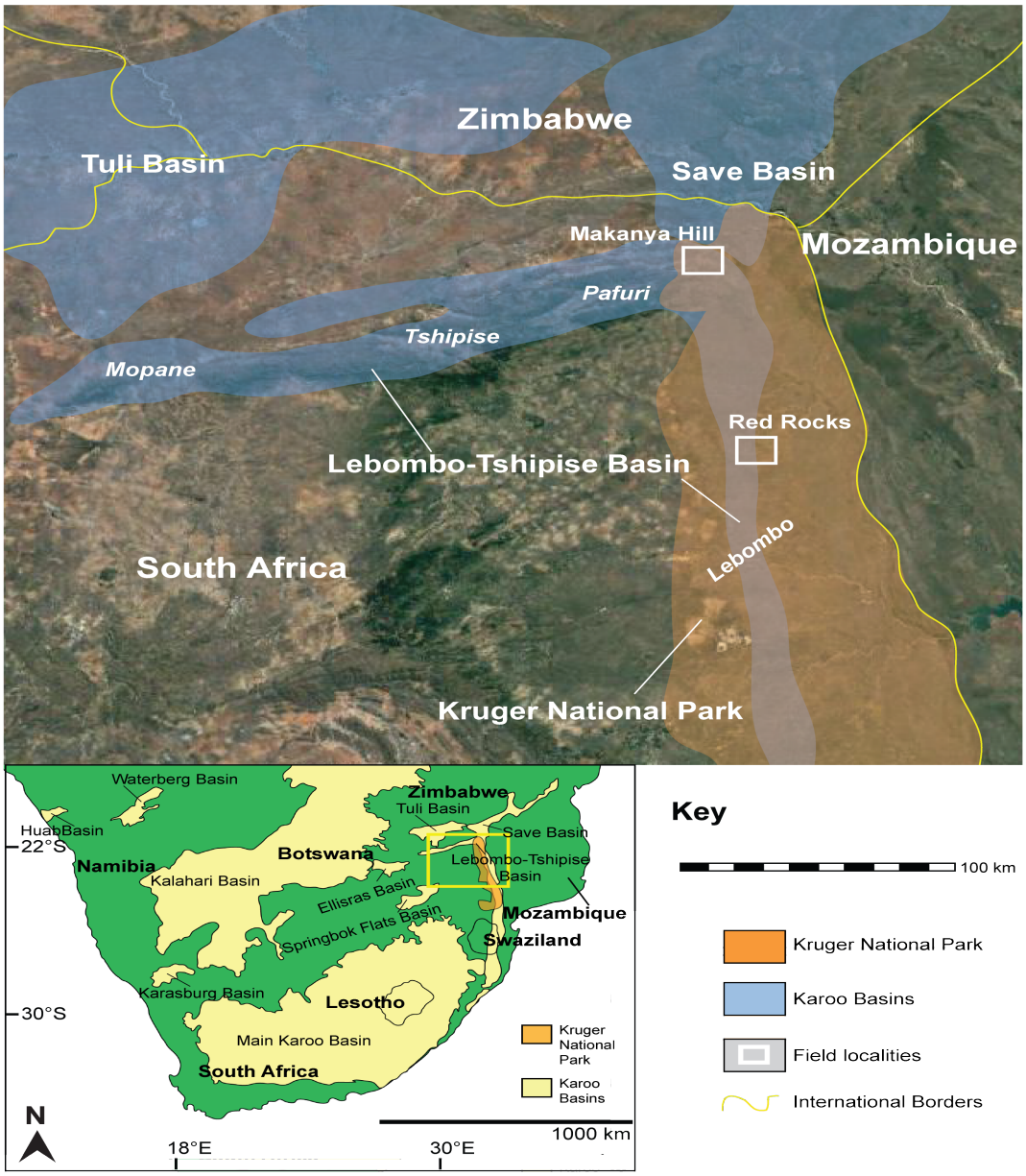

Figure 2-1: The Makanya Hill and Red Rocks field localities (indicated by white boxes) are located in the Kruger National Park (orange). These localities crop out in the Pafuri and Lebombo sub-basins of the Lebombo-Tshipise Basin; one of many Karoo Supergroup-containing basins in southern Africa (see inset map for Karoo Basins in southern Africa). Image credit: Google Maps 2017.

The stratigraphic section from Red Rocks represents approximately 18 m (see Figure 2-2), while the stratigraphic section from upper Makanya Hill covering the Elliot and Clarens Formations is a composite of two measured sections and represents approximately 180 m (see Figure 2-3).

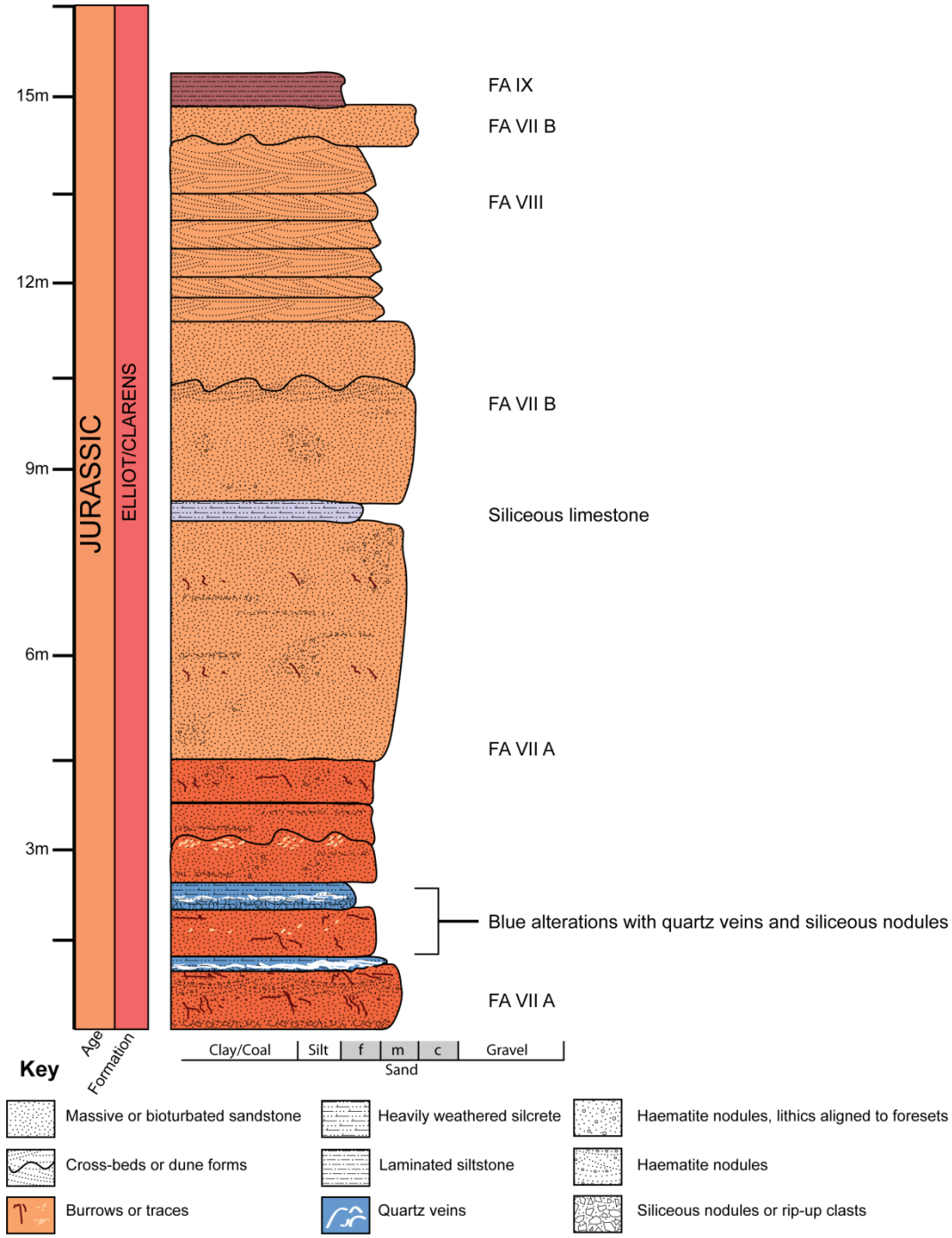

Figure 2-2: Stratigraphic section from the Red Rocks field locality (36K 326183 7436365), with identified facies associations (FA), discussed in Chapter 3.1.1. See Figures 2-1 and 2-4 for general locality map.

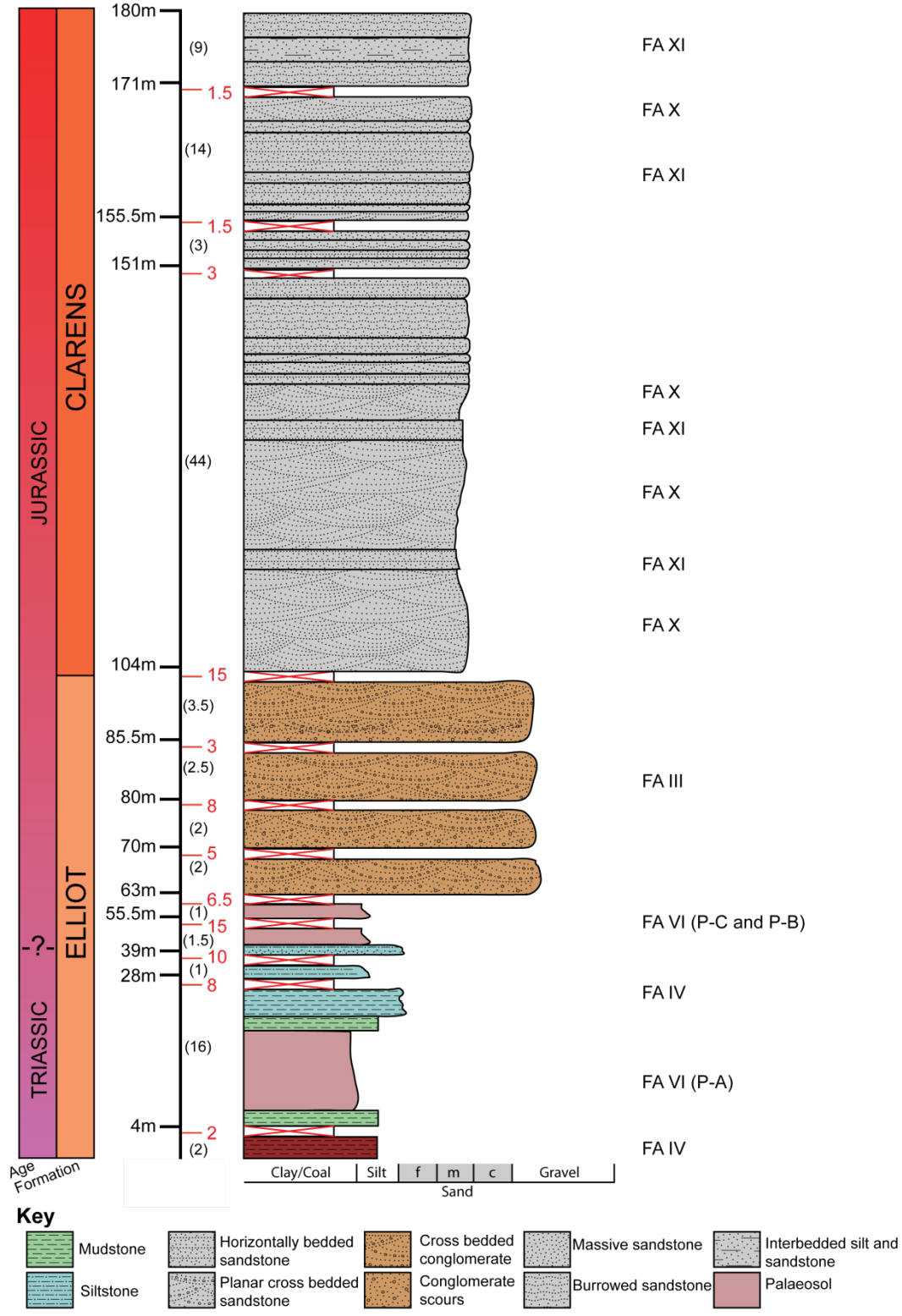

Figure 2-3: Stratigraphic section from the Makanya Hill field locality (S 22° 29.916, E 31° 03.612), with identified facies associations (FA), discussed in Chapter 3.1.1. FA VI represents palaeosols, and associated sites P-A, P-B, and P-C (see Table 2-1 for GPS coordinates and samples taken) are indicated in section. Red numbers to the right of the scale indicate missing or unexposed strata, while measurements in parentheses

represent measured section. Numbers left of stratigraphic marker represent the total measurement (unexposed + exposed). See Figures 2-1 and 2-4 for general locality map.

Both sites were chosen for survey because they were known to have at least 10 meters of outcrop, and sauropodomorph fossils were known from Makanya Hill (Durand, 1996). We visited Makuya Reserve to collect additional data, but were unable to find suitable outcrop to measure section due to poor exposure.

2.2 Kruger National Park Boreholes

Outcrop observations are supplemented by logs of 20 boreholes, representing an average of 296 m of the Karoo Supergroup (individual boreholes are illustrated in Appendix A). Exploration of the basin fill of the Lebombo-Tshipise basin was undertaken by the Council for Geosciences in the late 1970s, facilitated by twenty-five boreholes drilled within Kruger National Park (see Figure 2-4 for borehole localities).

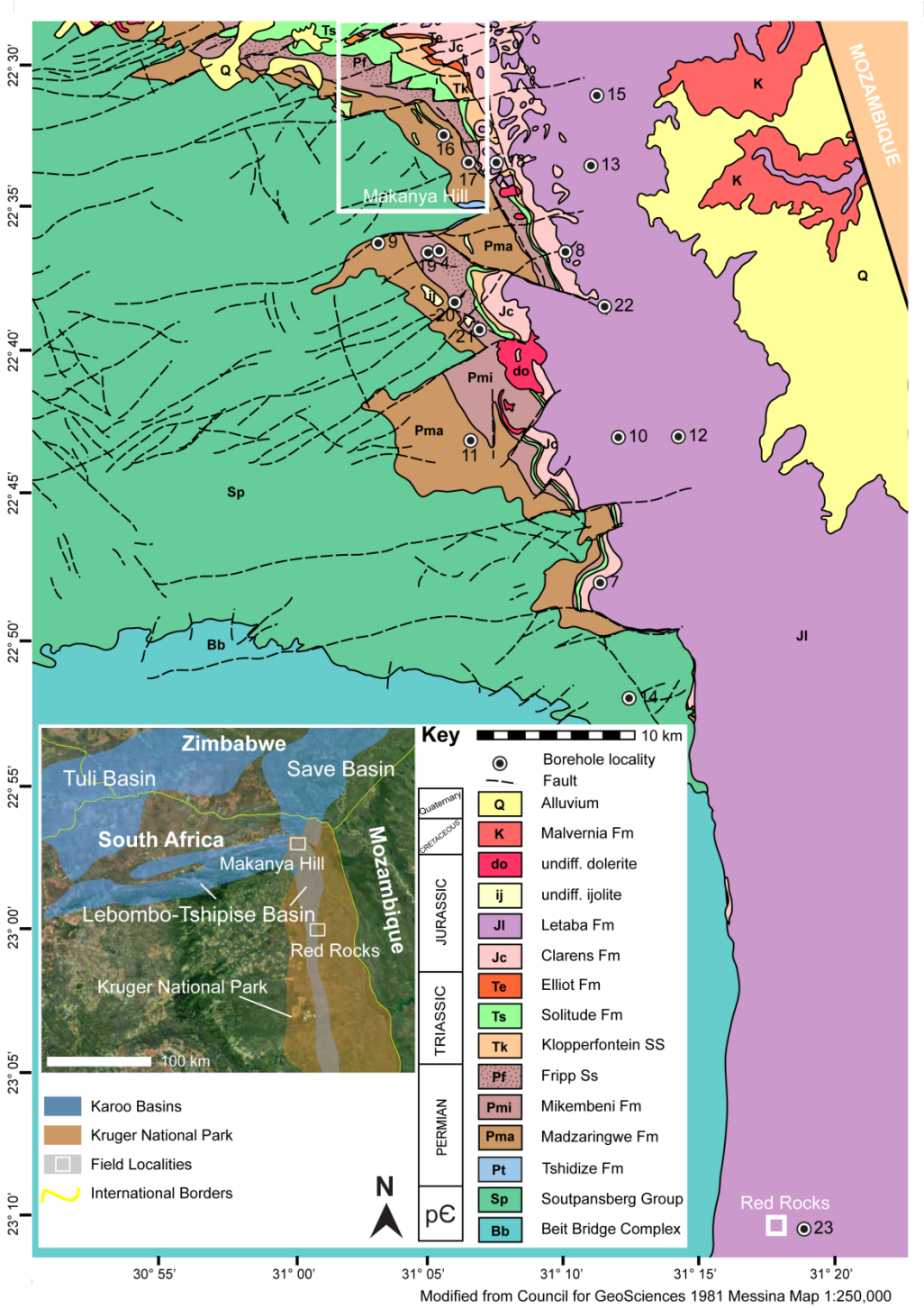

Figure 2-4: Pafuri sub-basin field localities (indicated by white boxes) and Kruger National Park borehole localities on geological map (modified from Council for Geosciences 1981 Messina Map 1:250,000). Inset map shows these field localities within the Kruger National Park (orange) and Lebombo-Tshipise Basin (blue).

The strata studied in these boreholes were incorporated with field descriptions of outcrop into the first general lithologic descriptions of the Karoo Supergroup in the Parfuri sub-basin (as identified by Hancox & Götz, 2014, Figure 2-1) of the Lebombo-Tshipise Basin (McCourt & Brandl, 1980). Though the total number of boreholes is recorded as 23 (i.e. KNP 23), two boreholes, KNP 15 and 12 had subsidiary boreholes drilled within very close proximity (KNP 15 “Wedge” and KNP 12A). None of the boreholes were published, but core logs kept at the Polokwane Council for Geoscience (CGS) office are included in this study to supplement the discussion of stratigraphy, general basin morphology, fill, and development. A summary of borehole location and depth is provided in Table 3-3. Of the total twenty-five cores drilled, five core logs (KNP 1, 2, 3, 5, and 6) were not accessible, and are therefore not included in this study.

Only one borehole core (KNP 12 and KNP12A) was available at the Council for Geoscience to review the information in the logs; during examination of this borehole several additional details were noted, such as evidence of subaerial exposure and weathering of the Mikembeni Formation before deposition of the overlying Fripp or possibly Solitude Formation (see Chapter 3.1.2 for borehole trends). The other core logs primarily identified lithological units by Group deposition (i.e. “Ecca”, “Beaufort”, “Red Beds”, and/or “Cave Sandstone”), and very few were divided into formations.

There are several difficulties in assigning formation names and boundaries in these boreholes due to irregular basin fill as the result of complex underlying basin morphology and apparent variable rates of sedimentation throughout the basin’s history (Bordy, 2000). Obstacles to formation and boundary identification include differentiating the Fripp and Klopperfontein sandstone units in attenuated sequences, as both are defined as micaceous or felspathic and thick; marking the boundary between the Madzaringwe and Mikembeni formations which are lithologically similar;

and the lack of detail in core log unit boundary descriptions (e.g. evidence of erosion indicating unconformable relationships).

In a few boreholes, core loggers identified formation contacts: the Madzaringwe/Mikembeni in KNP 15, 20, and 22; the Mikembeni/Fripp in KNP 12A, 15, 22; the Fripp/Solitude in KNP 12A, and the Solitude/Klopperfontein in KNP 7 and 12A. Madzaringwe identifiers including the “basal carbonaceous horizon”, “main [coal] seam”, and “Ecca middle marker” which marks the top of the Madzaringwe formation, were identified in KNP 4, 9, 19, 20; KNP 7, 12A, 15, 15 Wedge, 17, 19, 20, 22; and KNP 4, 7, 8, 10, 12A, 13, 15, 15 Wedge, 17, 19, and 20 respectively.

These divisions with relevant formation identifying lithological descriptions (e.g. the “carbonaceous zone” and “main seam”, and “middle marker” of the Madzaringwe Formation) were employed in assigning formation names and boundaries to the borehole units. Formation boundaries and identifications are denoted with a “?” in borehole illustrations that were not identified outright or with a relevant marker (i.e. the middle marker) by core loggers.

KNP 18 did not include any group or formation identification, however the presence of shale, silt, coal and sandstone allows confident placement of these in the Ecca Group, however, this borehole’s location (see Figure 2-1) indicates the sequence should include the Jurassic Clarens and Letaba Formations. Based on its location close to KNP 17 and that “Transition beds” closely resembling the Tshidize Formation are present at the base of the borehole, we have assigned overlying sediments as the Madzaringwe Formation. Likewise, KNP 11 did not include any formation designation, but we assign its contents as belonging to the Madzaringwe Formation due to the contents of nearby boreholes.

2.3 Palaeosol samples

Palaeosol samples from the Elliot Formation were excavated from a freshly eroded cliff face, at least 10 cm below the weathered surface of clay and mud lithologies identifiable as palaeosols by the presence of rhizoliths, heavy mottling, and/or soil horizons characterized by color change. One sample was collected from a brick-red palaeosol, approximately 1.5 meters thick, with bifurcated, blue rhizoliths in the Main Karoo Basin near the village of Blikana, Eastern Cape Province. This sample was collected to provide comparative data which is greatly augmented by geochemical data published by Sciscio and Bordy (2016) and this is discussed further in Chapter 4. Sample locations, stratigraphic position, and relevant analyses are summarized in Table 2-1.

Table 2-1: Rock samples collected and analyses conducted for present study

Field Site	Sample ID	GPS Coordinates	Formation	Facies Associations and Notes	XRD	SEM	TS	XRF
Red Rocks	KRR-1	36K 326183 7436365	Elliot/Clarens	Facies VII A: Base of Red Rocks			x	
	KRR-2	36K 326183 7436365	Elliot/Clarens	Facies VII A: Base of Red Rocks			x	
	KRR-3	36K 326187 7436369	Elliot/Clarens	Facies VIII: Top of Red Rocks			x	
Lower Makanya Hill	KDC-1	36K 305770 7500260	Soutpansberg Group	Precambrian Basement			x	
	KDC-2	22° 34.658 31° 6.274	Soutpansberg Group	Precambrian Basement			x	
	KDC-3	36K 305282 7501499	Madzaringwe or Fripp	Facies III: Micaceous sandstone			x	
	KDC-4	36K 305160 7502116	Madzaringwe or Fripp	Facies III: Micaceous sandstone			x	
	KDC-5	S 22° 35.193 E 31° 6.496	Tshidize	Facies I: Diamictite			x	
Upper Makanya Hill	KDS-1	S 22° 29.916 E 31° 03.612	Elliot	Facies VI: P-A 0.5 m above base	x	x		x
	KDS-2		Elliot	Facies VI: P-A 2.5 m above base	x	x		x

	KDS-3 A		Elliot	Facies VI: P-A 4.5 m above base				x
	KDS-3 B		Elliot	Facies VI: P-A 4.5 m above base: indurated siltstone	x	x		x
	KDS-4		Elliot	Facies VI: P-A 4.5 m above base	x	x		x
	KDS-5		Elliot	Facies VI: P-A 5.8 m above base	x	x		x
	KDS-6	36K 300890 7511640	Elliot	Facies VI: P-B	x	x		x
	KDS-7	36K 300892 7511370	Elliot	Facies VI: P- C	x	x		x
	KDS-8	22° 29.8536 31° 4.08474 356 m	Clarens	Facies III: Coarse-grained sandstone			x	
	KDS-9	22° 29.9688 31° 4.23402 323 m	Clarens	Facies XI: Bioturbated sandstone			x	
	KDS-10	36K 301105 7510962	Elliot	Facies IV: Nodular mudrock	x			X
Blikana	BPS-1	S 30.58213 E 27.49694	Elliot	Blikana Field Site: Facies VI	x	x		x
				Totals:	9	8	7	10

2.4 Fossil Material

Sauropodomorph fossils have been known from the remote area outside of Nyalaland Trail in the north of Kruger National Park, and in Makuya Reserve for two decades. Mr. Bearnard O'Riain is credited with the first discovery of material on a hike in 1995, and numerous subsequent finds are attributed to park ranger Adriaan Louw (Durand, 1996). In 1996, Adriaan Louw, François Durand and volunteers from the South African Society for Amateur Palaeontologists (SASAP) undertook fieldwork to collect and describe this material, which was subsequently published in a pamphlet and two scientific publications (Durand, 1996; 2001). Durand (2001) assigned these fossils to '*Euskelosaurus browni*', however, this wastebasket taxon has been reclassified into several currently diagnosable genera (Yates, 2004).

Three of the four sites published by Durand (2001) were revisited to reinvestigate fossil material left on the surface, and previously collected material currently stored at Berg-en-Dal camp in Kruger National Park was studied. Collection of two anterior caudal vertebrae and a sample of fossil wood was permitted from Makuya National Park to study and compare with specimens from the collections at the Evolutionary Studies Institute at the University of the Witwatersrand. Elements were found *ex situ,* often in dry washes or piles likely concentrated by modern human and ephemeral fluvial processes. These elements are heavily encrusted in ferricrete, which is a fairly common preservational state of similar material regularly recovered from the Main Karoo Basin. However, the extent of heavy encrustation is noteworthy and likely key to the long-term preservation of this material on the modern landscape surfaces.

Previously collected material stored at Berg-en-Dal include six dorsal and caudal vertebrae, one sacral vertebrae, one partial ilium (postacetabular process), one unidentified element potentially representing pelvic material, one proximal fibula head, and one pedal phalanx, all from a variety of individuals possibly representing multiple taxa and/or ontogenetic stages. Unfortunately, none of these elements are usable for taxonomic diagnosis. Of the numerous elements rediscovered in the field, three elements from adult-sized individuals are taxonomically informative; one anterior caudal vertebra, a left proximal femur possessing a posterior tubercle, and an elongate first left metacarpal (see Figures 3-18, 3-19, and 3-21). Measurements of these specimens were taken with calipers, or where appropriate, a measuring ribbon.

A sample of fossil wood approximately 8 cm long by 3 cm thick (Sample BP-16-1937) from Makuya National Reserve (near the upper Makanya Hill locality) was cut with a discoplan to make thin sections (Figure 3-24). These thin sections were polished on a Struers Acutom machine to about 40μm thickness. Photos were taken on a Zeiss Axioskop petrographic

microscope with an Olympus DP72 digital camera and Olympus Stream Essentials® software which are depicted in Figure 3-22. Prof. M. Bamford identified the material.

2.5 X-Ray Diffraction (XRD)

X-ray diffraction allows for phase identification of solid, crystalline materials. Crystal lattices of minerals diffract x-rays from an incident beam in predictable patterns which are specific to crystal structure. These patterns can then be compared to standard mineral patterns found in the ICDD (International Centre for Diffraction Data) database to identify constituent minerals of rock samples.

Interference patterns (produced in Appendix C) were produced for nine crushed whole rock samples –eight samples from the Elliot Formation in the Lebombo-Tshipise Basin (KDS1, 2, 3B, 4-7, 10), and one sample from Blikana field site (BPS-1) in the Main Karoo Basin– using a D2 Bruker instrument which employs a cobalt K-α X-ray tube with an x-ray wavelength of 1.79026 Å, accelerating voltage of 30 kV, and a current of 10 mA. Diffraction patterns were recorded for Bragg angles between 10 and 90° 2θ, and these analyses were conducted without spin. The scan step size of 0.00200318° was applied with a scan step time of 1.3 s. The XRD patterns derived from the palaeosol and mudrock samples were compared to patterns of standard minerals known to occur in sedimentary rocks using JADE 9 software at TerraTek, A Schlumberger Company, by Susan Lutz. Major, minor, or trace peaks for these minerals' occurrence are summarized in Table 3-5.

As the Y axis in XRD patterns is an arbitrary measurement of counts, the description of peaks as major, minor or trace functions as a semi-quantitative and imprecise indication of the amount of mineral present in the sample and identifiable in the XRD spectra. Individual sample XRD spectra are presented in Appendix C.

2.6Scanning Electron Microscope (SEM)

A scanning electron microscope uses an electron beam which interacts with atoms within the sample to produce high resolution images on the scale of micrometers. This is coupled with Energy Dispersive Spectroscopy (EDS), which generates an X-ray spectrum reflecting elemental composition, to identify mineral morphologies.

Scanning Electron Microscopy (SEM) was employed to examine clay crystal morphology to ascertain the detrital or authigenic nature of the species present within eight samples. Seven samples are from palaeosols of the Elliot Formation from the Lebombo-Tshipise Basin (KDS1, 2, 3B, 4-7, 10; sample information is listed in Table 2-1), and the eighth is from a palaeosol from the Blikana field site in the Main Karoo Basin (BPS-1). This analysis was conducted with an FEI Quanta 200 ESEM with a voltage of 30.00 kV and a 5.0 nm spot. All samples were coated with 10 μm of gold and palladium (AuPd), while samples KDS1-4 were coated with 30 μm of carbon (C) and then coated with an additional 10 μm of gold and palladium. Samples were analyzed with EDS to determine elemental composition and compared to spectra in *Electron Microprobe Analysis and Scanning Electron Microscopy in Geology* by Reed (2005). All sample images were produced by secondary electron (SE) signals and are found in Appendix C.

2.7 Petrography

Study of sandstone microstructure was conducted using a petrographic microscope. Microstructure includes grain size, rounding, and orientation, in addition to the nature of grain contacts, general mineralogy, cementation, and matrix description. Seven sandstone samples from Red Rocks (KRR1-3) and Makanya Hill (KDS8, 9, and KDC1-5) were collected from Karoo Supergroup sandstones in the Lebombo-Tshipise Basin, and mounted on 27 x 46 mm slides ground to 30 μm in thickness (samples in

Appendix B). Point counts were calculated by picking 250 grains at random from each slide, the results are summarized in a Q-F-L diagram (Figure B1, Appendix B) and photographs of the slides are found in Appendix B.

2.8 X-ray Fluorescence (XRF)

X-ray Fluorescence employs high energy x-rays which excite electrons in the material under investigation which escape in the form of radiation in patterns specific to the constituent atoms of the material. This allows quantification of major and trace elements present which are reported as oxide weight percentages and parts per million, respectively (see Tables 3-6 and 3-7 for results).

This analysis was conducted on ten crushed, whole rock samples- nine palaeosol and mudrock samples from the Elliot Formation in the Lebombo-Tshipise Basin (KDS1-7, 10) and one palaeosol sample from the Blikana field site in the Main Karoo Basin (BPS-1). Analysis was conducted at the Earth Lab at the University of the Witwatersrand by Marlin Patchappa. Samples were initially ignited at 250°C and then at 1000°C to measure the loss of organic carbon (CO_2) and carbonate ($CaCO_3$) respectively, so that the amount of CaO measured in the remaining sample represented CaO from the silicate fraction of the sample only.

Chemical Indices of Alteration (CIA) values were calculated using these XRF data. CIA values represent total weathering processes by quantifying the weathering of feldspars to clay minerals (Nesbitt & Young, 1982). This measurement compares amounts of insoluble Al_2O_3 to soluble Na_2O, CaO, and K_2O by the following equation: CIA = 100 x (Al_2O_3/(Al_2O_3+CaO+Na_2O+K_2O)). Low CIA values (<55) represent relatively unweathered rocks, and high values (>75) represent rocks that have undergone significant amounts of leaching, resulting in low amounts of soluble cations. CIA values are reported in Table 3-6.

Chapter 3: Results

3.1 Facies Associations and Stratigraphy

3.1.1 Facies Associations

This section provides lithofacies assignment and facies associations to determine the various depositional environments encountered at the field sites. Facies associations consist of lithofacies assemblages that commonly occur together in outcrop. Interpretation of these various facies associations is the primary qualitative tool in reconstructing various depositional environments. Through this approach, tracking palaeoenvironmental change from the Carboniferous to the Jurassic in the Madzaringwe, Mikembeni, Fripp, Solitude, Klopperfontein, Elliot and Clarens Formations is possible.

Lithofacies were classified per Miall's (1977, 1978, 1996, 2014) lithofacies classification scheme, which is based on grain-size (i.e. G for gravel, S for sand, and F for mud and silt) and sedimentary structures. Short descriptions and summaries of these lithofacies are found in Table 3-1, and Table 3-2 summarizes facies associations. Associated photographs are found in Figures 3-1 through 3.4 and 3-6 through 3-11.

Table 3-1: Lithofacies classification and descriptions (after Miall, 2014)

Facies	Grain size	Description	Geometry	Occurrence	Interpretation
Gmm Massively bedded conglomerate	Granule to cobble	(1) Intraformational quartzite, black brecciated shale, quartzite, and bedded metasandstone clasts 1-15 cm in diameter, in grey (5GY 8/1), blue (5B 5/1), orange (10 YR 6/6), mottled sandy clay. (2) Scour fills bearing angular to sub-rounded quartz pebbles (0.5-2cm in diameter).	(1) Massive irregular beds 30-90 cm thick. This facies is erosively overlain by Gmg. Contact with underlying strata was not observed. (2) Small (<20 cm long) scours at the	(1) Tshidize Formation (2) Clarens Formation	(1) Large debris flow consistent with fluvio-glacial processes. Large cobbles indicate viscous flows. (2) Small channel scours indicating variation in flow velocity

			base of troughs.		
Gmg Normal-graded conglomerate	Granule to pebble, rare cobbles	Black shale clasts in greater abundance than quartz, quartzite, and bedded metasandstone clasts in grey (5GY 8/1), blue (5B 5/1), orange (10 YR 6/6), mottled sandy clay. Clasts decrease in size and abundance upwards and matrix becomes more clay-ey.	Irregular beds 5-15 cm thick. Erosively contacts underlying Gmm. Contact with overlying strata was not observed in the field.	Tshidize Formation	Mass flow deposit. Fining upwards character denotes waning energy.
St Trough cross-bedded sandstone	Fine to coarse sand	Cross bedded units with curved bounding surfaces that truncate underlying structures. 1) Fine-medium grained, well sorted red (5R 6/6, 10R 6/6) and gray-white (N8, N9) sand 2) Coarse, moderate to poorly sorted, subangular to subrounded, gray and brown (10 YR 6/2, 5Y 7/2) sandstone 3) Coarse-grained, poorly sorted, subangular to subrounded, micaceous, yellow and white (N9, 10 YR 8/2) sandstone	Lenticular beds that vary in depth between 0.20-3m. Contacts are typically sharp, and often cross-cutting.	Madzaringwe, Mikembeni, Fripp, and Clarens Formations	Upper flow regime structure representing dune formation in water or air flow.
Sp Planar cross-bedded sandstone	Fine to coarse sand	Cross beds are typically 15-30° from the horizontal. 1) Fine-medium grained, well sorted red (5R 6/6, 10R 6/6) and gray-white (N8, N9) sand 2) Coarse,	Typically in tabular, sometimes inclined beds. These are often stacked in packages of 5-8 beds. Contacts are typically sharp and	Madzaringwe, Mikembeni, Fripp, and Clarens Formations	Lee-side deposits of migrating dunes. In aeolian settings, these are more continuous and thick. In fluvial settings, these can have coarse-grained

		moderate to poorly sorted, subangular to subrounded, gray and brown (10 YR 6/2, 5Y 7/2) sandstone 3) Coarse-grained, poorly sorted, subangular to subrounded, micaceous, yellow and white (N9, 10 YR 8/2) sandstone	planar, though irregular contacts are also observed.		forests and are frequently associated with conglomerates.
Sb Bioturbated, sandstone	Fine to medium sand	Grey (N8, N9) or red (5R 6/6, 10R 6/6) massively bedded sandstone, preserving local concentrations of cylindrical, vertically oriented burrows which are sometimes paired, and semi-undulatory, meniscate traces. Bedding features are faint, interrupted, or absent.	Lenticular and tabular beds 5cm-1m thick. Contacts are irregular, sharp and gradational.	Elliot and Clarens Formation	Bioturbated sandstone, locally preserving *Planolites isp,, Arenicolites isp., Entradensis isp,* and *Taenidium isp.*
Sl Low-angle cross-bedded sandstone	Fine to coarse sand	Low-angle (<15°), planar beds ~5-15 cm thick. 1) Coarse, moderate to poorly sorted, subangular to subrounded, gray and brown (10 YR 6/2, 5Y 7/2) sandstone 2) Coarse-grained, poorly sorted, subangular to subrounded, micaceous, yellow and white (N9, 10 YR 8/2) sandstone	Tabular beds with sharp contacts.	Madzaringwe, Mikemebeni Formations and Fripp Sandstone	Washed out dunes.
Ss	Medium	Tan or beige (5Y 8/1,	Lenticular	Madzaringwe,	Pulses of higher

Shallow scoured sandstone	to coarse sand	10 YR 7/4) sandstone in dish-shaped, typically fining upwards localized scours	and localized with sharp, erosive contacts.	Mikembeni Formations and Fripp Sandstone	energy flows which scour into the underlying strata.
Sm Massively bedded sandstone	Fine to coarse sand	Beds lacking sedimentary structures or bedding. 1) Fine-medium grained, well sorted red (5R 6/6, 10R 6/6) and gray-white (N8, N9) sand 2) Coarse, moderate to poorly sorted, subangular to subrounded, gray and brown (10 YR 6/2, 5Y 7/2) sandstone 3) Coarse-grained, poorly sorted, subangular to subrounded, micaceous, yellow and white (N9, 10 YR 8/2) sandstone	Typically tabular, laterally extensive. Contacts are usually gradational, though sharp contacts are also observed.	Madzaringwe, Mikembeni, Fripp, Solitude, Elliot and Clarens Formations	Associated with unchannelized flows, and upper flow regime deposition in channel bases. Also produced by bioturbation.
Sh Horizontally laminated sandstone	Fine to coarse sand	Laminated (<1cm) or thinly-bedded (>1 cm) strata. Fines upwards in some beds. 1) Fine-medium grained, well sorted red (5R 6/6, 10R 6/6) and gray-white (N8, N9) sand 2) Coarse, moderate to poorly sorted, subangular to subrounded, gray and brown (10 YR 6/2, 5Y 7/2) sandstone	Typically tabular and laterally extensive. Contacts can be sharp, gradational, and irregular.	Madzaringwe, Mikembeni, Fripp, Solitude, and Clarens Formations	Upper flow regime dominated channel bedforms, relatively horizontal interdune areas.

		3) Coarse-grained, poorly sorted, subangular to subrounded, micaceous, yellow and white (N9, 10 YR 8/2)sandstone			
Sr Ripple laminated sandstone	Fine to medium	Blue-green (10G 6/2) or beige (10 YR 7/4) sandstone preserving ripple forms or ripple cross-lamination.	Thin (<5 cm), tabular beds with sharp or gradational contacts, typically overlain by fines.	Solitude and Elliot Formations	Low flow regime structures formed in unchannelized flows.
Fsm Massively bedded mud or silt	Clay to silt	Structure-less or nodular siltstone and mudrock, often gray (N8), but also dull greens and yellows (5Y 7/2, 5G 7/2), red (5R 4/6) and blue-green (10G 6/2).	Tabular or sheet like beds ~10 cm thick, rarely in lenticular beds. Contacts are typically sharp, but gradational contacts are also observed.	Mikembeni and Solitude Formations	Indicative of water-saturated sediments such as those found in lakes, or unconfined, viscous flows across the floodplain.
Fl Finely laminated or mud or silt	Clay to silt	Finely laminated silt or mud in thin (~2-8 cm thick) beds. Often very colourful including pink (5R 8/2), purple (10R 6/2), blue-green (5BG 5/2) and yellows (10YR 8/6, 5Y 7/2).	Typically lenticular or sheet-like, commonly occurring with Fsm and various sandy lithofacies. Contacts are sharp.	Mikembeni, Solitude, and Elliot Formations	Represents low energy flow and/or sediment settling in standing water.
P Palaeosol	Clay, silt	Weakly bedded clay and silt in a variety of colours including grey (10GY 7/2, 10YR 8/2), maroon (5R 2/6, 5P 4/2), purple (5YR 7/2) with yellow-green green (10Y 6/6) sub-vertical oriented, branching fractures, and red-orange (10R 6/6) with yellow-green (5Y 7/6) mottling	Tabular beds, locally laterally extensive. No contacts with under or overlying strata were observed.	Elliot Formation	Ancient soil horizons.
C Coal	Coal	Bright, bituminous coal (N1), often laminated, with near-perpendicular	Thin, laminated, laterally extensive	Madzaringwe and Mikembeni Formations	Compressed and altered plant matter.

		cleavage.	beds or thin lenses. Contacts are gradational, but some sharp contacts are observed.		

Table 3-2: Karoo Supergroup Facies Associations from the Lebombo-Tshipise Basin

Facies Associations	Lithofacies	Interpretation	Formation Occurrence
I	Gmm, Gmg, St	Fluvio-glacial diamictite	Tshidize Formation, Makanya Hill
II	Sh, Sm, Fsm, Fl, C	Lacustrine and swamp deposits	Madzaringwe and Mikembeni Formations, Makanya Hill
III	Gmm, St, Sp, Sl, Ss, Sh	High energy fluvial channels and bedforms	Clarens, Klopperfontein, Fripp, Madzaringwe and Mikembeni Formations, Makanya Hill
IV	Sr, Fsm, Fl	Floodplain deposits	Solitude and Elliot Formations, Makanya Hill
V	Sh, Sm, Sr, Fl, Fsm	Crevasse-splay sandstones	Solitude Formation, Makanya Hill
VI	P	Palaeosol	Elliot Formation, Makanya Hill
VII (A&B)	Sm, St, Sb, Sl	Bioturbated aeolian dunes	Elliot/Clarens Formation, Red Rocks
VIII	Sm, St	Channel bedorms	Elliot/Clarens Formation, Red Rocks
IX	Sm, Fl	Overbank interdune deposits	Elliot Formation/Clarens, Red Rocks
X	St, Sp	Aeolian dunes	Clarens Formation, Makanya Hill
XI	Sm, Sh, Sb	Bioturbated, flooded interdunes	Clarens Formation, Makanya Hill

Facies Association I: FA I is represented by 7.5 m of poorly sorted, extraformational, polymictic diamictite (Figure 3-1 A, B) of the Tshidize Formation. The exposure at Lower Makanya Hilll field site can be informally divided into two units: an upward-coarsening, massive and irregularly bedded, yellow-orange (5GY 8/1, 10YR 6/6) lower unit (Gmm and Gmg), and an upward-fining, blue-grey (5B 5/1) sandstone and sandy mudstone upper unit (St and Gmm). Both units have granule to cobble sized clasts of quartzite, bedded metasandstone, and black shale.

The lower unit (Figure 3-1 A) consists of matrix-supported, brown (10YR 5/4) and green-grey (10YR 8/2) sandy mud which coarsens upwards, becoming sandier and yellow-orange (10YR 6/6). Indistinct, roughly horizontal bedding 10-25 cm thick tops the lower unit. Granule to cobble sized cream (5Y 8/4) and brown (5Y 7/6) quartzite and bedded metasandstone clasts are angular to rounded, poorly sorted, and common, unaligned to rarely present bedding. Angular to rounded black, brecciated shale pebbles are rare. Bedded metasandstone clasts resemble the underlying Soutpansberg Group quartzites, which is supported by observations in McCourt and Brandl (1980).

The lowermost third of the upper unit consists of blue-grey (5B 5/1) trough cross-bedded sand in 5-20 cm thick, undulatory, beds, with rare clasts (St), (Figure 3-1 B). This contact is sharp and irregular. The upper unit grades to massively bedded, mottled white (N9), black (N1) and blue-grey (5B 5/1) mud with quartz pebbles and black shale clasts (~4-10mm in diameter), with significantly fewer quartzite and metasandstone clasts than the lower unit, (Figure 3-1 C). The abundance of clasts decreases upwards in the unit, and clasts from the upper unit overall are less abundant and smaller than those in the lower unit.

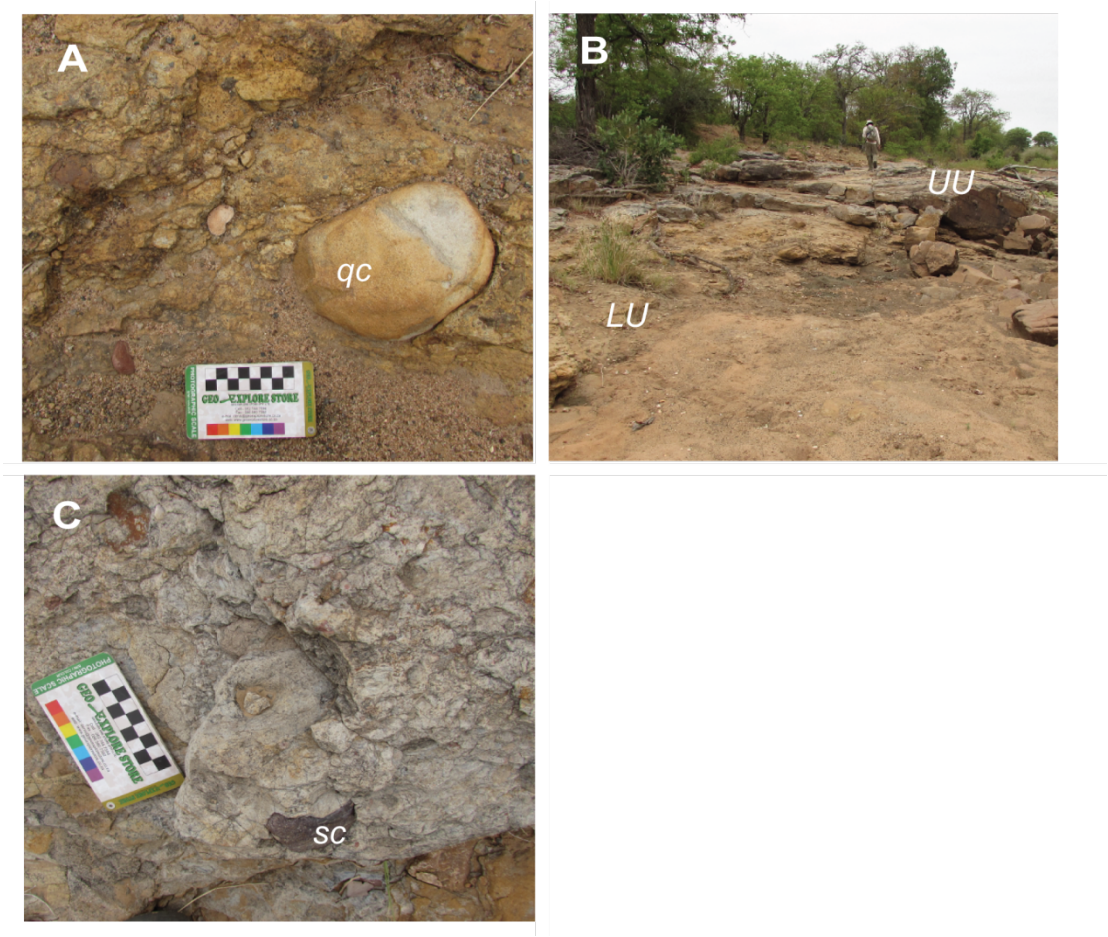

Figure 3-1: Facies Association I from the Lower Makanya Hill field locality. (A) Lower unit of the Tshidize Formation is weakly bedded with large clasts of underlying Soutpansberg quartzite (qc); (B) Boundary between sandy, weakly bedded lower (LU) and trough cross-bedded sandstone of the upper (UU) units, see geologist for scale;(C) Upper unit consisting of grey matrix and more shale clasts (sc) than lower, sandier unit.

Interpretation

The two units are primarily composed of diamictite, consistent with debris flows. Though the lower unit is poorly stratified, the faint bedding and rounded clasts suggests that meltwater was a primary source of deposition (Boggs, 2006). The upward-coarsening trend is typical of debris flows, and the indistinct bedding at the top likely represents repeated flow events. As cross bedding or other sedimentary features indicating fluvial reworking are not developed, this deposit is more consistent with distal flow (i.e., meltwater streams) than higher energy, outwash tills (Boulton & Deynoux, 1981).

The trough cross-bedded, undulating sandstone beds with fewer clasts at the base of the second unit show fluvial reworking of the till. The upper unit's prevalence of black shale clasts may indicate a change of sediment source, while upward-fining beds and the increasing rarity of larger metasedimentary cobbles are consistent with decreasing energy over time.

This facies association is interpreted as fluvio-glacial deposits. The lack of marine mud facies, dropstones or other marine features (i.e. fossils) support that this deposit was formed in the proximal glacial environment.

Facies Association II: Finely laminated sandstones and siltstones interbeddded with mudrocks and coal comprise FA II (Figure 3-2 A, B, and C). This facies association occurs in the Madzaringwe and Mikembeni Formations at the Lower Makanya Hill field locality. The sandstones are moderately sorted, medium-grained and both the sandstones and siltstones are micaceous and vary in color (Figure 3-2 A), including pink (5R 8/2), purple (10R 6/2), blue-green (5BG 5/2) and yellow or beige (10YR 8/6, 5Y 7/2). Sandstones are finely laminated, low-angle planar cross-bedded, or massively bedded, and sharply contact underlying siltstone and mudrock intervals. Sandstone layers are thicker and more common in the Madzaringwe than in the Mikembeni Formation, which is dominated by siltstones, mudstones, carbonaceous shale and coal.

Siltstone and sandstone units grade into interbedded mud and coal and contacts between the two units are typically gradual, though sharp contacts were also observed. Siltstone and mudrock successions commonly fine upwards. The carbonaceous shales and mudrocks are massive or poorly laminated, black in colour and interbedded with friable, bituminous coal (Figure 3-2 B and C). In the Mikembeni Formation, large (80 cm thick) ferruginous concretions within the mudstone beds are

common and can be laterally extensive, sometimes appearing bed-like. These concretions are rare in the siltstone intervals. This association interfingers with FA III, typically with sharp contacts (Figure 3-2 D).

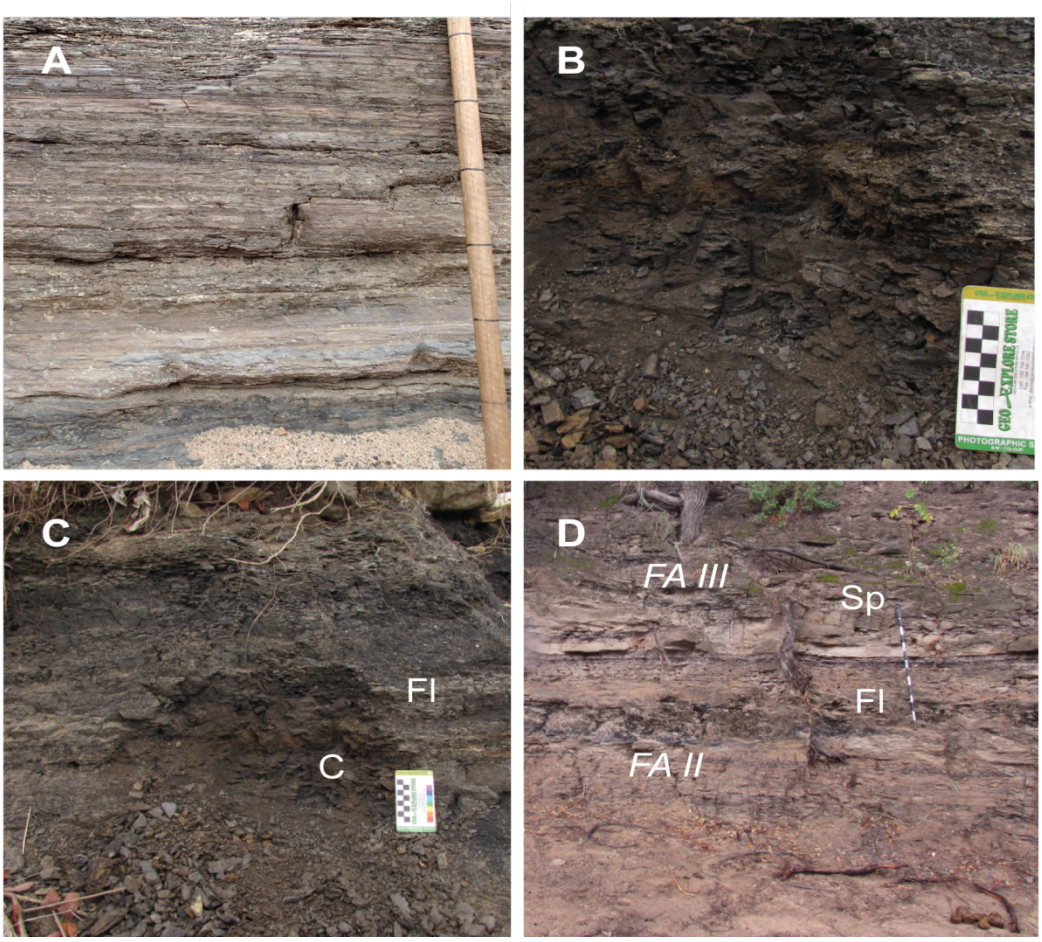

Figure 3-2: Facies Association II from the Lower Makanya Hill field locality. (A) Finely laminated siltstones and sandstones of the Mikembeni Formation; (B) weakly bedded coal and carbonaceous mudrock of the Madzaringwe Formation; (C) Interbedded coal, carbonaceous mudrock and laminated fines; (D) Laminated silts (Fl) of FA II overlain by planar cross-bedded sandstone (Sp) of FA III in the Madzaringwe Formation.

Interpretation

Carbonaceous mudrocks and coal form in a low energy environment, and are typical components of delta plain and fluvial deposits (Miall, 1996). Thinly-bedded siltstones and laminated mudrocks are deposited from suspension in lacustrine settings (Boggs, 2006), and upward-fining mudrocks and silt intervals may represent ox-bow lake environments. Thin

sandstone lenses and beds may represent near-shore deposits including deltas, beaches, spits or barriers (Boggs, 2006) in shallow lakes, as suggested by Malaza et al. (2013). Iron-rich concretions are likely formed diagenetically, from concentrated ground-water interactions.

FA II is interpreted as marsh or lacustrine deposits in a delta plain environment. The association FA II and the thick sandstone bodies of FA III indicate the marshy lacustrine environment was influenced by fluvial systems, (Figure 3-2 D).

Facies Association III: FA III is composed of medium to coarse-grained, moderate to poorly sorted sandstone in a variety of bedding types: lenticular and less frequently tabular bodies of planar cross-beds; lenticular or irregular bodies of trough cross-beds; lenticular bodies of low-angle planar cross beds; sheet-like or irregularly-shaped massive beds; and lenticular bodies of horizontal and wavy laminations (Figure 3-3 and 3-4). This facies association occurs in the Madzaringwe, Mikembeni, Fripp, Solitude and Clarens Formations at the Lower and Upper Makanya Hill field localities.

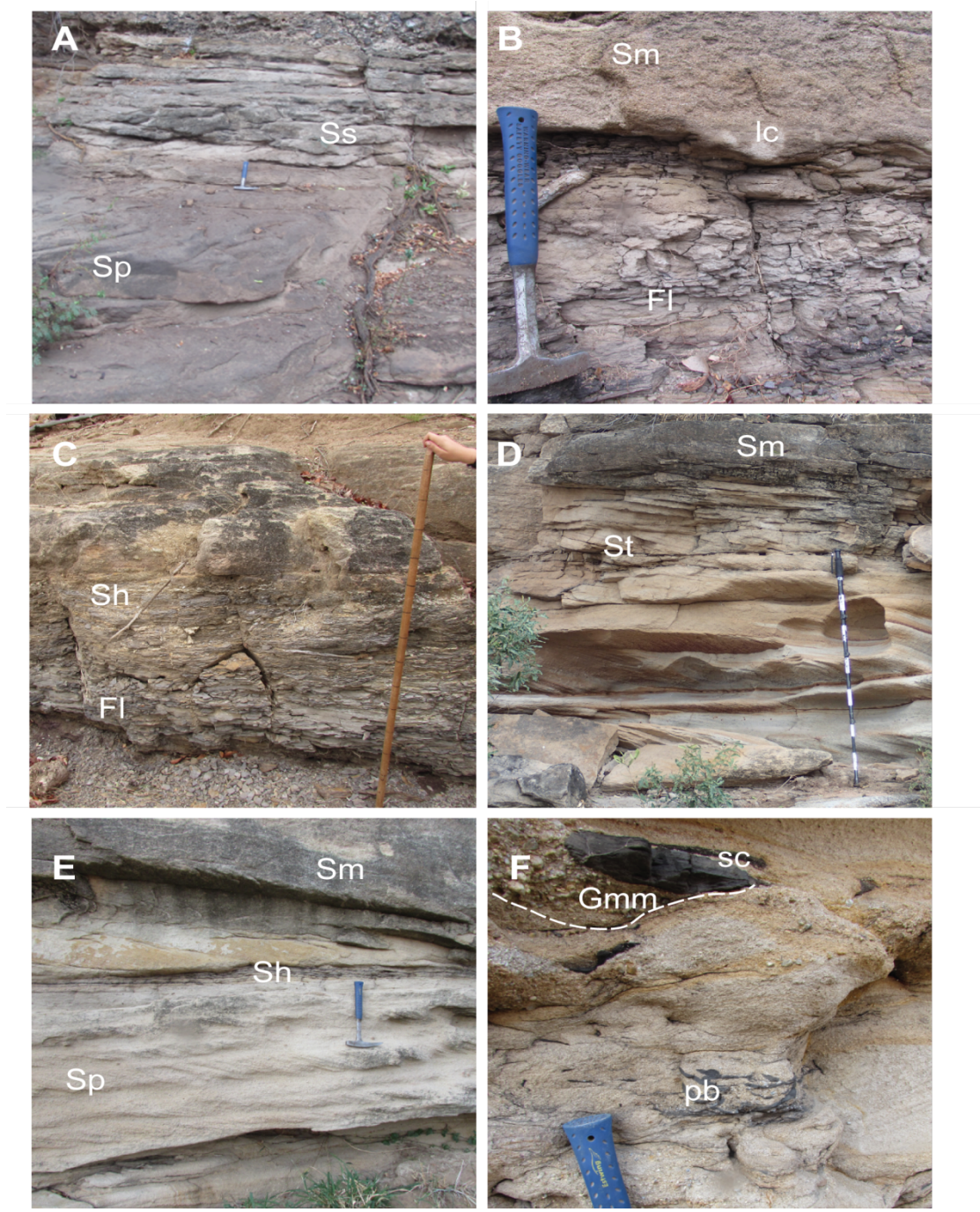

Figure 3-3: Facies Association III from the Lower Makanya Hill field locality. (A) Planar cross-bedded sandstone grading to scoured sandstone (Ss) in the Madzaringwe Formation; (B) Sharp contact between massive sandstone (Sm) and laminated silts (Fl) with load cast (lc) in the Solitude Formation; (C) Gradual contact between laminated mud and silt (Fl) and weakly bedded, horizontally laminated sandstone (Sh) in the Madzaringwe Formation; (D) Trough cross-bedded sandstone (St) and massive sandstone (Sm) overlying fine-grained sandstone of the Fripp Sandstone; (E) Sets of planar cross-bedded (Sp) sandstone gradually overlain by horizontally laminated (Sh) sandstone, and sharp contact overlying massively bedded sandstone (Sm) in the Fripp Sandstone; (F) Coarse, gritty (Gmm) lenses, with large shale clasts (sc)and carbonaceous plant debris (pd) indicate high energy intervals during deposition of the Fripp Sandstone.

Figure 3-4: Facies Association III from the Upper Makanya Hill field locality. (A, B, C) Coarse lags (Gmm) at the base of planar (Sp) and trough cross-bedded sandstones (St), in the Clarens Formation. (D, E) Lags are very coarse, pebble conglomerates sometimes containing bone fragments (bf).

Lenticular and tabular beds of planar cross-beds represent the majority (~65%) of this facies in outcrop (Figure 3-3 E). These beds range from 0.25-1.5 m thick. Tabular bodies often have sharp lower contacts and sharp or gradual, wavy upper contacts, and some beds are inclined at low (<15°) angles. These bodies are commonly stacked together, though typically separated by beds of Sh, or Sm. In some bodies, pebble conglomerates armour the tops of planar cross-beds, and are aligned to foresets. Others have shale rip-up clasts and carbonaceous plant material up to 28 cm in length and coarse, basal pebble lags (Gmm; Figure 3-3 F). Gritty, pebble conglomerates are common, especially in the Clarens Formation (Figure 3-4 B, C, D, and E).

Palaeocurrents from planar cross-beds are reported in Figure 3-5. These indicate south-southwest flows (157-238°, n=10) in the Madzaringwe Formation, south-southeast (93-220°, n=15) in the Mikembeni Formation, southeast (120-164°, n=25) flows in the Fripp Formation, southerly flows in the Solitude (118-210°), and easterly flows (59-104°, n=10) in the Clarens.

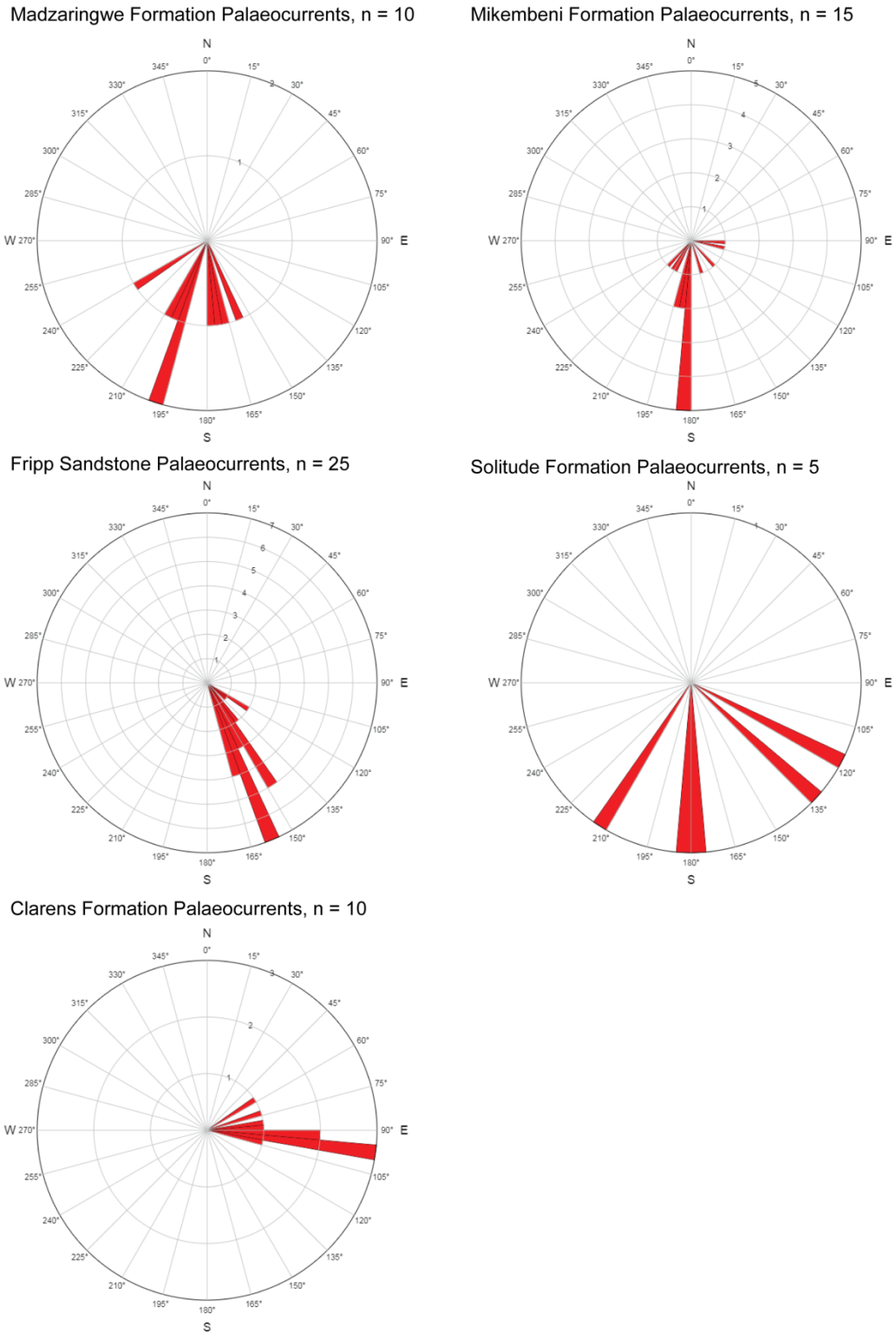

Figure 3-5: Palaeocurrents measured from planar cross-beds in the Madzaringwe (n = 10), Mikembeni (n = 15), Fripp (n = 25), Solitude (n = 5), and Clarens (n = 10) Formations at the Makanya Hill field locality.

Trough cross-bedded sandstones are lenticular, 15-50 cm thick beds which commonly contain scoured bases (Figure 3-4 A and C). Many of these have coarse lag deposits of quartzite pebbles (>5 mm in diameter) at their base. Trough cross-bedded units are commonly stacked, erosively cross-cutting underlying beds with sharp upper and lower contacts (Figure 3-3 D).

Low-angle (<15°) planar cross-bedded units are lenticular, 20-30 cm thick with sharp upper contacts and typically diffuse lower contacts. This facies is in many cases overlain by tabular, planar cross-bedded bodies.

Massively bedded sandstone bodies are irregularly shaped and large (~1 m thick). Massively bedded sand sheets (Ss) are typically lenticular beds 10-40 cm thick that are amalgamated up to a meter thick (Figure 3-3 A). Large massive beds typically have sharp upper and lower contacts, while amalgamations often have diffuse or gradual upper contacts with planar or horizontally laminated sandstones. These bodies also share gradual and sharp contacts with underlying silts (Figure 3-3 B and C).

Horizontally bedded or laminated sandstone (Sh) is the least common of the fluvial lithofacies. These beds are commonly 30-50 cm thick with 1-3cm thick laminations, and are lenticular or irregularly shaped. Laminations typically fine upwards, and many of these beds are draped by shale and silt laminations at the top. These beds have sharp lower and upper contacts, and are typically erosively overlain by planar laminated, coarse sandstone bodies (Figure 3-3 E).

Interpretation

The prevalence of sand and grits indicate a high energy environment. Trough cross-bedded units represent migrating dunes in fluvial channels and planar cross-bedded units stacked at low angles represent 2-D dune formation on top of bars (Miall, 1996; Boggs, 2006). Low-angle bedded

units are consistent with washed out dunes formed as channel dunes are eroded by an increase in flow from lower to higher flow regimes (Miall, 1996). Thus, this facies association is interpreted as dunes, bars and other channel bedforms from large, recurring fluvial systems.

Facies Association IV: FA IV consists of blue-green (10G 6/2) siltstone and mudrock with rare, intraformational quartz pebbles; blue-grey (10Y 4/2) mudrock, sometimes with orange mottles; and red (5R 4/6) massive mudrock. This facies association occurs in the Solitude and Elliot Formations at the Lower and Upper Makanya Hill field localities.

In the Solitude Formation, the mudrocks are typically interlaminated with blue, grey and brown siltstone, (Figure 3-6 A). These mudrocks and siltstones typically underlie and overlie channel bedforms of FA III (Figure 3-6 B), or the sandstones of FA V (Figure 3-7 A) with sharp contacts.

In the Elliot Formation, the mudrock is laminated, nodular, and in some outcrop, highly indurated (Figure 3-6 B). The weakly bedded mudrock is approximately 3 meters thick and thins upwards in planar beds from approximately 40 cm to 7 cm thick. The siltstone is weakly bedded with thin (~5-10 mm thick) planar laminations and ripples. The ripples measure ~30-50 mm high, and are asymmetric, elongate, continuous and fairly straight crested, though some curving is observed (Figure 3-6 C). Thin (~3-5 cm wide) stringers of granule-sized, well-rounded, intraformational quartz clasts occur randomly. This facies association was only observed in isolation in the field area.

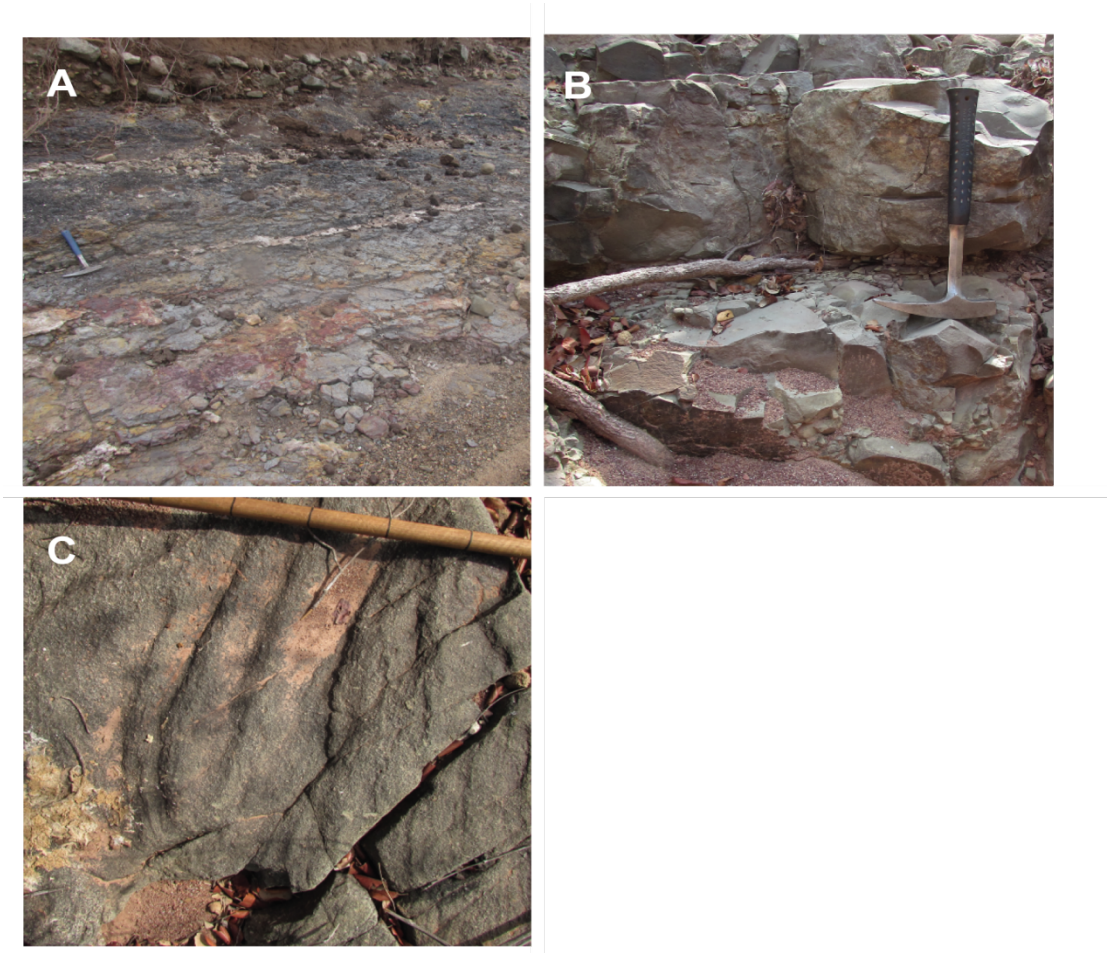

Figure 3-6: Facies Association VI from the Lower and Upper Makanya Hill field localities. (A) Colourful, weakly bedded mudrock from the Solitude Formation; (B) Nodular mudrock from the Elliot Formation; (C) Asymmetric ripples preserved in siltstone in the Elliot Formation.

Interpretation

Ripple and horizontal lamination are hallmarks of floodplain deposits, while stringers of granule-sized quartz clasts could represent short-lived high energy traction currents, consistent with the waning energy of distal deposits from crevasse splays (Miall 1996). Horizontal lamination and ripple cross-lamination are also consistent with distal crevasse splays (Lang, 1993; Miall, 1996; Brierley, 1997), but the lack of developed cross lamination and the faint preservation of laminations suggest these deposits formed distal to the channel. Nodular mudrock is more commonly associated with distal-most floodplain deposits or stagnant, standing water

(Miall, 1996). This facies association is interpreted as floodplain deposits of fine sediments.

Facies Association V: FA V is composed of medium-grained, thin (~10-45 cm thick), wedge-shaped and lenticular sandstone beds. This facies association occurs in the Solitude Formation at the Lower Makanya Hill field locality. Lenticular bodies tend to be massive or with very faint bedding, while the wedge-shaped beds are horizontally and/or ripple cross-laminated. Lenticular bodies are thicker than the wedge-shaped counterparts, and have sharp basal contacts with underlying fine-grained components of FA IV (Figure 3-7 A). Horizontally laminated and ripple cross-laminated beds are usually finer grained than adjacent lenticular bodies and typically reach 20 cm thick at maximum, Figure 3-7 B. These wedge out into siltstones and mudrocks.

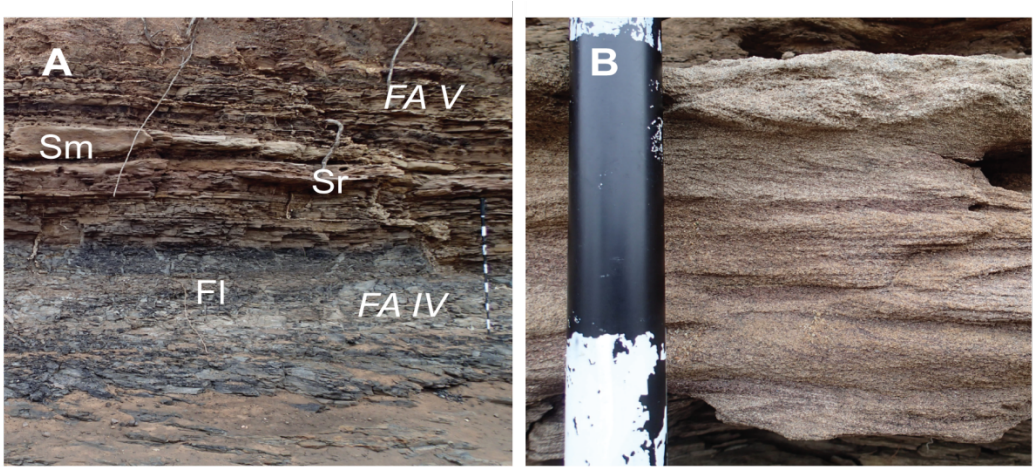

Figure 3-7: Facies Association V from the Lower Makanya Hill field locality. (A) Lenses of massively bedded sandstone (Sm) wedge out laterally into wedge-shaped bodies of ripple cross-laminated sandstone (Sr); these sandstones overlie laminated siltstones and mudrocks (Fl) of FA IV with sharp contacts; (B) Ripple cross-laminated sandstone bodies are thin, typically only 10-20 cm thick.

Interpretation

The geometry of the massively-bedded, lenticular sandstones is consistent with crevasse channels; while laminated and cross-laminated beds are typical components of represent crevasse splay deposits (Miall, 1996). Thus, this facies association is interpreted as crevasse-splay deposits.

The lack of preserved plant matter or interrupted bedding in the banks consistent with bioturbation could be attributed to frequent flooding and rapid burial.

Facies Association VI: FA VI consists of weakly-bedded mudrock in a variety of colours including grey (10GY 7/2), green (5Y 7/6), yellow-green, (10Y 6/6), red-brown (10R 6/6), and purple (5YR 7/2) mudrock (Figure 3-8). This facies association occurs in three locations: P-A, P-B, and P-C in the Elliot Formation of the Upper Makanya Hill field locality.

Two of the exposures (P-B and P-C) measure approximately 1.5 meters in height, and the other (P-A) measures 7 meters. The mineral content of all three exposures as determined by XRD (see section 3.2.1) primarily consists of illite and smectite clay, with minor amounts of plagioclase, quartz, and trace amounts of iron and titanium oxides. Bedding is very weak, though contacts between the differently coloured horizons are diffuse and primarily planar though minor undulations occur locally. Orange or yellow-green mottling occurs in many layers and is especially prevalent in P-B and P-C. Minor quartz pebbles (~8-10 mm in diameter) occur in the yellow-green horizons.

At the base of P-A, there is a zone of pervasive fractures which are green (10Y 6/6) and blue (5B 8/2) in color, oriented sub-vertically, and connected by regularly occurring sub-parallel veins (Figure 3-8 A). These are distinct from blue (5B 7/6) bifurcating, branched, vertically oriented features which measure approximately 20-40 cm in length and occur in a deep purple horizon approximately 2 meters above the base of P-A (Figure 3-8 C). A vertically-oriented dolerite dyke likely has hydrothermally altered immediately adjacent outcrop which is green and nodular (Figure 3-8 B). Additionally, diagenetic white, powdery calcite veins which are closely associated with modern plant roots that infiltrate upper strata exposed at P-A approximately a meter deep.

Figure 3-8: Facies Association VI from the Upper Makanya Hill field locality. (A) Exposure of pervasively fractured zone at the base of P-A (backpack for scale); (B) Large dyke (d) above geologist cross cuts P-A; (C) Bifurcating and branched rhizoliths in horizon of P-A indicated by arrows; (D) Exposure of P-B shows weak horizonation in comparison with P-A.

Interpretation

The argillaceous and horizonated nature of these exposures is consistent with palaeosols. Bifurcating, blue features are interpreted as rhizoliths. Purple and maroon colouring is consistent with subsurface (Bt and Bs) horizons (Retallack, 1984, 1988), while grey horizons in these palaeosols may represent A or E soil horizons which are often light coloured due to abundant quartz (Retallack, 2008).

These palaeosols do not preserve ped structures or burrows, and lack well developed O and A horizons (as defined by the USDA soil taxonomy

system), which suggests that subsurface portions of the ancient soil comprise these exposures (Retallack, 2008). Alternatively, arid conditions at the time of deposition might have contributed to poor or nonexistent ped development, or these structures may have been erased by diagenetic processes, though the existence of rhizoliths suggests little erasure of original structures and features has occurred.

The organic matter content of these palaeosols is very low, ruling out classification as a Histosol or Spodosol (Mack et al., 1993). Low organic content is consistent with soils developed in arid regions (Worden & Morad, 2009), however, these palaeosols also lack accumulations of soluble minerals
(i.e. calcite, gypsum) traditionally associated with aridisols, gypsisols, etc. The presence authigenic clay, sesquioxides, and traces of iron minerals as determined by XRD (see Chapter 3.2.1 for a more detailed discussion of mineral content and clay overgrowths) are consistent with both Oxisols and Argillisols (after Mack et al., 1993).

The fractured zone in P-A may have formed during the emplacement of the nearby dyke, though the fractures are regular, and do not appear to be enlarged nor more numerous near the dyke itself. The meter-long yellow-green and orange fractures in this purple horizon likely represent hydrothermal alteration subsequent to the dyke's emplacement through pre-existing weak planes in the soil. The orange colour may be from infill of oxidised sediments, or oxidised fluids moving through permeable conduits.

Facies Association VII A: FA VII A consists of fine-grained red to brown (5R 6/6, 10R 6/6), well-rounded and well-sorted sandstone which is heavily mottled beige and light brown (10 YR 7/4, 5 YR 7/2, 10 R 7/4; Figure 3-9 B). This facies association occurs in the Elliot/Clarens Formation at the Red Rocks field locality.

This facies is 4 meters thick, laterally extensive, and typically massive (~80% of the outcrop). Large sand bodies with relatively horizontal bases and undulating (~1 m, 2-3 m wavelength), sharp upper contacts and rare, lenticular, massive sand bodies are also present in this facies. These undulating surfaces strongly resemble sand dunes, and one of these preserved numerous, beige burrows aligned to cryptic, fairly high angle (~40°) foresets below the surface (Figure 3-22 C, Chapter 3.3.2). These dune forms represent approximately 10% of the facies association outcrop.

The beige mottles are cylindrical and elongate, though in some instances bulbous, and range in size from 5-8 cm in diameter and 50 cm in length to 0.5 cm in diameter and 5-6 cm in length (Figure 3-22 A and B, Chapter 3.3.2). These mottles are demarcated by color and are usually much lighter than surrounding sediment, though darker mottles were observed as well. Many of these mottles contain perpendicular cracks. In thin section, the size of the grains does not change significantly from the mottles to the surrounding sediment, but the matrix-supported sandstone is heavily clay-enriched within the mottles (Figure B6, KRR-2, Appendix B).

Lithic (granitic) and quartzite clasts approximately 1 cm in length, rip-up siliceous nodules (0.3-2 cm in length), and small spherical (<0.5 cm) hematite nodules demarcated from the surrounding sand by dark bands are common within this facies association (Figure 3-9 B, for nodules and lithics). These clasts represent 5-10% of the total rock, while mottles are locally abundant; both are found aligned to cryptic, large (~0.3-0.8 m tall), gently north-dipping, tangential cross-beds (~10 cm thick).

FA VII A is gradationally overlain by FA VII B, and overlies Precambrian schist in an erosive, altered contact (Figure 3-9 A). This contact is

irregular, with interstratified red sandstone and siliceous, blue, altered beds with large, white veins.

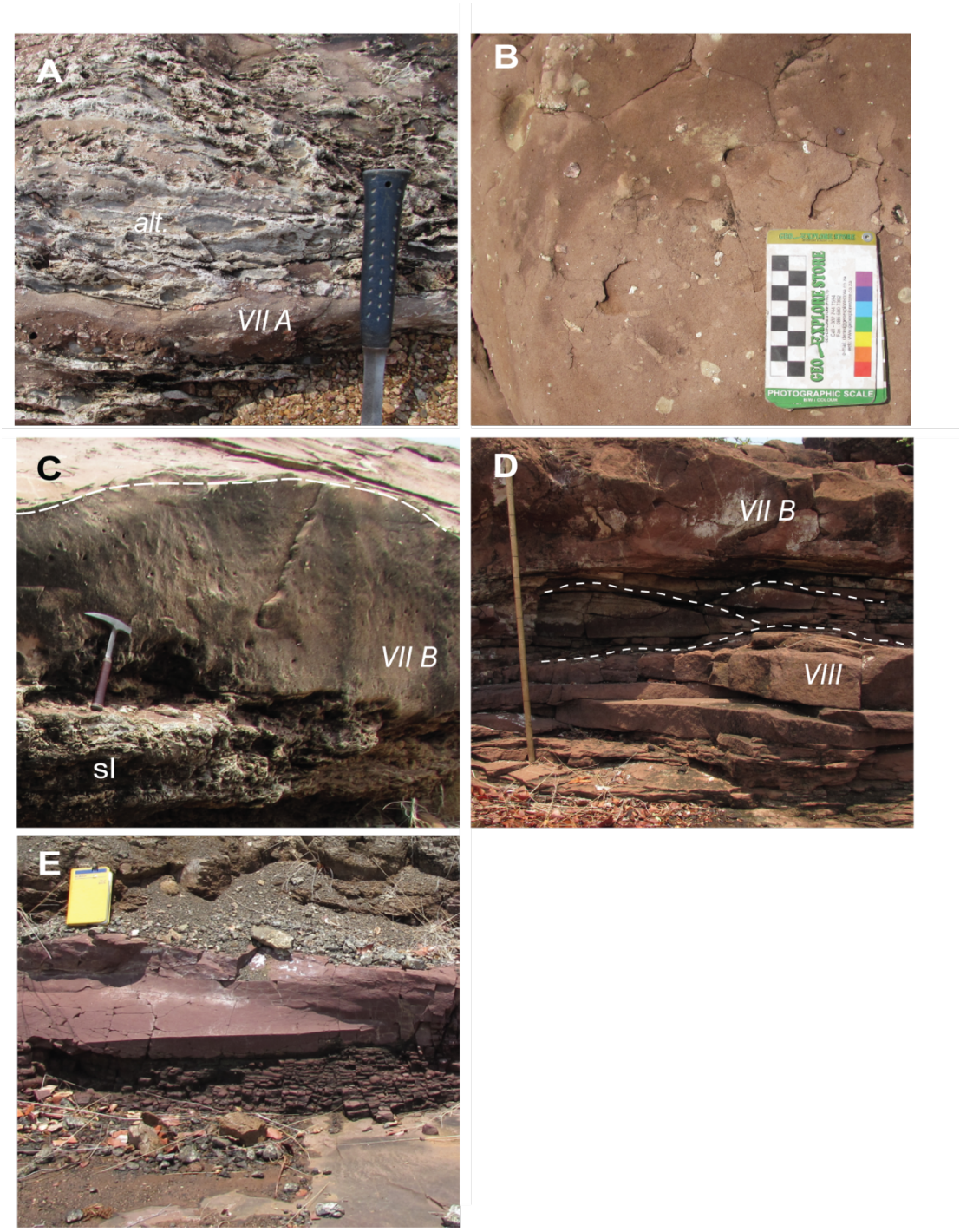

Figure 3-9: Facies Associations from the Red Rocks Locality. (A) The base of the outcrop consists of interstratified FA VII A and blue, siliceous layers with white veins; (B) FA VII A contains trace fossils and silicious nodules; (C) Dune form of VII A (dashed line indicates dune form top) overlying siliceous limestone (sl); (D) FA VII B contains fewer traces,

nodules and clasts, and here overlies discontinuous, wedges (outlined by dotted lines) of FA VIII. (E) FA IX consists of laminated silts overlain by massively bedded sandstone.

Interpretation

The small size and well-sorted grains indicate an aeolian origin. While much of the facies association is massively bedded, cryptic foresets delimited by aligned burrows or clasts reveal dune structures present in the outcrop. Invertebrate burrows in the lee side foresets of dunes have been documented in the Navajo Formation of the western United States (Ekdale et al., 2007), and are well-known from dune foresets in other inland erg settings (reviewed by Ekdale et al., 2007, see references therein). The pervasive bioturbation by these invertebrates could have destroyed other typical dune features (e.g. wind ripple deposits, cross bedding, grain fall lamination, sand flow lamination). FA VII A is interpreted as heavily bioturbated aeolian dune deposits.

The preservation of these burrows suggests fairly wet conditions were prevalent enough to prevent these structures from crumbling due to insufficient competence, and also to allow invertebrate life to thrive (Ekdale et al., 2007). Large communities of invertebrates, most likely arthropods, could survive by grazing on cyanobacteria or fungi as suggested by Friedmann and Galun (1974). However, the lack of evidence of macroscopic plants (e.g. rhizoliths) indicates these wet conditions were likely ephemeral, and not long-lasting enough to sustain vascular plants.

Facies Association VII B: FA VII B gradationally overlies FA VII A in the Elliot/Clarens Formation at the Red Rocks field locality, measures approximately 3.5 m thick and is laterally extensive, cropping out over a couple of kilometers. The red to brown (5R 6/6, 10R 6/6), fine-grained, well-rounded and well-sorted sandstone has less beige mottling than FA VII A, and is distinguished from FA VII A by containing approximately 50% fewer siliceous nodules and quartz clasts. Rare, angular granitic lithics approximately 4 cm in length and small (<0.5 cm) hematite nodules also

occur. The clasts in FA VII B, unlike those in FA VII A, are not aligned to sedimentary structures, and represent approximately 3% of the total outcrop.

Likewise, significantly fewer trace fossils are present than in FA VII A, and overall, these are smaller, sinuous, and more gracile than those in the underlying facies (Figure 3-22 F, Chapter 3.3.2). The majority of this facies is massively bedded, though rare, large dune forms are present, which measure ~0.5-1 m in height with wavelengths of ~2-3 m. A lenticular, 1 meter-thick, pervasively altered appearing, white-gray (N8, N9) silcrete or siliceous limestone layer occurs locally above the base of FAVII B (Figure 3-9 C). This siliceous limestone has undulating, uneven and irregular beds and has a crenulated appearance.

Interpretation

Like FA VII A, this facies is composed of fine-grained, well-rounded and well-sorted sandstone indicating an aeolian origin. In fact, FA VII B shares many similarities with FA VII A, with the exception of cryptic dune structures and well-preserved burrows. Rare dune forms suggest the presence of dunes despite a lack of bedding features, and together, these contrast with interdune deposits described by Loope and Row (2003) who describe vestiges of horizontal bedding from bioturbated interdunes.

FA VII B is interpreted as aeolian dune deposits which have been pervasively bioturbated but unlike FA VII A, do not preserve cryptic bedding structures, and rarely preserve trace fossils. The lack of burrows or tracks is likely related to moisture, which is integral to sand competency and preservation of delicate invertebrate traces (Ekdale et al., 2007). Alternately, or in addition to less moist conditions, increased bioturbation of the dunes could have destroyed burrows and cross-bedding during a hiatus or decrease in the rate of deposition. As dunes were buried more

slowly, invertebrates given more time to burrow would eventually erase any previous structures or sedimentary beds.

The silcrete layer, reported as a “siliceous limestone” by McCourt and Brandl (1980), may represent a spring deposit. Playa carbonates are known to occur in close proximity to bioturbated facies in aeolian settings (see Colson & Cojan, 1996; Smith & Mason, 1998). Alternatively, this could be a silicified calcrete, or silicified mud-rich playa deposit (Summerfield, 1983).

Facies Association VIII: FA VIII consists of approximately 1.8 meters of dark brown (5R 6/6), very fine-grained, well-sorted, well-rounded, sandstone arranged in stacked, thin (~15-50 cm thick), wedge-shaped bedforms without distinctive bedding structures (Figure 3-9 D). A thin section sample from this facies is classified as a lithic arenite, with little to no matrix (Figure b8, KRR-3, Appendix B). This facies association occurs in the Elliot/Clarens Formation at the Red Rocks field locality. Unlike laterally extensive FA VII A and B, FA VIII is an isolated, vaguely channel-shaped outcrop; measuring approximately 5-6 m sub-perpendicular to strike and 3 meters wide. FA VIII sharply contacts underlying massive beds of FA VII B, and has a sharp contact with overlying large dune forms (~1 m high) of FA VII B.

The discontinuous lenses and wedges typically wedge out westwards (205-285°) and share erosive contacts with each other. These bodies are stacked in wavy, irregular, lenticular packages. Very rarely, tangential cross-bedding is visible in some of the wedges.

Interpretation

The erosive nature of the internal contacts between the lenses and wedges indicates a high energy environment, while the fine-grained, well-sorted composition of the sand is identical to aeolian FA VII A and B.

While the well-sorted nature of the sand fits with interdunal fluvial systems as described by Langford (1989), Herries (1993), and Newell (2001), the prominent bedform development and lack of bedding structures is anomalous to other described aeolian fluvial deposits (see Langford & Chan, 1989; Scherer & Lavina, 2005). The bedforms' resemblance to fluvial dunes regardless of the lack of foreset development motivates the interpretation that FA VIII represents channel deposits of re-worked dune sand. Enigmatic structureless bedforms may be the result of insufficient clay content to preserve foresets. Clay poor sediments could be the result of winnowing by wind action, sources deficient in feldspar to facilitate clay formation, or extremely arid environments incompatible with soil development.

The erosive contacts of the dunes indicate fairly high energy flow conditions, which might have been generated by seasonal, westwards-flowing flash-flood events. The sharp contact between overlying dune deposits indicates the channel was suddenly choked off by migrating dunes after flow in the channel slowed or ceased.

Facies Association IX: FA IX consists of dark brown (5R 4/6) laminated silt (Fl) and massive sandstone (Sm) which crops out as a 0.5 m thick sheet (Figure 3-9 E). This facies association occurs in the Elliot/Clarens Formation at the Red Rocks field locality. The silty sandstone is generally finer-grained than the channel deposits of FA VIII; the lowermost 5 cm are silty, finely laminated and fine upwards to 35 cm of massively bedded sandstone. The contact between these units is planar and sharp. This facies association has a sharp contact with underlying dune deposits of FA VII B, and is truncated by overlying dolerite. This outcrop is laterally continuous with FA VIII as they both rest upon the continuous surface of FA VII B, but the contact between FA VIII and IX has been eroded.

Interpretation

The laminated basal bed is consistent with suspension deposition in quiet waters, while the massive upper bed likely represents deposition during flooding, likely during high energy flows which deposited sediment rapidly (Miall, 1996). Alternately, the massive bed may have been bioturbated as overbank interdunes are frequently associated with burrowing (Langford & Chan, 1989), though this seems unlikely as the underlying laminated unit shows no indications of being disturbed from activity in the overlying, massive layer.

FA IX is interpreted as overbank interdune deposits. These environments are known to form near channels (FA VIII) during flooding of the dune field. Channel incision into dunes re-works aeolian sediments, and interdune shales and sands are deposited in sheet-like or lenticular overbank deposits (Langford & Chan, 1989). The lack of evidence for plant life or bioturbation in the laminated unit could indicate that these deposits rapidly dried out after deposition, before invertebrate burrowing could commence (Miall, 1996). Limited bioturbation in the floodplain is consistent with semi-arid setting, where organic matter incorporated into the sediment is likely to be oxidized and not preserved (Reading, 1986).

This facies association is laterally equivalent to FA VIII which crops out approximately 2 meters away on top of the same FA VII B surface. This outcrop geometry suggests that the stacked fluvial dunes of FA VIII were restricted to a well-developed channel, as opposed to unchannelized sheet flows.

Facies Association X: FA X consists of fine-grained, well-sorted grey (10 YR 6/2, 5Y 7/2) sandstone in large, tangentially and planar cross-bedded, tabular cosets up to 2 m thick. This facies association occurs in the Clarens Formation at the Upper Makanya Hill field locality. Sets of high angle (>20°) cross-strata range from 5 to 20 cm thick, and share very low

angle (10°) contacts (Figure 3-10 A and B). Convolute bedding is also present in isolated beds; this can be wavy or folded bedding or large-scale fluid escape structures approximately 55 cm in height and 60-120 cm wide. These are tee-pee-shaped structures 20-80 cm in height, though recumbent folded convolutions are also observed (Figure 3-10 C and D). These units share planar, sharp boundaries with FA XI, with which they share an interfingering relationship.

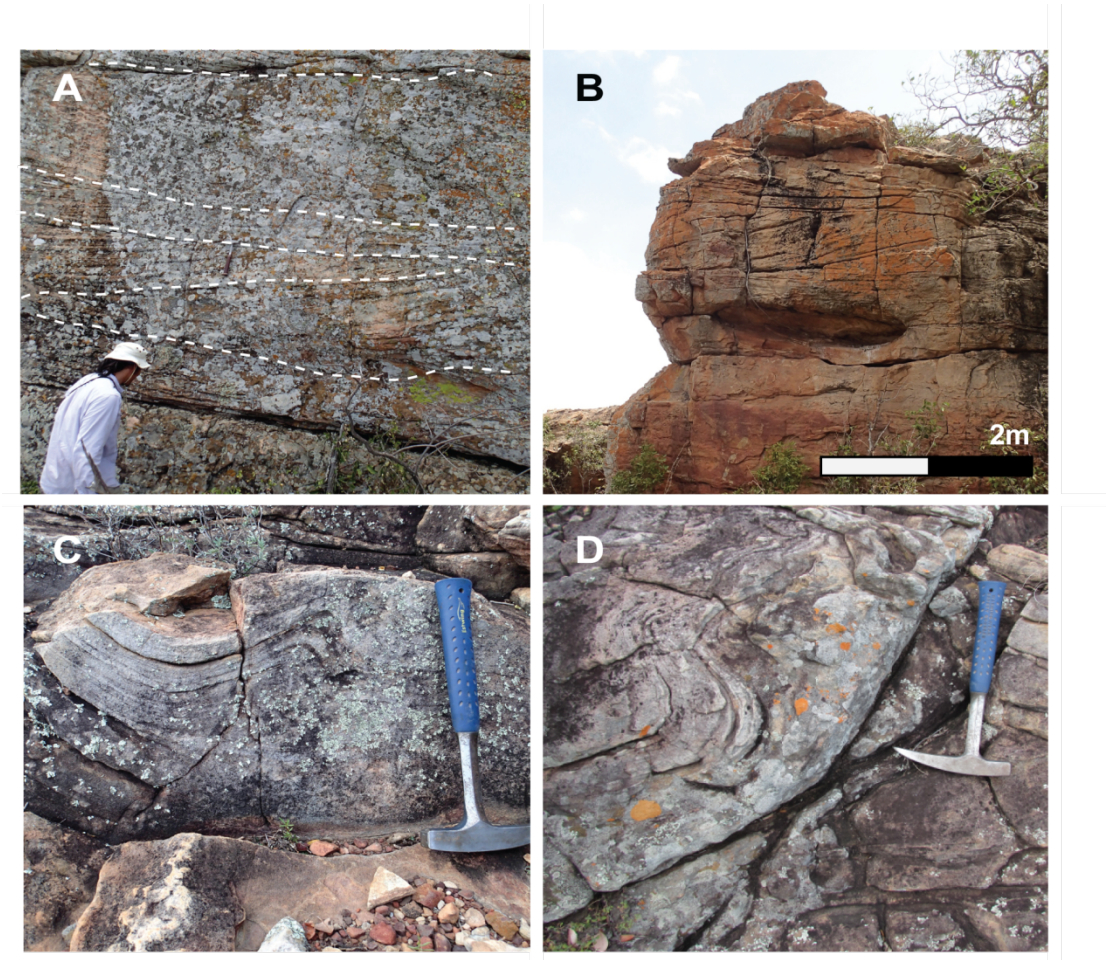

Figure 3-10: Facies Association X from the Upper Makanya Hill field locality. (A) Co-sets of tabular, trough cross-bedded sandstone, typical of dunes; (B) Large cross beds typically measure ~20 cm thick, while co-sets can reach 2 m thick; (C) Tee-pee shaped structures frequently occur; (D) Convoluted bedded is nearly vertically oriented.

Interpretation

Fine-grained sandstone bedded in large, high angle foresets is consistent with aeolian dunes. Planar, horizontal contacts between sets of beds dipping in the same direction represent 1st order bounding surfaces, while

inclined contacts between cosets represent 2nd order reactivation surfaces (Reading, 1986). The large-scale bedforms lack evidence of vegetation or animal life which could indicate dry conditions unable to sustain life or preserve trace fossils, in stark contrast to conditions at the Red Rocks locality. However, convoluted bedding and soft sediment deformation occurring in over-saturated sediments as suggested by Bordy (2008) would indicate periodic rises in the water table or flooding (see Strömbäck et al., 2005).
Surprisingly, these kinds of soft sediment deformation features do not occur in the interdune facies, which is in more continuous contact with rising and falling water tables than large-scale dunes. The large scale fluid escape structures are similar to sand volcanoes and other features described by Montenat et al. (2007) (Figure 3-10), and could originate from seismic activity.

Facies Association XI: FA XI is composed of grey (10 YR 6/2, 5Y 7/2), fine to medium-grained, well-sorted, massively bedded sandstone, in 5-40 cm thick, irregular, laterally extensive sandstone sheets (Figure 3-11 A) and interfingering tabular beds that are massively bedded, or planar laminated and heavily bioturbated. This facies association occurs in the Clarens Formation at the Upper Makanya Hill field locality. Massively bedded sheets have erosive, wavy, basal contacts, and are typically uniform, without observed grading, and these are sometimes isolated, but are frequently stacked in packages of 2-4 beds. Beds measure up to 0.5 m thick and are interbedded with FA X.

Planar, bioturbated layers are 10-30 cm thick, and have rare, silty lenses approximately 5 cm thick (Figure 3-11 B). These horizontally layered massive beds are frequently permeated by kidney-shaped to circular, vertical burrows (2-4 cm in diameter) that penetrate underlying strata up to 8 cm deep, identified as *Taenidium isp.*. Other traces in include elongate, low-sinuosity traces approximately 15-25 mm in width, some of which are

meniscate (*Planolites isp., Entradichnus isp)*; and small (1-5 cm in diameter) circular burrows that typically are paired (*Arenicolites isp.),*see Chapter 3.3.2 for trace fossil photos, identification and discussion.

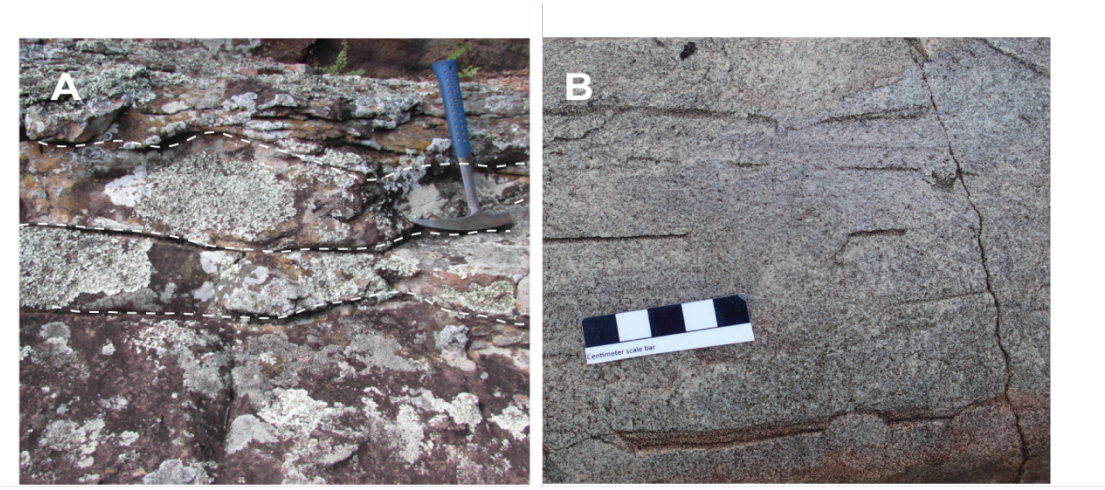

Figure 3-11: Facies Association XI from the Upper Makanya Hill field locality. (A) Irregular, planar beds of massive sandstone have erosive, wavy basal contacts; (B) Planar, laminated beds are interrupted by burrows.

Interpretation

Well-sorted, medium-grained sandstone is typical of aeolian environments, and vestiges of planar lamination are consistent with descriptions of flooded interdunes by Loope and Row (2003). FA XI is interpreted as flooded interdune deposits consisting of viscous flooding units and silty, bioturbated, marginal beds.

Numerous studies have found *Taenidium* in association with flooded desert systems (Smith et al., 1993; Smith & Mason, 1998; Melchor et al., 2012; Good & Ekdale, 2014). Abundant *Arenicolites isp., Planolites isp., Entradichnus isp., Skolithos isp.,* in addition to *Taenidium isp.* indicate presence of communal arthropods (Ekdale et al. 2007). This assemblage of ichnofossils is consistent with both *Scoyenia* and *Octopodichnus-Entradichus* ichnofacies, but differs from each in a paucity of arthropod trackways (Seilacher, 1964; Hung & Lucas, 2007), and is therefore consistent with freshwater lacustrine, fluvial and aeolian environments (Ekdale et al., 2007; Benton & Harper, 1997).

Massively bedded, fossil and ichnofossil-bearing strata have been interpreted as interdunal, non-carbonate lakes or standing bodies of water (Britt et al., 2016) in the Nugget Formation of western North America. However, the erosive bases and relative thinness of the sheets are more consistent with fairly viscous, sediment gravity flows (Miall, 1996). Sheets could have formed in response to (1) rain fall ponding in interdune areas; or (2) a rise in the groundwater table during long term climate change or temporary flooding from nearby fluvial sources (Ahlbrandt & Fryberger, 1981; Petit-Marie et al., 1980; Ward, 1988; Langford & Chan, 1989). Though bioturbation is a common cause of massive bedding, these sheets occur in close association with obviously bioturbated (and even burrow-bearing) strata, yet the contacts between these two lithofacies are undisturbed. Repetition of these sheets indicates that flooding conditions were fairly frequent.

3.1.2 Stratigraphy

Field Mapping

Outcrop at the lower Makanya Hill locality was found and described from the “Matsaringwe” dry wash, as the dense vegetation in the area obscures the majority of available outcrop (Figure 3-12 shows (A) original Council for Geoscience Messina 1:250,000 1981 geologic map and (B) suggested changes; letters A-T correspond to locations depicted in Figure 3-13 and mapped in Figure 3-14). Most of the formations mapped are consistent with formation descriptions observed in the field and described by McCourt and Brandl (1980) with a few exceptions explained below and mapped in Figure 3-12 B.

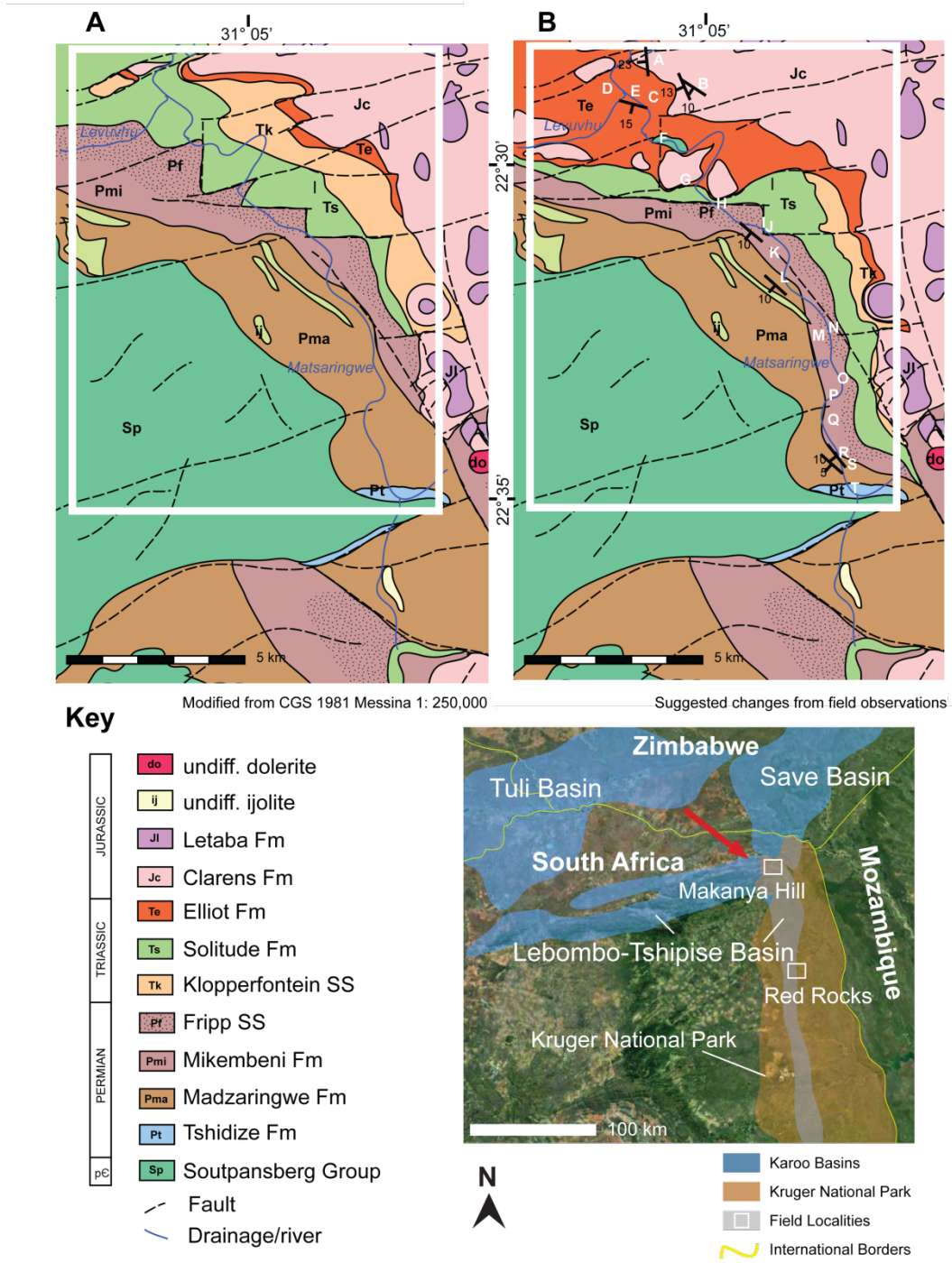

Figure 3-12: Geologic Map of the Makanya Hill field locality, indicated by red arrow on inset. (A) modified from the 1981 Council for Geoscience 1:250,000 map, (B) suggested changes based on field observations in the present study, see Figures 3-13 for outcrop photos corresponding to letters.

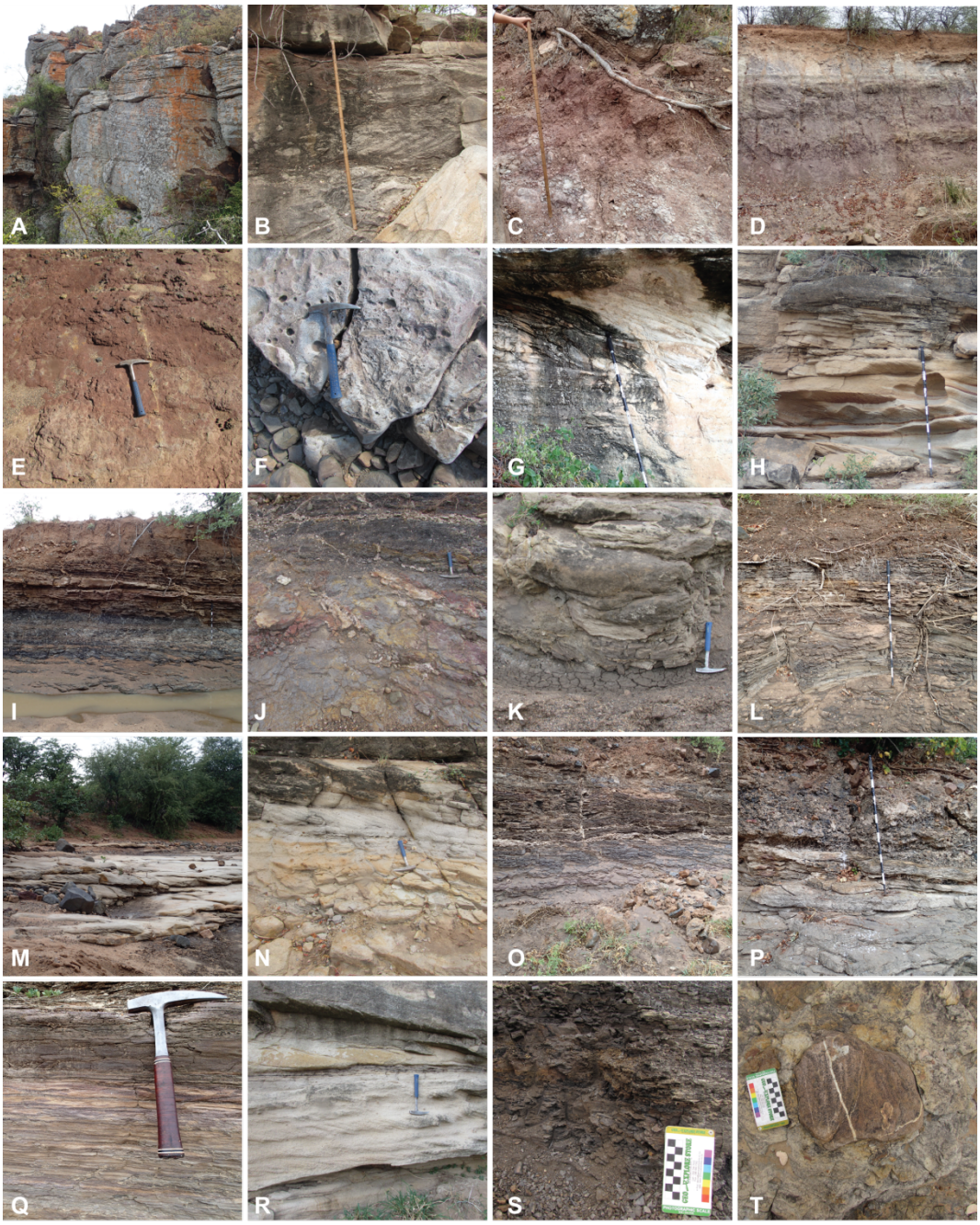

Figure 3-13: Photographs of outcrop mapped in Figures 3-12 B and 3-14. See 1.5 m scale, scale bar and geologic hammers for scale. (A) Aeolian sandstones from the Clarens Formation. (B) Coarse-grained fluvial sandstone from the base of the Clarens Formation (highlighted in orange in Figure 3-14). (C, D) P-C and P-A field sites, respectively, represent palaeosols from the Elliot Formation. (F) Crystalline basement rock. (G) Aeolian sandstones share same sedimentary features as sandstones in A, Clarens Formation. (H) Coarse-grained fluvial sandstones of the Fripp Sandstone. (I) Floodplain fines overlain by ripple cross-laminated crevasse splay sandstones in the Solitude Formation. (J) Multi-coloured mudstones of the Solitude Formation. (K) Coarse-grained sandstone bodies are rare in the Mikembeni Formation. (L) Interbedded horizontally laminated sandstones, siltstones and mudrocks of the Madzaringwe Formation. (M)

Coarse-grained sandstones in the Mikembeni Formation closely resemble the Fripp Sandstone (N), but are smaller in scale. (O, P, Q) Interbedded sandstones, siltstones and mudrocks from the Mikembeni Formation. (R) Another large (~10 meter tall) outcrop of the Fripp Formation. (S) Interbedded coal and mudrocks from the Madzaringwe Formation. (T) Diamictite from the Tshidize Formation.

A number of very resistant, large (~15 m), sandstone outcrops at R, O, N, and H (pictured in Figure 3-13-R,O,N, and H; mapped in Figures 3-12 B and 3-14), match the description of the Fripp Sandstone, instead of sandstone bodies from the Madzaringwe or Mikembeni Formations as mapped on the CGS Messina Map (Figure 3-12A). Figure 3-14 highlights the continuous, resistant outcrop on a satellite image which is thus identified as the Fripp Sandstone (Figure 3-12 B).

North of location H (pictured in Figure 3-13 and mapped in Figures 3-12 and 3-14), field observations more frequently contradict the identifications from the Messina Map (1981). The fine-grained, high angle cross-bedded, cliff-forming sandstone at G (Figure 3-13 G) and traces (*Arenicolites sp.*) observed there are typical of the Clarens Formation and do not resemble the largely crevasse-splay sandstones observed in the Solitude Formation from locations I and J.

Fine-grained mudrocks, siltstones and palaeosols (Figure 3-13 C, D, and E) are not necessarily out of place in the Solitude Formation, but the mudrocks lack characteristic mottling described from Solitude overbank deposits (McCourt and Brandl, 1980). *Ex situ* sauropodomorph fossils resemble Elliot taxa from the Main Karoo Basin (see Chapter 3.3.1 for fossil descriptions) indicate these locations do not represent the Solitude Formation as mapped (Figure 3-12 A) but the Elliot Formation (Figure 3-12 B).

Location B is mapped as Klopperfontein Sandstone (Figure 3-12 A), however, Brandl (2002) notes that the Klopperfontein Sandstone does not tend to form large, resistant outcrops. The sandstones and grits from

location B (Figure 3-13 B) is lithologically consistent with the basal conglomerate of the Clarens Formation described by McCourt & Brandl (1980), and appears to form a continuous bench in the area which is depicted in orange in Figure 3-14.

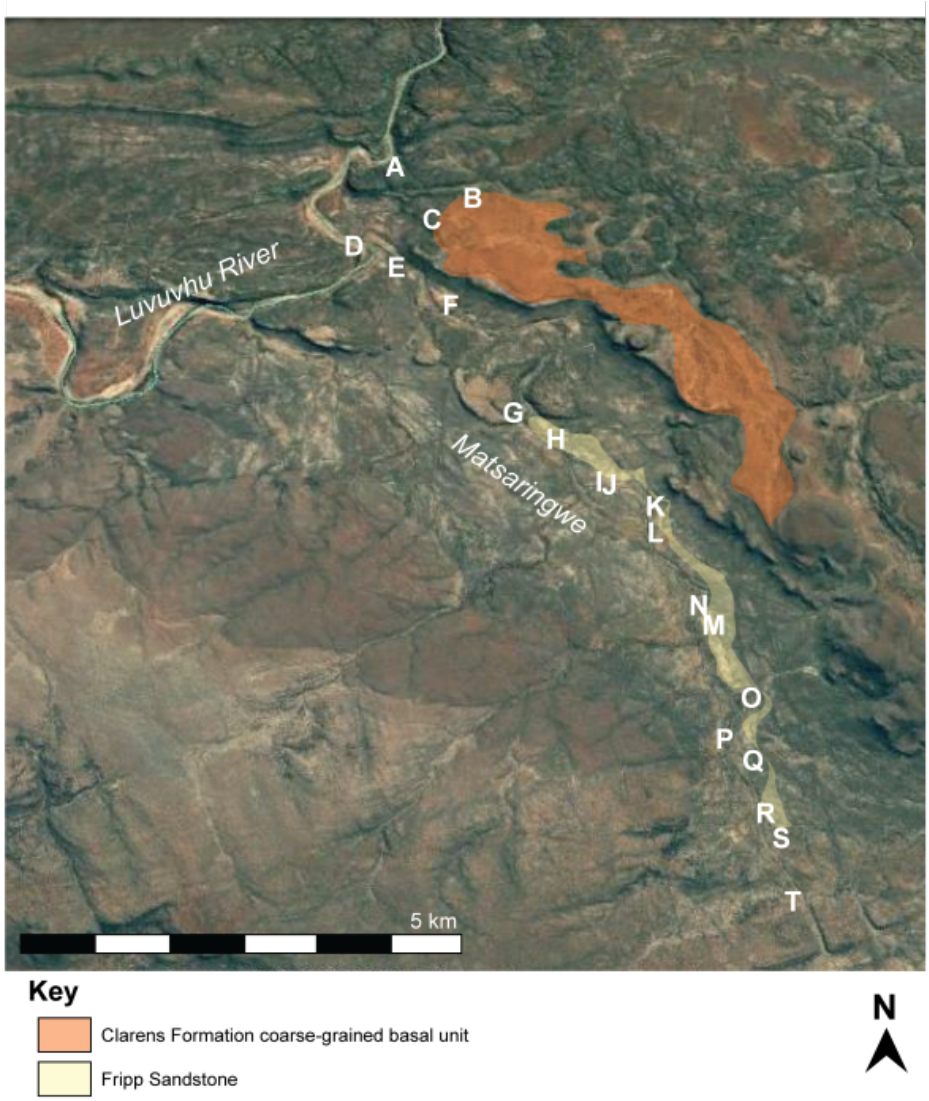

Figure 3-14: Makanya Hill satellite image with continuous, resistant sandstone outcrops identified in this study as the Fripp Sandstone (yellow) and basal, coarse-grained Clarens Formation (orange) highlighted. Letters correspond to pictures in Figure 3-13.

Due to heavy vegetation which obscured the majority of the outcrop, no formation contacts were observed but information from McCourt and Brandl (1980) and the Kruger National Park boreholes allow for a more

complete discussion of the stratigraphy and basin development of the Pafuri sub-basin (see following section and Chapter 4).

Kruger National Park Boreholes

The boreholes drilled in Kruger National Park to study the Pafuri sub-basin were divided by core loggers primarily into group designations (e.g. “Ecca Group”, “Beaufort Group”), and very occasionally into constituent formations. Using lithologic descriptions from the core logs, several formation identities are suggested in the borehole stratigraphic columns (which are designated with a “?” by the formation name or contact in borehole stratigraphic columns in Appendix A).

Though none of the formations in the Lebombo-Tshipise basin have been studied with radiometric dating methods, correlative work by Van Eeden et al. (1955) between the Karoo basins has historically placed the Tshidize as Carboniferous/Permian in age; the Madzaringwe, Mikembeni Formations, and Fripp Sandstone as “Ecca Group” and Permian in age; the Solitude as “Beaufort Group” and Triassic in age; and the Elliot and Clarens Formations, and Drakensberg Group (“Stormberg Group”) as Triassic-Jurassic in age. The Triassic-Jurassic boundary has long been placed within the Elliot Formation (Smith & Kitching, 1997; Bordy et al., 2004b). As the specific locations of the Carboniferous-Permian and Triassic-Jurassic boundaries are not known from the Lebombo-Tshipise Basin, the whole of the Tshidize and Elliot are allocated to the Permian and Triassic periods, respectively, in borehole, stratigraphic section and geologic map figures, to avoid confusion with suggested identification of formations (noted with a “?”).

Table 3-3: Summary of Kruger National Park Boreholes (drilled in 1979 by Council for Geosciences)

Name	Location	Latitude	Longitude	Start (m)	Finish (m)	Total height (m)
KNP 1	20 km N of Punda Milis	22° 30' 57"	31° 03' 35"	-	-	-
KNP 2	19 km NNE of PM	22° 32' 15"	31° 05' 56"	-	-	-
KNP 3	16.5 km NE of PM	22° 34' 41"	31° 07'26"	-	-	-
KNP 4	11 km NE of PM	22° 36' 50"	31° 05' 19"	18.00	286.70	268.70
KNP 5	11.5 km ESE of PM	22° 42' 18"	31° 07' 44"	-	-	-
KNP 6	14.5 km E of PM	22° 41' 31°"	31° 09' 33"	-	-	-
KNP 7	24.5 km ESE of PM	22° 48' 09"	31° 11' 22"	6.00	176.19	170.19
KNP 8	18 km ENE of PM	22° 36' 51"	31° 10' 11"	7.17	425.51	418.34
KNP 9	15.5 km NE of PM	22° 36' 16"	31° 03' 07"	22.91	152.68	129.77
KNP 10	19 km ESE of PM	22° 43' 01"	31° 12' 05"	10.15	652.36	642.21
KNP 11	10.5km ESE of PM	22° 43'18"	31° 06'53"	13.94	167.42	153.48
KNP 12	26 km ESE of PM	22° 43'00"	31° 14' 26"	25.55	466.92	441.37
KNP 12A	26 km ESE of PM	22° 43'00"	31° 14' 26"	432.00	646.56	214.56
KNP 13	22 km NE of PM	22° 33' 47"	31° 11' 06"	7.85	578.09	570.24
KNP 14	36 km SSE of PM	22° 52' 50"	31° 12' 37"	21.94	425.34	403.4
KNP 15	26 km NE of PM	22° 31' 03"	31° 11' 19"	6.45	773.65	767.2
KNP 15	"Wedge"	22° 31' 03"	31° 11' 19"	459.70	750.78	291.08
KNP 16	16 km NNE of PM	22° 32' 39"	31° 05' 42"	7.65	145.46	137.81
KNP 17	17.5 km NE of PM	22° 33' 40"	31° 06'48"	6.10	202.03	195.93
KNP 18	14 km NE of PM	22° 33' 40"	31° 07' 49"	6.40	55.29	48.89
KNP 19	10.5 km NE of Punda	22° 36' 58"	31° 05' 00"	7.80	218.80	211.00
KNP 20	10.25 km NE of PM	22° 38' 23"	31° 06' 00"	9.12	212.61	203.49
KNP 21	10.6 km ENE of PM	22° 39' 29"	31° 07' 18"	15.90	162.36	146.46
KNP 22	18.75 km ENE of PM	22° 38' 52"	31° 11' 41"	21.91	1200.07	1178.16
KNP 23	13.6 km SW of Shingwedzi	23° 10' 44"	31° 19' 37"	41.00	167.32	126.32

*Grey backfill indicates boreholes east of 31° 10'

The trends and thicknesses of the Pafuri sub-basin's fill are summarized here.

The Pafuri sub-basin boreholes drilled in Kruger National Park have an average depth of 311.63 m. Boreholes to the east of 31° 10' contain the most complete sequences of the Karoo Supergroup sediments, and are significantly thicker (mean = 430.64 m) than the western boreholes (mean = 149.55 m). Western boreholes do not preserve the Fripp Sandstone or subsequent formations. Though the eastern boreholes are more stratigraphically representative, most lack at least one formation. The only exception appears to be KNP 15 (767.20 m); however, the Klopperfontein Sandstone was not marked in the core log and the candidate sandstone has been identified based on lithological similarity to the formation in McCourt and Brandl (1980).

The southernmost boreholes, KNP 23 (167.32 m) and KNP 14 (425.34 m) are among the shortest from the east and lack the lower Karoo sequence (Dwyka, Ecca and Beaufort Groups); these boreholes consist mostly of Letaba basalt over a thin succession of upper Karoo sandstones which rest on crystalline basement rock. These were identified as "Red Beds" in the core logs, and are described as "baked" with pervasive, large calcite veins. Based on proximity to the Red Rocks locality (which crops out less than 5 km to the west), assigning these rocks to the Clarens Formation is reasonable. The location of KNP 14 may have been recorded in error or the area mapped in insufficient detail as this borehole is located, according to the 1981 Messina area map, in the Palaeoproterozoic Soutpansberg Group.

Palaeoproterozic Basement

Less than half the studied boreholes (n = 8) intersect the Precambrian basement: the western boreholes KNP 4, 9, 11, and 18, and the boreholes at the western, eastern and southern margins of the eastern borehole

group, KNP 8, 12A, 14, and 23. These are among the shortest of the eastern boreholes.

Tshidize Formation

Ten boreholes intersect the Tshidize Formation, 3 of which also intersect the Precambrian basement; KNP 12 in the east and KNP 9 and 18 in the west. The Tshidize Formation is present in nearly all the western boreholes (7 of the 9), while it is more sporadic in the eastern boreholes (3 of 7). The formation varies in thickness from ~5-20 m in the west, while the formation is consistently ~10 m thick in the eastern boreholes (KNP 7, 12A and 22).

Core logs of the western boreholes KNP 16, 17, 18, 19, 20, and 21 described Madzaringwe rocks overlying “tillite” or pebbly conglomerate. These strata were often identified as “Pre-Karoo” or “transition beds.” However, lithological descriptions from the core logs match the Tshidize Formation and contrast with crystallized basement rock described from KNP 4, 9, 11, and 18.

In the east, the Tshidize Formation appears to be preferentially preserved in the more central boreholes (KNP 7, 12A, and 22). The northernmost boreholes KNP 13 and 15, and central KNP 10 are some of the deepest boreholes (579.09 m, 773.65 m, and 652.07 m, respectively), but none reach the Tshidize Formation or Precambrian basement.

Madzaringwe Formation

All of the Kruger National Park boreholes intersect the Madzaringwe Formation which ranges from 40 to 180 m thick. In boreholes containing bracketing formations (overlying Mikembeni and underlying Tshidize or Precambrian basement) the Madzaringwe Formation consistently measures ~150-170 m thick.

In western boreholes, the Madzaringwe consistently overlies the Tshidize Formation except in KNP 4 and 11 where it overlies Precambrian basement. In the eastern boreholes the Madzaringwe only overlies the basement in KNP 8, and overlies the Tshidize Formation in KNP 22, 12, and 7 (towards the southern end of the cluster). Underlying sediments were not drilled into in KNP 15, 13, and 10 in the north of the western borehole cluster.

The Madzaringwe Formation has the most consistent thickness of the Karoo Supergroup in the western boreholes, ranging only ~40 m (~110 in KNP 21 and ~150 in KNP 19). The only exception is KNP 18 which only contains roughly 40 m of this formation. The core log did not identify any formations in this short borehole (218.80 m), nor markers of the Madzaringwe Formation (Carbonaceous Horizon, Main Seam, or Middle Marker), but 5 m of Precambrian basement, 15 m of Tshidize and 40 m of the Madzaringwe Formation appear to be present based on lithological descriptions.

In the eastern boreholes the formation is thickest in the centre of the borehole cluster (ranging from ~150 m in KNP 8 and 13, to ~180 m in KNP 22), while the northern and southern-most boreholes measure only ~80 m. This thinning trend is probably genuine southwards; the southernmost borehole (KNP 7) reaches the underlying Tshidize Formation, but the northernmost borehole (KNP 15) does not extend to underlying formations or crystalline basement, so the total thickness of the Madzaringwe Formation there is unknown. The easternmost boreholes (KNP 4, 17, 18, and 21) have fewer sand bodies which tend to be thinner when present, than western sequences. Generally, more sandy bodies are present in the northern boreholes than the southern, while central boreholes have many intrusive bodies that obscure the relative amounts of sandy and muddy lithologies.

Mikembeni Formation

The Mikembeni Formation varies in thickness more than the Madzaringwe, measuring ~210 m (maximum, KNP 22 and KNP 15 “Wedge”) to ~15 m (minimum, KNP 7) in the eastern boreholes, and ~110 m (maximum, KNP 21) to 20 m (KNP 17) in the western boreholes.

In the east the central portion of the basin has the thickest deposits of Mikembeni sediments, reaching 200 m KNP 22. Towards the north, the Mikembeni thickens from ~110 m (KNP 8) to 130 m (KNP 15). The southern boreholes contain progressively more truncated sequences from ~100 m (KNP 10) to ~15 m (KNP 7) before disappearing completely in the southernmost boreholes (KNP 14 and 23). This drastic shortening and the heavily weathered top of the Mikembeni observed in KNP 12A indicates erosion affecting the southern portion of the basin sometime after Permian deposition.

In the western boreholes, the thickness of the Mikembeni is less variable, measuring ~20 (KNP 17) to 110 m (KNP 4). The Mikembeni Formation is not present in the western (KNP 9, 16), northern (KNP 18) and southern (KNP 11) peripheral boreholes. These are all some of the shortest boreholes (<155 m), yet all (excluding KNP 11) preserve thick sequences of the Tshidize Formation (~20 m).

Fripp Sandstone

The western boreholes only contain Permian and older sediments, so discussion of the Fripp, Solitude, Klopperfontein, Elliot and Clarens Formations will refer only to the eastern boreholes.

The most complete Triassic sequence is represented in the northernmost borehole KNP 15, which has nearly 200 m of Triassic strata. While core loggers did not identify the Fripp or Klopperfontein outright in this borehole, the thick bodies of white, gray and purplish sandstone

bracketing green, red and gray mudrocks are good candidates for these formations. In fact, the Klopperfontein is only positively identified by core loggers in KNP 12A, which contains only ~35 m of Triassic sediment.

The Fripp was identified by core loggers in KNP 12A, 15, and 22; however, in KNP 12A the Fripp is tentatively identified as a 2 meter interval of coarse-grained sandstone and siltstone with mudrock lenses and siderite nodules. This is lithologically consistent with intervals of the Solitude Formation and it has been identified thusly on the stratigraphic column (see Appendix A, Figure 9).

The formation is thickest (~50 m) in KNP 22, and coarse-grained candidate sandstones are present in numerous, northern boreholes (KNP 8, 10, 13, and 15). Southern boreholes lack the Fripp Formation, or good candidate sandstone bodies identifiable as the Fripp. This fits with McCourt and Brandl's (1980) account of the Fripp thickening to the north. The Fripp may pinch out to the south or could have been removed prior to deposition of overlying Triassic strata.

Solitude Formation

The Solitude Formation was only identified by core loggers in KNP 12A, but candidate sequences appear as part of the "Beaufort series" identified in KNP 7, 10, 15 and 22. Minor silts and muds (less than 5 m thick) between the two thick, coarse-grained sandstone bodies (likely the Fripp and Klopperfontein Formations) in KNP 13 might also represent the Solitude Formation.

The Solitude is represented by ~50 m of strata in KNP 15 and KNP 22 and generally thins to the south and east to less than 15 m (KNP 7 and 12A), and is absent in boreholes further south. This trend matches the reduction of the Solitude in Kruger Park from 85 m in the north to 10 in the south reported by McCourt and Brandl (1980), and a decrease from 120 m to 60

m to the west in the northern arm of the Lebombo-Tshipise Basin (Brandl, 2002).

Klopperfontein Sandstone

This coarse-grained, felspathic sandstone unit was only identified in KNP 12A, however, this 20 m of sediments was likely misidentified by core loggers. The reddish-brown conglomerate bracketed by fine-grained sandstone more closely resembles conglomerate present at the base of the Red Rocks Member of the Clarens Formation found in “some boreholes” (McCourt & Brandl, 1980; see Elliot and Clarens Formations in this chapter for more description).

However, other boreholes including KNP 7, 8, 10, 13, and 15 have candidate sandstone bodies that could represent the Klopperfontein Sandstone. Surprisingly, no candidate sandstone is present in the deepest borehole, KNP 22 (1178.16 m). The formation reaches a maximum of ~40 m (KNP 13 and 15) and thins to the southwest to a minimum of ~15-20 (KNP 7 and 10).

McCourt and Brandl (1980) note the formation is ~20 m in the Kruger National Park and that it thins to ~10 m east of Tshipise, where it is described as coarse-grained and gritty with “abundant” pink feldspar. Brandl (2002) notes that in the “extreme west” the formation is very thin or absent.

Elliot and Clarens Formations

Previous workers have neglected to describe the contact between the Elliot Formation and the underlying Klopperfontein. In places where the Klopperfontein is missing, Brandl (2002) describes the contact between the Elliot and Solitude as “arbitrary,” which implies a gradual contact.

The overlying Red Rocks member of the Clarens Formation share a gradational contact with the Elliot Formation (Brandl, 2002), and core loggers did not differentiate the Elliot Formation from the Red Rocks Member, but referred to the red sandstones, siltstones, and mudrocks below the “Cave Sandstone” (Tshipise Member of the Clarens) together as “Red Beds.” This move presaged Bordy and Eriksson’s (2015) recommendation to subsume the Red Rocks Member into the Elliot Formation.

The Elliot Formation is typically composed of siltstones and mudrocks and is described as poorly developed in Kruger Park, but reaches maximum thickness of 150 m near the town of Tshipise in the central Tshipise sub-basin of the Lebombo-Tshipise Basin (McCourt & Brandl, 1980). The Red Rocks Member of the Clarens Formation consists of red, argillaceous sandstones with irregular patches of beige or cream sandstone identical to the overlying Tshipise Member (McCourt and Brandl, 1980). The Red Rocks Member disappears east of Tshipise according to McCourt and Brandl (1980), though this likely strictly refers to the Tshipise sub-basin, as the type locality of this member crops out 100 km southeast of Tshipise at the Red Rocks locality field area in the Pafuri sub-basin. These authors also note that in “some boreholes,” the Red Rocks Member is represented by conglomerate units.

South-eastern boreholes KNP 7, 12, and 12A contain pebble conglomerates at the base of the Clarens Formation instead of typical Elliot or Red Rocks Member deposits. The compositions of these conglomerates vary slightly; in the Makanya Hill field area the conglomerate is primarily composed of quartzite pebbles, while KNP 12 and 12A’s units have angular quartzite, arenaceous sandstone, and Soutpansberg quartzite clasts. The conglomerate in KNP 7 is composed of quartzite, calcareous concretions and occasional mudrock rip-ups, and the

succession has numerous sharp, “downcutting” contacts which evoke channel lags deposited in high energy fluvial successions.

The northern boreholes KNP 8, 10, and 15 preserve 20-60 m of the typical Elliot/Red Rocks sequence of mudrocks capped with fine-grained sandstones. In the north (KNP 13), east (KNP 12A), and southernmost boreholes (KNP 14 and 23) the red beds are not represented by mudstones but only 5-20 m of red sandstones. The nearby Red Rocks field locality likewise preserves ~15 m of fine-grained sandstone and minor siltstones directly overlying Precambrian basement.

Beige or cream-colored “Cave Sandstone” deposits (the Tshipise Member of the Clarens Formation) sharply overlies the Red Rocks Member in all the eastern boreholes except for KNP 22 where it overlies “Beaufort” multicolored mudrocks, siltstones and grits. The Tshipise Member is thickest near the central portion of the eastern boreholes, reaching a maximum of ~130 m (KNP 22) and approximately 100 m less than 10 km to the south (KNP 10). These sediments are thicker in the western periphery of the eastern boreholes, measuring between 30 and 60 m (KNP 7 and 8, respectively), while the thinnest sequences <10-20 m occur at the eastern margin (KNP 12 and 12A respectively). To the north, the formation thins drastically to 40 m (KNP 13), but doubles to ~80 m (KNP 15) at the northern margin, and measures some 70-100 m at Makanya Hill field locality. The Tshipise Member disappears completely in the southernmost boreholes (KNP 14 and 23).

The Elliot and Clarens together are thickest in the north and central portions, especially if the coarse-grained lithology currently marked as “Solitude?” in KNP 22 instead represents the basal conglomerate of the Clarens Formation. These formations thin towards the south and east of the basin; reduced to nearly a tenth (10-20 m thick in KNP 7, 12, 14, and 23) of the maximum ~180 m (KNP 10).

3.2 Clay Composition and Quantitative Palaeoenvironmental Reconstruction of the Elliot Formation

The majority of methods used to quantitatively reconstruct paleoenvironment are preferentially performed on palaeosol samples, as authigenic clay formed in this environment most accurately records environmental signatures such as temperature and precipitation (see Sheldon and Tabor, 2009 for nuanced explanations of various methods, techniques and calculations). As palaeosols were only found and sampled in the Elliot Formation of the upper Makanya Hill area, quantitative palaeoenvironmental reconstruction was only undertaken for the Elliot Formation.

3.2.1 X-Ray Diffraction (XRD) and Scanning Electron Microscopy (SEM)

XRD

X-Ray Diffraction (XRD) analyses were performed on seven palaeosol samples from the Lebombo-Tshipise Basin and one from the Main Karoo Basin. Whole rock compositions of these samples indicate lithological similarity of the palaeosols/mudrocks in both basins; this data is summarized in Table 3-4. For individual sample XRD spectra and SEM images with associated Energy Dispersive Spectra (EDS) results, see Appendix C. The pattern for albite is preferred to anorthite or other Ca-Na intermediate feldspars in terms of fit to sample spectra, but represents all plagioclase present in the samples. Illite/Smectite + Mica in Table 3-4 corresponds to the combined XRD patterns of the 2M form of muscovite and illite which represents interlayered illite and smectite, as these minerals often occur together. Additional analyses of separate clay fractions from these samples using glycol solvation (Moore & Reynolds, 1997) would be required to quantify the amount of interlayered smectite present in the illite structure. Though the high temperature stable

polymorph of muscovite (2M) is unlikely to actually be present in these samples, the pattern provided a better fit to the data, and is employed to represent all forms of mica.

Table 3-4: XRD Major (M), minor (m), and trace (t) summary of whole rock palaeosol and mudrock samples

SAMPLE LOCATION	SAMPLE ID	QUARTZ	K-FELDSPAR	PLAGIOCLASE	CALCITE	ANKERITE/ FE-DOLOMITE	PYRITE	BARITE	MAGHEMITE	HEMATITE	GOETHITE	ANATASE	**CLAY SPECIES**	ILLITE/SMECTITE +MICA	KAOLINITE	CHLORITE
Upper Makanya Hill: P-A	KDS-1	M	t	m			t		t	t		t		M	m	t
	KDS-2	M	m	m						t	t			M	m	t
	KDS-3B	M	t	M		t		t	t	t				t	m	m
	KDS-4	M	t	m					t	t	t			M	m	t
	KDS-5	M	t	m						t	t	t		M	m	t
Upper Makanya Hill: P-B	KDS-6	M	t	M						t				M		t
Upper Makanya Hill: P-C	KDS-7	M	t	m	t			t				t		M	m	
Upper Makanya Hill	KDS-10	M	t	M	t			t	t	t				m	t	m
Blikana Field Area	BPS-1	M	m	M	t					t				M	M	

All samples have major quartz peaks and major/minor amounts of feldspar; more plagioclase appears to be present than potassium feldspar in all the samples. As expected, the palaeosol samples are enriched in clay, and have major/minor peaks for illite/smectite and mica, and minor/trace peaks for kaolinite and chlorite. All samples except KDS-7 have trace amounts of iron oxides including maghemite, hematite, and goethite, while only one sample (KDS-1) has small peaks consistent with pyrite. A few samples additionally have trace amounts of barite, calcite and the titanium oxide anatase. Ankerite (iron-dolomite) is present in trace amounts in KDS-3B.

Samples from P-A (KDS-1 – KDS-5) were collected in stratigraphic order from the outcrop base to the top. KDS-3B was collected from a horizon in the palaeosol directly adjacent to a small dyke, and has compositional differences from other samples in the palaeosol including an enrichment in plagioclase, reduction in clay species, and the presence of ankerite/iron-dolomite and barite, which are not present in other samples from P-A. These differences suggest diagenic alteration of this horizon, whereby illite/smectite clay common in the other palaeosol samples has been altered to kaolinite/chlorite. KDS-10 is the only other sample lacking in clay; less weathering and clay genesis is expected to have occurred in a mudrock sample compared to palaeosol samples.

BPS-1 is more enriched in feldspar than the other samples, indicating that massive weathering massive weathering (i.e. chemical weathering dominating physical weathering *sensu* Pédro in Paquet & Clauer, 1997) was likely not occurring in the Main Karoo Basin, or at least not the extent present in the Lebombo-Tshipise samples.

SEM

Minerals most commonly identified by Scanning Electron Microscopy (SEM) analyses of seven Lebombo-Tshipise Basin and one Main Karoo Basin palaeosol samples include mixed layer illite/smectite, quartz, mica, potassium and sodium feldspars, chlorite, and iron oxides. Many spectra include unidentified peaks near 2 and 10 keV; these are palladium and gold peaks contributed by sample coatings.

Micas and clays are especially vulnerable to cation substitutions, impurities and highly variable structures, largely due to the high surface area to volume ratio of the phyllosilicate crystal structure and the electrically active nature of these surfaces (Velde, 1995). It is unsurprising, then, that none of the micas in the SEM samples produced EDS results that exactly match those of the mica end-members biotite and muscovite,

but the closer match is indicated in parentheses after the identification of mica (e.g. mica (biotite) in Appendix C).

No reference EDS spectrum for mixed layer illite/smectite is provided in the literature, though mixed layer illite and smectite is common in nature, forming in a variety of environments through weathering, burial diagenesis, and hydrothermal alteration (Weaver, 1958; Velde, 1995; Kahle et al., 2002). Complex spectra with subequal aluminum and silicon peaks and relevant associated peaks (K, Na, Mg, and Fe) are interpreted as mixed-layer illite and smectite. Calcium and titanium, and sulfur and chlorine are typical cation and anion substitutions in smectite, so spectra including these peaks are also identified as illite/smectite clay. These spectra closely resemble the spectrum of stilpnomelane, but this mineral is typical of metamorphic and igneous rocks and therefore unlikely to be present in palaeosol samples.

The maximum magnification (>20 μm) was often inadequate to capture exceedingly small and delicate, singular iron oxides. There are no spectra of solitary iron/titanium oxides, though the pervasive presence of iron and titanium peaks throughout the analyses strongly indicate these are present in abundance, especially as thin crusts.

In contrast to the XRD results, potassium feldspar was encountered more frequently than plagioclase during SEM analyses. The dominant clay identified by EDS is authigenic mixed layer illite and smectite, though some morphologies indicate detrital clay is also present (e.g. rounded grains). The most common morphologies are flakes and lathes, often formed as pore linings or grain coatings, and non-aligned pore fillings typical of authigenic clays (Wilson & Pittman, 1977). Copper replacement in the octahedral sheets of smectite is the likely source for large copper peaks in KDS-3B (Mosser et al., 1990). Chlorite was detected in most

samples, while kaolinite was tentatively identified only in KDS-3B. Chlorite in the samples is almost entirely authigenic flakes and laths.

SEM images of BPS-1 are visibly less clay-rich than other samples and are primarily composed of blocky quartz and mica grains with clay flakes filling instead of lining pores. The grains on average are larger than the other samples and less covered in iron and clay coverings.

Mineral EDS spectra from “Electron Microprobe Analysis and Scanning Electron Microscopy in Geology” S.J.B. Reed (2005) are provided in Appendix C for comparisons to the subsequent sample analyses.

3.2.2 X-Ray Fluorescence (XRF) and Chemical Indices of Alteration (CIA)

The major element geochemistry for nine palaeosol samples and one mudrock sample from the Lebombo-Tshipise Basin, and one palaeosol sample from the Main Karoo Basin are presented in Table 3-5 and trace element geochemistry and loss on ignition results are presented in Table 3-6.

Table 3-5. XRF Major Elements and CIA values

Location	Sample ID	SiO_2	Al_2O_3	Fe_2O_3	FeO	MnO	MgO	CaO	Na_2O	K_2O	TiO_2	P_2O_5	Cr_2O	NiO	LOI	Total	CIA	CIA (m)
Palaeosol A	KDS-1	73.27	12.35	0.46	3.73	0.01	0.78	0.10	0.86	1.86	0.72	0.02	0.01	0.00	5.75	99.91	76.92	2.82
	KDS-2	65.15	16.11	0.58	4.65	0.01	1.04	0.08	0.84	2.30	0.79	0.03	0.01	0.01	8.54	100.14	79.11	3.23
	KDS-3A	84.51	6.05	0.24	1.94	0.07	0.59	0.94	0.70	1.38	0.48	0.12	0.02	0.00	2.80	99.85	60.31	1.36
	KDS-3B	84.30	5.76	0.25	2.04	0.07	0.54	0.94	0.57	1.35	0.48	0.10	0.02	0.00	3.19	99.61	60.35	1.36
	KDS-4	68.27	14.76	0.54	4.34	0.01	1.03	0.07	1.04	1.93	0.71	0.02	0.02	0.00	7.31	100.04	78.77	3.18
	KDS-5	84.65	4.10	0.23	1.79	0.04	0.27	0.50	0.23	0.98	0.51	0.08	0.01	0.00	6.13	99.52	64.26	1.49
Palaeosol B	KDS-6	87.08	3.61	0.19	1.51	0.15	0.12	0.16	0.13	0.99	0.59	0.08	0.02	0.00	5.11	99.73	67.75	1.59
Palaeosol C	KDS-7	84.92	3.38	0.18	1.49	0.04	0.08	0.10	0.13	0.97	0.58	0.06	0.02	0.00	8.23	100.17	67.72	1.57
Makanya Hill	KDS-10	88.52	3.99	0.17	1.42	0.03	0.10	0.11	0.16	1.10	0.50	0.06	0.02	0.00	4.31	100.48	68.47	1.73
Blikana Field Site	BPS-1	90.14	2.58	0.09	0.71	0.00	0.04	0.05	0.06	0.88	0.22	0.02	0.01	0.00	4.83	99.62	65.87	1.67

Major Elements are presented as a weight percentage of the total sample weight

Table 3-6. Trace Elements and Loss on Ignition values

Sample ID	Sc	V	Cr	Co	Ni	Cu	Zn	Ga	Rb	Sr	Y	Zr	Nb	Mo	Ba	Pb	Th	U	LOI
KDS-1	10.44	52.14	45.11	11.45	26.61	16.82	56.05	15.83	115.27	46.45	21.47	416.24	16.94	1.41	258.32	20.24	17.82	d.l.	5.61
KDS-2	12.24	99.68	47.43	10.33	30.79	24.14	57.40	22.53	134.75	52.45	21.44	297.34	19.27	1.38	275.45	36.42	10.15	d.l.	8.83
KDS-3A	5.49	26.62	37.90	18.49	12.17	25.26	42.94	7.39	31.52	58.25	17.67	466.91	9.63	0.63	224.46	13.34	6.39	d.l.	3.03
KDS-3B	8.14	37.13	37.36	19.03	18.90	18.66	63.66	7.99	37.55	71.38	19.40	550.54	11.40	1.14	333.88	15.92	7.82	d.l.	3.30
KDS-4	11.04	68.16	43.00	3.57	26.66	17.12	42.32	17.22	106.40	44.66	20.71	292.62	16.73	1.80	263.01	22.63	9.48	d.l.	7.51
KDS-5	9.97	72.47	55.10	14.42	22.17	22.02	32.78	15.54	101.76	72.34	23.65	388.69	16.89	1.15	254.07	17.05	15.60	2.51	6.09
KDS-6	7.89	54.49	70.54	2.38	29.73	19.69	33.43	14.22	131.74	55.55	27.09	328.15	14.97	0.27	424.62	29.57	12.59	2.25	5.11
KDS-7	7.95	100.04	81.03	3.92	69.34	16.24	22.38	13.16	62.84	64.97	20.05	425.26	10.79	d.l.	1026.18	20.37	8.77	0.94	8.21
KDS-10	10.84	54.87	68.23	16.41	28.74	24.40	32.65	9.38	41.97	75.42	27.66	637.37	12.45	0.52	622.33	13.27	10.39	d.l.	3.96
BPS-1	9.66	47.51	42.79	7.82	16.15	22.97	49.66	14.53	119.46	158.80	22.39	281.02	12.34	0.80	594.52	25.61	12.14	1.94	4.83

LOI is measured in grams and Trace elements are measured in Parts Per Million

XRF Major Element Geochemistry:

The Lebombo-Tshipise samples display positive linear co-variance of Al_2O_3 with Fe_2O_3, MgO, Na_2O and K_2O ($R^2 \geq 0.8$), while there is a weaker co-variance with TiO_2 ($R^2 = 0.63859$) (Figure 3-15 A- G). The weaker correlation between TiO_2 and Al_2O_3 could indicate TiO_2 is hosted in other minerals besides clays, consistent with the identification of titanium oxides in the XRD results (see Appendix C), while the stronger relationships suggest these other oxides are constituents of clay and other aluminosilicates (Jin et al., 2006). Co-variance is not established with CaO ($R^2 = 0.0581$) (Figure 3-15 F), and this is resultant of very small concentrations of CaO present in all samples (0.05-0.94). CaO concentration is especially low in comparison results from the Elliot Formation in the Main Karoo Basin (avg. 4.42, Sciscio & Bordy, 2016).

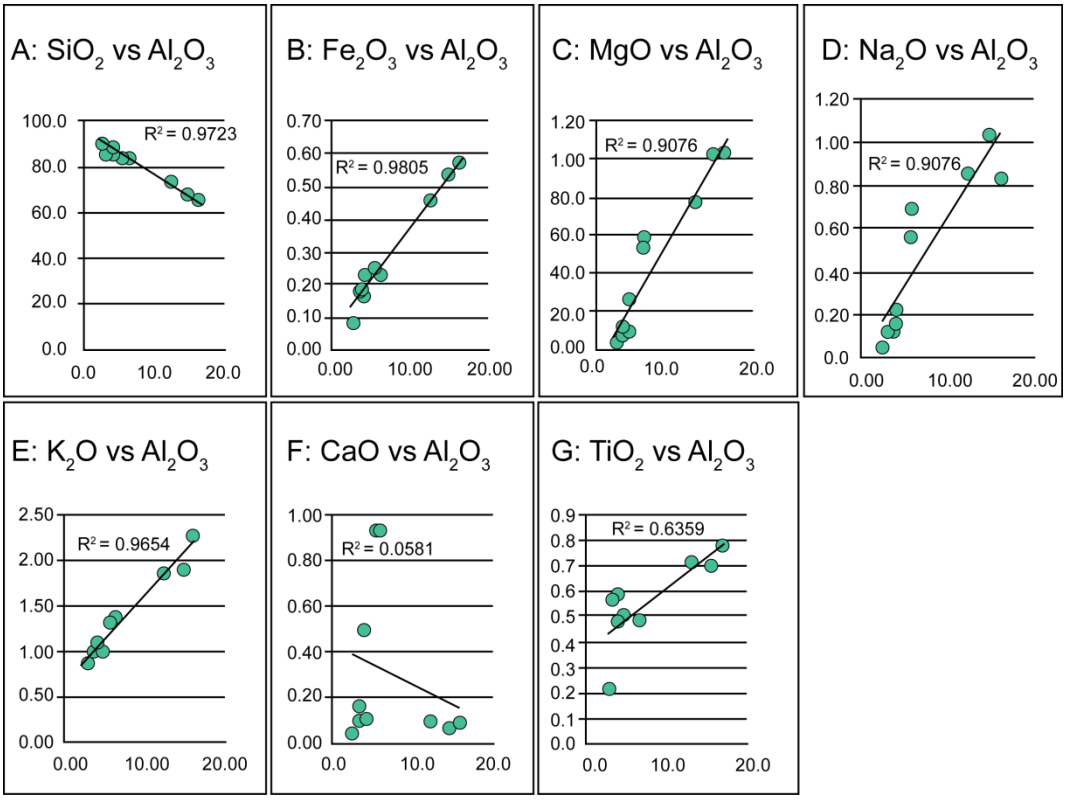

Figure 3-15: Various oxides present in relation to alumina from 9 samples from the Lebombo-Tshipise Basin (see Table 2-1 for sample list) as measured by XRF.

The ratio of silica to aluminum in samples can be employed as a proxy for sediment maturation, with larger ratios reflecting more mature sediment as resistive quartz increases while feldspars, micas and other aluminosilicate content decreases during transport and recycling (Akarish & El-Gohary, 2011). In general, SiO_2/Al_2O_3 ratios for the Lebombo Tshipise Basin are high, with an average (mean) of 17.02, considering Roser et al. (1996) report values between and greater than 5 and 6 as indicative of sedimentary maturation. The largest ratios are from the Main Karoo Basin palaeosol sample (BPS-1: 34.94), samples from P-B and C (KDS-6: 24.12, KDS-7: 25.12), the LTB mudrock sample (KDS-10: 22.19), and the uppermost sample from P-A (KDS-5: 20.65). Samples KDS-3A and B also have high ratios (13.97 and 14.64, respectively), however quartz enrichment may be a result of diagenic alteration; these samples are significantly enriched in CaO compared to the other samples by as great as a factor of 18. Additional evidence for alteration is presented in Chapter 3.2.1 (SEM and XRD) and Appendix C. Only two of the palaeosol samples (KDS-2 and 4) are considered immature with ratios of 4.04 and 4.63 respectively.

Excluding samples BPS-1, KDS-10, and KDS-3A and B, to further elucidate the sediment maturation of strictly Lebombo-Tshipise palaeosols that do not show evidence of alteration, the mean SiO_2/Al_2O_3 ratio is reduced to 14.08 with a standard deviation of 9.33, indicating there is still a very large variance in ratios and therefore soil maturation throughout these soil horizons. Most surprisingly, there is no upward trend in less mature sediment in the extensively sampled P-A; the largest ratio comes from the uppermost strata in the deposit. KDS-5 may represent a new, less weathered generation of soil development on top of older, more clay-rich soil.

All of the Lebombo-Tshipise samples have larger amounts of iron (2.86 avg) and titanium (0.59) than the Main Karoo Basin sample and the

average of samples reported from the Main Karoo Basin in Sciscio and Bordy (2016; 0.8 and 0.22; 2.28 and 0.48, respectively). Samples from Sciscio and Bordy (2016) do not report FeO (due to instrumentation), so a direct comparison to this study's samples cannot be made. These samples have, on average, 8 times more FeO than Fe_2O_3 present. The resultant abundance of soluble ferrous iron in the Lebombo-Tshipise samples suggests the soils were poorly drained.

XRF Trace Element Geochemistry

All trace elements are present in concentrations below 100 ppm with the exceptions of Rb (31.52 – 131.74) Zr (281.02 – 637.37) and Ba (224.46 – 1026.18); this is comparable to results published from the Elliot Formation of the Main Karoo Basin: Sr (86.4 – 268 ppm), Zr (143 – 215 ppm), and Ba (335 – 1884 ppm) (Sciscio and Bordy, 2016).

CIA

Chemical Indices of Alteration are calculated to determine overall weathering of fresh parent material. These values can be compared to the relative amounts of potassium (K), alumina (A), calcium and sodium (CN) determined by XRF, and plotted in a ternary diagram to represent clay species likely to be present and degree of weathering (Figure 3-16). Samples from the present study are plotted and compared with three locations from the Main Karoo Basin published by Sciscio and Bordy (2016), which indicate that the Lebombo-Tshipise samples are more likely to contain greater amounts of illite compared to smectite, and are more weathered (intermediate weathering vs. weak weathering) than the Main Karoo Basin counterparts. The sample taken from Blikana field area surprisingly plots out very close to the illite line, and more closely resembles samples from the Lebombo-Tshipise Basin than the Main Karoo Basin samples.

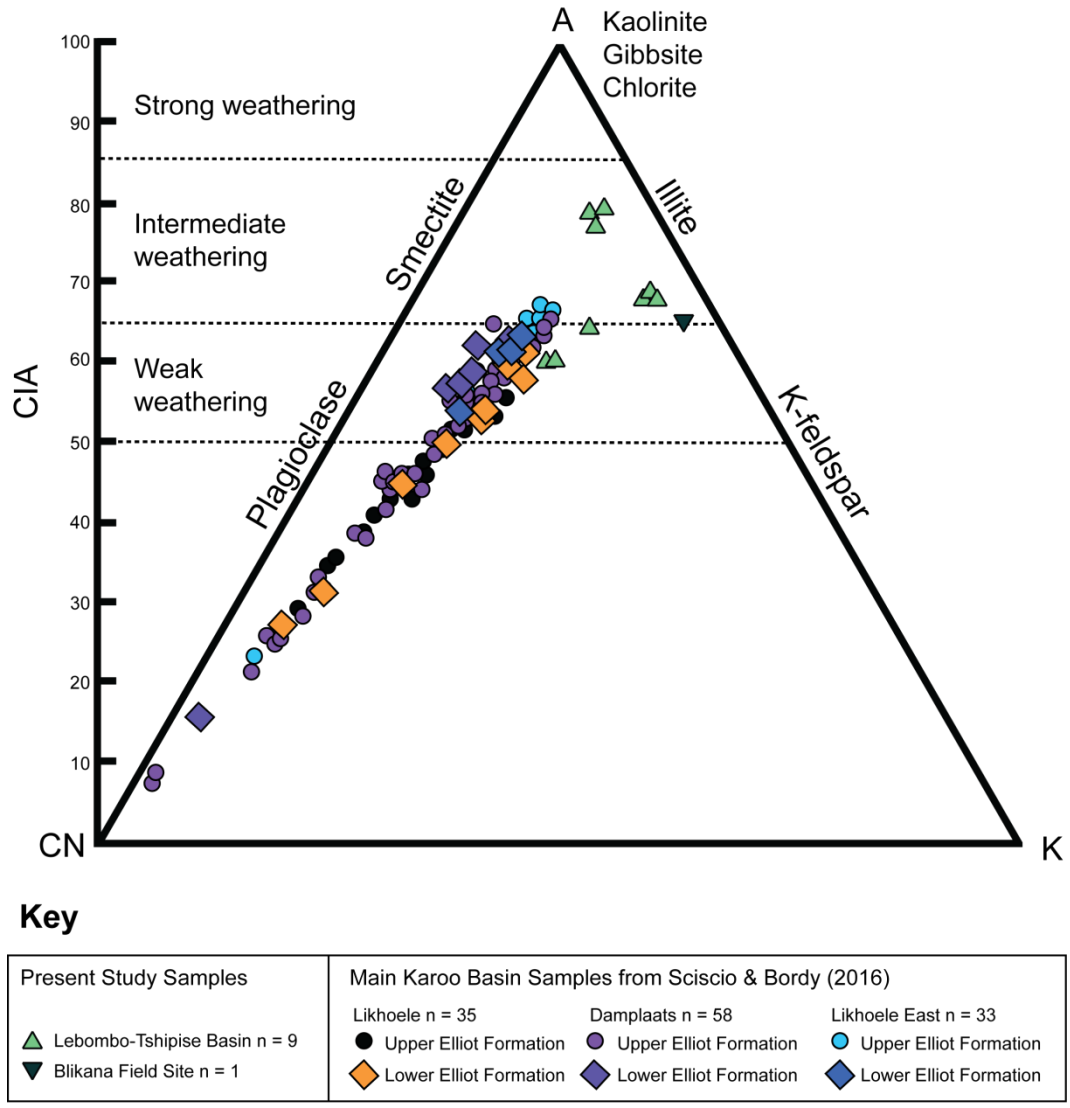

Figure 3-16: Ternary diagram of Chemical Indices of Alteration (CIA) values vs. Combined calcium (C)/sodium (N), Potassium (K), and alumina (A) amounts present in 10 samples from the present study and 126 samples published by Sciscio and Bordy (2016). Amounts of cations and CIA values are calculated from XRF results. Samples below CIA 50 represent relatively unweathered rocks, while samples enriched in alumina are highly weathered and have lost mobile cations.

CIA molar values can be compared to potassium (K)/sodium (Na), and alumina (Al) values as determined by XRF to determine the relative aridity of the environment in which the samples were formed (Figure 3-17). Samples from the present study are again compared to data published by Sciscio and Bordy (2016) from the Main Karoo Basin. The samples from the present study tend to have higher CIA values consistent with more

subtropical (i.e. wetter) weathering conditions than samples from the Main Karoo Basin.

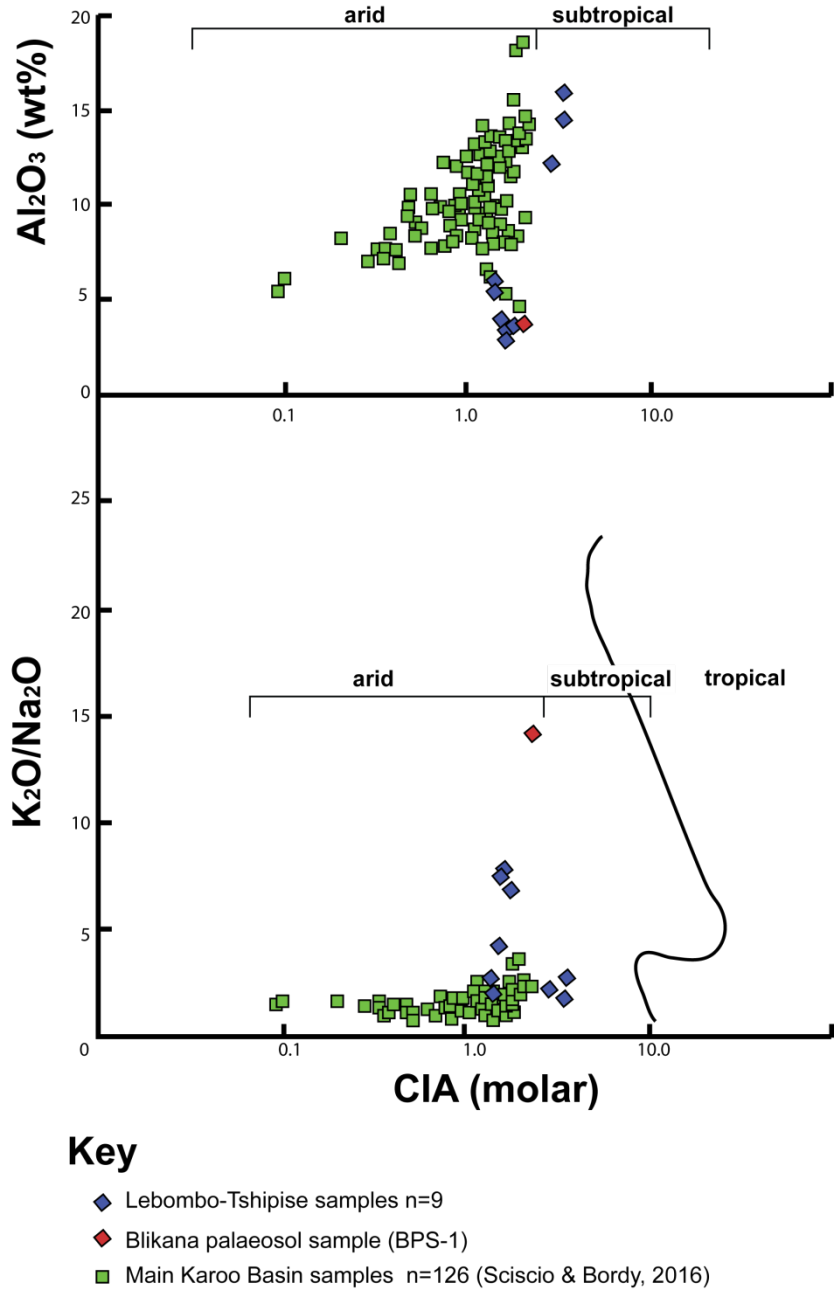

Figure 3-17: Chemical Indices of Alteration (CIA) molar values compared to potassium/sodium ratio, and alumina (XRF values) from 10 samples from the present study (blue and red) and 126 samples published by Sciscio and Bordy (2016). Samples from the present study plot closer to and within the subtropical depositional climate as established by Goldberg and Humayun (2010).

3.3 Fossils of the Elliot and Clarens Formations

3.3.1 Sauropodomorph Fossils

The fossil material recovered from Kruger National Park and Makuya National Reserve had originally been assigned by Durand (2001) to *Euskelosaurus browni* based primarily on the size and robust nature of the large, adult specimens recovered. This interpretation followed the biostratigraphic range zones established by Kitching and Raath (1984) for the Elliot Formation within the main Karoo Basin: the *Euskelosaurus* Range Zone for the lowermost subunit (typified by the nearly exclusive occurrence of large-bodied 'prosauropods'), and the *Massospondylus* Range Zone for the 'middle' and uppermost subunits (typified by abundant remains of the comparatively gracile *Massospondylus*). However, recent taxonomic revision has demonstrated *Euskelosaurus* to be a "waste-basket" taxon (Yates & Kitching, 2003; Yates 2003; 2004; 2007a,b), and numerous new sauropodomorph taxa have since been described from both the upper and lower sections of the Elliot Formation (Yates, 2003b; 2004b; 2007a,b; Yates et al., 20010; McPhee et al., 2015a, b).

Current consensus recognizes five species occurring in the lower Elliot Formation (LEF): *Blikanasaurus cromptoni, Melanorosaurus readi, Eucnemesaurus entaxonis, Plateosauravus cullingworthi,* and *Antetonitrus ingenipes* (Yates, 2007; McPhee et al., 2015a); and four genera occurring in the upper Elliot Formation (UEF): *Massospondylus, Aardonyx, Pulanesaura,* and *Arcusaurus* (McPhee et al., 2015b), though this is subject to increase due to the uncertain status of taxa referred to as *Massospondylus* (i.e. *Ignavusaurus* and *Gyposaurus*, Cooper 1981; Yates et al., 2011). This stratigraphic distribution represents a marked departure from older assessments of sauropodomorph biostratigraphy of the Elliot Formation that assumed a more morphologically and taxonomically diverse assemblage of sauropodomorphs within the Late Triassic lower Elliot Formation compared to the 'depauperate' Early Jurassic upper Elliot Formation (Barrett, 2004, 2009; McPhee et al., 2016).

The Lebombo-Tshipise sauropodomorph material was found *ex situ*, and represents numerous individuals from multiple ontogenetic phases and potentially several different genera. Elements were recovered from dry stream beds in topographic lows between two highlands and could have originated from a single bonebed or multiple deposits of unknown composition. Thus, this material does not necessarily represent a single population of animals, a monospecific assemblage, or even single temporal horizon. Nonetheless, a select subset of these fossils present a modest amount of informative morphology that allows comparison with the better-known fossil remains from the main Karoo Basin. This subset includes an anterior caudal vertebra, first metacarpal, and proximal left femoral head which are described and discussed below.

Caudal vertebra: The anterior caudal vertebra (Figure 3-18) has a centrum that is much taller dorsoventrally than it is anteroposteriorly long, with an anteroposterior length 0.32 times its dorsoventral height. Anteroposterior shortening of anterior caudal vertebrae is considered a putatively derived feature in Sauropodomorpha, and is noted in *Pulanesaura* (McPhee et al., 2015b) and *Tazoudasaurus naimi* (Allain & Aquesbi, 2008). However, this feature is otherwise rare within the Elliot sauropodomorph assemblage. Similar features observed in a referred specimen of *Melanorosaurus* (NMQR 1551; Galton et al., 2005) complicate the phylogenetic connotations of this character. The transverse processes are positioned high on the centrum and are located roughly the level of the neurocentral suture. This feature distinguishes it from the anterior caudal vertebrae of *Pulanesaura* and from more derived sauropod taxa in which the transverse processes extend well onto the lateral surfaces of the centrum. The phylogenetic distribution of this feature is ambiguous, with the basal sauropods *Tazoudasaurus* and '*Kotasaurus*' possibly retaining the plesiomorphic condition in the positioning of the transverse processes (Yadagiri, 1988; Allain et al., 2004).

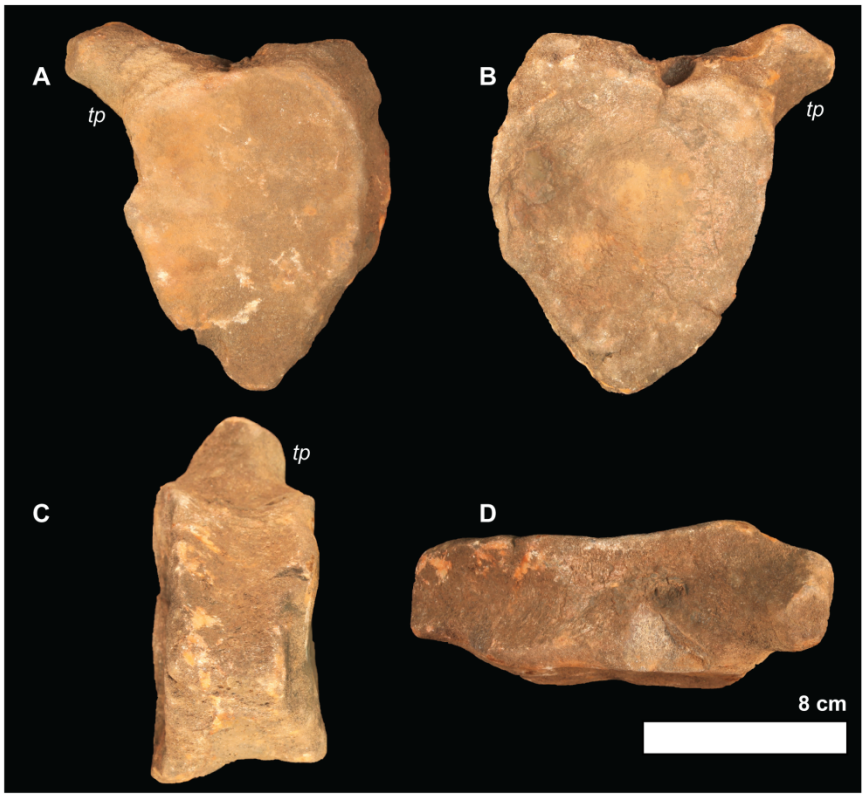

Figure 3-18: Sauropodomorph anterior caudal vertebra in anterior (A), posterior (B), lateral (C), and dorsal (D) views. Note the high positioning of the transverse processs (*tp*) and anteroposterior shortening.

Metacarpal I: The first metacarpal (mc I) is volumetrically large but relatively elongate in comparison to the similarly-sized taxa like *Aardonyx* (Figure 3-19 and 3-20). The proximal surface is roughly trapezoidal, with nearly equidimensional mediolateral (5.5 cm) and dorsovental (5.4 cm) maximum measurements. This surface is flat, lacking the proximal concavity typical of phalanges. The mediolateral width of the proximal end is approximately 0.60 of the length of the total length of the bone (9.1 cm), in marked contrast to the similar-sized animal *Aardonyx celestae* which has a very stout mc I with a ratio of 1.12 (McPhee et al., 2014). *Anchisaurus* and *Plateosaurus* have similarly elongate first metacarpals with ratios of 0.65 and 0.7, respectively (McPhee et al., 2014). The medial condyle is bulbous while the lateral appears much reduced.

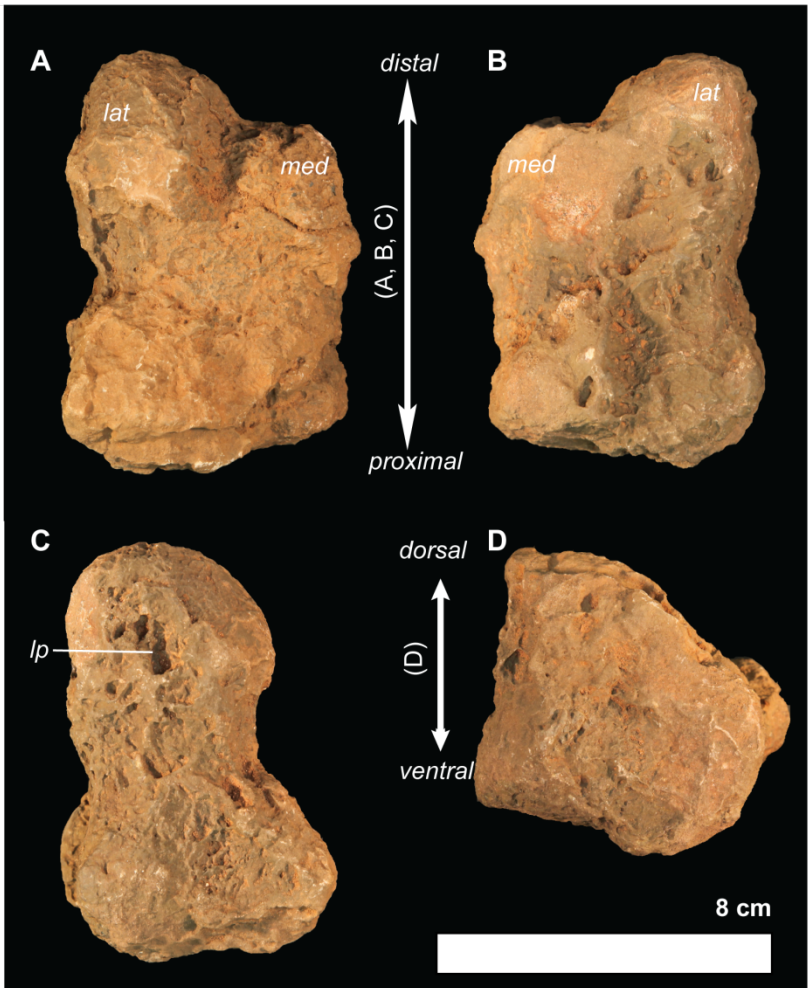

Figure 3-19: Sauropodomorph first metacarpal in dorsal (A), palmer (B), medial (C), and proximal (D) views. This elongate element is heavily encrusted in ferricrete; *lat* = lateral, and *med* = medial condyles, *li* = ligament pit.

The relative elongation of the Lebombo-Tshipise mc I is intriguing as no equivalent from such a large specimen is known from the Elliot sauropodomorph assemblage (see Figure 3-20 for comparison with other Elliot sauropodomorph metacarpals). In the Main Karoo Basin the morphology of sauropodomorph metacarpals appears to have a vague correlation with stratigraphic position (i.e. short and stocky in the upper Elliot Formation and elongate in the lower Elliot Formation). As few Early Jurassic taxa from southern Africa display a similarly elongate mc I (even morphologically disparate *Antetonitrus* and *Massospondylus* have proximodistally shortened first metacarpals), the element's morphology could motivate a lower Elliot stratigraphic placement for the Lebombo-

Tshipise assemblage. However, the Elliot assemblage (and especially that of the lower Elliot), is depauperate in sauropodomorph manus material, which may play a role in overstating the correlation of mc I morphology and stratigraphic placement. Additionally, a relatively elongate mc I exists in the putative near-sauropod *Lamplughsaura* from the Early Jurassic of India (Kutty et al., 2007), so caution should be taken when associating atomized anatomical information with stratigraphic position.

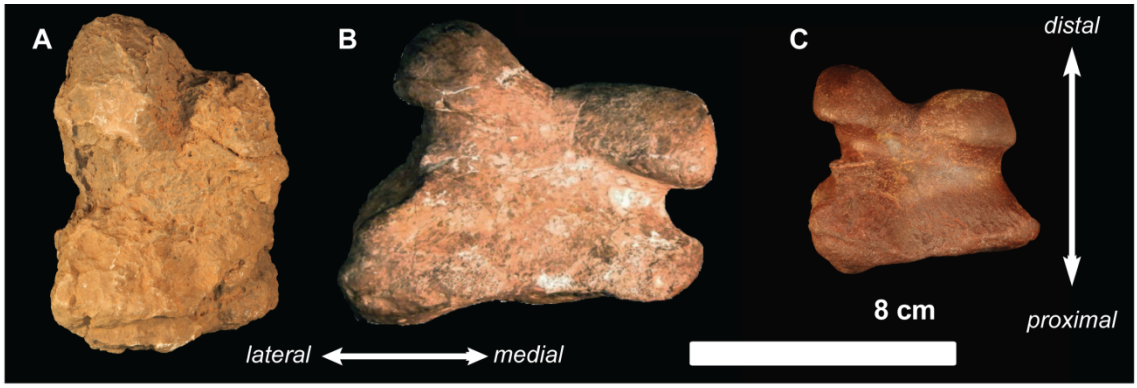

Figure 3-20: Sauropodomorph first metacarpals: (A) Lebombo-Tshipise specimen, (B) *Antetonitrus* (BPI/1/4952), and (C) *Aardonyx* (BPI/1/5379). While these animals are similar in size, their manual architecture is markedly different.

Femur: A number of isolated femora were figured by Durand (2001), who cited the appreciable size range of these elements from several ontogenetic stages as evidence of gregarious herding behaviour in basal Sauropodomorpha. However, this conclusion was drawn with minimal discussion of the elements' taphonomic context which refutes this hypothesis, and the material was not figured in detail to establish taxonomic affinity beyond indet. Sauropodmorpha. The fragmentary femora encountered in the study do not present autapomorphies that enable identification at low taxonomic levels; however, recovery of a partial left femur offers modest taxonomic insight.

The left femur is represented only by the head and the proximal-most portion of the shaft (Figure 3-21). The circumference of the shaft measured proximal to the lesser trochanter and distal to the greater trochanter is 31.1 cm, which places this element in the same size class as

Eucnemesaurus fortis (BPI/1/6111) and *Aardonyx celestae* (BPI/1/6510) which measure 31.5 and 32.5 cm, respectively. These animals probably weighed close to 700 kg, significantly smaller than the estimated 5,600 kg of *Antetonitrus ingenipes* (BPI/1/4952) which measures 42.3 cm in circumference (Benson et al., 2014).

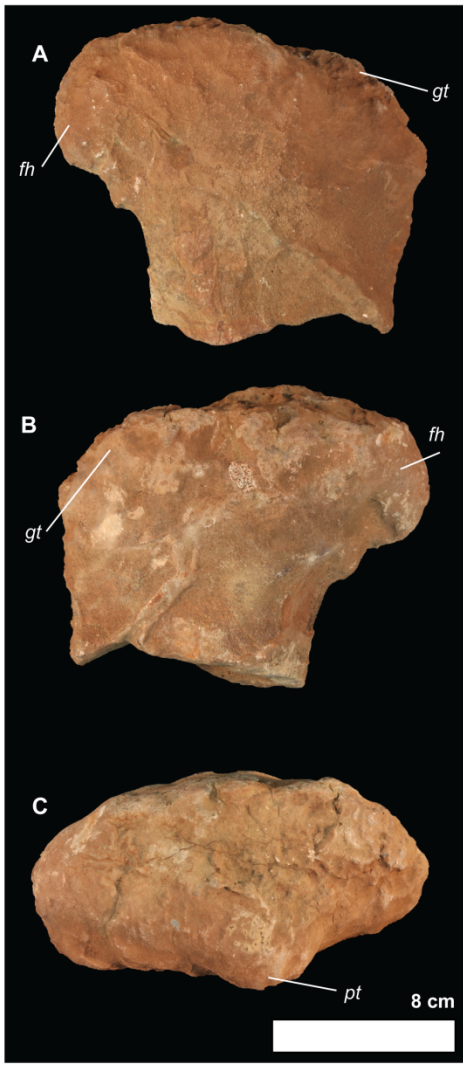

Figure 3-21: Sauropodomorph proximal left femur in anterior (A), posterior (B), and proximal (C) views, *fh* = femoral head, *gt* = greater trochanter, *pt* = posterior tubercle.

Of particular interest is the presence of a pronounced protuberance on the posterior surface of the femoral head. This posterior tubercle was suggested as a possible autapomorphy of *Eucnemesaurus* by Yates (2007a,b). However, McPhee et al. (2015a) have recently suggested that

this feature is probably more variable than generally appreciated, and question its utility as a diagnostic character.

Diagnosis: The absence of articulated, *in situ* specimens makes taxonomic assessment of this material particularly difficult. However, this assemblage compares well to the Elliot Formation sauropodomorph assemblage in overall morphology and relative body size, belonging to animals similar to *Eucnemesaurus* though smaller than *Antetonitrus*. As the material lacks any evidence of the presence of gracile, massospondylid-like morphologies typical of the upper Elliot Formation, the study can tentatively suggest a lower Elliot equivalent stratigraphic placement of this material.

Should the femoral posterior tubercle remain a valid autapomorphy, this would place some of the material within ‘Riojasauridae’ at the base of Massopoda. Though the anterior caudal vertebra features a putatively derived (i.e. sauropod-like) condition, this is less pronounced than in *Pulanesaura.*

The pleisomorphic, elongate metacarpal suggests affinities with both *Plateosaurus,* which falls outside of Massopoda, and *Anchisaurus* which is recovered within Massopoda but sister-taxon to Massospondylidae (McPhee et al., 2015). Phylogenetically, the animal to which it belonged is most likely to occur at the base or just outside of Massopoda. The metacarpal’s morphology suggests it belongs to a new species, or represents an unknown element from a described species.

3.3.2 Trace Fossils

Burrows from the Elliot Formation at the Red Rock locality (Figure 3-22) are unlined, unbranched, cylindrical and elongate, ranging in size from 5-50 cm in length and 0.5-8 cm in diameter. Their infill, when present, is typically finer-grained and different coloured (dustier, or yellow) from the

surrounding, massive sediment. These burrows are preserved in full and epirelief, and are oriented vertically through the substrate (*Skolithos isp.*) and horizontally along bedding planes (*Planolites isp.*) (Figure 3-22 B), and in some places, gently aligned to dune foresets (Figure 3-22 C). They are typically discrete and do not overlap, but commonly occur together in clusters (Figure 3-22 A and E).

Figure 3-22: Trace fossils from the Elliot/Clarens Formation at the Red Rocks locality. (A) Small burrows often cluster in transect, but do not overlap (FA VII A). (B) *Planolites isp.* present on the palaeosurface and *Skolithos isp.* vertically oriented through strata (FA VII A). (C) Small burrows in beige are aligned to dune foresets in cryptic dune (FA VII B). (D) Circular traces in epirelief likely represent *Skolithos isp.* in epirelief (FA VII A). (E) Small burrows preserved in epirelief are clustered but to not significantly overlap each other (FA VII A). (F) Elongate traces (*Planolites?*) in epirelief are sparse and delicate in appearance and only found in FA VII B.

The trace fossil assemblage from the Clarens Formation at Makanya Hill is dominated by kidney-shaped to circular, unlined, oblique burrows (2-4 cm in diameter) that penetrate underlying strata up to 8 cm deep. These burrows appear to have a faint, meniscate infill. Circular to almond-shaped, convex bodies 2-3 cm in length are preserved in epirelief above

these burrows (Figure 3-23 A, C, D). The convex bodies in epirelief combined with the unlined and oblique burrowing orientation are consistent with *Taenidium isp.* (Good & Ekdale, 2014). These burrows are not nested in ellipsoidal packets, so the term AMB (adhesive meniscate burrows) is not applicable to these traces (Bown and Kraus 1983; Hasiotis and Dubiel 1994; Smith et al. 2008). Other traces include elongate, low-sinuosity, unlined, traces approximately 15-25 mm in width. These are present in epirelief, and commonly found in association with *Taenidium isp.* Many of these have meniscate infill and are assigned to *Entradichnus isp.* (after Ekdale et al., 2007), while burrows without this interior structure are assigned to *Planolites isp.* (Figure 3-23-F, and C, G respectively). Additionally, numerous small (1-5 cm in diameter) circular burrows which are typically paired are assigned to *Arenicolites isp.* Figure 3-23-H).

The abundance of *Arenicolites isp., Planolites isp., Entradichnus isp., Skolithos isp.,* and *Taenidium isp.* indicate the presence of communal invertebrates (Ekdale et al. 2007). There are several possible tracemakers present in Late Triassic aeolian environments including gastropods, isopods, myriapods, arachnids, and a variety of insects such as non-gregarious wasps, crickets, flies, cockroaches, beetles, and cicadas (from the orders Hymenoptera, Orthoptera, Diptera, Blattodea, Coeloptera, and Hemiptera respectively) (Good & Ekdale, 2014). There are a variety of behaviours represented by these tracemakers; meniscate traces like *Taenidium* and *Entradichnus* are related to either locomotion (repichnia) or feeding (pascichnia) behaviours, while *Skolithos, Planolites,* and *Arenicolites* are dwelling structures (dominichnia).

Taken together, these ichnofossils are consistent with both *Scoyenia* and *Octopodichnus-Entradichus* ichnofacies. However, neither assemblage has arthropod trackways, but this omission is likely a preservational artefact as these delicate traces rarely preserve (Seilacher, 1964; Hunt & Lucas, 2007). This assemblage is therefore consistent with freshwater

lacustrine, fluvial, and aeolian environments (Benton & Harper, 1997; Ekdale et al., 2007). The aeolian sedimentary features of both field sites is consistent with a desert palaeoenvironment, though abundance of traces would require fairly wet conditions for sustaining life and preserving these ichnofossils (Ekdale et al., 2007).

Figure 3-23: Trace fossils from the Clarens Formation at Makanya Hill locality. (A) Almond-shaped *Taenidium isp.* in epirelief (note hammer ~30 cm for scale), and (B) associated disturbed bedding. (C) *Taenidium isp*. and meniscate, undulatory *Entradichnus isp.* in epirelief. (D) Oblique *Taenidium isp*. burrows in full relief. (E) *Arenicolites isp*. and other large, cylindrical traces in epirelief. (F) *Entradichnus isp.* showing meniscate infill in epirelief. (G) Undulatory *Planolites isp.* in epirelief. (H) Paired, minute *Arenicolites isp.* in epirelief.

3.3.3 Fossil Wood

In contrast to the relatively rare preservation of wood in the Elliot Formation of the Main Karoo Basin, the upper Makanya Hill locality and the Makuya field site are littered with *ex situ* fossil wood, with fragments ranging in size from 2-3 cm thick to 15 x 30 cm. The samples exhibit structures typical to *Agathoxylon*, a well-known Gondwanan conifer. However, the lobes viewed in transverse section (Figure 21 A) are similar to *Rhexoxylon*, which has been identified in the Late Triassic Molteno Formation (Bamford, 2004). Several species of *Rhexoxylon* are known from South Africa and South America (Archangelsky & Brett, 1961; Anderson & Anderson 1985; Artabe et al., 1999), but further diagnosis was not possible due to the small size of the sample and generally poor preservation of its internal structure, typical of wood from the Late Triassic Molteno Formation (Bamford, 2004).

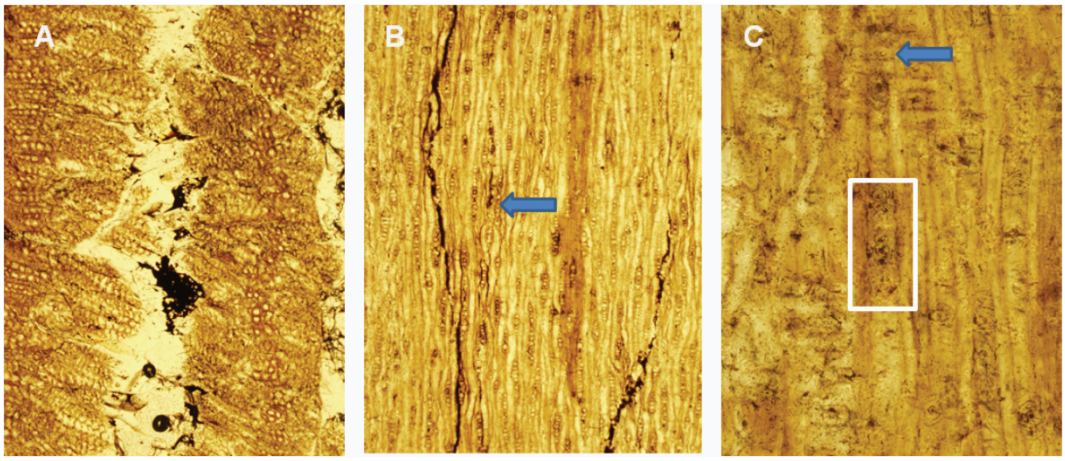

Figure 3-24: Fossil wood thin sections from the Elliot Formation at Makanya Hill locality. (A) Transverse section showing arrangement of tracheids is irregular with gaps and lobes, magnification = 40x. (B) Tangential longitudinal section shows uniserite rays 30-14 cells high (arrow), magnification = 40x. (C) Radial longitudinal section shows the crowded, compressed uniserate bordered pits on the radial walls of the tracheids (white box), numerous cross-file pits are also visible (arrow), magnification = 200x.

Assignment of this wood to *Rhexoxylon* indicates a Triassic age for the sediments. The Elliot Formation is notorious for very rare preservation of plant material, with only one sphenophyte, one bennettitalean and three

conifers identified as *Agathoxylon* reported from this formation until this present study (Bamford, 2004). This paucity of preserved wood has been explained in the literature (Bamford, 2004) as reflective of climactic change: as the warm, wet environment during the deposition of the Molteno Formation changed to a drier climate of the Elliot Formation, the geographic distribution of plants would have become more localized, reducing the likelihood of preservation.

Chapter 4: Discussion

4.1 Palaeoenvironments of the Karoo Supergroup:

The Karoo sediments of the Lebombo-Tshipise Basin record similar environments present in the Main Karoo Basin. Though previous workers suspected the Tshidize Formation might represent pre-Karoo sedimentation (McCourt & Brandl, 1980), researchers generally regard this formation as part of the Dwyka Group. When present, this formation directly overlies the Precambrian basement (Brandl, 2002; Durand, 2012; Malaza et al., 2013). The formation is composed of diamictite with pebble to boulder-sized clasts that reach up to a maximum of 2 m in diameter at the type location southwest of Masisi, though typically clasts are smaller (~60 cm maximum) (Brandl, 2002). At the Makanya Hill locality, the upper unit of the deposit fines upward, with fewer large, cobble-sized clasts upsection, attesting to diminishing energy in the debris flow consistent with fluvioglacial processes. Thought to be deposited during the end of glaciation during the Late Carboniferous/Early Permian (Malaza et al., 2013), this diamictite represents fluvio-glacial deposits which are preserved sporadically throughout the Pafuri sub-basin. The discontinuous presence and irregular thickness of the Tshizie is likely due to the highly variable discharge associated with glacial processes.

Throughout the Permian, mud, silts, and coarse-grained felspathic sands were deposited in well-drained swamps, lakes and fluvial systems in the Lebombo-Tshipise Basin (Malaza et al., 2013). The landscape was well vegetated as evidenced by rip-up clasts including plant matter, plant fossils described by Louw (1981), and coal seams during the deposition of the Madzaringwe and Mikembeni Formations. The Madzaringwe Formation, in addition to laminated silts, muds and coal seams, records high energy fluvial deposits in coarse-grained sandstones deposited in bars and channels. The Mikembeni conformably overlies the Madzaringwe (McCourt & Brandl, 1980; Malaza et al., 2013), recording a lower energy environment dominated by lakes, ponds, swamps and overbank deposits.

Ferriginous concretions in mudrock from the “upper unit” identified by McCourt and Brandl (1980) and observed in the Lower Makanya Hill field area (see Chapter 3.1) could have formed in water-logged, anoxic conditions.

The Fripp Sandstone was laid down as point bars and channel lags deposited unconformably on top of the Mikembeni Formation (Brandl, 2002). This coarse-grained sandstone is similar to deposits in the Madzaringwe, but much thicker, reaching up to 125 m at its type locality (Brandl, 2002). Shale lenses, in addition to coalified wood and other plant rip-up clasts were observed in outcrop, and attest to well vegetated overbank environments. The coarse-grained sandstone bodies are consistent with high energy fluvial environments. This formation has been posited as a clastic wedge formed in response to tectonic uplift in the north, and as such has no direct correlative in the Main Karoo Basin (Brandl, 2002), though Bordy and Catuneanu (2002c) contend the Fripp may represent a facies equivalent of the Molteno Formation due to the presence of *dicrodium* fossils.

The Solitude Formation consists of mudrock, siltstone, and gritty sandstones deposited in fluvial systems with well-developed overbank environments which gradually overlie the Fripp Sandstone (Brandl, 2002). These fluvial overbank deposits are correlated to the Beaufort Group mudrocks by previous researchers (McCourt & Brandl, 1980; Brandl, 2002), though the lack of developed palaeosols may indicate wet, saturated conditions, in contrast to the aridification events evidenced by pedogenic carbonate horizons, desiccation cracks, and gypsum rosettes in the Main Karoo Basin (Keyser, 1966; Catuneanu et al., 2005).

The Klopperfontein Sandstone consists of grit and sandstone with minor shale and mudrock units and lenses, in addition to calcareous nodules and other rip-up clasts from underlying sediments. These sand bodies and the

formation's unconformable relationship with the underlying Solitude Formation indicate high energy, fluvial environments. Like the Fripp, this formation has been posited as evidence of renewed tectonism from the northeast, and likely represents a clastic wedge. Previous workers have noted its similarity in terms of lithology and timing (i.e., directly before Elliot Formation sedimentation) to the Molteno Formation in the Main Karoo Basin (de Jager, 1983b; Chidley, 1985; Johnson, 1994; Johnson et al., 1996; Catuneanu et al., 2005).

4.2 Late Triassic-Early Jurassic Palaeoenvironments and Climate:

The Elliot Formation muds and palaeosols preserved in the Lebombo-Tshipise Basin are similar to floodplain environments preserved in the Main Karoo basin. These floodplain and associated fluvial sediments were abruptly drowned in aeolian deposits of an erg or series of dune fields across the whole of southern Africa. Previous workers have long interpreted these sedimentological and associated palaeontological data to correlate to progressive aridification in southern Africa across the Late Triassic and into the Early Jurassic (Haughton, 1924; Beukes, 1970; Ellenberger, 1970; Eriksson 1984; 1985; Bordy & Eriksson, 2015). However, more recent studies have focused on climate change in the Tethyan realm during the Early Jurassic, which documents a precipitous change to stronger seasonality and increased humidity (Ruckwied et al., 2008; Ruckwied & Götz, 2009; Götz et al., 2009; Bonis et al., 2009; 2010; Ryseth, 2014; Pálfy & Kocsis, 2014) though this is mostly documented in south-western Europe, and the southern extent of this humidification event is unknown.

Most palaeoclimate reconstructions of Gondwanan Triassic-Jurassic formations are based exclusively on lithologic indicators such as the locations of coal, laterite, tillite, evaporite, and calcrete deposits, in addition to relevant palaeofaunal and floral occurrences (e.g. crocodiles and mangrove swamps; Péron et al., 2005; Rais et al., 2007; Stigall et al.,

2008; Bond & Wignall, 2010; Bialik et al., 2013). While these data are not as accurate as quantitative methods, they do allow for areas to be assigned to climatic zones corresponding to widely available lithological and palaeobiological data (see maps from Paleomap Project, Scotese, 2001). These zones include: tropical (warm and moist year-round); arid (warm or cool but dry year-round); warm temperate (seasonal climate); cold temperate (seasonal climate); and cold (typically identified by evidence of glaciers) (Scotese, 2001). It's important to note that these zones do not always correspond to modern geographical zonations (i.e. modern "tropical" climates restricted to those present between the Tropics of Cancer and Capricorn).

Palaeosol samples from the Elliot Formation of the Lebombo-Tshipise Basin are enriched in smectite, corresponding to "intermittently poorly drained environments, including monsoonal and xeric climates, characterized by strongly seasonal precipitation" (Sheldon & Tabor, 2009). The presence of large amounts of authigenic smectite indicates massive weathering (i.e. large-scale replacement of stable aluminosilicates by secondary minerals such as gibbsite, kaolinite, or smectite as defined in Pedro, 1997) occurred during the Late Triassic. This massive weathering regime is not consistent with truly arid environments, and unlike most of the Elliot Formation described in the Lebombo-Tshipise (McCourt & Brandl, 1980; Brandl, 2002) the palaeosol samples were very low in calcium and lacked calcic pedogenic nodules or calcrete horizons typical of the upper Elliot in the Main Karoo Basin (Bordy et al., 2004 b and c).

The presence of iron and titanium oxides observed from XRD and SEM analyses indicates that periodically dry conditions occurred during formation of the soil during Elliot time. Iron and titanium substitution in authigenic smectite indicates that these elements were present in fairly high concentrations during, and likely after, soil formation. This is likely to have affected the preservation of sauropodomorph fossils, which were all

found heavily encrusted in ferricrete. While hematite coverings are typical of the upper Elliot Formation (Kitching & Raath, 1984), the thickness and completeness of the coverings is exceptional in the Lebombo-Tshipise Basin. The thicker iron oxide coatings may be caused by higher concentrations of dissolved iron in the groundwater subsequent to carcass burial (Bao et al., 1998). Alternately, these authigenic mineral coatings may have formed significantly after fossilization, and may not correlate to palaeoclimate. However, Bao et al., (1998) suggest these coatings are primarily a pedogenic feature and could serve as a source for studying continental palaeoclimate. Further research on the origin and geochemical nature of these coatings could elucidate groundwater conditions either at the time of burial, or the divergence between diagenetic conditions in these two basins.

Perhaps the most meaningful fossil evidence for palaeoclimate in the Lebombo-Tshipise, is from fossilized wood in the Elliot Formation. The large chunks of *Rhexoxylon* indicate the presence of fairly large trees. While no *in situ* fossils evincing a petrified forest were found, the large amount of scattered fossil fragments represents multiple trees, which may indicate fairly humid conditions, or the presence of oases as suggested by Bordy and Catuneanu (2002a).

Recently developed quantitative methods have been applied to palaeosols to investigate palaeoclimate proxies, including provenance, weathering intensity, mean annual precipitation and others (e.g. Sheldon & Tabor, 2009). Many of these were calculated for a suite of samples in the Elliot Formation of the Main Karoo Basin (Sciscio & Bordy, 2016), though these were performed not on palaeosols, but instead on mudrocks and sandstones. Because the formation of authigenic clays and other minerals in the soil record the environment in which they form, analyses of detrital grains in sandstones and mudrocks (as in Sciscio and Bordy, 2016) may not as accurately represent the palaeoenvironment present in the Main

Karoo Basin at the time of deposition. This may account for the differences found in the single Main Karoo Basin sample in this study and the published results of in Sciscio and Bordy (2016).

Chemical Indices of Alteration derived from X-Ray Fluorescence values ranging from 60.31-79.11 indicate intermediate weathering consistent with sediments that have been cycled or that are particularly clay-rich. Though this range appears to overlap with samples from the Main Karoo Basin (CIA values: 8.8-60.3 in Sciscio & Bordy, 2016), only two samples actually overlap (KDS-3A and B) with CIA values of 60.31 and 60.35 respectively. These samples have undergone diagenetic alteration (for more discussion see Chapter 3.2 XRD and XRF), and thus these two datasets do not have a continuous relationship, but represent two distinct clusters on an A-CN-K ternary diagram (see Figure 13). Sample BPS-1, which is the only sample from the Main Karoo Basin in our dataset, has CIA value of 65.87, which is much higher than any values from Sciscio and Bordy's dataset (2016). These intermediate CIA values, when plotted on an A-CN-K ternary diagram indicate illite enrichment of the Lebombo-Tshipise samples compared to samples from the Main Karoo Basin. This is likely due to overall larger volumes of clay in palaeosol samples compared to sandstones and mudrocks. The trend of this data on an A-CN-K diagram indicates less smectite than amounts suggested by SEM and XRD, and this is likely due to the very low concentrations of calcium as carbonate or oxides present in the Lebombo-Tshipise samples (average value of CaO in our dataset is 0.31% compared to the 1.19% in the Main Karoo Basin).

CIA molar values have been demonstrated to provide a more sensitive measure of humidity than CIA values (Goldberg & Huyaman, 2010) during soil formation, with values tightly clustered at 1 representing arid conditions, and values greater than 1 and less than 10 representing sub-tropical conditions, in this case simply meaning wetter conditions than found in arid environments. CIA molar values from our dataset range from

1.36-3.23, but removing diagenetically altered samples KDS-3A and B shortens this range to 1.49-3.23 with an average of 2.15. This contrasts with the very low average of 1.10 reported from the Main Karoo Basin samples, which led Sciscio and Bordy (2016) to interpret the deposition of the Elliot Formation as occurring in semi-arid to arid settings where chemical weathering was less dominant than physical weathering. CIA molar values from the Lebombo-Tshipise basin indicate a “subtropical” environment, characterized by well developed palaeosols formed in warm, periodically wet conditions (see Figure 3-16 for comparison of CIA molar values in the Lebombo-Tshipise and Main Karoo Basins).

While no suitable palaeosols were found in the overlying Red Rocks unit or Clarens Formation to provide quantitative results comparable to the Elliot Formation, ichnofossils can provide some clues to palaeoenvironment and climate at the interface of the Triassic and Jurassic periods.

Both the Red Rocks site in the south of the basin and Makanya Hill field site in the north preserve *Scoyenia* ichnofacies in aeolian-dominated strata. While dune fields form under arid conditions, modern studies have shown that desert-dwellers prefer to burrow in moist substrate (Hadley et al., 1990), suggesting this environment was wet enough to support animal life and preserve its traces.

The Red Rocks site preserves ichnofossils primarily in dune foresets, though they are also present on horizontal surfaces likely representing interdune environments. To preserve tracks or other impressions in sand, clay content and moisture have been determined to be the two most important factors (Walker & Harms, 1972; McKeever, 1991). While the sand is very clay-poor, resulting in poor preservation of bedding features, the delicate, often minute traces indicate moist enough conditions for preservation. Though *Scoyenia* typically is characterized by plenty of

trackways, tracks are often unlikely to preserve even under ideal conditions. The lack of trackways at Red Rocks is likely due to slow sedimentation rates resulting in non-preservation. The burrow containing Facies VII A is succeeded by heavily bioturbated Facies VII B that only rarely preserves traces, indicating that preservational biases changed at this time. This change could be an aridification event in which burrows simply fell in on themselves, or a reduction in sedimentation rate leading to more pervasive bioturbation by animals living near the surface.

The ichnofauna present in the Clarens Formation at Makanya Hill is similar to that at Red Rocks, but its distribution and frequency suggest wetter conditions were present for longer periods of time than at the Red Rocks locality. Ichnofossils here are primarily found in interdune deposits characterized by horizontal, irregularly bounded sand sheets, bioturbated beds, and soft sediment deformation. As *Taenidium*-like traces are formed in moist sand (Counts & Hasiotis 2009), and it is posited that the meniscate structure in *Entradichnus* needs moisture to form (Ekdale et al., 2007), the presence of these traces are evidence of a relatively wet environment.

The irregularly bounded sheets of FA XI are reminiscent of the non-carbonate interdunal lakes present in the Jurassic Nugget Sandstone Formation in the western United States (Britt et al., 2016), though these deposits are thicker. The Saints and Sinner's Quarry (Nugget Sandstone) in Utah, preserves a similar ichnofauna consisting of *Entradichnus, Taenidium, Planolites, Skolithos,* and the trackways *Octopodichnus* and *Paleohelcura* (Good & Ekdale, 2014). Additionally, modern studies of burrows and tracks show that *Taenidium* and *Scoyenia* are often present along lake shorelines (Buatois & Mángano, 2011). The repeated sequences of aeolian dunes with soft sediment deformation and heavily bioturbated layers associated with thin sand sheets, suggest repeated

flooding events that could have created ephemeral, interdune lakes within the erg.

Similar trace fossils have been described in the Clarens Formation from the Main Karoo, Tuli and Tshipise basins which occur preferentially in structureless, massive facies (Bordy, 2008). While playa lakes are known from the Clarens in the Main Karoo Basin, the northernmost portion of the Main Karoo and other northern basins appear to have been subjected to wetter conditions than most of the Main Karoo basin during deposition of the Clarens (see Beukes, 1970; Eriksson 1981, 1986). This has been linked to the rain shadow effect of the Cape Fold Belt, and to the latitudinal drift of Gondwana at this time (Bordy, 2008).

4.3 Stratigraphy and basin development discussion

The Palaeozoic and Mesozoic (Carbonifeous-Jurassic) Karoo Supergroup makes up the fill of the Lebombo-Tshipise Basin and rests nonconformably on top of Palaeoproterozoic schists and quartzites of the Soutpansberg Group. This basin likely formed initially as a sag basin along established weaknesses in the crust over the Limpopo belt between the Kaapval and Zimbabwe cratons (Cox, 1970; Bordy, 2000). The basin fill varies in presence and thickness at every stage, recording a complex history of changing subsidence and basin partitioning throughout the deposition of the Karoo Supergroup.

The Carboniferous-Permian strata (Tshidize, Madzaringwe, and Mikembeni Formations), wedge out southwards from a maximum of ~430 m in KNP 22, to <150 m in KNP 7, and eventually disappear completely in KNP 14 and 23.

The Tshidize Formation is the most discontinuous formation in the boreholes. Three boreholes (KNP 10, 13, and 15) do not intersect the Tshidize or underlying formations, and in another three (KNP 4, 8, and 11)

the Tshidize Formation is missing and the overlying Madzaringwe Formation directly contacts crystalline basement. These latter three boreholes may represent central and southern palaeotopographic highs where the Tshidize Formation was never deposited. The Tshidize Formation is rarer in the eastern boreholes; only ~10 m is present in south-central KNP 7, 12 and 22. Variation in the presence of Tshidize Formation may be due to erosion prior to deposition of the Madzaringwe Formation, but is most likely caused by irregular fluvio-glacial deposition across a landscape characterized by small hills and ridges (Stagman, 1978).

The Madzaringwe Formation appears to gently thicken towards the centre of the western boreholes, reaching a maximum of ~200 m in KNP 22. However, because the northern boreholes (KNP 13, 15, and 15 “Wedge”) were not drilled into the basement or Tshidize Formation, the Madzaringwe Formation could be more extensive than the 80-150 m present in these cores. Towards the south, the Madzaringwe Formation thins slightly from 150 m (KNP 8) to ~80-100 m (KNP 7 and 12A). It’s note worthy that the shortest sequence recorded (KNP 7) identifies the “Main Seam” (coal) near the top of the Madzaringwe Formation, consistent with other boreholes across the basin, meaning that the formation’s variation in thickness in this area is not due to erosion of the top of the formation prior to deposition of the Mikembeni Formation.

The basin was likely undergoing more rapid subsidence where the Madzaringwe Formation is thickest (150-180 m), near the centre of the borehole cluster. The thicker, more prevalent sandy intervals in the north indicate this portion of the basin was more proximal to source areas. The “Main Seam” and “Middle Member” markers near the top of the formation are consistently identified throughout the basin, indicating variation in thickness is intrinsic to the ancient landscape or the formation’s deposition, and not subsequent erosion.

Like the Madzaringwe Formation, the Mikembeni Formation is thickest in the central portion of the basin, and reaches a maximum of ~200 m in KNP 22. This formation thickens by 10 m northwards, while towards the south it thins dramatically to 15 m in KNP 7 before disappearing completely in the southernmost boreholes KNP 14 and 23.

The low energy deposits of the Mikembeni Formation reflect a period of quiescence in the basin, as the tectonic events which drove deposition of coarse-grained sandstone bodies in the Madzaringwe Formation ceased. Subsidence may have decreased as the result of decreasing tectonic loading. Subsequent erosion of at least one south-eastern borehole (KNP 12A) indicates subaerial erosion may have affected portions of the basin and contributed to significant thinning of the Mikembeni Formation in the south. Figure 4-1 illustrates formation variation north to south.

Trends in the Triassic strata are more difficult to summarize as identification of the Fripp, Solitude, Klopperfontein, and Elliot Formations was largely ignored by core loggers. In general, the Triassic strata are the most variable in presence and depth of all the Karoo formations in the boreholes.

The Fripp Sandstone was laid down as point bars and channel lags deposited unconformably on top of the Mikembeni Formation (Brandl, 2002). If coarse-grained basal candidate sandstones present in the Triassic sequences indeed represent the Fripp Sandstone, numerous boreholes intersect this formation (KNP 8, 10, 13, and 15). This formation was positively identified by core loggers and is thickest (~50 m) in KNP 22. The sandstone thins westward from ~60 m in KNP 15 to less than 5 m in KNP 8.

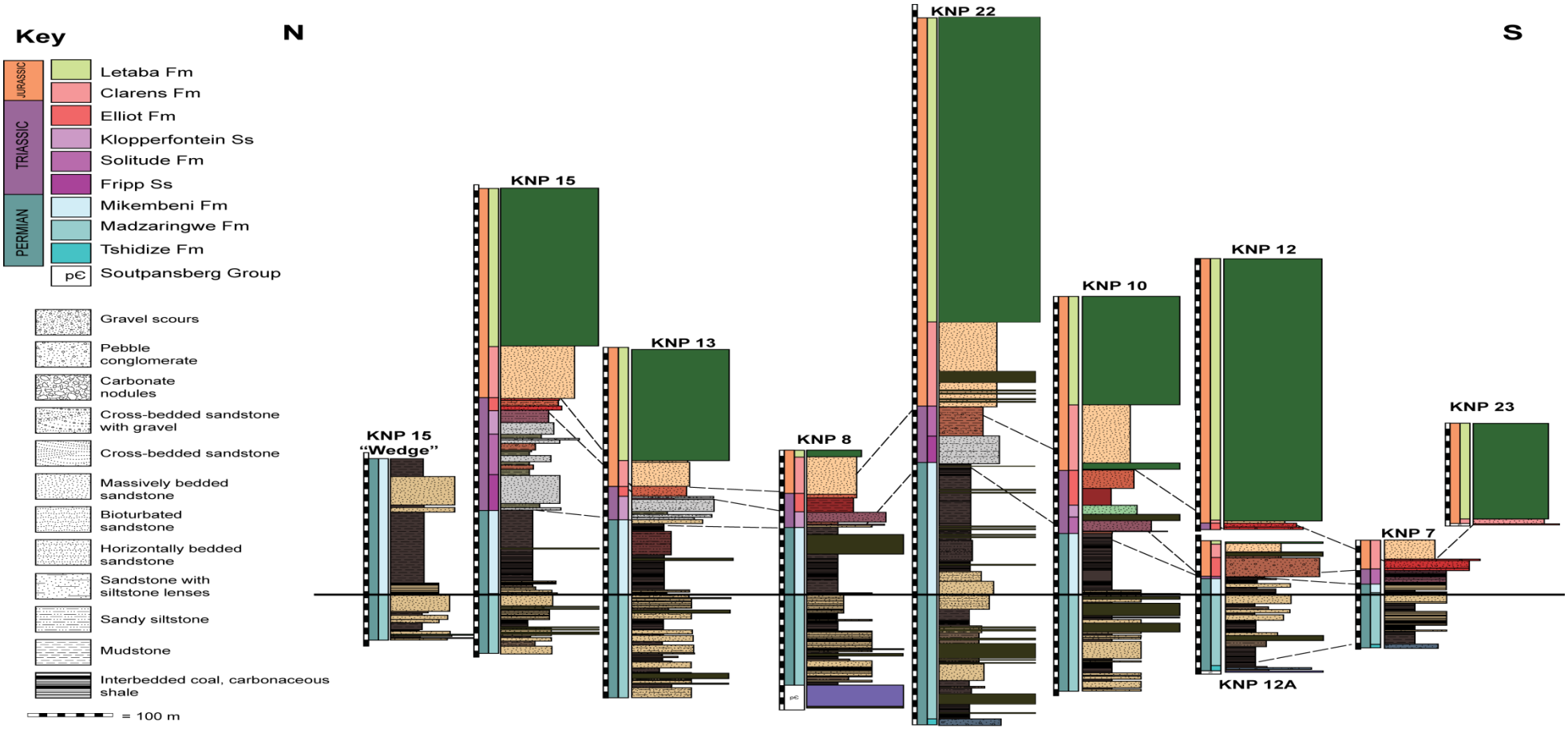

Figure 4-1: North-south transect of ten boreholes from the western cluster drilled in Kruger National Park. The stratigraphic sections are centred across the boundary between the Madzaringwe and Mikembeni Formations, as markers from the Madzaringwe noted by core loggers indicate little to no erosion of this formation.

This formation has been posited as a clastic wedge formed in response to tectonic uplift in the north (Brandl, 2002). McCourt & Brandl (1980), and Brandl (2002) report that the Fripp is thickest (125 m) at its type locality southwest of Tshipise and that it wedges out eastwards from Punda Milia (southwest of KNP 22).

McCourt and Brandl (1980) noted the Fripp Sandstone is extremely felspathic in the Tuli Basin (often in excess of 25% feldspar, (Brandl, 2002)), and is increasingly quartzitic (and correspondingly, less felspathic) in the northern part of Kruger and east of Masisi in the northern (east-west trending) arm of the Lebombo-Tshipise Basin. This distribution indicates a northwesterly granitic source area, consistent with south-east palaeocurrent data taken from the Pafuri sub-basin (Figure 3-5, Chapter 3.1.1).

The Fripp Sandstone may have been preferentially deposited in the northeastern portion of the Pafuri sub-basin as subsidence rapidly increased in response to tectonic unloading from the north. Alternatively, the Fripp Sandstone may have been preferentially eroded in the southern and western portions of the basin prior to deposition of the Solitude Formation (see KNP 7, 12A; as the underlying Mikembeni Formation is substantially shortened by erosion in these boreholes, absent overlying formations are to be expected). As underlying sediments (the Madzaringwe and Mikembeni Formations) wedge out southwards, the Fripp Sandstone's disappearance in the east may represent a transition from axial flow in the under-filled rift to transverse flow across the overfilled rift. Another possibility is thickness change along the rift axis consistent with formation of a bajada.

The Solitude Formation was only identified in KNP 12A by core loggers, but "Beaufort Group" mudrocks and siltstones were identified in several boreholes. "Beaufort" grit and mud were identified in KNP 22, though this

coarse-grained section, which contains evidence of faulting (slickensides, recementation, etc.), might actually represent a basal conglomerate known to replace the Red Rocks Member in some areas of the basin as described by McCourt and Brandl (1980). The Solitude or undifferentiated “Beaufort Group” is thickest in KNP 15 and wedges out to the south and east.

The Solitude Formation mudrocks and overbank deposits represent another period of quiescence in the basin. Trends in thickness (wedging out in the south and east) could be the result of palaeotopogphy, subsequent erosion prior to deposition of the overlying Klopperfontein Sandstone, or a continuation of transverse deposition across an overfilled rift.

The Klopperfontein Sandstone was deposited unconformably on top of the Solitude Formation and is thought to have formed in response to renewed tectonism in the north and syndepositional scarp development (Brandl, 2002). The sandstone thins west and southwards from a maximum of ~40 m in KNP 15 to ~15-20 m in KNP 8 and 10. The formation is approximately 20 m thick in the Kruger National Park (McCourt and Brandl, 1980). These authors note that the formation is thinner, ~10 m, but coarse-grained and gritty with “abundant” pink feldspar, east of Tshipise. Brandl (2002) notes that in the “extreme west” the formation is very thin or absent. Southwest-wards thinning of the formation is consistent with the northeast rift flank, which fits the coarse, braid-channel nature of the deposits.

De Jager (1983) identified the Klopperfontein Sandstone as a contemporary of the Molteno Formation in the Main Karoo Basin, which has also been noted by subsequent researchers (Chidley, 1985; Johnson, 1994; Johnson et al., 1996; Brandl, 2002; Catuneanu et al., 2005). As the Molteno Formation in the main Karoo Basin represents a northwards thinning, clastic wedge sourced from the Cape Fold Belt (Catuneanu et al.,

2005), the Molteno Formation does not share the same source area as the Klopperfontein Sandstone. Should the two formations represent synchronous deposition, we can broadly state that the Lebombo-Tshipise and other northern, peripheral basins were undergoing rift flank uplift at the same time as orogenic uplift in the Main Karoo Basin. As the southern basin was compressed, northern impactogens extended. Further studies might focus on uncovering the link between compressive tectonism in southern Africa and scarp genesis in the north, where progressively south-moving extensional tectonism dominated the landscape (Catuneanu et al., 2005).

The siltstones and mudrocks of the Elliot Formation are thickest in KNP 8 and 10 and in Makanya Hill field area (~20-30 m). Though the siltstones and mudrocks do not crop out well at Makanya Hill, sauropodomorph fossils from the field site are morphologically consistent with Elliot Formation fauna in the Main Karoo Basin (see Chapter 3.2.1 for more detailed descriptions of recovered fossils).

Ephemeral fluvial, loessic and aeolian deposits that resemble the Red Rocks Member have been described from the upper Elliot Formation in other basins (Visser and Botha, 1980; Eriksson 1983; 1986; Smith et al., 1993; Bordy et al., 2004b, Bordy & Eriksson 2015). A thick, red and beige sandstone body representing the Red Rocks Member appears to overlie the silts and mudrocks of the Elliot Formation in KNP 8, 10, 13 and 15. The southernmost basins contain 10-20 m of red fine-grained sandstones; these are the only Karoo Supergroup formations in the southern margin of the Pafuri sub-basin and directly overlie Precambrian basement. Their presence indicates the extent of subsidence in the basin increased southwards during the latest Triassic.

The Red Rocks Member is described by McCourt and Brandl (1980) as being replaced by conglomerates in several boreholes. At Makanya Hill

there are no red sandstone units consistent with the Red Rocks Member; instead siltstones and mudrocks of the Elliot Formation are overlain by ~25 m of coarse-grained, cross-bedded sandstones with basal conglomerate channel scours and east-flowing palaeocurrents (FA III). Similar conglomerates in Makuya Reserve west of the Makanya Hill field locality interfinger with bioturbated, flooded interdune deposits (FA XI), instead of aeolian dune deposits (FA X) like at Makanya Hill. The conglomerates and sandstones crop out at the base of the Clarens at Makanya Hill, but at Makuya Reserve, these coarse-grained deposits crop out near the top of the Clarens Formation. Possibly, capping aeolian Clarens sediments have been eroded in the west at Makuya Reserve, and these coarse sandstones and conglomerates are stratigraphically equivalent to those at Makanya Hill. Alternatively, this distribution could represent a stream-dominated alluvial fan shifting west-ward during the early Jurassic, or that wetter conditions resulted in bioturbation near active braided fluvial systems in the west, while bioturbation primarily took place in physical and temporal proximity to ephemeral flooding events in the east.

At the southern end of the boreholes, conglomerates in KNP 7 are composed of quartzite pebbles, calcareous concretions and occasional mudrock rip-ups. The succession has numerous sharp, “downcutting” contacts which evoke channel lags deposited in high energy fluvial successions. Similar conglomerates in KNP 12, 12A, and 22 are present and likely represent the same fluvial facies association at Makanya Hill and Makuya Reserve.

McCourt and Brandl (1980) suggest the Red Rocks Member may be a lateral correlative to the poorly developed Elliot Formation which is only sporadically present in the Kruger National Park. Eriksson and Bordy (2015) likewise have included the Red Rocks Member in the Elliot Formation. However, the Red Rocks member is described as lithologically identical to the overlying Tshipise Member of the Clarens Formation which

it gradationally overlies (McCourt and Brandl, 1980). The only differentiable aspect of the Red Rocks and Tshipise members are their respective red and beige colours. Colour is a notoriously poor quality to divide lithological units, as the characteristic color of many Triassic red beds has been shown to be a diagenetic feature and, therefore not an intrinsic quality of the sediment itself (Turner, 1980). The contact between these two members is described by McCourt and Brandl (1980) as “gradual”, implying no hiatus in deposition. In terms of depositional environments, the Red Rocks type locality preserves similar desert environments to those present in the Tshipise Member outcrop at Makanya Hill field locality, which contrasts with the fluvial sandstones and floodplain siltstones and mudstones of the Elliot Formation described from numerous African basins (Bordy, 2004 a, b, c; Catuneau et al., 2005). Contact between the Red Rocks Member and the Elliot Formation was not observed in the field and has not been described in the literature.

The beige, cream-coloured Tshipise Member of the Clarens gradually overlies the Red Rock Member sandstones or conglomerates in all the eastern boreholes except for KNP 22 where it overlies multicolored mudrocks, siltstones and grits identified as “Beaufort” sediments. This central area of the basin may have experienced erosion during the early Late Triassic which removed the Klopperfontein Sandstone and Elliot Formation. Deposition of the Clarens Formation then took place when rapid subsidence resumed in the Early Jurassic.

The distribution of late Triassic and early Jurassic formations indicates that Elliot Formation siltstones and mudrocks were only deposited in the deepest portions of the basin. Renewed tectonism then formed multiple alluvial fans along the northern and eastern margins of the basin where coarse-grained grits, conglomerates and sandstones were deposited. This tectonic activity is correlated with a southwards increase in basin subsidence as Red Rock Member aeolianites were deposited in a newly

subsiding southern portion of the Pafuri sub-basin. Fluvial flows measured from the Red Rocks field locality reflect rapid subsidence towards the west along the large fault which separates the eastern from the western boreholes.

Following this last spasm of tectonic activity, the dune fields of the Tshipise Member of the Clarens Formation blanketed the topography. However, in the southernmost portion of the basin, either rapid erosion of these deposits, scarp development cut off deposition in this part of the basin, or changes in subsidence affected deposition here. Soft sediment deformation structures observed in the Clarens Formation at Makanya Hill field locality and by Bordy (2008) have been attributed to sediment saturation, but the tee-pee like structures could also be interpreted as seismites and suggest tectonic activity continued during Clarens Formation deposition, as suggested by Bordy and Catuneanu (2001) and Bordy (2008).

Chapter 5: Conclusions

The Limpopo Mobile belt, sandwiched between the Kaapvaal Craton to the south and the Zimbabwe Craton in the north, has a long history of deformation which has been associated with the location and formation of the Lebombo-Tshipise basin (Cox, 1970). By the end of the Palaeozoic, this area had been tectonically quiet and had undergone erosion for hundreds of millions of years, likely resulting in an uneven topography (Cox et al., 1965; Stagman, 1978) which influenced subsequent Karoo deposition. This explains many absences of the otherwise thin Tshidize Formation throughout the Pafuri sub-basin, with variations in thickness due to the nature of fluvioglacial deposits and possibly some erosion prior to deposition of the swamps, lakes, and river systems of the Madzaringwe Formation.

While the Madzaringwe Formation has many coarse-grained, micaceous fluvial and lacustrine sandstone bodies, the Mikembeni Formation is characterized by significantly more mud and fines than sandstones (see borehole stratigraphic columns in Appendix A). The Mikembeni Formation varies in thickness across the basin, though this variation is most noticeable in the eastern boreholes where erosion has removed much of the sediment and overlying formations. The southern and eastern-most boreholes of the western cluster in addition to displaying evidence of subaerial erosion of the Mikembeni Formation, contain truncated overlying Triassic sequences; these boreholes may represent basin flanks or horsts. However, the Madzaringwe Formation is fairly uniform in thickness across the boreholes indicating a period of steady subsidence, coincident with findings of Malaza et al. (2016) of rapid subsidence dominating the Permian in the Tshipise and Pafuri sub-basins.

The arenaceous Fripp Sandstone marks renewed tectonism at the beginning of the Triassic in the area, where a granitic source was uplifted

to the northwest and a clastic wedge built into the basin. Thickness changes from north to south may represent a bajada-type morphology where thickness varies along the basin axis, or preferential erosion as southern portions of the basin is where the underlying Mikembeni is truncated and shows evidence of subaerial weathering.

The mudrocks, siltstones, and occasional sandstone bodies of the Solitude Formation represent quiescence in the basin and a return to steady subsidence, coincident with Malaza et al.'s (2016) second period of rapid subsidence as determined by backstripping. Variations of the strata in the western boreholes can be attributed to erosion or non-deposition in the southernmost boreholes, and flank or horsts in the eastern-most boreholes where the formation is often present but thin.

The Klopperfontein Formation represents another period of tectonism and flank uplift. Syndepositional scarp formation at this time may have been the driver of other faulting in the basin, and perhaps the cause of the apparent vertical offset of the western and eastern boreholes. The Klopperfontein Formation is thickest in the northern portion of the eastern boreholes, but missing or thin along the eastern margin, where either the clastic wedge was not deposited due to topographic highs, or where it has been subsequently eroded.

Deposition of the mudrocks and palaeosols of the Elliot Formation represent a return to subsidence in the basin coincident with the first of two slow subsidence phases identified by Malaza et al. (2016). Geochemical analyses indicate deposition of the Elliot Formation occurred under subtropical conditions and massive weathering. The environment appears to have been wetter than that recorded from this formation in the Main Karoo Basin. Fossil discoveries suggest conditions were wet enough to support large sauropodomorph dinosaurs and trees.

If the Red Rocks unit formerly of the Clarens Formation actually represents the Elliot Formation, this period of subsidence represents the southernmost extent of sedimentation in the Pafuri sub-basin. While aeolian facies of the Red Rocks field locality indicate desert conditions, exceptional preservation of trace fossils show conditions capable of supporting significant invertebrate communities.

Conglomerate units at the base of the Clarens Formation from the Makanya Hill and Makuya Reserve field areas and KNP 7, 12, 12A indicate high energy alluvial fan building episodes at this time. As these conglomerates appear to interfinger with the bioturbated interdune facies (FA XI) of the Clarens' Formation at Makuya Hill, further research could be aimed at fully explaining the timing of this period of apparent tectonic renewal that has received little attention from past researchers.

The dune fields of the Tshipise Member of the Clarens Formation were deposited during the second subsidence phase of the Early Jurassic described by Malaza et al. (2016). As this formation is not found in the southern-most eastern basins, the aerial extent of sedimentation decreased at this time, or the dunes were eroded prior to eruption of the Letaba Formation lavas. While facies associations consistent with aeolian dunes comprise the majority of outcrop in this formation, bioturbated interdune deposits and soft sediment deformation features indicate the desert was subjected to wet conditions during deposition.

References

Ahlbrandt, T.S., & S.G. Fryberger. 1981. Sedimentary features and significance of interdune deposits, In: Recent and Ancient Nonmarine Depositional Environments: models for exploration (Eds: F.G. Ethridge and R.M. Flores). Society of economic paleontology and mineralogy, Tulsa, Oklahoma, Special Publication 31: 293-314

Akarish, A.L. & A.M. El-Gohary. 2011. Pre-Cenonmanian sandstones, East Sinai, Egypt. *Journal of Applied Sciences* 11(17), 3070-3088.

Aldiss, D. T., Benson, J. M., & C.C. Rundle. 1984. Early Jurassic pillow lavas and palynomorphs in the Karoo of eastern Botswana. *Nature*, 310(5975), 302-304.

Allain, R., & N. Aquesbi. 2008. Anatomy and phylogenetic relationships of *Tazoudasaurus naimi* (Dinosauria, Sauropoda) from the late Early Jurassic of Morocco. *Geodiversitas*, 30(2), 345-424.

Allain, R., Aquesbi, N., Dejax, J., Meyer, C., Monbaron, M., Montenat, C., Richir, P., Rochdy, M., Russell, D. & P. Taquet. 2004. A basal sauropod dinosaur from the Early Jurassic of Morocco. *Comptes Rendus Palevol*, *3*(3), 199-208.

Allsopp, H. L., Manton, W. I., Bristow, J. W., & A.J. Erlank. 1984. Rb-Sr geochronology of Karoo felsic volcanics. Petrogenesis of the volcanic rocks of the Karoo Province. *Special Publications of the Geological Society of South Africa*, 13, 273-280.

Anderson J.M., & H.M. Anderson. 1985. Palaeoflora of southern Africa. Devonian to Lower Cretaceous. A.A., Balkema, Rotterdam, the Netherlands, 423 p.

Archangelsky, S., & Brett, D. W. 1961. Studies on Triassic fossil plants from Argentina. I. Rhexoxylon from the Ischigualasto Formation. *Philosophical Transactions of the Royal Society of London B: Biological Sciences*, 244(706), 1-19.

Artabe, A. E., Brea, M., & A.B. Zamuner. 1999. *Rhexoxylon brunoi* Artabe, Brea et Zamuner, sp. nov., a new Triassic corystosperm from the Paramillo de Uspallata, Mendoza, Argentina. Review of Palaeobotany and Palynology, 105(1), 63-74.

Bahlburg, H., & N. Dobrzinkski. 2011. A review of the Chemical Index of Alteration (CIA) and its application to the study of Neoproterozoic glacial deposits and climate transitions. *Geological Society, London, Memoirs* 36(1), 81-92.

Bamford, M.K. 1999 Permo-Triassic fossil woods from the South African Karoo Basin. *Palaeontologia africana*, 35, 25-40.

Bamford, M.K. 2004. Diversity of the woody vegetation of Gondwanan southern Africa. *Gondwana Research* 7, 153-164

Bao, H., Koch, P. L., & R. P. Hepple. 1998. Hematite and calcite coatings on fossil vertebrates. *Journal of Sedimentary Research*, *68*(5).

Barrett, P. M. 2004. Sauropodomorph dinosaur diversity in the upper Elliot Formation (Massospondylus range zone: Lower Jurassic) of South Africa: research letter. *South African Journal of Science*, *100*(9-10), 501-503.

Barrett, P. M. 2009. A new basal sauropodomorph dinosaur from the upper Elliot Formation (Lower Jurassic) of South Africa. *Journal of Vertebrate Paleontology*, *29*(4), 1032-1045.

Benson, R. B., Campione, N. E., Carrano, M. T., Mannion, P. D., Sullivan, C., Upchurch, P., & D. C. Evans. 2014. Rates of dinosaur body mass evolution indicate 170 million

years of sustained ecological innovation on the avian stem lineage. *PLoS Biology* 12(5), e1001853.

Benton, M. J., & Harper, D. A. (1997). *Basic palaeontology*. Prentice Hall.

Beukes, N.J. 1970. Stratigraphy and sedimentology of the Cave Sandstone stage, Karoo System. In Haughton S.H., (ed.), Proceedings and Papers, 2nd Gondwana Symposium, Pretoria, South Africa. p. 321-342

Bialik, O. M., Korngreen, D., & C. Benjamini. 2013. Carnian (Triassic) aridization on the Levant margin: evidence from the M1 member, Mohilla Formation, Makhtesh Ramon, south Israel. *Facies*, *59*(3), 559-581.

Bond, D. P., & P. B. Wignall. 2010. Pyrite framboid study of marine Permian–Triassic boundary sections: a complex anoxic event and its relationship to contemporaneous mass extinction. *Geological Society of America Bulletin*, *122*(7-8), 1265-1279.

Bonis, N.R., Kürschner, W.M., & L. Krystyn. 2009. A detailed palynological study of the Triassic-Jurassic transition in key sections of the Eiberg basin (Northern Calcareous Alps, Austria). *Review of Palaeobotany and Palynology* 156, 376-400

Bonis, N.R., Ruhl, M., & W.M. Kürschner. 2010. Climate change driven black shale deposition during the end-Triassic in the western Tethys. *Palaeogeography, Palaeoclimatology, Palaeoecology, 290, 151-159*

Bordy, E.M. 2000. Sedimentology of the Karoo Supergroup in the Tuli Basin (Limpopo River area, South Africa) PhD thesis, Rhodes University

Bordy, E.M. 2008 Enigmatic trace fossils from the aeolian Lower Jurassic Clarens Formation, Southern Africa. *Palaeontologia Electronica* Vol. 11, Issue 3; 16A: 16p

Bordy, E. M. & O. Catuneanu 2001. Sedimentology of the upper Karoo fluvial strata in the Tuli Basin, South Africa. *Journal of African Earth Sciences* 33: 605–629.

Bordy, E. M.,& O. Catuneanu. 2002a. Sedimentology and palaeontology of upper Karoo aeolian strata (Early Jurassic) in the Tuli Basin, South Africa. *Journal of African Earth Sciences*, *35*(2), 301-314.

Bordy, E. M. &O. Catuneanu 2002b. Sedimentology of the lower Karoo Supergroup fluvial strata in the Tuli Basin, South Africa. *Journal of African Earth Sciences* 35(4):503-521.

Bordy, E. M. & O. Catuneanu. 2002c. Sedimentology of the Beaufort-Molteno Karoo fluvial strata in the Tuli Basin, South Africa. *South African Journal of Geology*, *105*(1), 51-66.

Bordy, E. M., Hancox, P. J. & B. S. Rubidge. 2004a. A description of the sedimentology and palaeontology of the Late Triassic-Early Jurassic Elliot Formation in Lesotho. *Palaeontologia Africana* 40: 43-56

Bordy, E. M., Hancox, P.J. & B. S. Rubidge. 2004b. Basin development during the deposition of the Elliot Formation (Late Triassic–Early Jurassic), Karoo Supergroup, South Africa. *South African Journal of Geology* 107: 397–412.

Bordy, E.M., Hancox, P.J., & Rubidge, B.S. 2004c. Fluvial style variations in the Late Triassic-Early Jurassic Elliot Formation, main Karoo Basin, South Africa. *Journal of African Earth Sciences*, 38, 383-400.

Bordy, E. M., Hancox, P. J. & B. S. Rubidge. 2005. The contact of the Molteno and Elliot Formations through the main Karoo Basin, South Africa: a second-order sequence boundary. *South African Journal of Geology* 108: 351–364.

Bordy, E. M., Prevec, R. & C. Makhwelo. 2006. Late Triassic (Norian) palaeoecosystems of the lowermost Elliot Formation (Salpeterberg, Eastern Cape, South Africa). A century of research at Petrified Forest National Park: geology and paleontology. W. G. Parker, S. R. Ash and R. B. Irmis, Museum of Northern Arizona Bulletin. 62.

Bordy, E. M. 2008. Enigmatic trace fossils from the aeolian lower Jurassic Clarens Formation, Southern Africa. *Palaeontologia Electronica*, 11, 16a-16p.

Bordy, E. M. & R. Prevec. 2008. Sedimentology, palaeontology and palaeo-environments of the Middle (?) to Upper Permian Emakwezini Formation (Karoo Supergroup, South Africa). *South African Journal of Geology*, *111*(4), 429-458.

Bordy, E. M., Knoll, F. & A. Bumby. 2010. New data on the palaeontology and sedimentology of the Lower Jurassic Lisbon Formation (Karoo Supergroup), Ellisras Basin, South Africa. *Neues Jahrbuch für Geologie und Paläontologie-Abhandlungen*, *258*(2), 145-155.

Bordy, E.M., Segwabe, T., & B. Makuke. 2010. Sedimentology of the Upper Triassic–Lower Jurassic (?) Mosolotsane Formation (Karoo Supergroup), Kalahari Karoo Basin, Botswana. *Journal of African Earth Sciences* 58.1: 127-140.

Bordy, E.M. & P. Eriksson. 2015. Lithostratigraphy of the Elliot Formation (Karoo Supergroup), South Africa. *South African Journal of Geology* 118(3), 311-316.

Boulton, G., & M. Deynoux. 1981. Sedimentation in glacial environments and the identification of tills and tillites in ancient sedimentary sequences. *Precambrian Research*, 15(3-4), 397-422.

Brandl, G. 2002. The geology of the Alldays area. Explanation Sheet 2228 Scale: 1:250,000. Council for Geoscience. 71p.

Bristowe, A., & M.A. Raath. 2004. A juvenile coelophysoid skull from the Early Jurassic of Zimbabwe, and the synonymy of *Coelophysis* and *Syntarsus*. *Palaeontologica Africana* 40: 31-41

Britt, B. B., Chure, D. J., Engelmann, G. F. & J.D. Shumway. 2016. Rise of the erg—paleontology and paleoenvironments of the Triassic-Jurassic transition in northeastern Utah. *Geology of the Intermountain West*, 3, 1-32.

Bromley, R.G. & U. Asgaard. 1979. Triassic freshwater ichnocoenoses from Carlsberg Fjord, East Greenland: *Palaeogeography, Palaeoclimatology, Palaeoecology*, v. 28, p. 39–80.

Brusatte, S. L., Benton, M. J., Ruta, M., & G.T. Lloyd. 2008. The first 50 Myr of dinosaur evolution: macroevolutionary pattern and morphological disparity. *Biology Letters*, 4(6), 733-736.

Buatois, L. A., & M.G. Mángano. 2011. Ichnology: Organism-substrate interactions in space and time. Cambridge University Press.

Burke, K., & J.F. Dewey. 1973. Plume-generated triple junctions: key indicators in applying plate tectonics to old rocks. *The Journal of Geology*, 406-433.

Butler, R. J., Smith, R. M., & D.B. Norman. 2007. A primitive ornithischian dinosaur from the Late Triassic of South Africa, and the early evolution and diversification of Ornithischia. *Proceedings of the Royal Society of London B: Biological Sciences*, *274*(1621), 2041-2046.

Cadle, A. B., Cairncross, B., Christie, A. D. M., & D.L. Roberts. 1993. The Karoo Basin of South Africa: type basin for the coal-bearing deposits of southern Africa. *International Journal of Coal Geology*, *23*(1-4), 117-157.

Cairncross, B., & A.B. Cadle. 1987. A genetic stratigraphy for the Permian coal-bearing Vryheid Formation in the east Witbank Coalfield, South Africa. *South African Journal of Geology*, *90*(3), 219-230.

Catuneanu, O., Beaumont, C., & P. Waschbusch. 1997. Interplay of static loads and subduction dynamics in foreland basins: Reciprocal stratigraphies and the “missing” peripheral bulge. Geology, 25(12), 1087-1090.

Catuneanu, O., Hancox, P. J., & B.S. Rubidge. 1998. Reciprocal flexural behaviour and contrasting stratigraphies: a new basin development model for the Karoo retroarc foreland system, South Africa. *Basin Research*, *10*(4), 417-439.

Catuneanu, O., & H.N. Elango. 2001. Tectonic control on fluvial styles: the Balfour Formation of the Karoo Basin, South Africa. *Sedimentary Geology*, *140*(3), 291-313.

Catuneanu, O. 2004. Basement control on flexural profiles and the distribution of foreland facies: The Dwyka Group of the Karoo Basin, South Africa. *Geology*, 32(6), 517-520.

Catuneanu, O., Wopfner, H., Eriksson, P.G., Cairncross, B., Rubidge, B.S., Smith, R.M.H., & P.J. Hancox. 2005. The Karoo basins of south-central Africa. *Journal of African Earth Sciences*, 43, 211-253.

Chidley, C.M. 1985. The geology of the country around Evangelina and Pontdrift (1:50000 Sheets 2228BD & 2229A). Unpublished South African Geological Survey Report. Pietersburg, South Africa.

Cloeting, S., de Wit, M.J., Lankrcijer, A. & I. Martinez. 1992. Subsidence history analysis and forward modeling of the Cape and Karoo Supergroups, In: Inversion Tectonics of the Cape Fold Bell, Karoo and Cretaceous Basins of Southern Africa, (eds. M. J. de Wit and I. G.U. Ransome). Batkema. Rotterdam, the Netherlands. 239-248 pp

Colson, J. & I. Cojan. 1996. Growndwater dolocretes in a lake-marginal environment: An alternative model for dolocrete formation in continental settings (Danian of the Provence Basin, France). *Sedimentology* 43: 175-188

Cooper, M. R. 1981. The prosauropod dinosaur *Massospondylus carinatus* Owen from Zimbabwe: its biology, mode of life and phylogenetic significance. *Occasional Papers of the National Museums and Monuments of Rhodesia B, Natural Sciences*, 6: 689–840.

Counts, J. W., & S.T. Hasiotis. 2009. Neoichnological experiments with masked chafer beetles (Coleoptera: Scarabaeidae): Implications for backfilled continental trace fossils. *Palaios*, 24(2), 74-91.

Cox, K.G. 1970. Tectonics and volcanism of the Karoo period. In: African magmatism and tectonics, (eds. T.N. Clifford and I.G. Gass). Oliver & Boyd Press, Edinburgh, Scotland, 211-236 pp

Cox, K. G., Johnson, R. L., Monkman, L. J., Stillman, C. J., Vail, J. R., & D.N. Wood. 1965. The geology of the Nuanetsi igneous province. *Philosophical Transactions of the Royal Society of London A: Mathematical, Physical and Engineering Sciences*, *257*(1078), 71-218.

Cox, K.G. 1989. The role of mantle plumes in the development of continental drainage patterns. *Nature* 342, 873-877.

Cox, R., Lowe, D.R., & R.L. Cullers. 1995. The influence of sediment recycling and basement composition of evolution of mudrock chemistry in the southwestern United States. *Geochimica et Cosmochimica Acta* 59, 2919-2940

Crompton, A. W. & A. J. Charig. 1962. A new Ornithischian from the Upper Triassic of South Africa. *Nature* 4859: 1074–1077.

Crompton, A.W. & F.A. Jenkins. 1968. Molar occlusion in Late Triassic mammals. *Biological Reviews*, 43: 427–458. doi: 10.1111/j.1469-185X.1968.tb00966.x

Day, M. O., Ramezani, J., Bowring, S. A., Sadler, P. M., Erwin, D. H., Abdala, F., & B.S. Rubidge. 2015. When and how did the terrestrial mid-Permian mass extinction occur? Evidence from the tetrapod record of the Karoo Basin, South Africa. In *Proceedings of the Royal Society B* (Vol. 282, No. 1811, p. 20150834).

de Jager, F.S.J. 1983a. Coal reserves of the Republic of South Africa – an evaluation at the end of 1982. *Bulletin of the Geological Survey of South Africa*, 74, 17pp.

de Jager, F.S.J., 1983b. The Geology of the Springbok Flats, Waterberg, Soutpansberg and Limpopo Coal Fields (with an addendum on the geology of the Komatipoort coal field). – Unpublished Report 1983-0120, 11 pp.; Pretoria (South African Geological Survey).

de Wit, M.J., Jeffery, M., Nicolaysen, L.O.N.,& H. Bergh. 1988. Explanatory notes on the Geologic Map of Gondwana. *American Association Petroleum Geol*ogy, Tulsa

de Wit, M.J., & I.G.D. Ransome. 1992. Regional inversion tectonics along the southern margin of Gondwana. In: Inversion Tectonics of the Cape Fold Belt, Karoo and Cretaceous Basins of Southern Africa, (eds. de Wit, M.J., Ransome, I.G.D.). Balkema, Rotterdam, Edinburgh, London, 611 p.

Du Toit, A.L. 1954. Geology of South Africa. Oliver and Boyd, Edinburgh, London, 611 p.

Duncan A.R., & J.S. Marsh. 2006. The Karoo Igneous Province In: The Geology of South Africa, (eds. Johnson M.R., Anhaeusser C.R. and Thomas R.J.). Geological Society of South Africa, Johannesburg/Council for Geoscience, Pretoria, 501-520.

Durand, J.F. 1996. First vertebrate fossil discovery in the Kruger National Park. *South African Journal of Science*, 92, 302.

Durand, J.F. 2001. The oldest juvenile dinosaurs in Africa. Journal of African Earth Sciences, 33, 597-603.SAHRA (2014) www.sahra.org.za/fossil-layers/nyoka-formation Accessed 30 October 2014.

Durand, J.F. 2012. Proposed Diamond mine adjacent to Venetia Mine, Limpopo Province. Scoping report Palaeontology compiled for G&A Heritage. May 18, 2012.

Ekdale, A. A., R. G. Bromley, & D. B. Loope. 2007. Ichnofacies of an ancient erg: a climatically influenced trace fossil association in the Jurassic Navajo Sandstone,

southern Utah, USA, In: Miller W., ed., Trace Fossils: Concepts, Problems, Prospects. Elsevier, Amsterdam: 562-574

Eriksson, P.G. 1979. Mesozoic sheetflow and playa sediments of the Clarens Formation in the Kamberg area of the Natal Drakensberg. *Transactions Geologic Society of South Africa* 83: 257–258

Eriksson, P.G. 1981. A palaeoenvironmental analysis of the Clarens Formation in the Natal Drakensberg. *Transactions of the Geological Society of South Africa*, 84:7-17

Eriksson, P.G. 1982 Palaeoenvironmental Study of the Molteno, Elliot, and Clarens Formations in the Natal Drakensberg and Northeastern Orange Free State. Unpublished PhD thesis, University of Natal, South Africa 109 pp

Eriksson, P.G. 1983. Palaeoenvironmental Study of the Molteno, Elliot and Clarens Formations in the Natal Drakensberg and Northeastern Orange Free State. Ph.D. Thesis, University of Natal, South Africa, 209pp

Eriksson, P.G. 1985. The depositional environment of the Elliot Formation in the Natal Drakensberg and north-east Orange Free State. *Transactions of the Geological Society of South Africa* 88, 19-26

Eriksson, P.G. 1986. Aeolian dune and alluvial fan deposits in the Clarens Formation of the Natal Drakensberg. *Transactions of the Geological Society of South Africa*, 89:389-394

Erwin, D. H. 2009. Climate as a driver of evolutionary change. *Current Biology*, *19*(14), R575-R583.

Faure, K., Armstrong, R. A., Harris, C., & J.P. Willis. 1996. Provenance of mudstones in the Karoo Supergroup of the Ellisras basin, South Africa: geochemical evidence. *Journal of African Earth Sciences*, *23*(2), 189-204.

Fitch, F. J. & J. A. Miller. 1984. Dating Karoo igneous rocks by the conventional K-Ar and $^{40}Ar/^{39}Ar$ age spectrum methods.

Friedmann, E.I. & M. Galun. 1974. Desert algae, lichens, and fungi. In: Desert biology: Special Topics on the Physical and Biological Aspects of Arid Regions, Volume II. (eds. Brown, Jr. G.W.) Academic Press, New York, pp. 165–212.

Galton, P. M. & J. Van Heerden. 1998. Anatomy of the prosauropod dinosaur *Blikanosaurus cromptoni* (Upper Triassic, South Africa), with notes on the other tetrapods from the Lower Elliot Formation. Palaontologische Zeitschrift 72: 163–177.

Galton, P. M., J. Van Heerden & A. M. Yates. 2005. Postcranial anatomy of referred specimens of the sauropodomorph dinosaur *Melanorosaurus* from the Upper Triassic of South Africa, In: Thunder-lizards: the sauropodomorph dinosaurs (eds. V. Tidwell and K. Carpenter). Bloomington, Indiana University Press: 1-37.

Gastaldo, R. A., Adendorff, R., Bamford, M., Labandeira, C. C., Neveling, J. & H. Sims. 2005. Taphonomic trends of macrofloral assemblages across the Permian–Triassic boundary, Karoo Basin, South Africa. *Palaios*, *20*(5), 479-497.

Goldberg, K., & M. Humayun. 2010. The applicability of the Chemical Index of Alteration as a paleoclimatic indicator, an example from the Permian of the Paraná Basin, Brazil. *Palaeogeography, Palaeoclimatology, Palaeoecology* 293(1), 175-183.

Good, T. R. & A.A. Ekdale. 2014. Paleoecology and taphonomy of trace fossils in the eolian Upper Triassic/Lower Jurassic Nugget Sandstone, Northeastern Utah. *Palaios*, 29(8), 401-413.

Götz, A.E., Ruckwied, K., Pálfy, J., & J. Haas. 2009 Palynological evidence of synchronous changes within the terrestrial and marine realm at the Jurassic boundary (Csövár section, Hungary). *Review of Paleobotany and Palynology* 156, 401-409

Gow, C. E. 2000. The skull of *Protosuchus haughtoni*, an early Jurassic crocodyliform from southern Africa. *Journal of Vertebrate Paleontology* 20(1): 49–56.

Groenewald, P.B., Grantham, G.H., and Watkeys, M.K., 1991. Geological evidence for a Proterozoic to Mesozoic link between south-eastern Africa and Dronning Maud Land, Antarctica. Journal of the Geological Society of London, 148: 1115-1123

Hancox, P. J., & A.E. Götz. 2014. South Africa's coalfields—A 2014 perspective. *International Journal of Coal Geology*, *132*, 170-254.

Hansma, J., Tohver, E., Schrank, C., Jourdan, F., & D. Adams. 2016. The timing of the Cape Orogeny: New 40 Ar/39 Ar age constraints on deformation and cooling of the Cape Fold Belt, South Africa. *Gondwana Research*, *32*, 122-137.

Hawkesworth C., Kelly, S., Turner, S., leRoex, A., & B. Storey. 1999. Mantle processes during Gondwana break-up and dispersal. *Journal of African Earth Sciences* 28, 239-261

Herries, R.D. 1993. Contrasting styles of fluvial-aeolian interaction at a downwind erg margin: Jurassic Kayenta-Navajo Transition, Northeastern Arizona, USA. In: Characterization of Fluvial and Aeolian Reservoirs (eds. C.P. North and J.D. Prosser), Geological Society of London Special Publication 73: 199-218

Hooper, P. R., Rehacek, J., Duncan, R. A., Marsh, J. S., & A.R. Duncan. 1993. The basalts of Lesotho, Karoo province, southern Africa. *EOS, Transactions of the American Geophysical Union*, *74*, 553.

Irmis, R. B., & J. H. Whiteside. 2012. Delayed recovery of non-marine tetrapods after the end-Permian mass extinction tracks global carbon cycle. In *Proceedings of the Royal Society B* (Vol. 279, No. 1732, pp. 1310-1318).

Jin, Z., Li, F., Cao, J., Wang, S., & J. Yu. 2006. Geochemistry of Daihai Lake sediments, Inner Mongolia, north China, implications for provenance, sedimentary sorting, and catchment weathering. *Geomorphology* 80(3), 147–163.

Johnson, M. R. 1976. Stratigraphy and sedimentology of the Cape and Karoo sequences in the Eastern Cape Province. Unpublished PhD thesis, Rhodes University, Grahamstown, South Africa.

Johnson, M. R. 1991. Sandstone petrography, provenance and plate tectonic setting in Gondwana context of the southeastern Cape-Karoo Basin. *South African Journal of Geology*, *94*(2-3), 137-154.

Johnson, M.R. 1994. Lexicon of South African Stratigraphy. Part 1: Phanerozoic Units. Publication, South African Committee for Stratigraphy. Council for Geoscience Pretoria, 56 p.

Johnson, M.R., Van Vuuren, C.J., Hegenberger, W.F., Key, R. & U. Show. 1996. Stratigraphy of the Karoo Supergroup in southern Africa: an overview. *Journal of African Earth Sciences* 23(1): 3-15

Johnson, M. R., Van Vuuren, C. J., Visser, J. N. J., Cole, D. I., Wickens, H. D. V., Christie, A. D. M., & D.L. Roberts. 1997. The Foreland Karoo Basin, South Africa. *Sedimentary basins of the world*, *3*, 269-317.

Johnson, M. R., Anhauesser, C. R., & R.J. Thomas. 2006. The Geology of South Africa. Geological Society of South Africa. 691 pp.

Jordan, T.E, Flemings, P.B. & J.A. Beers. 1988. Dating Thrust-Fault Activity by Use of Foreland-Basin Strata. In: New Perspectives in Basin Analysis, (eds. K. Kleinspehn, K. and C. Paola). Springer-Verlag, 307-330.

Keyser, A. W. 1966. Some indications of arid climate during the deposition of the Beaufort Series. *Annals of the Geological Survey of South Africa*, *5*, 77-79.

Kitching, J. W. 1979. Preliminary report on a clutch of six dinosaurian eggs from the Upper Triassic Elliot Formation, Northern Orange Free State.

Kitching, J. W. & M. A. Raath. 1984. Fossils from the Elliot and Clarens Formations (Karoo sequence) of the northeastern Cape, Orange Free State, and Lesotho, and a suggested biozonation based on tetrapods. *Palaeontologia africana* 25: 111-125.

Langford R.P. 1989. Fluvial-eolian interactions: Part I, modern systems. *Sedimentology* 36: 1023-1035

Langford, R. P., & M.A. Chan. 1989. Fluvial-aeolian interactions: Part II, ancient systems. *Sedimentology*, 36(6), 1037-1051.

Lee, Y.I. 2002. Provenance derived from the geochemistry of Late Paleozoic – Early Mesozoic mudrocks of the Pyeongan Supergroup, Korea. *Sedimentary Geology*, 149(4). 219-235.

Leeder, M. R., Harris, T., & M.J. Kirkby. 1998. Sediment supply and climate change: implications for basin stratigraphy. *Basin Research*, *10*(1), 7-18.

Le Roux, J. P., & B.B. Hambleton-Jones. 1991. The analysis of termite hills to locate uranium mineralization in the Karoo Basin of South Africa. *Journal of geochemical exploration*, *41*(3), 341-347.

Lock, B.E. 1978. The Cape Fold Belt of South Africa; tectonic control of sedimentation. *Geological Association of London Proceedings 89*, 263-281

Lock, B.E. 1980. Flat-plate subduction and the Cape Fold Belt of South Africa. *Geology*, 8, 35-39

Loope, D. B., & C.M. Rowe. 2003. Long-lived pluvial episodes during deposition of the Navajo Sandstone. *The Journal of Geology*, 111(2), 223-232.

Mack, G. H., James, W. C., & Monger, H. C. (1993). Classification of paleosols. Geological Society of America Bulletin, 105(2), 129-136.

Malaza, N., K. Liu & B. Zhao. 2013 Facies Analysis and Depositional Environments of the Late Palaeozoic Coal-Bearing Madzaringwe Formation in the Tshipise-Pafuri Basin, South Africa. ISRN *Geology* 2013

Malaza N., Liu K. & B. Zhao B. 2015. Paleostress analysis of Karoo Supergroup of the Tshipise-Parfuri Basin, South Africa. *South African Journal of Geology* 118.2: 173-184.

Malaza, N., Liu, K. & B. Zhao. 2016. Petrology and geochemistry of clastic sedimentary rocks as evidences for provenance of the Late Palaeozoic Madzaringwe Formation, Tshipise-Pafuri Basin, South Africa. *Science China Earth Sciences*, 59(12), 2411-2426.

Mallison, H. 2010. The digital *Plateosaurus* II: an assessment of the range of motion of the limbs and vertebral column and of previous reconstructions using a digital skeletal mount. *Acta Palaeontologica Polonica*, *55*(3), 433-458.

MacRae, C.S. 1988. Palynostratigraphic correlation between the lower Karoo sequence of the Waterberg and Pafuri coal-bearing basins and the Hammanskraal plant macrofossil locality, Republic of South Africa. *Geological Survey of South Africa Memoir* 75, 1-217

McCourt, S., & G. Brandl. 1980. A lithostratigraphic subdivision of the Karoo Sequence in North-Eastern Transvaal. *Annals of Geological Survey of South Africa* 14(1): 51-56.

McKeever, P.J. 1991. Trackway preservation in eolian sandstones from the Permian of Scotland: *Geology*, v. 19, p. 726-729

McLennan, S.M., Hemming, S., McDaniel, D.K. & G.N. Hanson. 1993. Geochemical approaches to sedimentation, provenance and tectonics. *Geological Society of America Special Paper* 284, 21-40.

McPhee, B.W., Bordy, E.M., Sciscio, L. & J.N. Choiniere. 2016. A revised Sauropodomorph-based biostratigraphy of the Elliot Formation, Late Triassic-Early Jurassic, South Africa. *Journal of Vertebrate Paleontology, Program and Abstracts, 2016*, p. 71

McPhee, B.W. & J.N. Choiniere. 2016. A hyper-robust sauropodomorph dinosaur ilium from the Upper Triassic–Lower Jurassic Elliot Formation of South Africa: Implications for the functional diversity of basal Sauropodomorpha. *Journal of African Earth Sciences* 123: 177-184.

McPhee, B.W., Choiniere, J.N., Yates, A.M., & P.A. Viglietti. 2015. A second species of *Eucnemasaurus* Van Hoepen, 1920 (Dinosauria, Sauropodomorpha): new information on the diversity and evolution of the sauropodomorph fauna of South Africa's lower Elliot Formation (latest Triassic). *Journal of Vertebrate Paleontology,* 35:5, e980504, DOI:10.1080/02724634.2015.980504

McPhee, B. W., Bonnan, M. F., Yates, A. M., Neveling, J., & J.N. Choiniere. 2015. A new basal sauropod from the pre-Toarcian Jurassic of South Africa: evidence of niche-partitioning at the sauropodomorph–sauropod boundary. *Scientific reports*, 5.

McPhee, B. W., Yates, A. M., Choiniere, J. N. & F. Abdala. 2014. The complete anatomy and phylogenetic relationships of *Antetonitrus ingenipes* (Sauropodiformes, Dinosauria): implications for the origins of Sauropoda. *Zoological Journal of the Linnean Society*, 171: 151–205. doi: 10.1111/zoj.12127

Melchor, R. N., Genise, J. F., Umazano, A. M., & M. Superina. 2012. Pink fairy armadillo meniscate burrows and ichnofabrics from Miocene and Holocene interdune deposits of Argentina: palaeoenvironmental and palaeoecological significance. *Palaeogeography, Palaeoclimatology, Palaeoecology*, 350, 149-170.

Miall, A. D. 1977. Lithofacies types and vertical profile models in braided river deposits: a summary. *Fluvial Sedimentology* — Memoir 5, 597-604

Miall, A. D. 1978. Tectonic setting and syndepositional deformation of molasse and other nonmarine-paralic sedimentary basins. *Canadian Journal of Earth Sciences*, 15(10), 1613-1632.

Miall, A.D. 1996. The Geology of Fluvial Deposits – Sedimentary Facies, Basin Analysis, and Petroleum Geology. Springer, Berlin 582 pp.

Miall, A.D. 2014. Fluvial depositional systems (Vol. 14). Berlin: Springer.

Moore, D.M., & R.C. Jr. Reynolds. 1997. X-ray diffraction and the identification and analysis of clay minerals, 2nd edn., Oxford University Press, Oxford, New York.

Mpodozis, C. & S.M. Kay. 1992. Late Paleozoic to Triassic evolution of the Gondwana margin: Evidence from Chilean Frontal Cordilleran batholiths (28 S to 31 S). *Geological Society of America Bulletin*, *104*(8), 999-1014.

Nesbitt, I. I. W. & G. M. Young. 1982. Early Proterozoic climates and plate. *Nature* 299: 21.p 715-717

Newell, A.J. 2001. Bounding surfaces in a mixed aeolian-fluvial system (Rotliegent, Wessex Basin, SW UK). *Marine and Petroleum Geology* 18, 339-347.

Olsen, P. E. & P. M. Galton. 1984. A review of the reptile and amphibian assemblages from the Stormberg of southern Africa, with special emphasis on the footprints and the age of the Stormberg. *Palaeontologia africana* 25: 87–110.

Owen, R. 1854. Descriptive catalogue of the fossil organic remains of Reptilia and Pisces contained in the Museum of the Royal College of Surgeons of England, Taylor & Francis.

Oesterlen, P. M. & J. Lepper. 2005. The Lower Karoo coal (k2–3) of the Mid-Zambezi basin, Zimbabwe: depositional analysis, coal genesis and palaeogeographic implications. *International Journal of Coal Geology*, *61*(1), 97-118.

Pálfy, J. & Á. T. Kocsis. 2014. Volcanism of the Central Atlantic magmatic province as the trigger of environmental and biotic changes around the Triassic-Jurassic boundary. *Geological Society of America Special Papers*, 505, 245-261.

Parrish, J. T. 1990. Gondwanan paleogeography and paleoclimatology. In: Antarctic Paleobiology (pp. 15-26). Springer New York.

Pedro, G. 2012. Clay minerals in weathered rock materials and in soils, In: Soils and sediments: mineralogy and geochemistry, (eds. Paquet, H., & Clauer, N.). Springer Science & Business Media.

Petit-Marie, N., Casta L., Delibrias, G., Gavin, C.H. & A.M. Testud. 1980. Preliminary data on Quaternary palaeolucustrine deposits in the Wadi ash Shati' area Libya. In: The Geology of Libya Volume III (eds. M.J. Salem and M.T. Busrewil), pp. 979-808. Academic Press, London.

Péron, S., Bourquin, S., Fluteau, F. & F. Guillocheau. 2005. Paleoenvironment reconstructions and climate simulations of the Early Triassic: impact of the water and sediment supply on the preservation of fluvial systems. *Geodinamica Acta*, *18*(6), 431-446.

Porro, L. B., Butler, R. J., Barrett, P. M., Moore-Fay, S., & R.L. Abel. 2011. New heterodontosaurid specimens from the Lower Jurassic of southern Africa and the early ornithischian dinosaur radiation. *Earth and Environmental Science Transactions-Royal Society of Edinburgh*, *101*(3), 351.

Potter, P.E., Maynard, J.B., & P.J. Depetris. 2005. Mud and mudstones, introduction and overview. Springer Berlin Heidelberg pp. 157-174.

Pysklywec, R. N. & J. X. Mitrovica. 1999. The role of subduction-induced subsidence in the evolution of the Karoo Basin. *The Journal of Geology*, 107(2), 155-164.

Raath, M. A. 1969. A new coelurosaurian dinosaur from the Forest Sandstone of Rhodesia. *Arnoldia (Rhodesia)* 4(28): 1–25.

Raath, M. A. 1977. The anatomy of the Triassic theropod *Syntarsus rhodesiensis* (Saurischia: Podokeosauridae) and a consideration of its biology. Doctor of Philosophy, Rhodes University.

Rais, P., Louis-Schmid, B., Bernasconi, S. M., & H. Weissert. 2007. Palaeoceanographic and palaeoclimatic reorganization around the Middle–Late Jurassic transition. *Palaeogeography, Palaeoclimatology, Palaeoecology*, *251*(3), 527-546.

Reed, S. J. B. 2016. *Electron Microprobe Analysis and Scanning Electron Microscopy in Geology*. 2nd ed. Cambridge: Cambridge University Press, 2005.

Reeves, C. V., de Wit, M. J. & B. K. Sahu. 2004. Tight reassembly of Gondwana exposes Phanerozoic shears in Africa as global tectonic players. *Gondwana Research*, *7*(1), 7-19.

Reisz, R. R., Scott, D. Sues, H.-D., Evans, D.C., & M. A. Raath. 2005. Embryos of an Early Jurassic prosauropod dinosaur and their evolutionary significance. *Science* 309: 761–764.

Remane, J., Bassett, M. G., Cowie, J. W., Gohrbandt, K. H., Lane, H. R., Michelsen, O., & W. Naiwen. 1996. Revised guidelines for the establishment of global chronostratigraphic standards by the International Commission on Stratigraphy (ICS). *Episodes-Newsmagazine of the International Union of Geological Sciences*, *19*(3), 77-81.

Retallack, G. J. (1988). Field recognition of paleosols. Geological Society of America Special Papers, 216, 1-20.

Retallack, G. (1984). Completeness of the rock and fossil record: some estimates using fossil soils. Paleobiology, 10(1), 59-78.

Rubidge, B. S., Johnson, M. R., Kitching, J. W., Smith, R. M. H., Keyser, A. W. & G.H. Groenewald. 1995. An introduction to the biozonation of the Beaufort Group. In: Biostratigraphy of the Beaufort Group (Karoo Supergroup) (Vol. 1, pp. 1-2). Biostratigraphic Series, 1: South African Committee for Stratigraphy.

Rubidge, B. S. 2005. Re-uniting lost continents--Fossil reptiles from the ancient Karoo and their wanderlust. *South African Journal of Geology*, *108*(1).

Ruckwied, K., Götz, A., Pálfy J. & Á. Török. 2008. Palynology of a terrestrial coal-bearing series along the Triassic/Jurassic boundary (Mecsek Mts., Hungary). *Central European Geology* 51, 1-15

Ruckwied, K. & A. Götz. 2009. Climate change at the Triassic/Jurassic boundary, palynological evidence from the Furkaska section (Tatra Mountains, Slovakia). *Geologica Carpathica* 60, 139-149

Rust, I.C. 1959. On the sedimentation of the Molteno Sandstones in the vicinity of Molteno. Cape Province.Unpublished MSc Thesis, University of Stellenbosch.

Rust, I.C. 1962. On the sedimentation of the Molteno sandstones in the vicinity of Molteno, Cape Province. University of Stellenbosch (Annals) 37, 165-236

Rust, I.C. 1975. Tectonic and sedimentary framework of Gondwana basins in southern Africa. In: K.S.W. Campbell (ed.): Gondwana Geology. Canberra: Australian National University Press, 537-564

Ryseth, A. 2014. Sedimentation at the Jurassic-Triassic boundary, south-west Barents Sea, indication of climate change. *International Association of Sedimentologists Special Publication* 46, 187-214

Scherer, C., & E.L. Lavina. 2005. Sedimentary cycles and facies architecture of aeolian–fluvial strata of the Upper Jurassic Guará Formation, southern Brazil. *Sedimentology*, 52(6), 1323-1341.

Sciscio, L. & E.M. Bordy. 2016. Palaeoclimatic conditions in the Late Triassic-Early Jurassic of southern Africa: A geochemical assessment of the Elliot Formation. *Journal of African Earth Sciences* 119 (2016): 102-119.

Scotese C.R., Boucot, A.J. & W.S. McKerrow. 1999. Gondwanan palaeogeography and palaeoclimatology. *Journal of African Earth* Sciences 28, 99-114

Scotese, C. R. 2001. *Atlas of earth history*. University of Texas at Arlington. Department of Geology. PALEOMAP Project.

Sheldon, N.D., & N.J. Tabor. 2009. Quantitative palaeoenvironmental and paleoclimatic reconstruction using paleosols. *Earth Science Reviews* 95, 1-52.

Stagman, J.G. 1978. An outline of the geology of Rhodesia. *Rhodesia Geological Survey Bulletin*, 80, p. 126

Smellie, J. L. 1981. A complete arc-trench system recognized in Gondwana sequences of the Antarctic Peninsula region. *Geological Magazine*, *118*(02), 139-159.

Smith, R. M., & T.R. Mason. 1998. Sedimentary environments and trace fossils of Tertiary oasis deposits in the central Namib Desert, Namibia. *Palaios*, 13(6), 547-559.

Smith, R. M. H., Eriksson, P.G. & W. J. Botha. 1993. A review of the stratigraphy and sedimentary environments of the Karoo-aged basins of Southern Africa. *Journal of African Earth Sciences (and the Middle East)* 16, no. 1: 143-169.

Smith, R.H.M., Rubidge, B.S., & M.V.M. Van Der Walt. 2012. Therapsid biodiversity patterns and palaeoenvironments of the Karoo Basin, South Africa, In: The forerunners of mammals (ed.A. Chinsamy-Turan). Indianapolis, Indiana University Press, pp. 31–64

South African Committee for Stratigraphy (SACS). 1980. Stratigraphy of South Africa (Part 1). Geological Survey of South Africa. Pretoria

SOEKOR. 1996. Major offshore petroleum exploration opportunities. Intera Information Technologies Ltd, pp 1-19

Stagman, J. G. N., & N.M. Harrison. 1978. An outline of the geology of Rhodesia (No. 80). Government Printer.

Stavrakis, N. 1980. Sedimentation of the Katberg Sandstone and adjacent formations in the south-eastern Karoo Basin. *Transactions of the Geological Society of South Africa* 83, 361-374

Stigall, A. L., Babcock, L. E., Briggs, D. E. & S. A. Leslie. 2008. Taphonomy of lacustrine interbeds in the Kirkpatrick Basalt (Jurassic), Antarctica. *Palaios*, *23*(6), 344-355.

Summerfield, M. A. (1983). Silcrete. Chemical Sediments and Geomorphology, 59-91.

Tankard, A. J., Jackson, M. P. A., Eriksson, IL A., Hobday, D. K., Hunter, D. R., & W. E. L. Minter. 1982. Crustal evolution of Southern Africa. Springer Verlag, New York, 523 pp.

Tankard, A., Welsink, H., Aukes, P., Newton, R. & E. Stettler. 2009. Tectonic evolution of the Cape and Karoo basins of South Africa. *Marine and Petroleum Geology*, *26*(8), 1379-1412.

Tohver, E., Lanci, L., Wilson, A., Hansma, J. & S. Flint. 2015. Magnetostratigraphic constraints on the age of the lower Beaufort Group, western Karoo basin, South Africa, and a critical analysis of existing U-Pb geochronological data. *Geochemistry, Geophysics, Geosystems*, *16*(10), 3649-3665.

Torsvik T.H. & L.R.M. Cocks. 2011. Paleogeography of Central Gondwana In: The formation and evolution of Africa from the Archaean to Present: A synopsis of 3.8 Ga of Earth's History, (eds. Van Hinsbergen, D. J. J., Buiter, S. J. H., Torsvik, T. H., Gaina, C. & Webb, S. J.). Special Publications of the Geological Society, London, 357, 137-166

Tucker, M. E. & M. J. Benton. 1982. Triassic environments, climates and reptile evolution. *Palaeogeography, Palaeoclimatology, Palaeoecology*, *40*(4), 361-379.

Turner, P. 1980. *Continental red beds* (Vol. 29). Elsevier.

Turner, B. R. 1975. Statistical appraisal of Molteno (Triassic) sedimentary cycles from the upper part of the Karroo (Gondwana) system in South Africa. *Journal of Sedimentary Research*, *45*(1).

Turner, B. R. 1977. Sedimentary patterns of uranium mineralisation in the Beaufort Group of the southern Karoo (Gondwana) Basin, South Africa.

Turner, B.R. 1999. Tectonostratigraphical development of the Upper Karoo foreland basin: orogenic unloading versus thermally-induced Gondwana rifting. *Journal of African Earth Sciences*, 28, 251-238

Vail J.R., Hornung, G. & K.G.Cox. 1969. Karoo basalts of the Tuli syncline. *Rhodesia Bulletin of Volcanology* 33, 398-418

Van Eeden, O. R., Visser, H. N., Van Zyl, J. S., Coertze, F. J., & Wessels, J. T. (1955). *The Geology of the Eastern Soutpansberg and the Lowveld to the North...*SA Geological Survey.

van der Walt, M., Day, M., Rubidge, B., Cooper, A. K., & I. Netterberg. 2010. A new GIS-based biozone map of the Beaufort Group (Karoo Supergroup), South Africa.

van Reenen, D.D., Roering, C., Ashwal L.D. & M.J., de Wit. 1992. Regional geological setting of the Limopopo Belt. *Precambrian Research*, 55 1-5

Veevers J.N.J., Cole, D.I. & E.J. Cowan. 1994. Southern Africa: Karoo Basin and Cape Fold Belt, In: Permian-Triassic Pangean basins and foldbelts along the Panthalassan margin of Gondwanaland, (eds. J.N.J Veevers and McA. Powell). *Geological Society of America*, Memoir 184, 223-280

Visser, J.N.J. 1984. A review of the "Stormberg" Group and Drakensberg Volcanics in Southern Africa. *Palaeontologia Africana* 25, 5-27.

Visser, J. N. J. 1986. Lateral lithofacies relationships in the glacigene Dwyka Formation in the western and central parts of the Karoo Basin. *Transactions of the Geological Society of South Africa*, *89*, 373-383.

Visser, J.N.J. 1991a. The paleoclimatic setting of the late Paleozoic marine ice sheet in the Karoo Basin of southern Africa. *Geological Society of America Special Papers*, *261*, 181-190.

Visser, J.N.J. 1991b. Geography and climatology of the Late Carboniferous to Jurassic Karoo Basin in south-western Gondwana: *Annals of the South African Museum*, v. 99, p. 415-431

Visser J.N.J. & B.J.V. Botha. 1980. Meander belt, point bar, crevasse splay and aeolian deposits from the Elliot Formation in Barkly Pass, northeastern Cape. *Transactions Geological Society of South Africa*, 83, 55-62

Visser, J. N. J. & B. A Dukas. 1979. Upward-fining fluviatile megacycles in the Beaufort Group, north of Graaff-Reinet, Cape Province. *Transactions of the Geological Society of South Africa*, *82*(149), e154.

Visser, J.N.J. & L.S. Kingsley.1982. Upper Carboniferous glacial valley sedimentation in the Karoo Basin, Orange Free State. *Transactions of the Geological Society of South Africa* 85, 71-79

Walker, T.R. & J.C. Harms. 1972. Eolian origin of flagstone beds, Lyons Sandstone (Permian), type area, Boulder County, Colorado: *The Mountain Geologist*, v.9, p. 279-288

Ward, J.D. 1988. Eolian, fluvial, and pan (playa) facies of the Tertiary Tsondab Sandstone in the central Namib Desert, Namibia. *Sedimentary Geology* 55: 143-162.

Watkeys, M.K., and Sweeney, R.J., 1988 Tuli-Lebombo colanism and Gondwana rifting. Extended abstracts-Geocongress 88, Durban: University of Natal, 38, 725-728

Watkeys, M. K. 1979. Explanation of the geological map of the country west of Beitbridge. Government Printer, South Africa.

Whetstone, K. N. & P. Whybrow. 1983. A "cursorial" crocodilian from the Triassic of Lesotho (Basutoland), southern Africa. Occasional Papers of the Museum of Natural History, The University of Kansas 106: 1–37.

White, R. & McKenzie, D. 1989. Magmatism at rift zones: the generation of volcanic continental margins and flood basalts. *Journal of Geophysical Research: Solid Earth*, *94*(B6), 7685-7729.

Winter, H. de la R. 1984. Tectonostratigraphy, as applied to the analysis of South African Phanerozoic basins. *Transactions of the Geological Society of South Africa* 87, 169-179

Wopfner, H. 1991. Extent and timing of the late Palaeozoic glaciation in Africa. Geologisches Institut, Universität Köln, Sonderveröffentlichungen, 82, 447-453.

Wopfner, H. 1994. The Malagasy Rift, a chasm in the Tethyan margin of Gondwana. *Journal of Southeast Asian Earth Sciences*, 9(4), 451-461.

Wopfner, H. 2002. Tectonic and climatic events controlling deposition in Tanzanian Karoo basins. *Journal of African Earth Sciences*, *34*(3), 167-177.

Yadagiri, P. 1988. A new sauropod *Kotasaurus yamanpalliensis* from Lower Jurassic Kota Formation of India. *Records of the Geological Survey of India* 11: 102-127.

Yates, A. M. 2003. A definite prosauropod dinosaur from the Lower Elliot Formation (Norian: Upper Triassic) of South Africa. *Palaeontologia africana* 39: 63–68.

Yates, A. M. 2004. The Death of a Dinosaur: dismembering *Euskelosaurus*. *Geoscience Africa*: 715.

Yates, A. M. 2005. A new theropod dinosaur from the Early Jurassic of South Africa and its implications for the early evolution of theropods. *Palaeontologia africana* 41: 105–122.

Yates, A. M. 2007a. Solving a dinosaurian puzzle: the identity of *Aliwalia rex* Galton. *Historical Biology* 19:93-123.

Yates, A. M. 2007b. The first complete skull of the Triassic disnosaur *Melanorosaurs* Haughton (Sauropodomorpha: Anchisauria). *Special Papers in Paleontology* 77:9-55.

Yates, A. M. 2008. A second specimen of *Blikanosaurus* (Dinosauria: Sauropoda) and the biostratigraphy of the Lower Elliot Formation. *Palaeontologia africana* 43: 39–43.

Yates, A. M. & J. W. Kitching. 2003. The earliest known sauropod dinosaur and the first steps towards sauropod locomotion." Proceedings of the Royal Society of London, Series B 270: 1753–1758.

Yates, A.M., Hancox, J.P. & B.S. Rubidge. 2004. First record of a sauropod dinosaur from the upper Elliot Formation (Early Jurassic) of South Africa: research letter. *South African Journal of Science* 100 (9&10): 504-506

Yates, A. M. & P. M. Barrett. 2010. *Massospondylus carinatus* Owen 1854 (Dinosauria: Sauropodomorpha) from the Lower Jurassic of South Africa: Proposed conservation of the usage by designation of a neotype. *Palaeontologia africana* 45: 7–10.

Yates, A. M., Bonnan, M.F., Neveling, J., Chinsamy A. & M. G. Blackbeard. 2010. A new transitional sauropodomorph dinosaur from the Early Jurassic of South Africa and

the evolution of sauropod feeding and quadrupedalism." *Proceedings of the Royal Society of London, Series B* 277: 787–794

Yates, A. M., Bonnan, M.F. & J. Neveling. 2011. A new basal sauropodomorph dinosaur from the Early Jurassic of South Africa. *Journal of Vertebrate Paleontology* 31: 610–625.

APPENDIX A: KRUGER NATIONAL PARK (KNP) BOREHOLES

Legend to KNP borehole stratigraphic sections

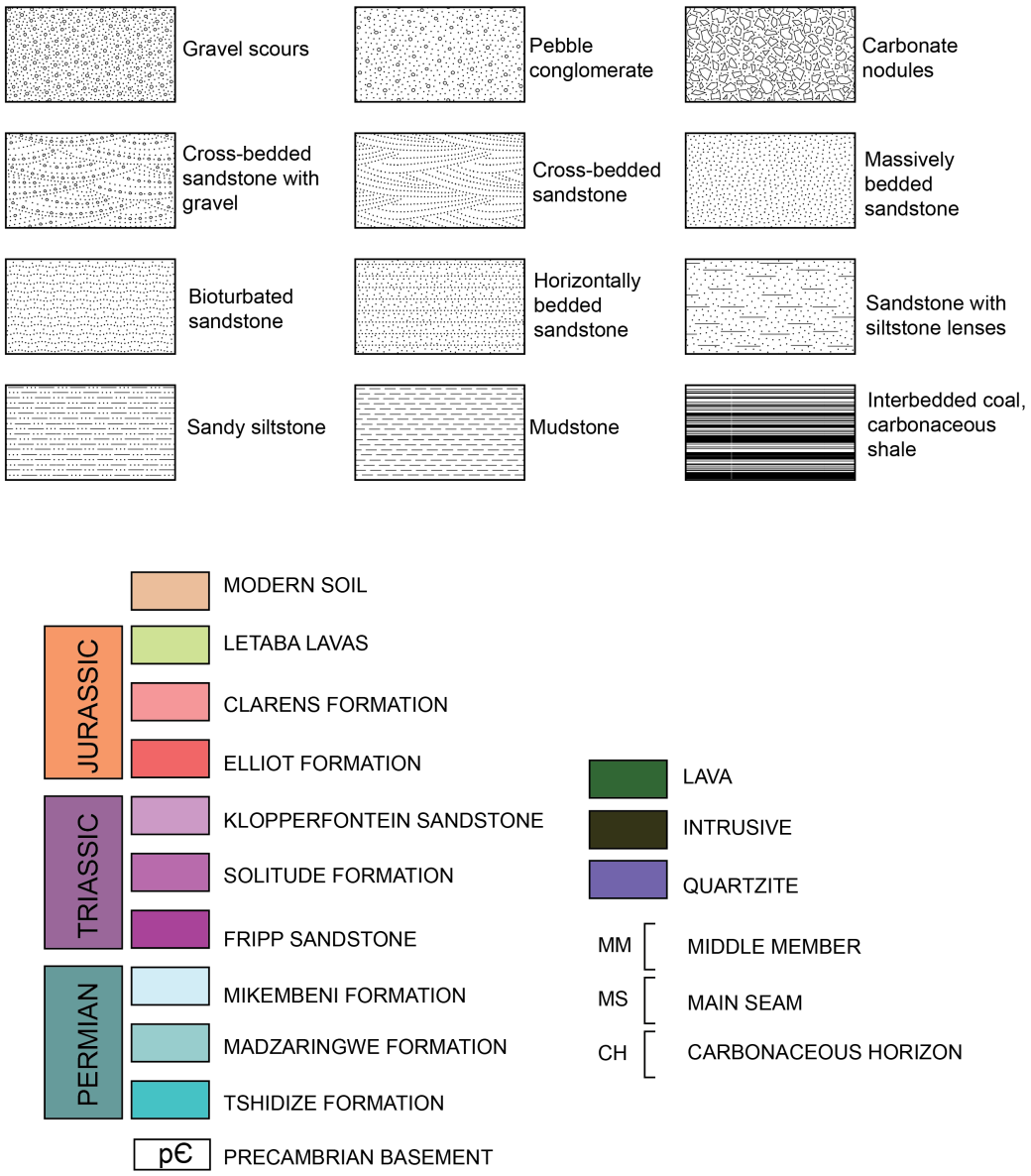

Figure A1.

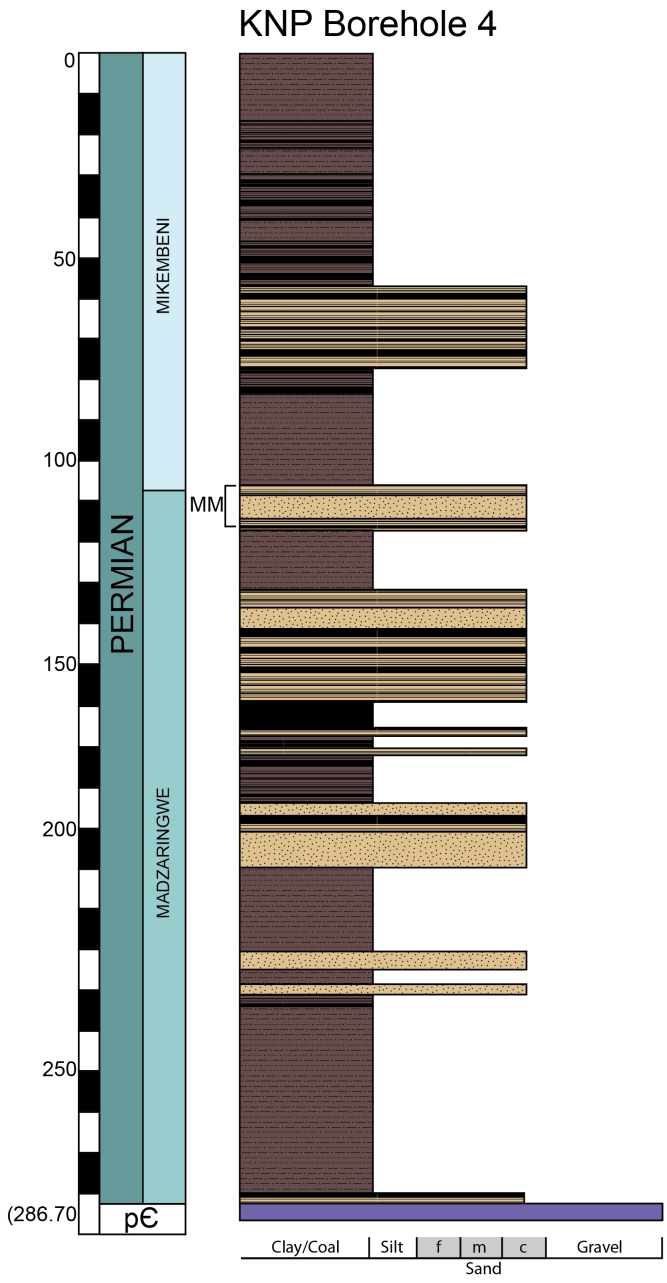
KNP Borehole 4
0
50
100
150
200
250
(286.70
PERMIAN
MIKEMBENI
MADZARINGWE
MM
pЄ
Clay/Coal
Silt
f
m
c
Gravel
Sand

Figure A2.

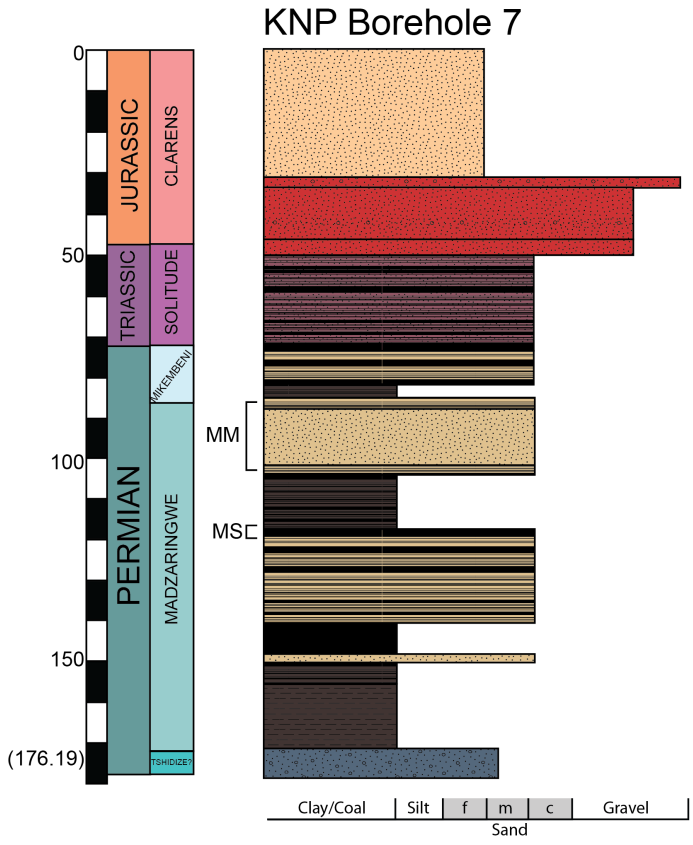
KNP Borehole 7
0
50
100
150
(176.19)
JURASSIC
TRIASSIC
PERMIAN
CLARENS
SOLITUDE
NIKEMBENI
MADZARINGWE
TSHIDIZE?
MM
MSC
Clay/Coal
Silt
f
m
c
Gravel
Sand

Figure A3.

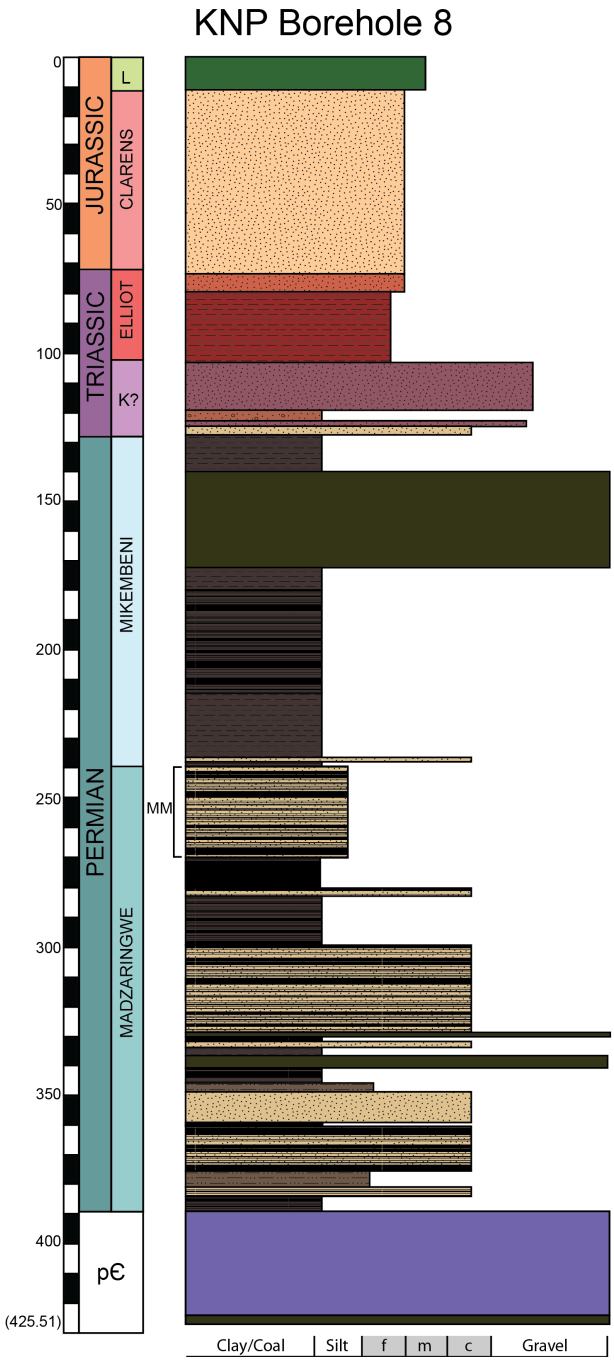
KNP Borehole 8
0
50
100
150
200
250
300
350
400
(425.51)
JURASSIC
TRIASSIC
PERMIAN
pЄ
L
CLARENS
ELLIOT
K?
MIKEMBENI
MADZARINGWE
MM
Clay/Coal
Silt
f
m
c
Gravel

Figure A4.

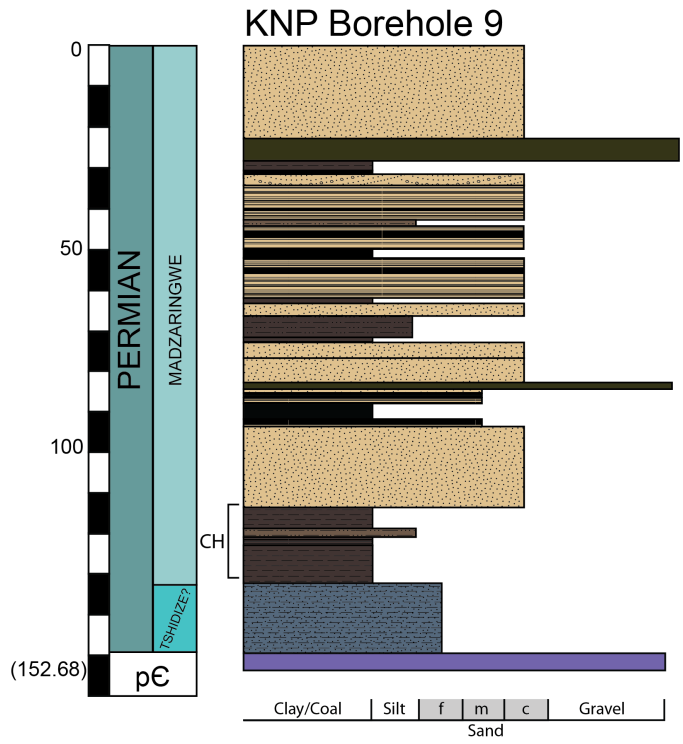
KNP Borehole 9
0
50
100
(152.68)
PERMIAN
MADZARINGWE
TSHIDZE?
pЄ
CH
Clay/Coal
Silt
f
m
c
Gravel
Sand

Figure A5.

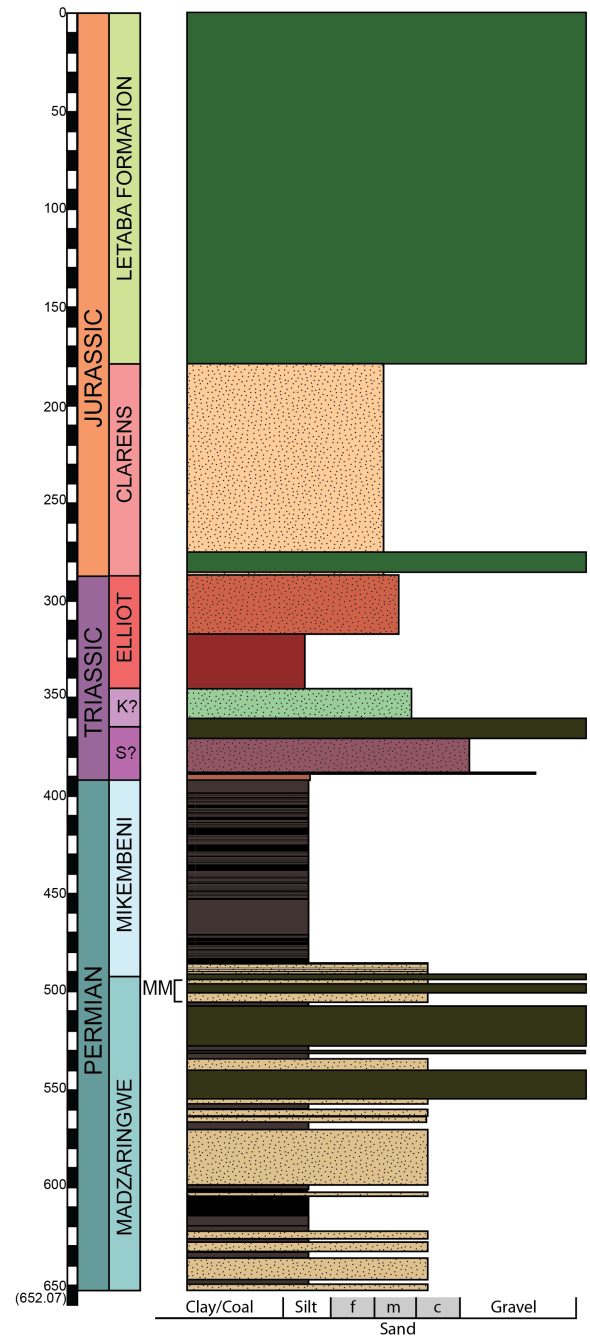
0
50
100
150
200
250
300
350
400
450
500
550
600
650
(652.07)
JURASSIC
TRIASSIC
PERMIAN
LETABA FORMATION
CLARENS
ELLIOT
K?
S?
MIKEMBENI
MADZARINGWE
MM
Clay/Coal
Silt
f
m
c
Gravel
Sand

Figure A6.

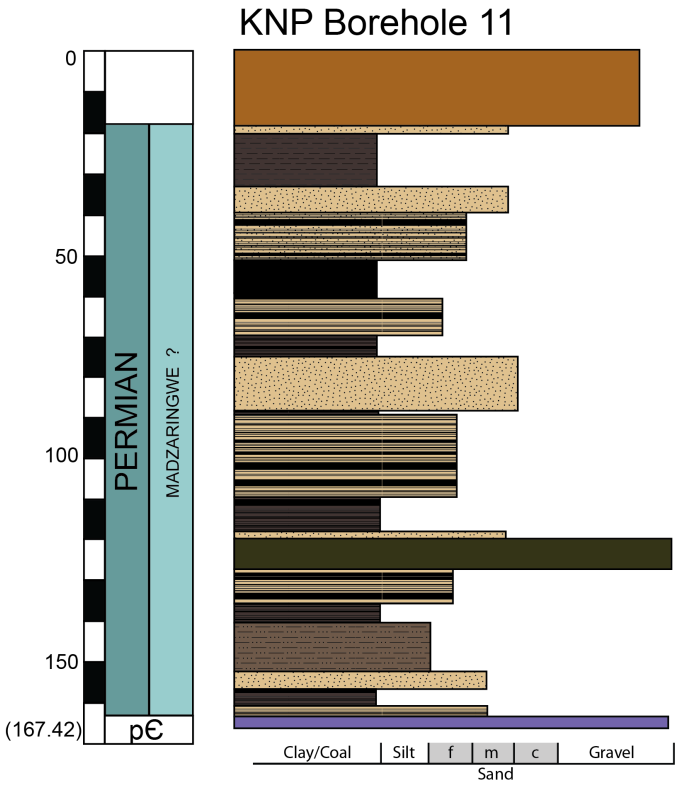
KNP Borehole 11
0
50
100
150
(167.42)
PERMIAN
MADZARINGWE ?
pЄ
Clay/Coal
Silt
f
m
c
Gravel
Sand

Figure A7.

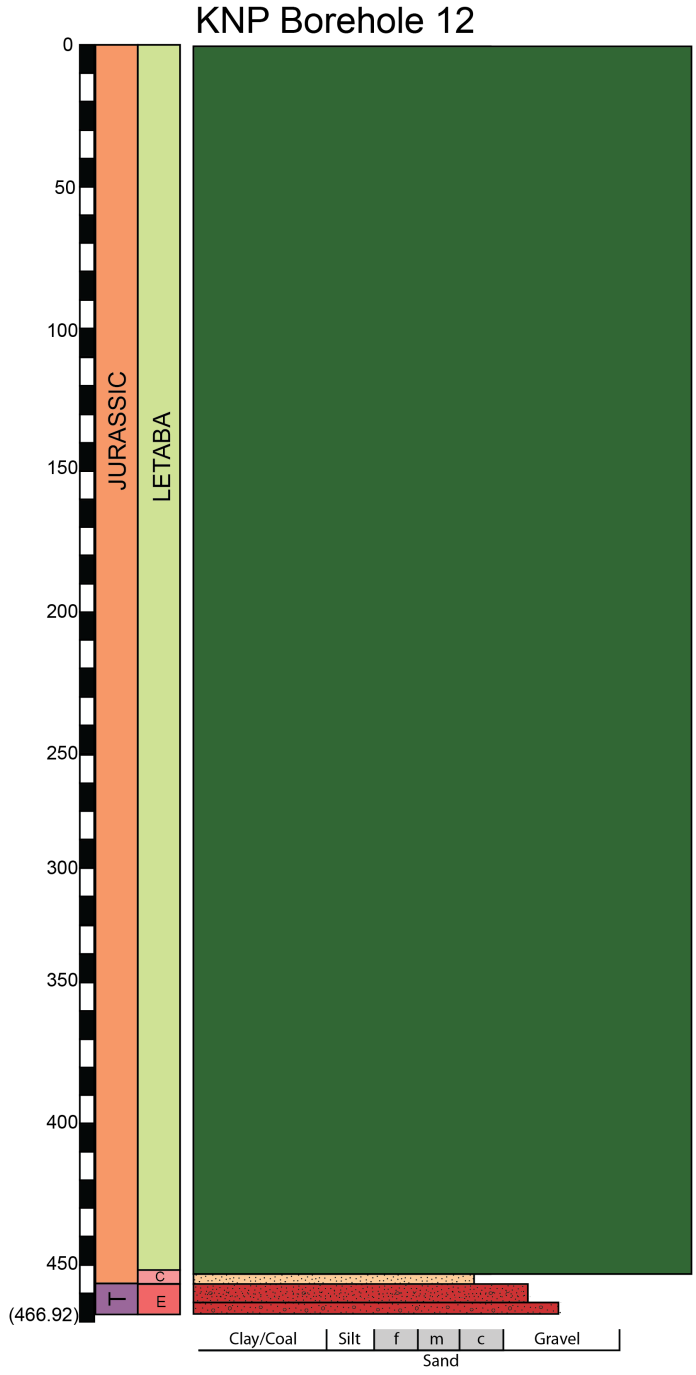
KNP Borehole 12
0
50
100
150
200
250
300
350
400
450
(466.92)
JURASSIC
LETABA
C
T
E
Clay/Coal
Silt
f
m
c
Gravel
Sand

Figure A8.

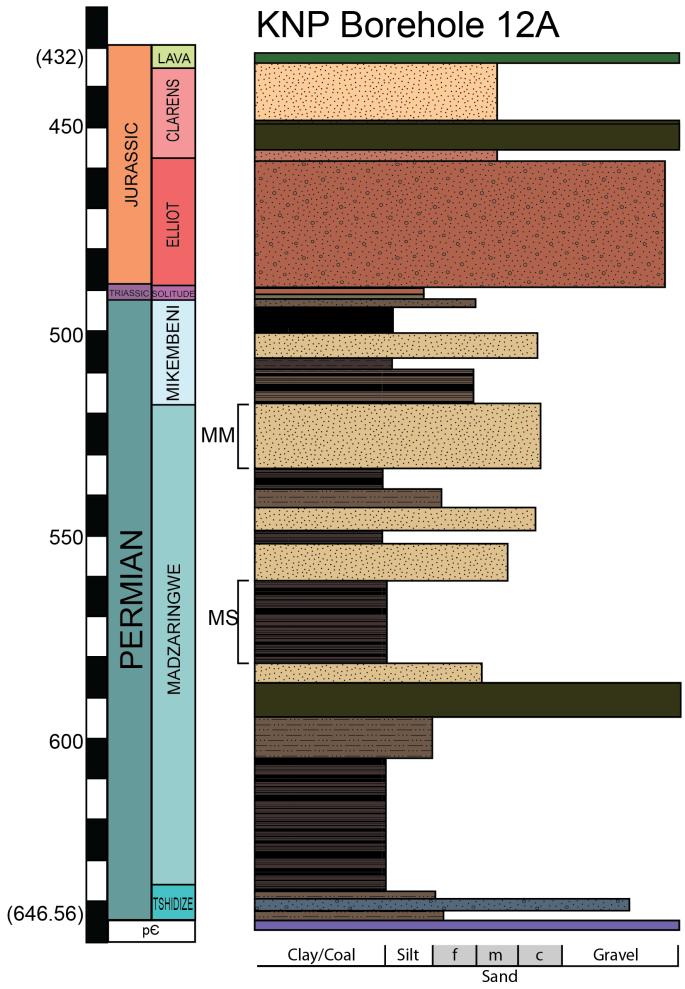
KNP Borehole 12A
(432)
450
500
550
600
(646.56)
JURASSIC
LAVA
CLARENS
ELLIOT
TRIASSIC
SOLITUDE
PERMIAN
MIKEMBENI
MADZARINGWE
TSHIDIZE
pЄ
MM
MS
Clay/Coal
Silt
f
m
c
Gravel
Sand

Figure A9.

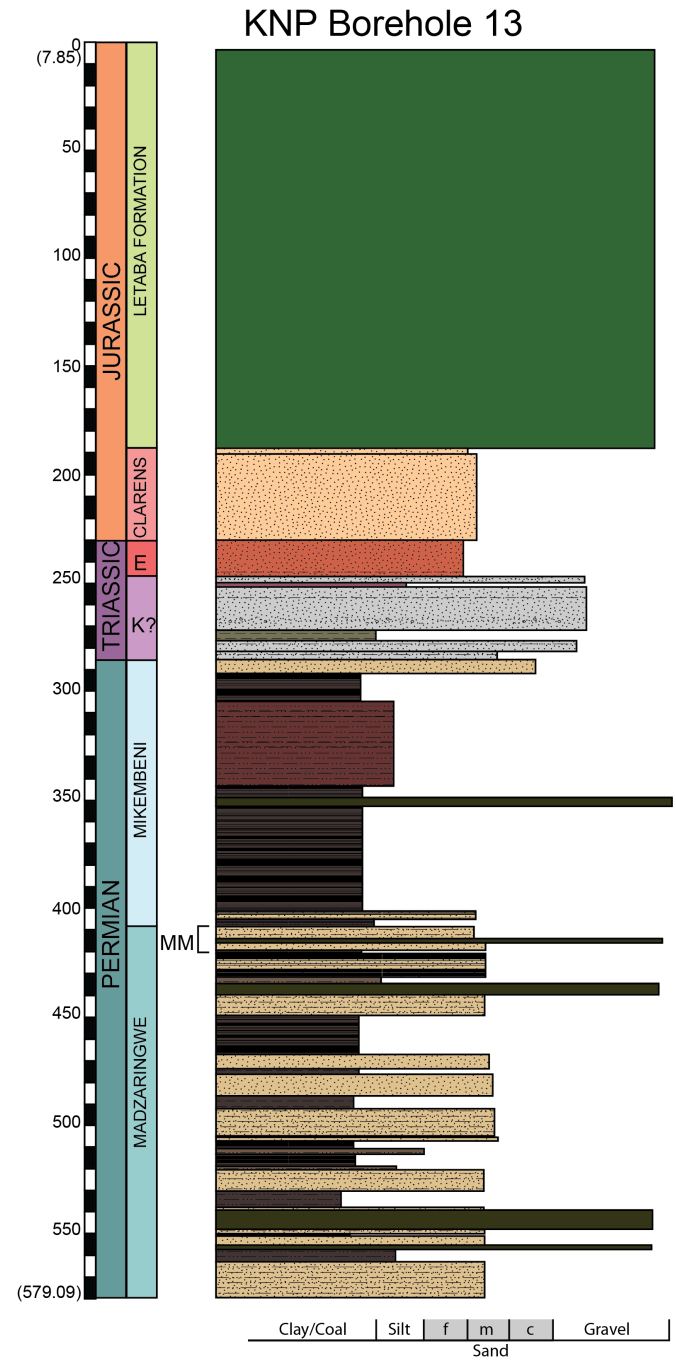
KNP Borehole 13
0
(7.85)
50
100
150
200
250
300
350
400
450
500
550
(579.09)
JURASSIC
TRIASSIC
PERMIAN
LETABA FORMATION
CLARENS
m
K?
MIKEMBENI
MADZARINGWE
MM
Clay/Coal
Silt
f
m
c
Gravel
Sand

Figure A10.

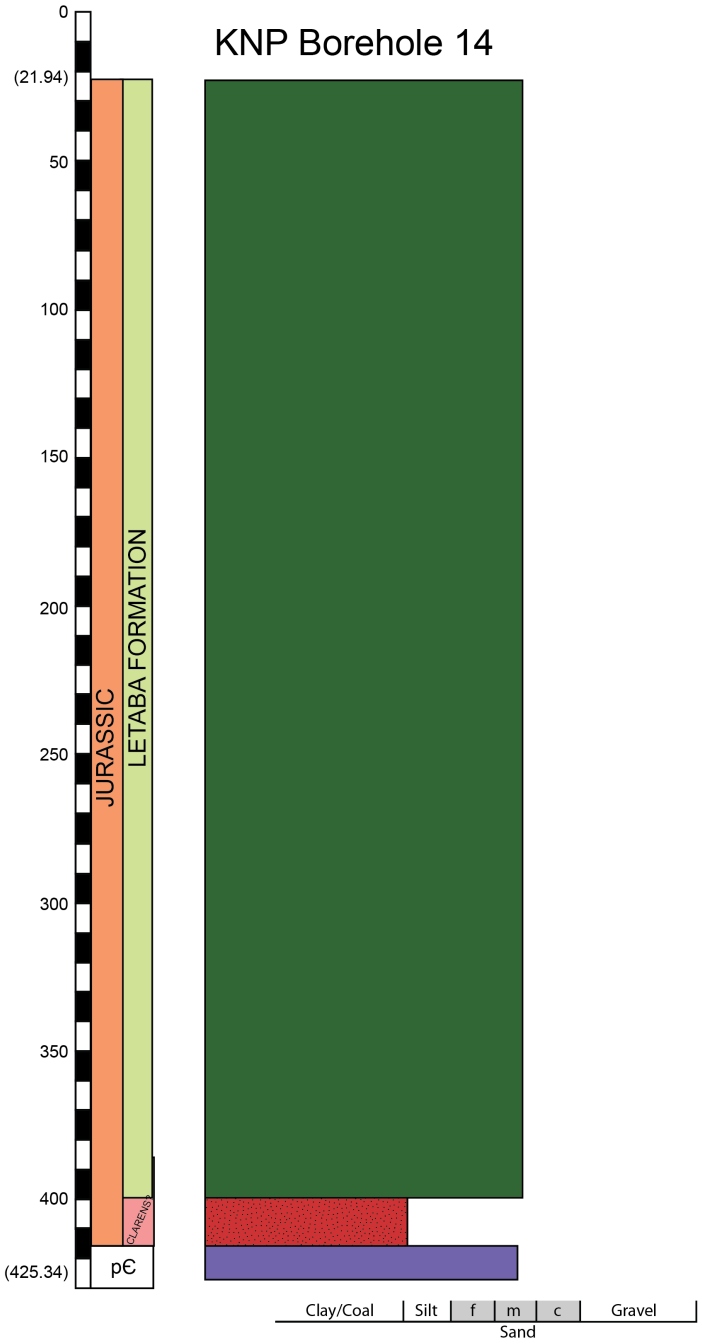
KNP Borehole 14
0
(21.94)
50
100
150
200
250
300
350
400
(425.34)
JURASSIC
LETABA FORMATION
CLARENS
pЄ
Clay/Coal
Silt
f
m
c
Gravel
Sand

Figure A11.

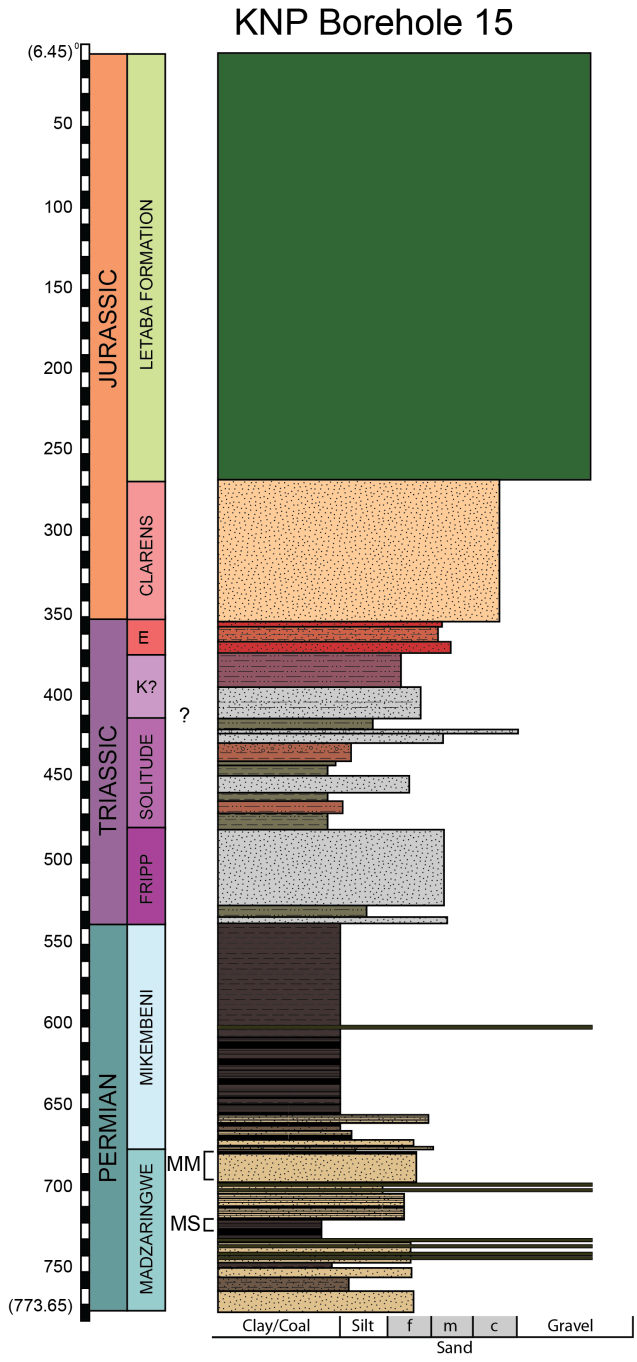
KNP Borehole 15
(6.45)
50
100
150
200
250
300
350
400
450
500
550
600
650
700
750
(773.65)
JURASSIC
TRIASSIC
PERMIAN
LETABA FORMATION
CLARENS
m
K?
SOLITUDE
FRIPP
MIKEMBENI
MADZARINGWE
?
MM
MS
Clay/Coal
Silt
f
m
c
Gravel
Sand

Figure A12.

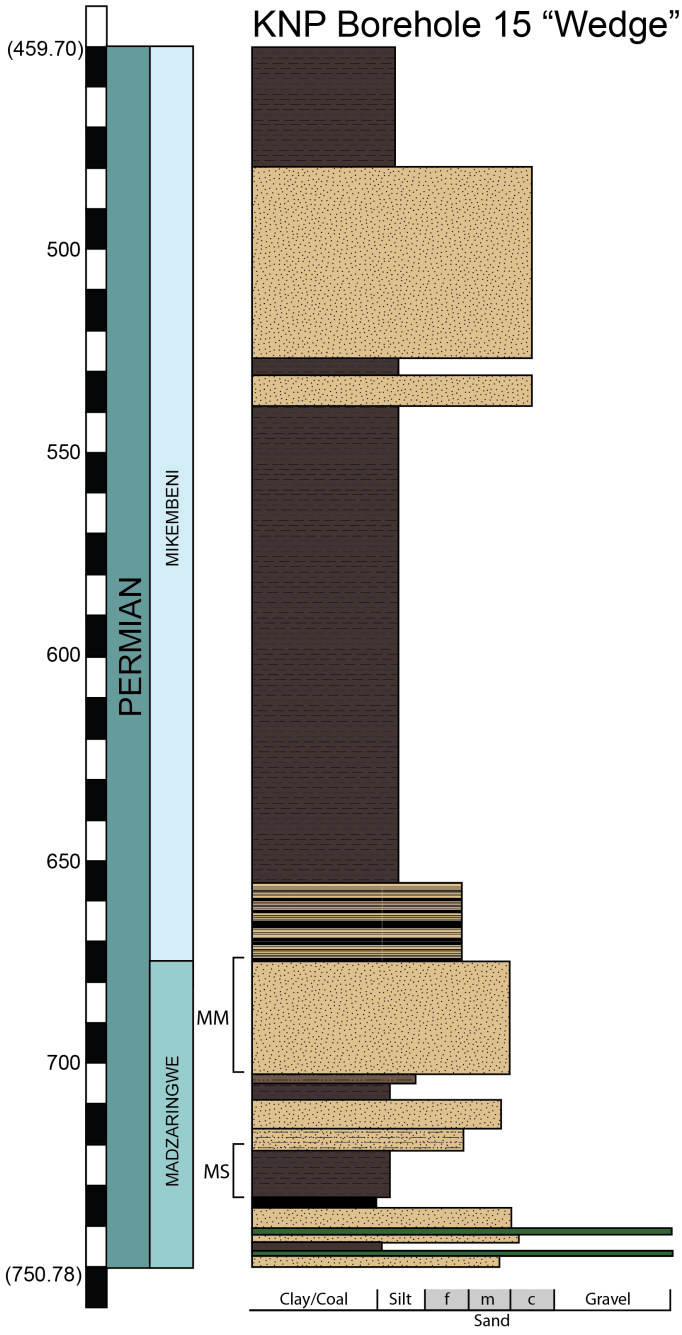
KNP Borehole 15 “Wedge”
(459.70)
500
550
600
650
700
(750.78)
PERMIAN
MIKEMBENI
MADZARINGWE
MM
MS
Clay/Coal
Silt
f
m
c
Gravel
Sand

Figure A13.

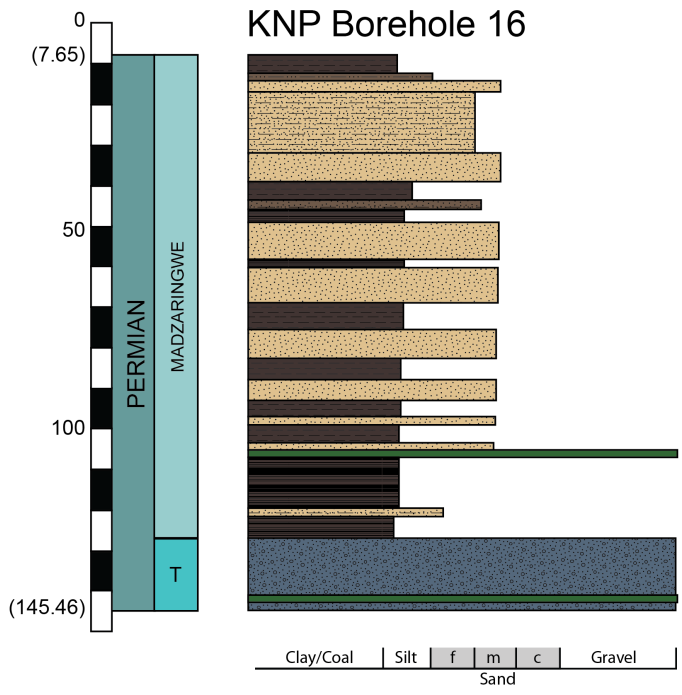
KNP Borehole 16
0
(7.65)
50
100
(145.46)
PERMIAN
MADZARINGWE
T
Clay/Coal
Silt
f
m
c
Gravel
Sand

Figure A14.

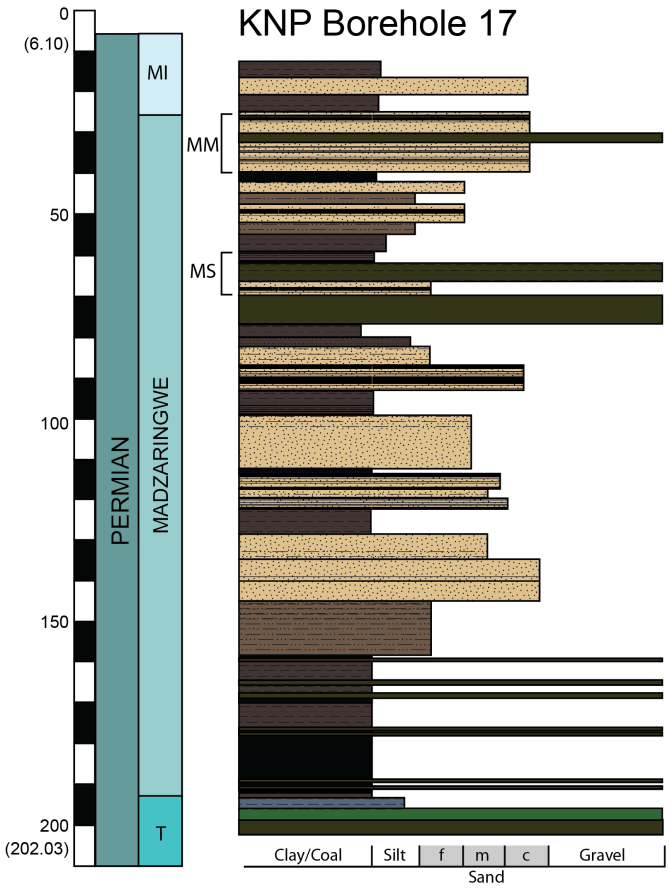
KNP Borehole 17
0
(6.10)
50
100
150
200
(202.03)
PERMIAN
MADZARINGWE
MI
T
MM
MS
Clay/Coal
Silt
f
m
c
Gravel
Sand

Figure A15.

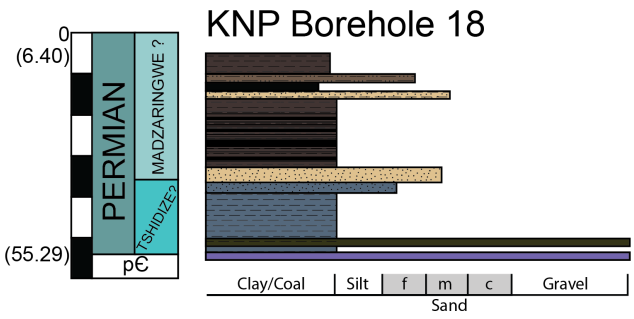
KNP Borehole 18
0
(6.40)
(55.29)
PERMIAN
MADZARINGWE ?
TSHIDIZE?
pЄ
Clay/Coal
Silt
f
m
c
Gravel
Sand

Figure A16.

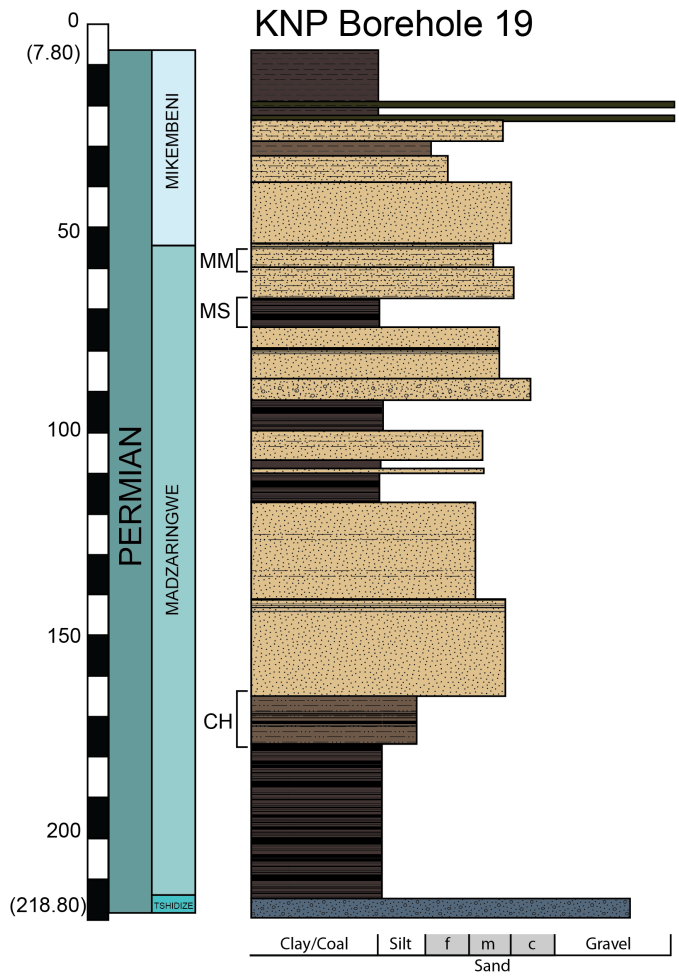
KNP Borehole 19
0
(7.80)
50
100
150
200
(218.80)
PERMIAN
MIKEMBENI
MADZARINGWE
TSHIDIZE
MM
MS
CH
Clay/Coal
Silt
f
m
c
Gravel
Sand

Figure A17.

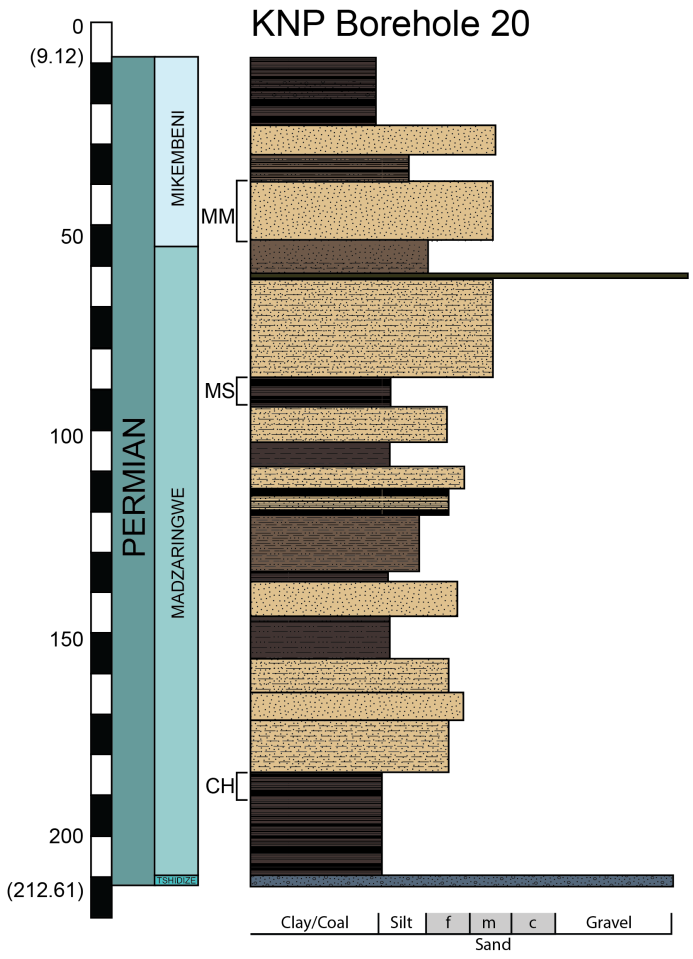
KNP Borehole 20
0
(9.12)
50
100
150
200
(212.61)
PERMIAN
MIKEMBENI
MADZARINGWE
MM
MS
CH
Clay/Coal
Silt
f
m
c
Gravel
Sand

Figure A18.

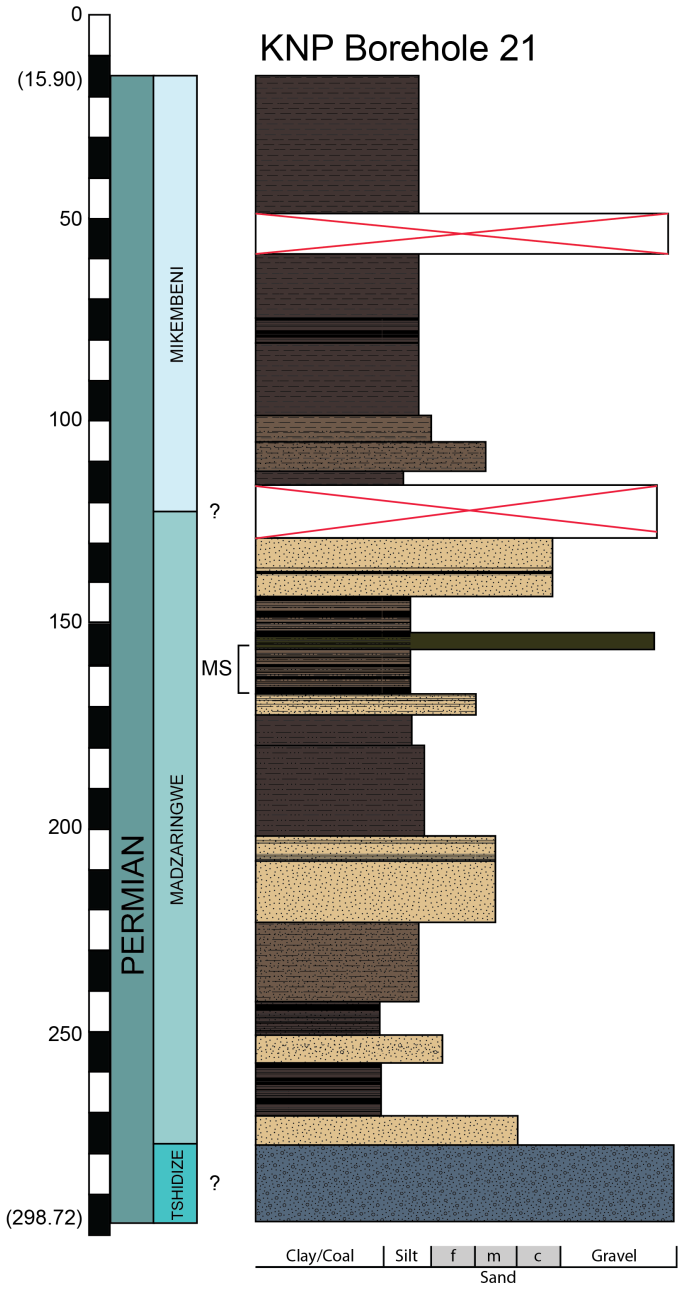
KNP Borehole 21
0
(15.90)
50
100
150
200
250
(298.72)
PERMIAN
MIKEMBENI
MADZARINGWE
TSHIDIZE
?
MS
?
Clay/Coal
Silt
f
m
c
Gravel
Sand

Figure A19.

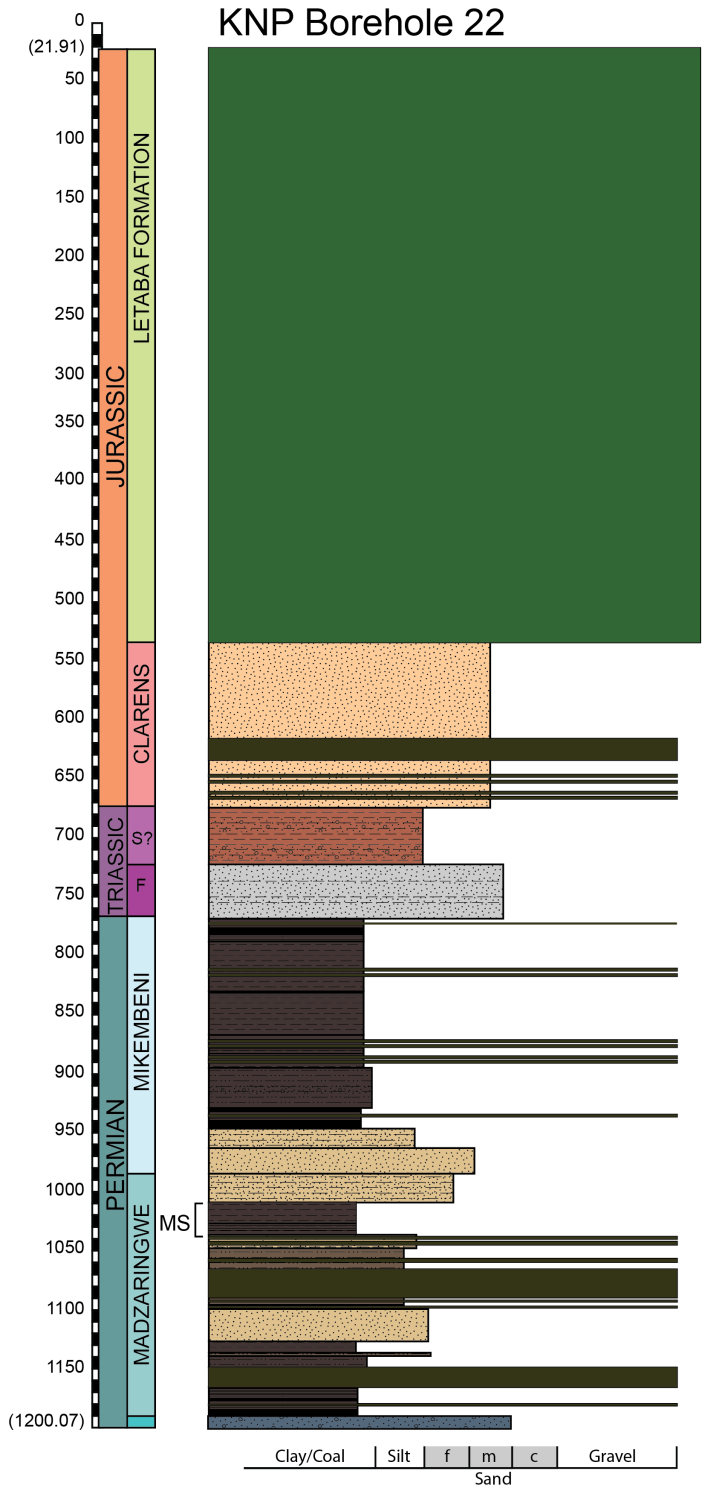
KNP Borehole 22
0
(21.91)
50
100
150
200
250
300
350
400
450
500
550
600
650
700
750
800
850
900
950
1000
1050
1100
1150
(1200.07)
JURASSIC
LETABA FORMATION
CLARENS
TRIASSIC
S
F
PERMIAN
MIKEMBENI
MADZARINGWE
MS
Clay/Coal
Silt
f
m
c
Gravel
Sand

Figure A20.

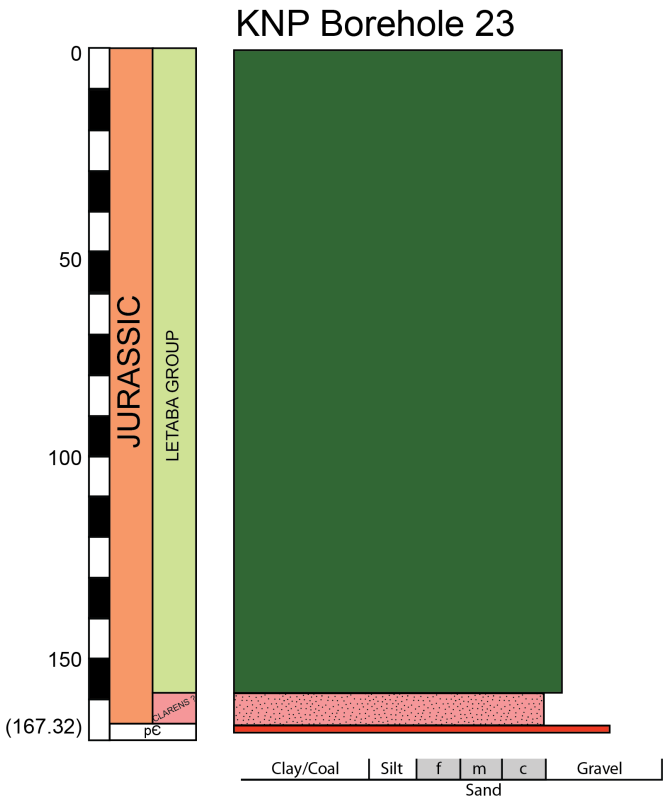
KNP Borehole 23
0
50
100
150
(167.32)
JURASSIC
LETABA GROUP
pC
Clay/Coal
Silt
f
m
c
Gravel
Sand

APPENDIX B: PETROGRAPHY OF SAMPLES FROM STUDY AREA

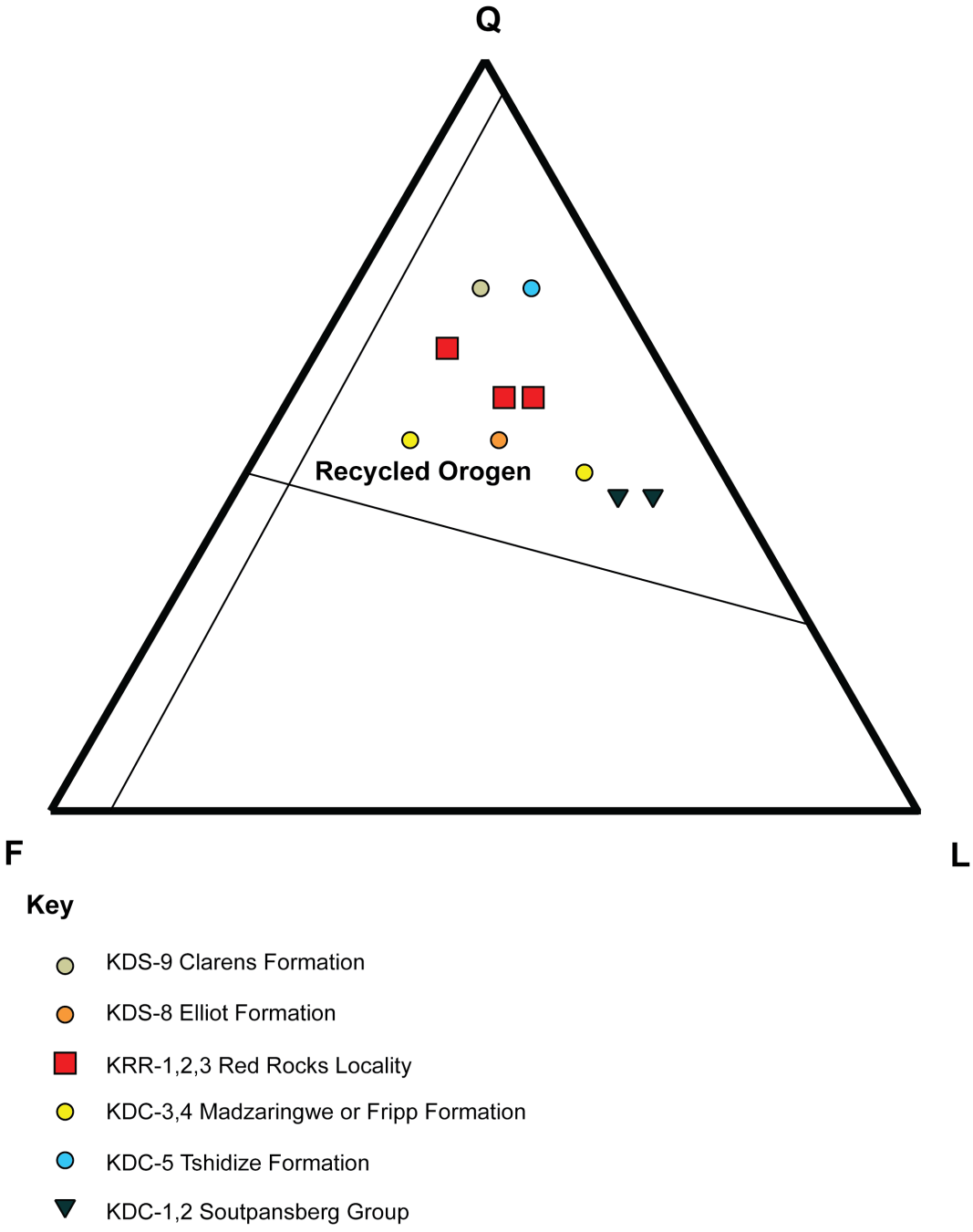

Figure B1: QFL Diagram of 10 petrography samples collected from Lower and Upper Makanya Hill (KDC-1,2,3,4,5, KDS-8,9) and Red Rocks Localities (KRR-1,2,3)

Base of Facies Association VII A:

Figure B2: Facies Association VII A in outcrop consists of alternating fine-grained red sandstone and fine, altered blue layers.

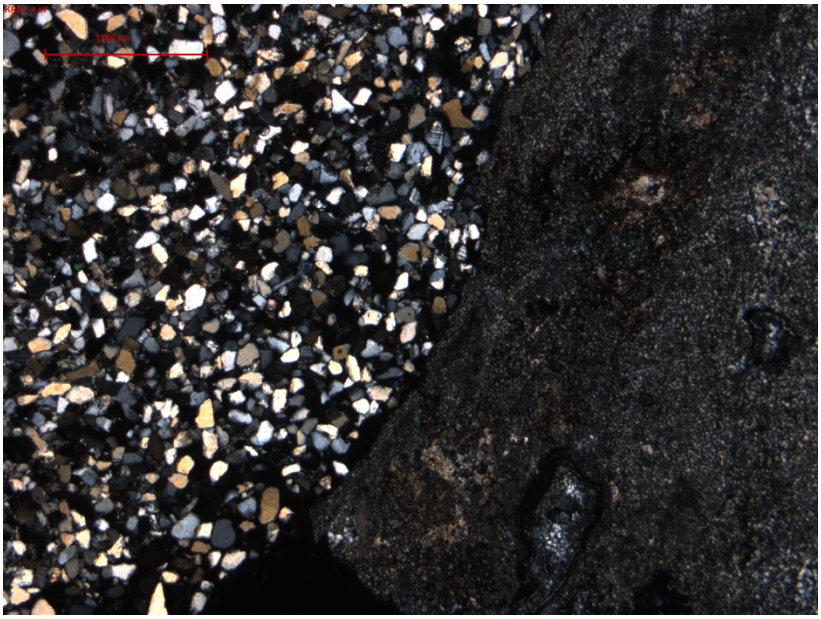

Figure B3: Thin section of FA VII A. Overview illustrates contact between fine red sandstone (left) and altered calcretized blue layers (right) in KRR-1. Cross-polarized light, scale bar = 1000 µm

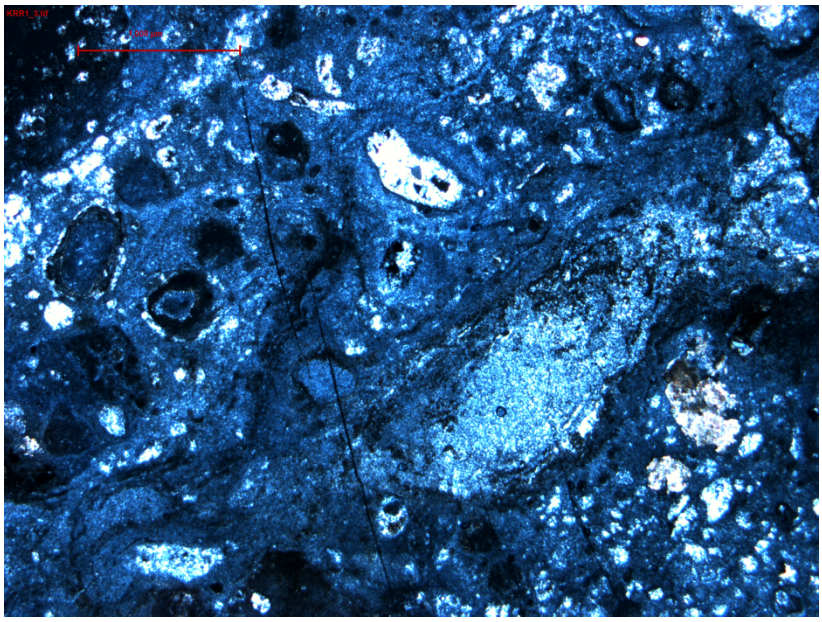

Figure B4: Thin section of FA VII A. Blue interlayers have large vugs that appear to contain re-crystallized quartz in KRR-1. Cross- polarized light, scale bar = 1000 µm

KRR-1 is composed of very fine (70-80 µm), sub to well-rounded, well-sorted quartz grains which are tightly packed, sharing point and long contacts. By point count, the sample consists of 62% quartz, 24% feldspar, the majority of which are orthoclase, and 14% lithics, of which 43% are polycrystalline quartz. Additionally, minor amounts of clay grains were also present. The clay matrix is in places slightly calcretized and accounts for less than 5% of the sample; the fabric is homogenous. This thin section was taken from the base of the Red Rocks locality and contains pervasively altered, siliceous nodules. In hand sample, this alteration is blue with large white veins. In thin section, the alterations are primarily composed of microcrystalline quartz, while veins are composed of calcite and quartz. Calcite veins tend to have smaller crystals near the vein margin and much larger crystals in the center. Quartz veins contain isopachous quartz crystals. Also within this nodule are large vugs, typically around quartz grains. This sample is classified as an arkosic arenite and is texturally mature while mineralogically submature.

Facies Association VII A:

Figure B5: Outcrop of Facies Association IA consists of fine-grained, bioturbated sandstone with numerous burrows.

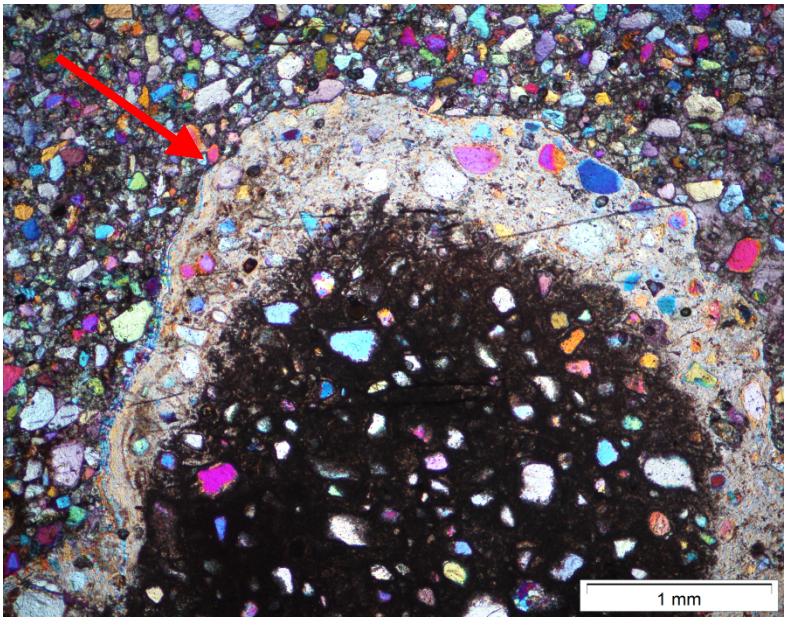

Figure B6: Thin section of FA VII A. KRR-2 has clay-rich matrix, but invertebrate burrows (external boundary marked by arrow) has significantly more clay enrichment, with few grains. Cross-polarized light with gypsum plate, scale bar = 1000 µm

KRR-2 is a clay matrix-supported sample (~20%) with fine (70-80 µm) grains that are sub to well-rounded, and moderately to poorly sorted. Some grains share point contacts. By point counts, this sample consists of

56% quartz, 20% feldspar, and 24% lithics of which 75% are polycrystalline quartz. The fabric of this sample is homogenous, excluding what appears to be an invertebrate burrow, which is significantly enriched in clay with few, larger (80 µm) grains and diagenic calcite veins. This sample is classified as a lithic greywacke, and is texturally and mineralogically immature.

Facies Association VIII:

Figure B7: Facies Association VIII consists of fine-grained, red sandstone fluvial deposits.

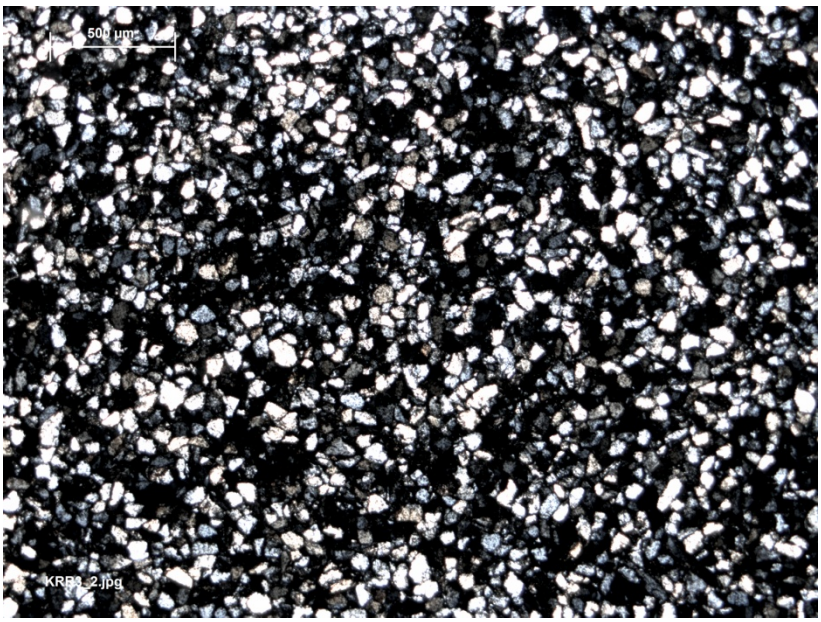

Figure B8: Thin section of FA VIII. KRR-3 is very fine-grained and quartz rich. Cross-polarized light,
scale bar = 500 µm.

KRR-3 is composed of very fine (70-100 μm), sub to well-rounded, well-sorted grains, with ~15% clayey matrix. Grains are closely packed, sharing point and long contacts. By point counts, the sample consists of 56% quartz, 18% feldspar, and 26% lithics, 62%% of which are polycrystalline quartz. Biotite and clay grains are also present in this sample. The fabric is homogenous and lacks any apparent bedding features. The sample is classified as a lithic arenite and is texturally and mineralogically immature.

Facies Association XI:

Figure B9: Facies Association XI in outcrop contains numerous *Arenicolites* burrows, and is heavily bioturbated.

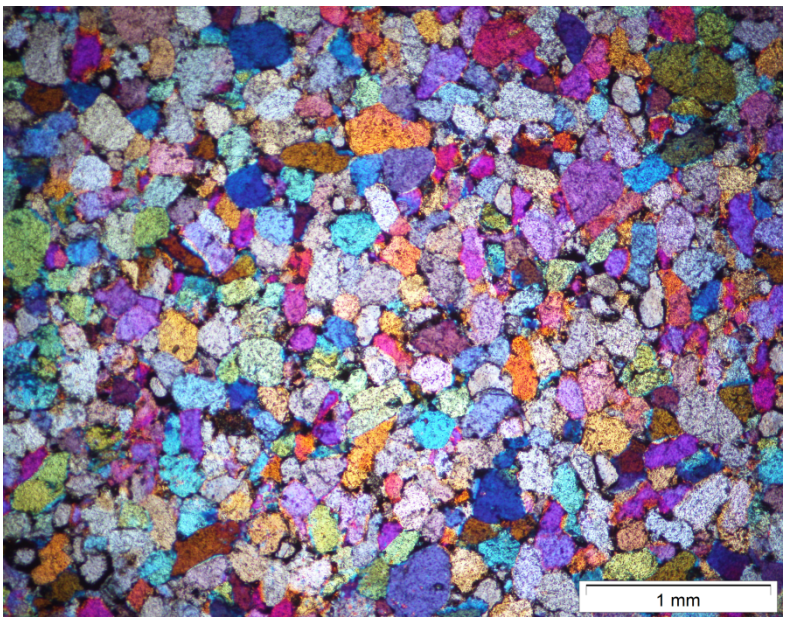

Figure B10: Thin section of FA XI. KDS-9 is feldspar-rich in contrast to typical Clarens arenites. Cross-polarized light and gypsum plate, scale bar = 1000 μm

KDS-9 is composed of fine to medium (80-120 μm), well rounded, well sorted, tightly packed grains with ~5% clay matrix. Grains share long contacts, though some concave-convex contacts are also observed. The fabric is homogenous. By point counts these grains are composed of 70% quartz, 16% feldspar, and 14% lithics of which 57% are polycrystalline quartz. Minor amounts of detrital clay grains are present. This sample is mineralogically and texturally submature and classified as a feldspathic greywacke.

Facies Association III:

Figure B11: Facies Association III represents fluvial channels, bars, and bedforms. In the Mikembeni or Fripp Formation (left), the sandstone is coarse and micaceous. The sandstone is medium-coarse and has high energy scours near the base of the Clarens Formation (right), filled with small quartzite pebbles.

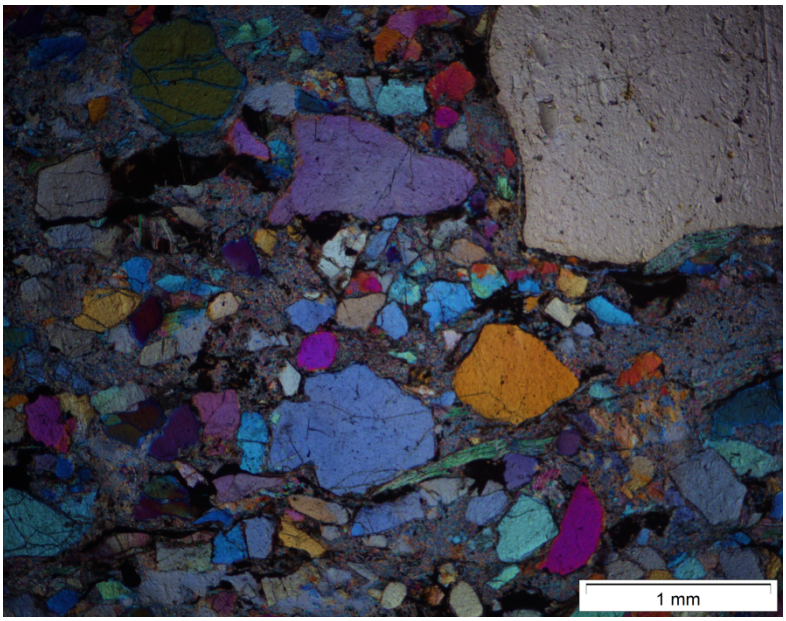

Figure B22: Thin section of FA III. KDC-3 from the Madzaringwe or Fripp Formation is poorly sorted and contains micas aligned to bedding planes, roughly horizontal here. In hand sample, this sandstone is very micaceous. Cross-polarized light, scale bar = 1000 µm

KDC-3 is composed of fine to coarse (200-600µm), angular, poorly sorted, loosely packed grains which share point and long contacts and ~15% clay matrix. By point counts the sample consists of 46% quartz, 16% feldspar, and 38% lithics of which 84% are represented by polycrystalline quartz. Mica, biotite and clay grains are also abundant and are aligned along bedding planes. This sample is mineralogically and texturally immature, classified as a lithic greywacke.

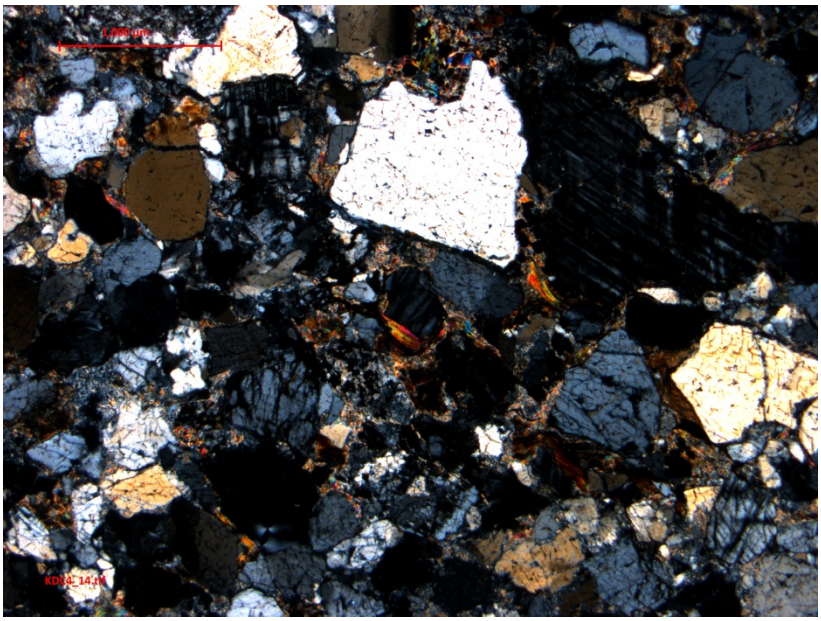

Figure B13: KDC-4 has large feldspar grains (f), and lots of red and orange micas and biotite in cross-polarized light. Scale bar = 1000 µm

KDC-4 is composed of fine to coarse (100-1000µm), subangular to subrounded, poorly sorted, tightly packed grains which share long, concavo-convex, and sutured contacts. The sample contains ~10% clay matrix, and by point counts the grains are composed of 50% quartz, 34% feldspar, of which the majority is potassium feldspar, and 16% lithics, of which 75% are polycrystalline quartz. Detrital clay, mica and biotite are also abundant. Clays and micas aren't necessarily aligned to bedding planes, and the sample's fabric is homogenous. This sample is mineralogically and texturally immature, is classified as an arkosic arenite.

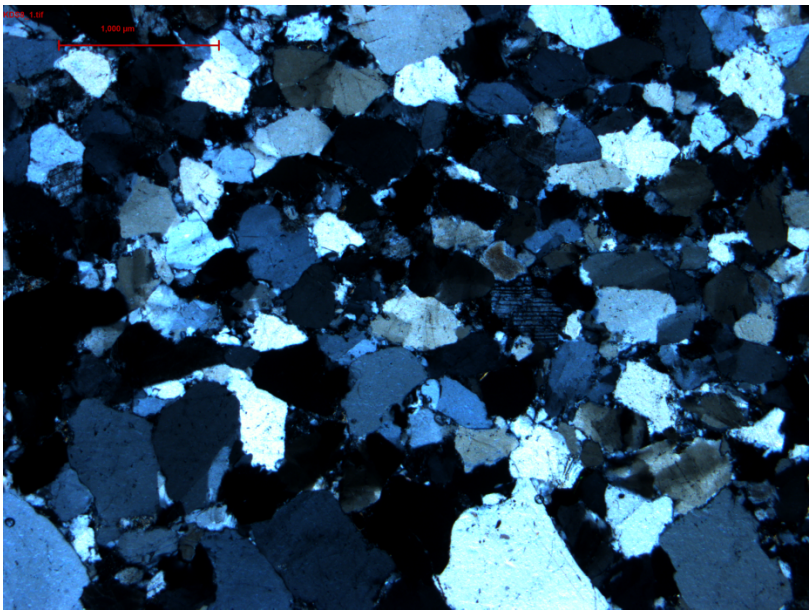

Figure B14: KDS-8 has fairly large grains and lots of lithics and feldspars in contrast to the aeolianite sandstones of the Clarens Formation. Cross-polarized light, scale bar = 1000 µm

KDS-8 is composed of fine to coarse (100-1000µm), subangular to subrounded, moderate to well-sorted, packed grains with 5% clay matrix. The grains mostly share long contacts, though concave-convex contacts are also observed. These grains by point counts are composed of 50% quartz, 24% feldspar, of which the majority is potassium feldspar, and 26% lithics of which 84% are polycrystalline quartz. Mica, biotite and authigenic and detrital clay are also abundant. This sample is mineralogically immature and texturally submature, and classified as a lithic arenite.

Facies Association I:

Figure B35: Facies Association I in outcrop has numerous pebble and cobble clasts in a fine mud. This conglomerate was formed during a high energy event.

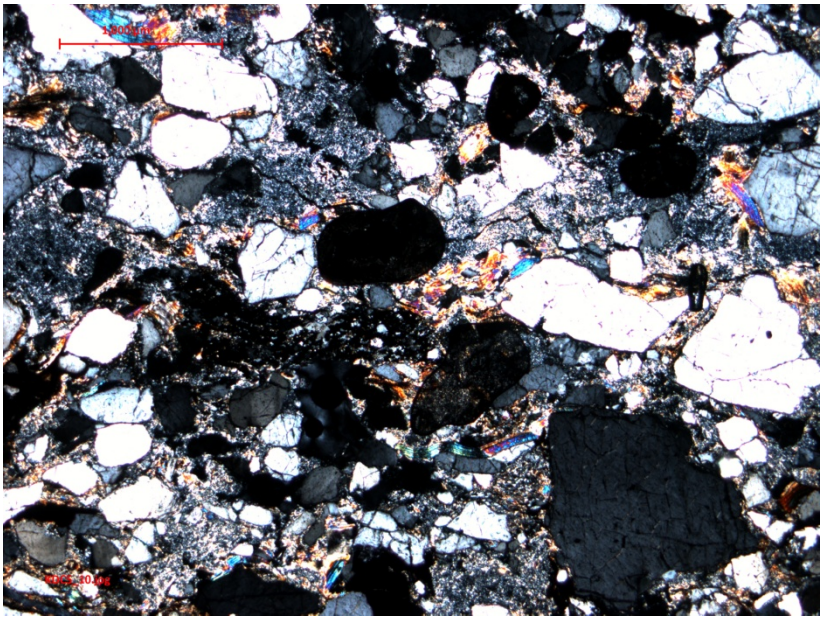

Figure B46: KDC-5 is clay rich with poorly sorted, mineralogically immature grains. Cross-polarized light, scale bar = 1000 µm

KDC-5 is composed of ~ 20% clay matrix and fine to coarse (100-1000µm), sub-angular to well rounded, very poorly sorted, grains. Grains are matrix supported, but some share point and long contacts. By point counts, the grains are composed of 70% quartz, 10% feldspar and 20% lithics of which 60% are polycrystalline quartz. Micas and clay grains are aligned to bedding planes, and rare zircons are present in the sample.

Many clay grains are authigenic and formed by conversion of feldspars. This sample is mineralogically submature, classified as a lithic greywacke.

Loskop Formation:

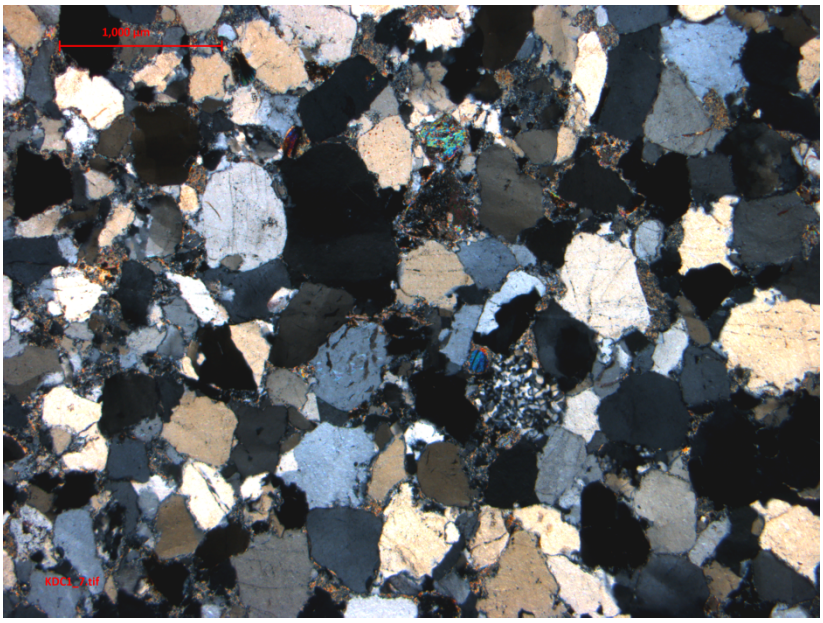

Figure B17: KDC-1 has numerous lithics and tightly packed, large grains. Cross-polarized light, scale bar = 1000 µm

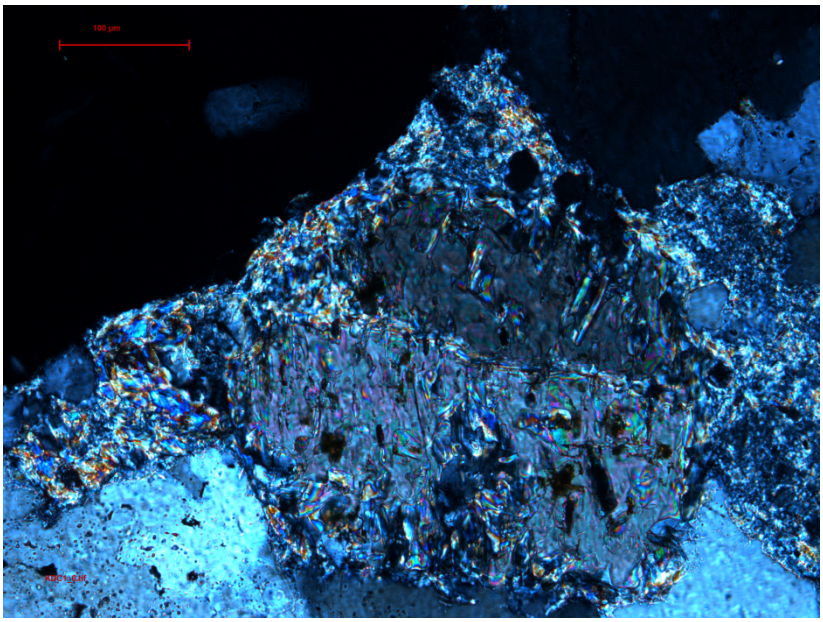

Figure B58: Degraded grain has converted partially to clay. Scale bar = 100 µm

KDC-1 is composed of fine to coarse (200-600μm), angular, moderate to well-sorted, tightly-packed grains with ~10% clay matrix. By point counts, the sample consists of 42% quartz, 14% feldspars, and 44% lithics, of which 86% are represented by polycrystalline quartz. Micas, biotite and both detrital and authigenic clay grains are abundant. Grains are tightly packed, sharing long, concavo-convex and sutured contacts. Some grains are heavily degraded and are a likely source for authigenic clay. This sample is mineralogically immature and texturally immature, and is classified as a lithic arenite.

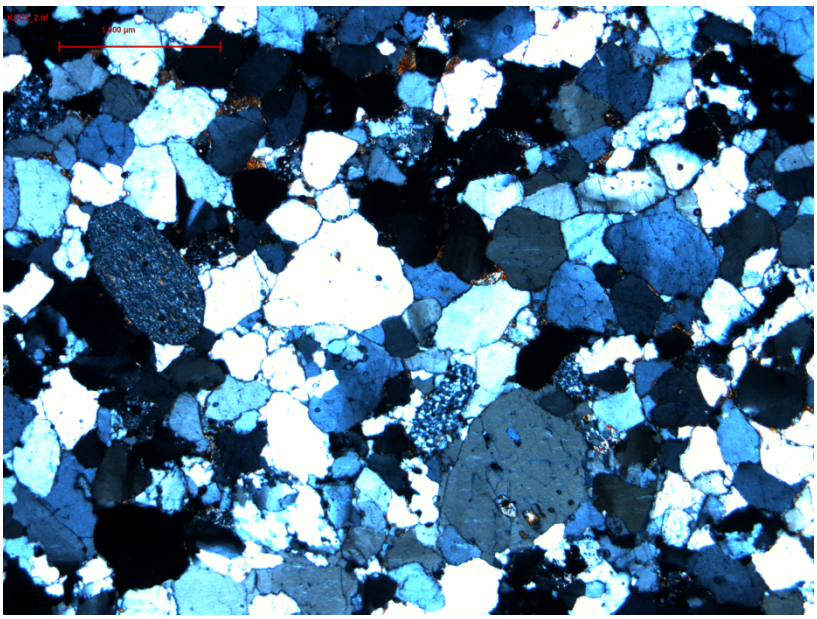

Figure B19: KDC-2 also has tightly packed grains. Well-rounded, lithic grains are abundant. Cross-polarized light, scale bar = 1000 μm

KDC-2 is composed of fine to medium (200-400μm), sub-angular to sub-rounded, moderate to poorly sorted, tightly packed grains with ~2% clay matrix. Grain composition by point counts consists of 42% quartz, 10% feldspar plagioclase, 48% lithics of which 88% are represented by polycrystalline quartz. Zircons, micas and detrital clay grains are also abundant. Grains are tightly packed, and share long, concavo-convex, and sutured contacts. This sample is mineralogically immature and texturally sub-mature, and is classified as a lithic arenite.

APPENDIX C: SEM AND XRD RESULTS

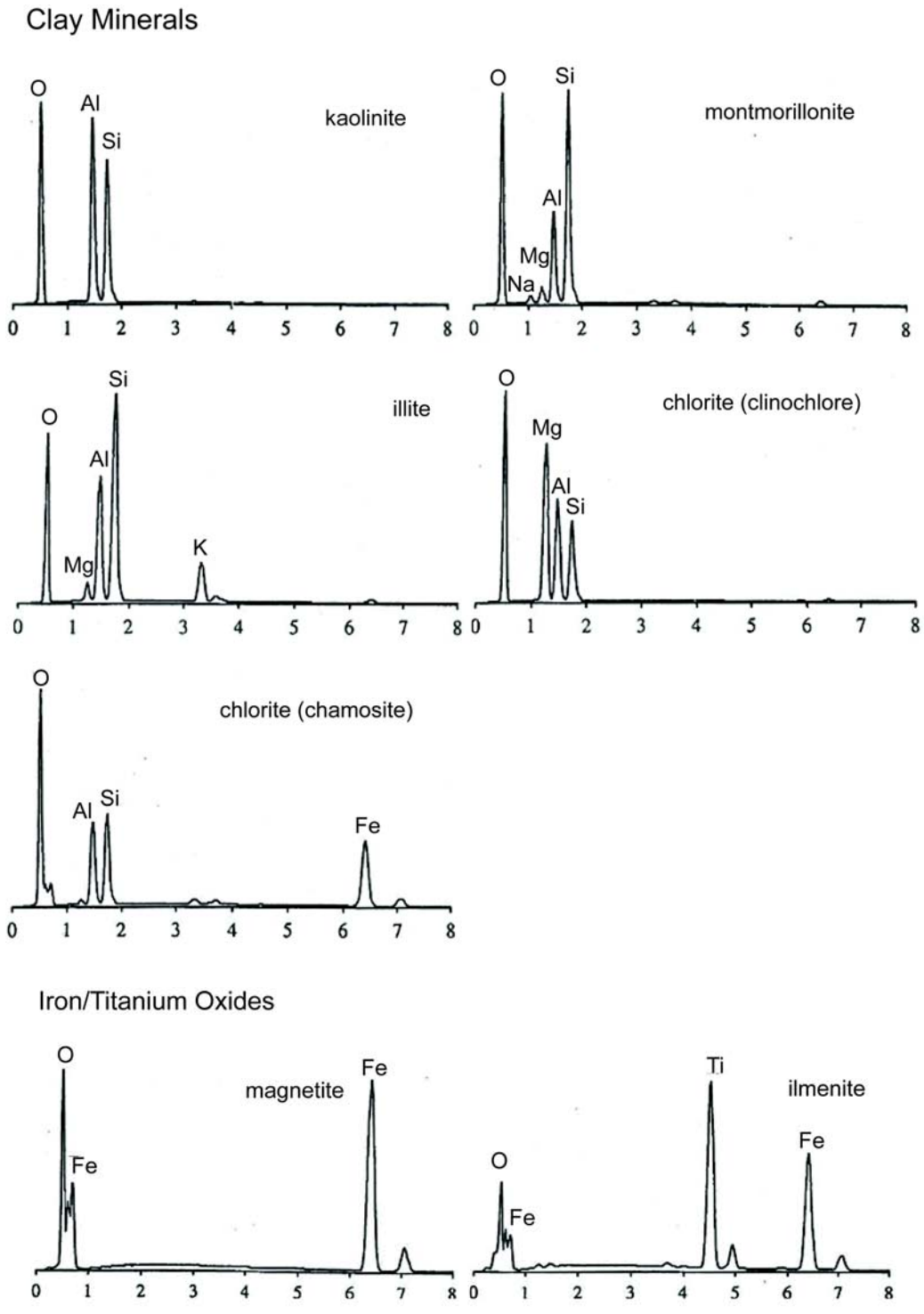

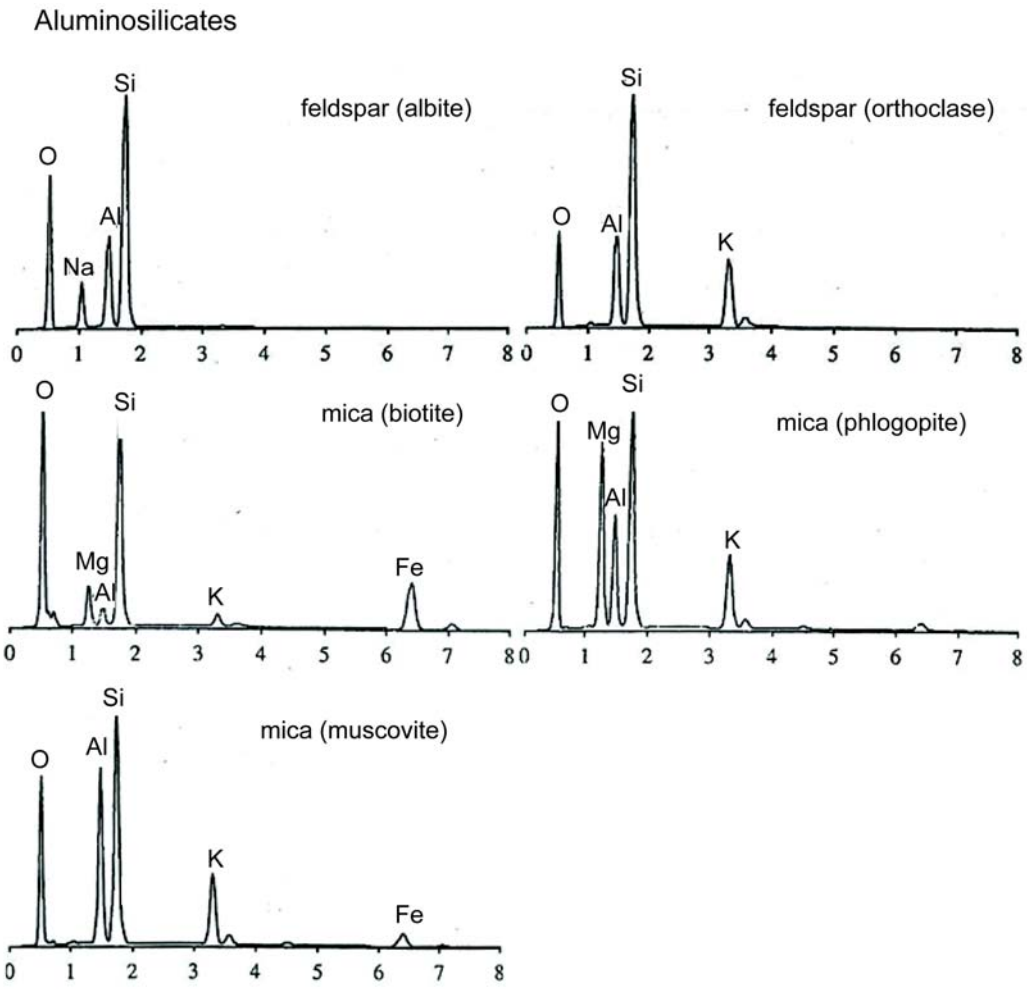

Reference EDS spectra of relevant minerals from Reed, 2016.

BPS-1 Image 1

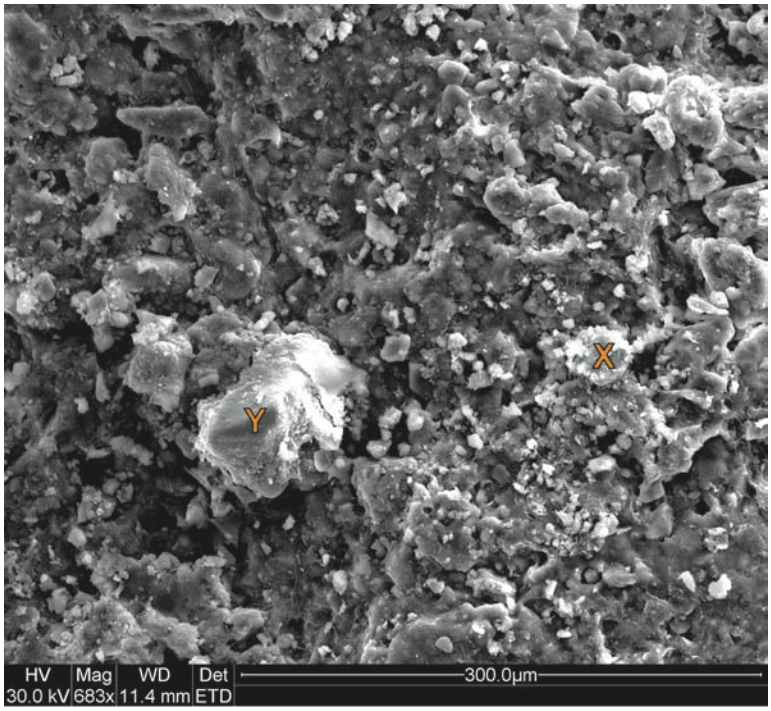

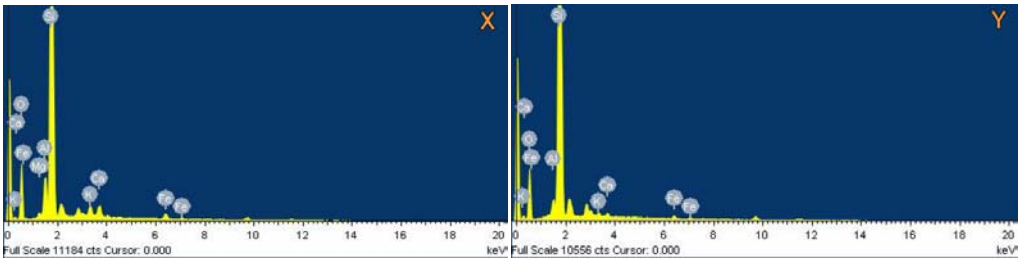

BPS-1 was collected from the Main Karoo Basin from a brick red (Munsell code), indurated palaesol with blue (Munsell code), forked rhizoliths. The above overview image shows a mix of very large grains, especially in comparison to the other samples collected from the Lebombo-Tshipise Basin. There is a less well developed clay matrix. The sample's XRD spectrum has strong peaks for quartz, sodium feldspar, plagioclase, mixed illite/smectite, and mica, and trace peaks for calcite and hematite. Note the XRD spectrum is shifted about +6 degrees (to the right) 2θ.

Spectrum X is consistent with mica (biotite), and though the grain (X) appears to be heavily degraded and webby, the spectrum does not seem to include extra clay. Spectrum Y has an even smaller aluminium peak, and likely represents a large quartz grain covered with minor smectitic clay which could account for small aluminium, potassium, calcium and iron peaks.

BPS-1 XRD Spectrum

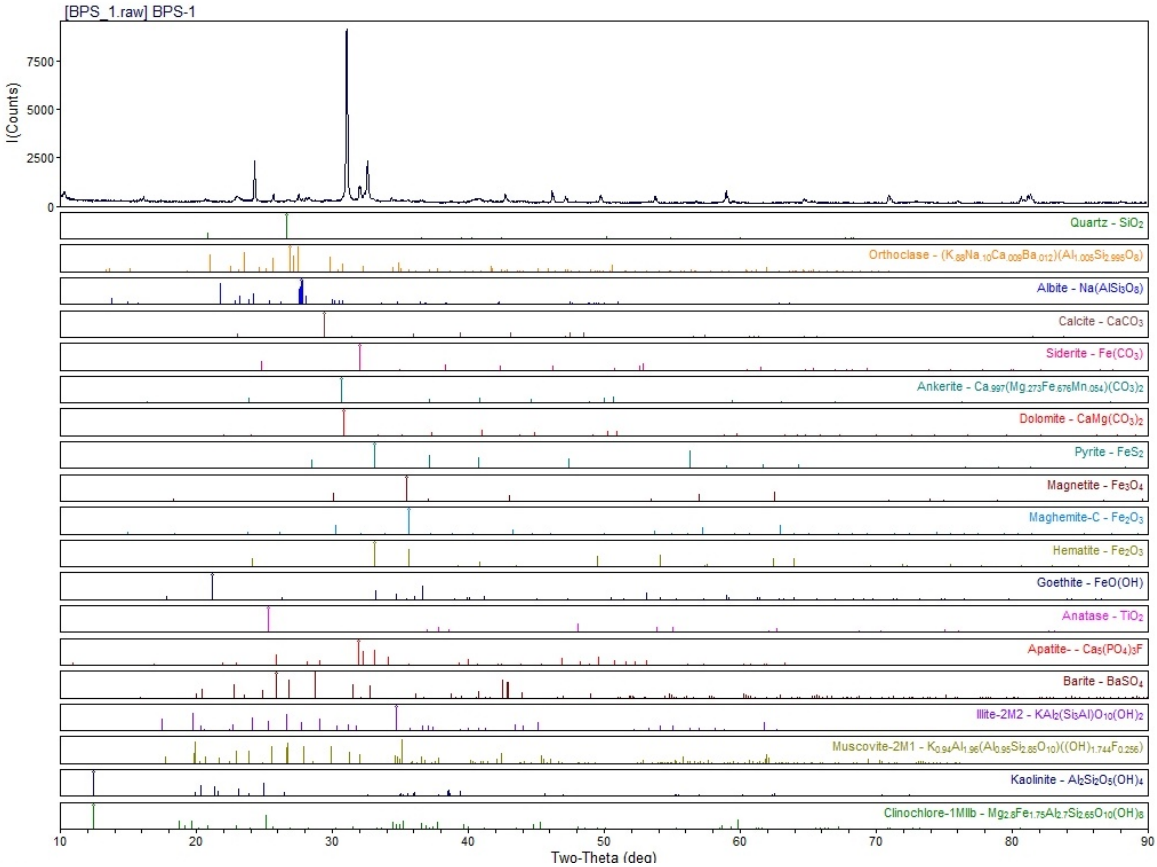

BPS-1 Image 3

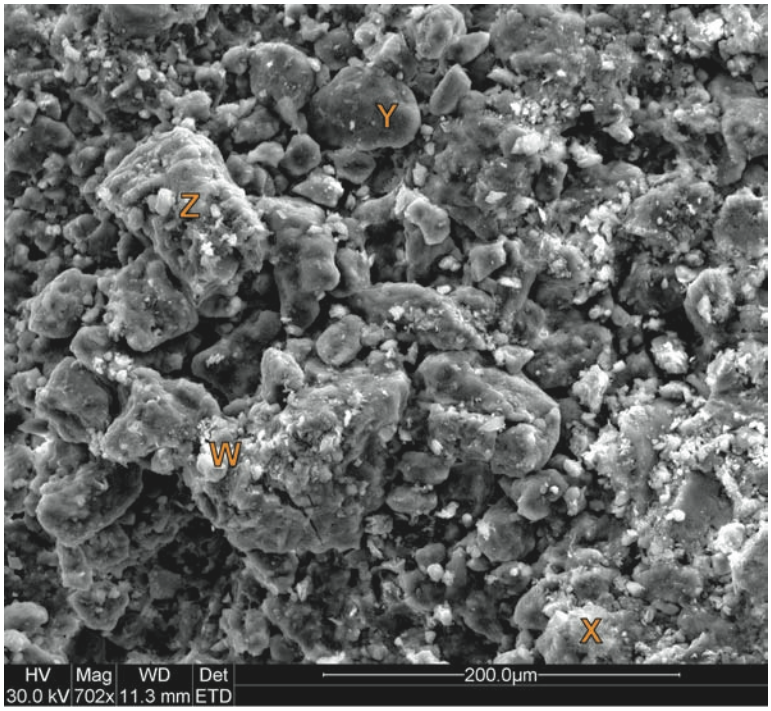

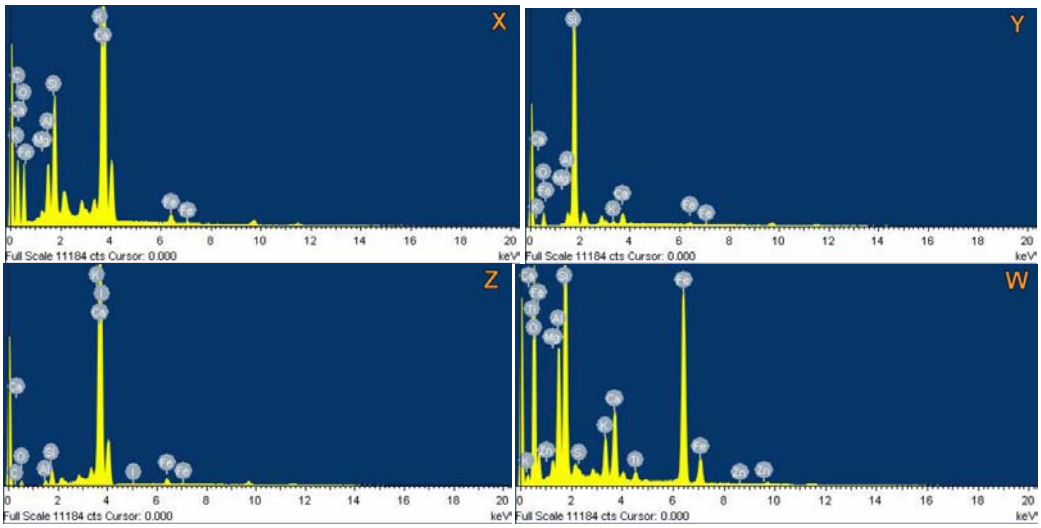

Spectrum X has unexpectedly large potassium and calcium peaks, but otherwise is similar to illite clay. X has a webby, flaky appearance consistent with clay. Large amounts of potassium and calcium may represent zeolites or other alteration products. Grain Y is large and polygonal and is likely quartz. Minor additional peaks may be clay products covering the grain or nearby. Z marks a crust forming over a grain. Its spectrum (Z) has a very large potassium peak, with smaller calcium, silicon and iron peaks, and a very small aluminium peak (the iodine peak is erroneous and overlaps with potassium). This spectrum is difficult to interpret, but this crust appears to be an alteration product of mica or feldspar. Spectrum W has very large iron peaks and resembles chlorite with intermixed illite. Zinc is likely an impurity in the chlorite.

KDS-1 Image 1

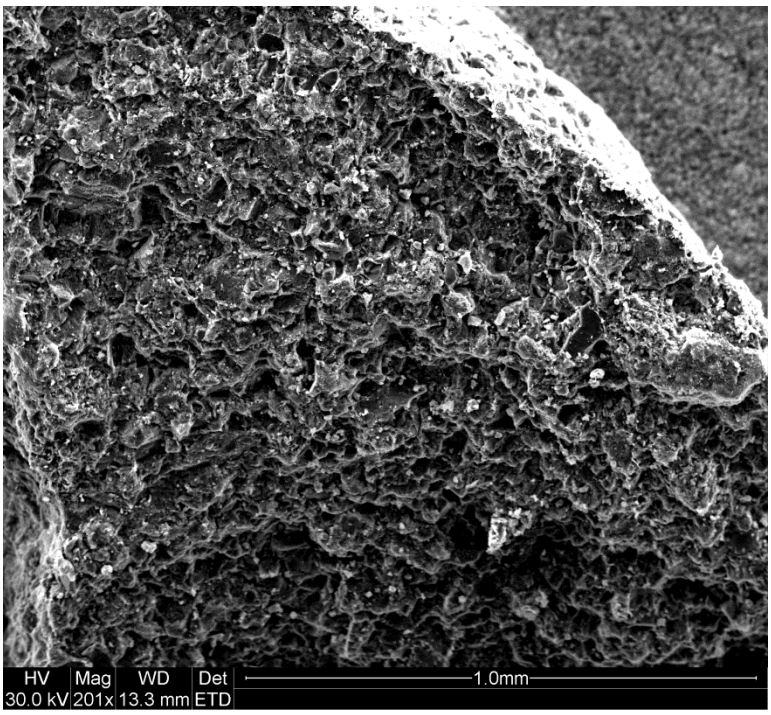

Sample KDS-1 was collected from Palaeosol A, 0.5 m from the base of the outcrop, and 26.5 m east of a large (~3m wide), subvertically oriented, dolerite dike. The above overview image of the sample shows some dissolution pockets where grains have been disolved. A variety of clay morphologies, and large quartz and/or feldspar grains are present. The sample's XRD spectrum has strong quartz, mixed layer illite/smectite, and mica peaks, and sodium plagioclase, and kaolinite peaks. Trace potassium feldspar, pyrite, maghemite, hematite, anatase and chlorite peaks are also identified.

KDS-1 XRD Spectrum

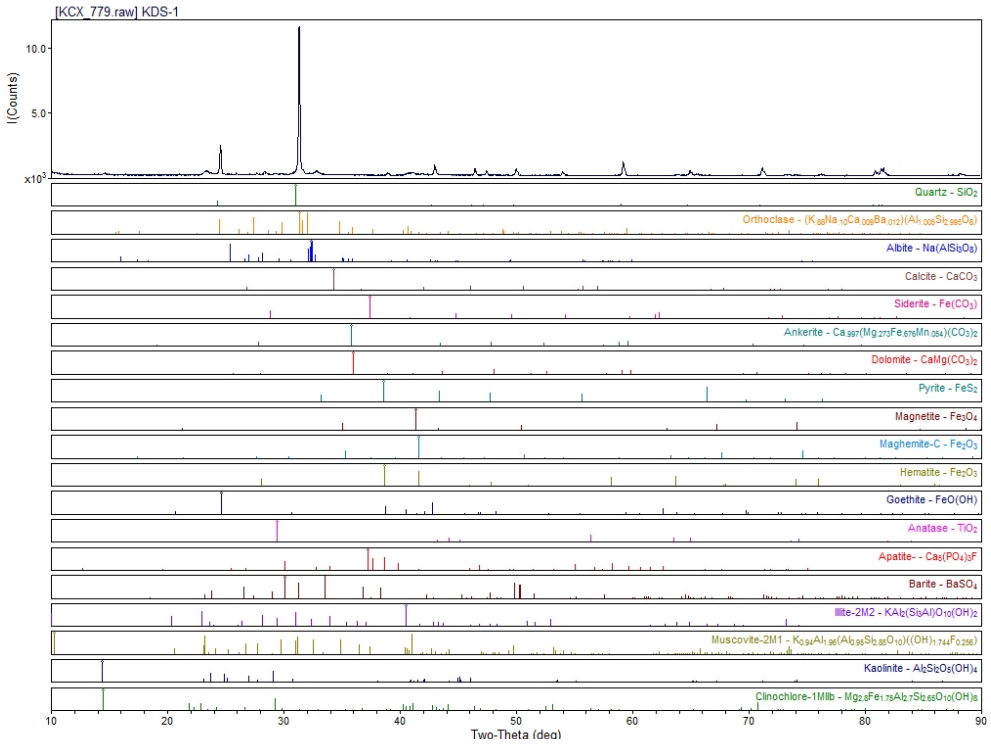

KDS-1 Image 3

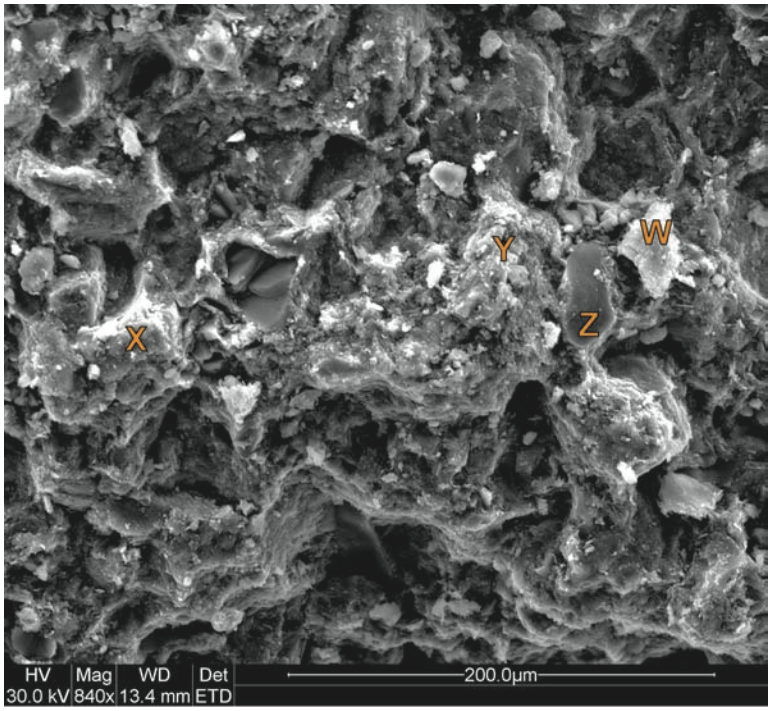

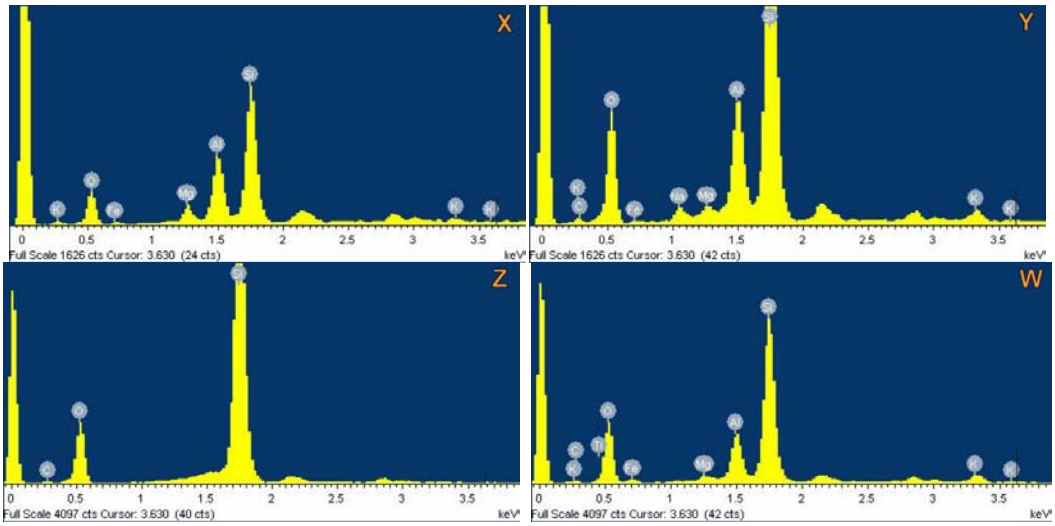

Spectrum X is relatively complex and likely represents mica or illite with minor iron and titanium oxides. The grain appears to be heavily degraded, and small, light colored flakes at its periphery might be authigenic clay. Spectrum Y is more complex containing sodium, potassium, and a relative increase in aluminium to sodium, magnesium, and potassium in comparison to X. This is consistent with mixed illite and smectite clay. The clumpy morphology of Y may be representative of a more advanced decay of mica to authigenic clay. Z is a quartz grain, which is rounded and appears to be larger than other mica, feldspar or clay grains. Spectrum W is very similar to X and likely represents a slightly different morphology of the same illite with minor iron and titanium oxides; this grain appears more separated from the matrix than X and may represent a detrital grain.

KDS-1 Image 4

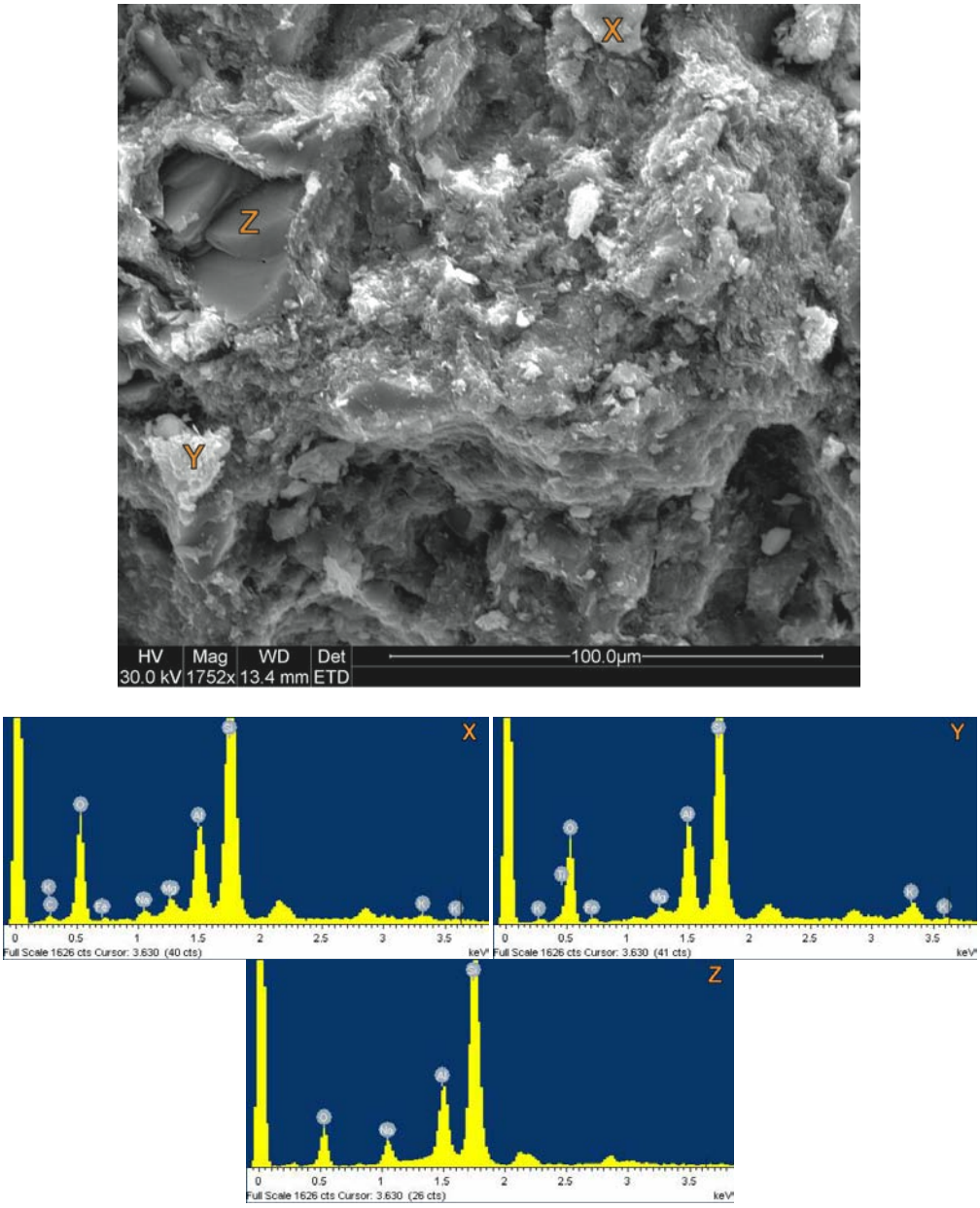

Image 4 shows the same grains as Image 3, but is more magnified (840x). Spectrum X is consistent with mixed illite and iron-rich smectite clay. Spectrum Y has smaller iron and titanium peaks, and lacks sodium, making this grain more consistent with illite with minor iron and titanium oxides. Z marks albite grains encased in clay matrix. These are the likely source of sodium for authigenic smectite clay.

KDS-1 Image 5

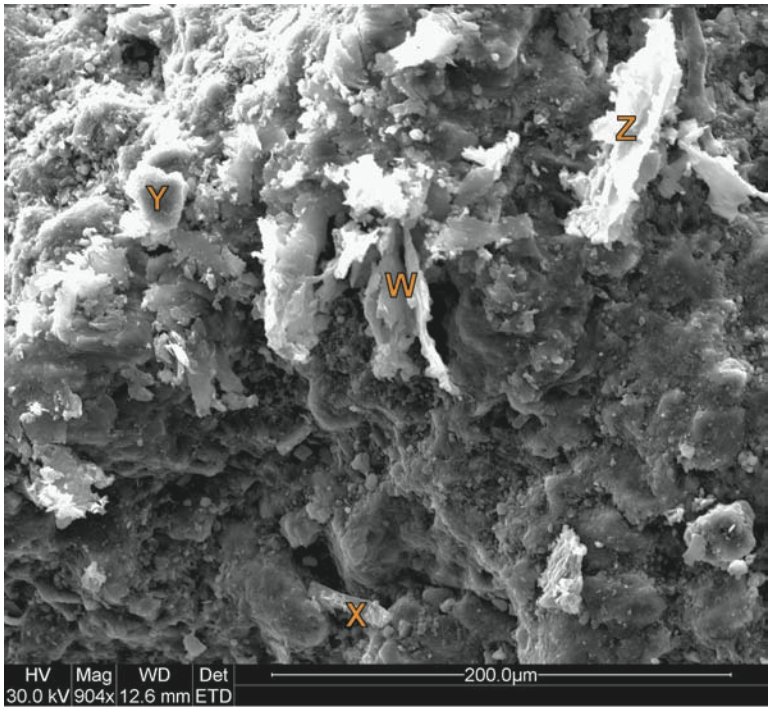

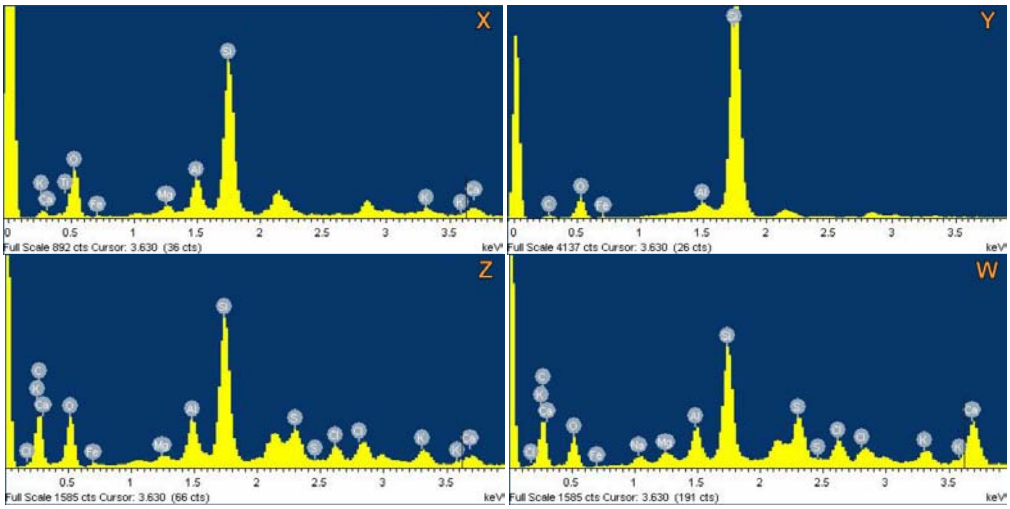

X represents flakey, calcium-containing smectite and illite clay which appears to be a fine, authigenic covering over a rectangular mineral. Y appears to be a quartz grain with minor iron and aluminium forming an oxide covering. The large, platey flakes of Z and W both represent illite and iron containing smectite clays with chlorine and sulfur likely substituting in the hydroxyl group. Z lacks sodium, while W contains sodium and relatively more calcium than is present in Z. These differences are likely due to different cation replacement after burial.

KDS-1 Image 6

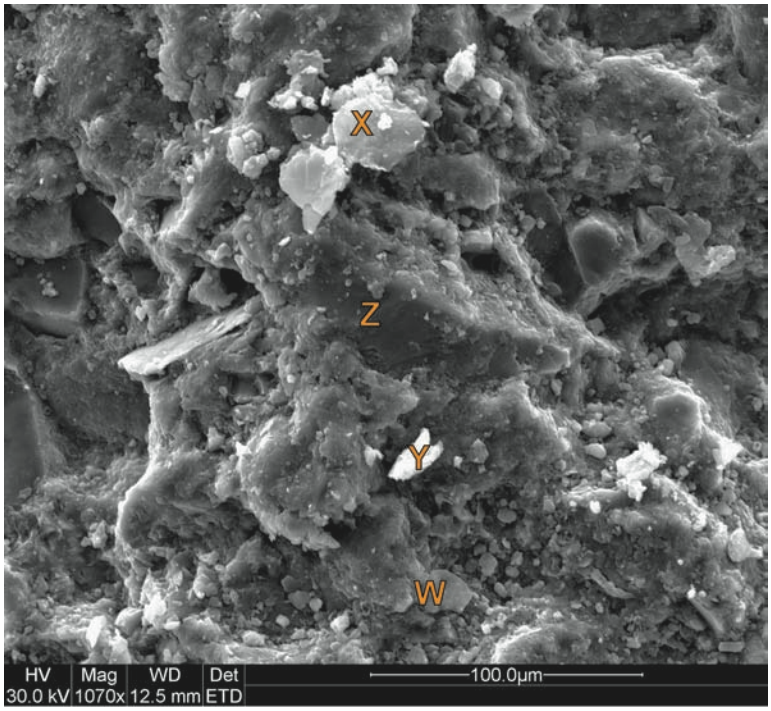

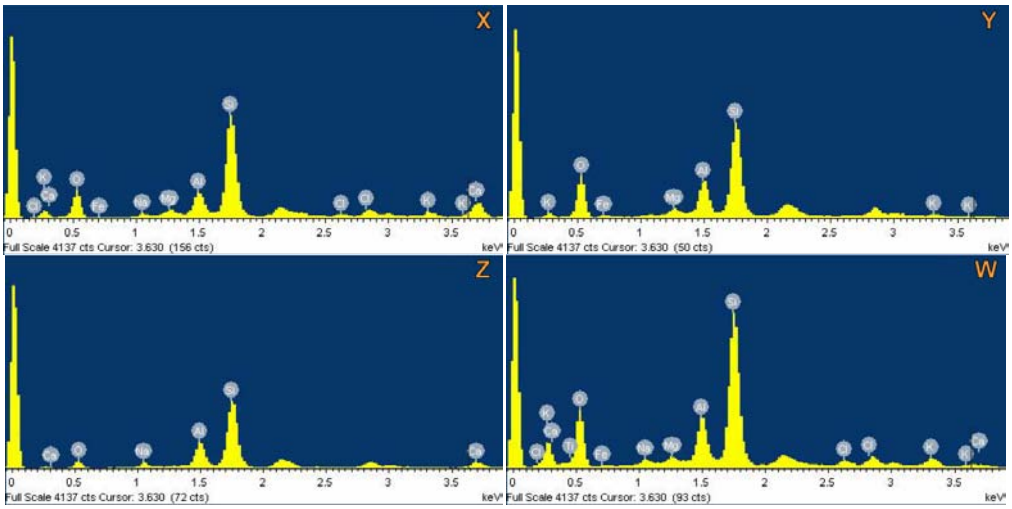

X and W are iron-containing smectite with minor iron, and chlorine substitution in the hydroxyl group. The platy, stacked morphology of these grains indicates they are detrital, rather than authigenic. Spectrum Y is most consistent with a mica (biotite) grain, though the aluminium peak's proportion to silicon is similar to illite clay, perhaps indicating a break-down of mica to constituent clays. Z is a rather large (~100 µm across) grain embedded in clay matrix which likely represents intermediate (Ca-Na) plagioclase, though the spectrums overall small number of counts (72) obfuscates the true proportion of aluminium to silicon, the morphology of the grain indicates this is not likely to be clay or mica.

KDS-1 Image 7

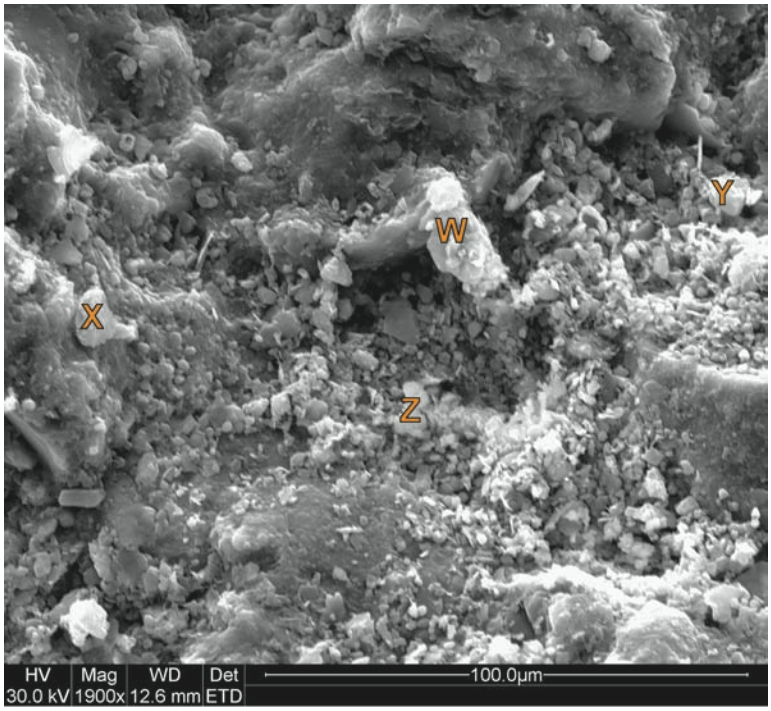

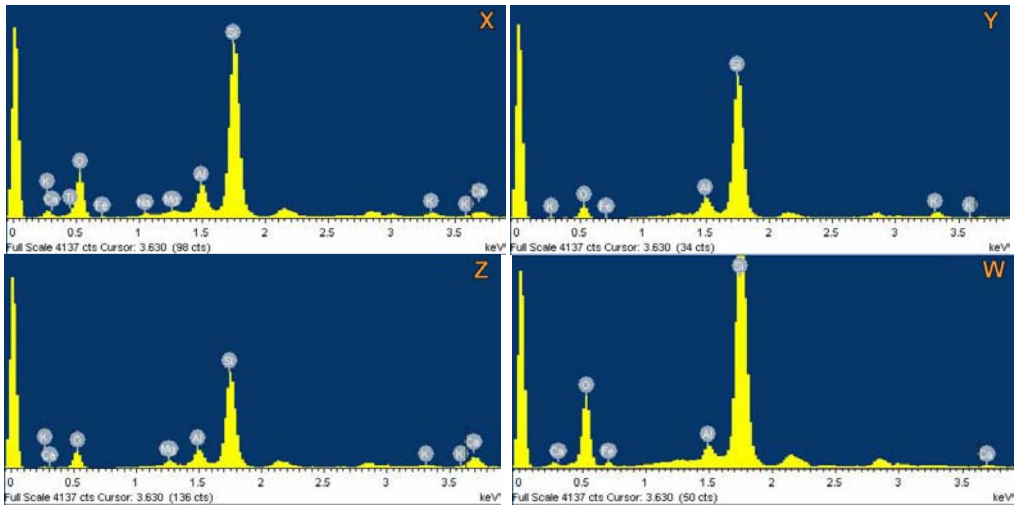

X appears to be a rounded smectite grain with iron and titanium likely present within the clay through cation replacement. The grain morphology is consistent either with a fine authigenic covering of a mineral grain, or a detrital clay grain. Spectrum Y is intermediate between biotite and muscovite, and the platy, boxy morphology of the grain (Y) is typical of mica. Spectrum Z likely represents illite and smectite clay, though the aluminium peak is much reduced. However this is likely caused by the EDS spot penetrating a topographic low in the sample. Spectrum W is difficult to interpret due to its exceedingly small aluminium peak which is inconsistent with calcium plagioclase- it could represent either a quartz grain with smectite-like clay, or a mica (biotite) grain with calcium and iron replacing potassium and magnesium. Its large, platy appearance favors a large mica grain with an irregular spectrum, though additional flakes of authigenic appearing clay on grain W complicate interpretation.

KDS-2 Image 1

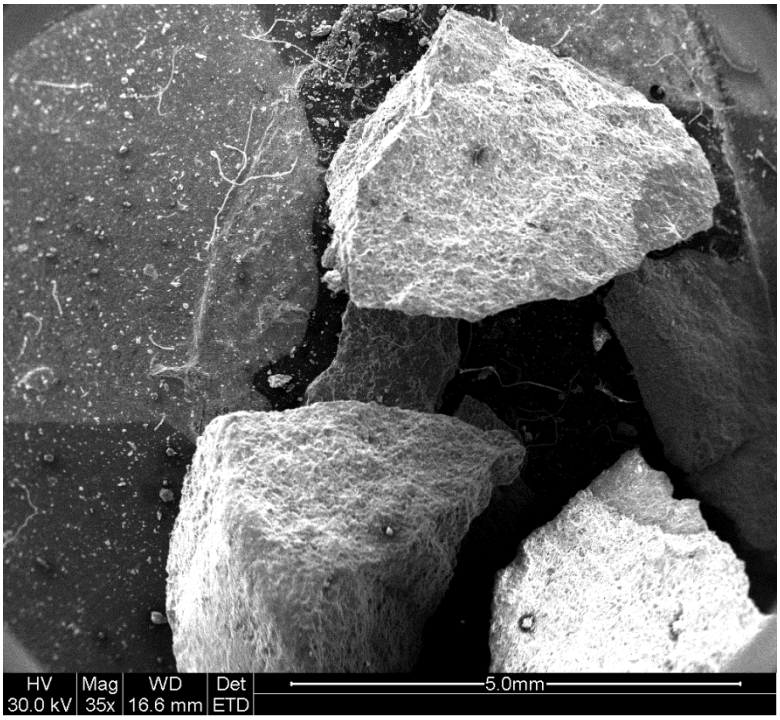

Sample KDS-2 was collected from Palaeosol A, 4.5 m above the outcrop base and 29.5 m east from the intrusive dolerite dike. It is purple in color and very fine grained. The fine-grained texture of the sample crumbs is evident in the above overview image. The sample's XRD spectrum has strong quartz, mixed layer illite/smectite and mica peaks, and minor potassium feldspar, plagioclase, and kaolinite peaks. Trace peaks for hematite, goethite and chlorite are also present.

KDS-2 XRD Spectrum

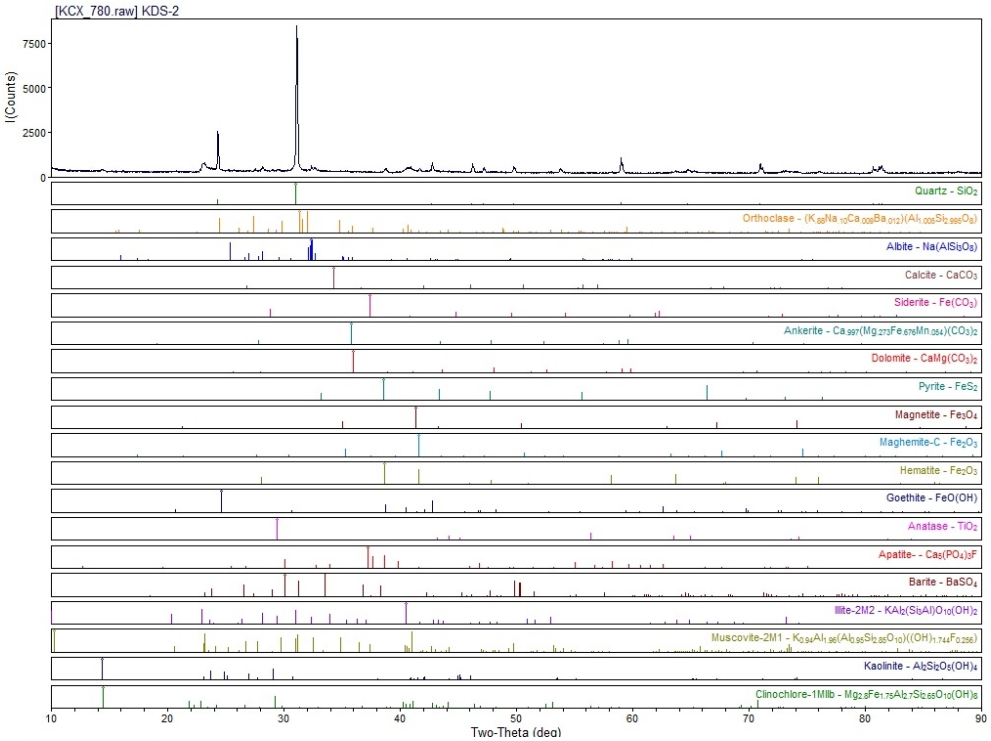

KDS-2 Image 3

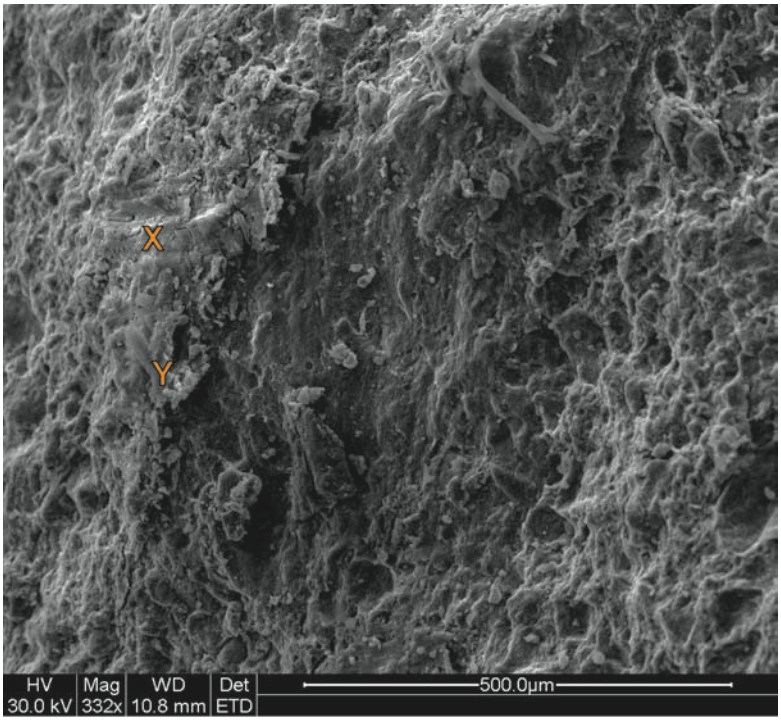

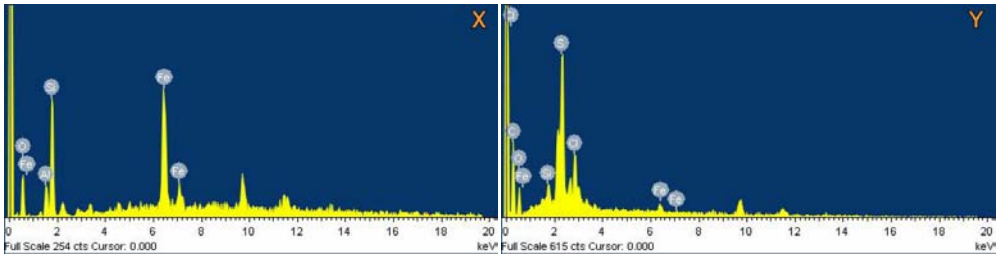

Spectrum X is very iron-rich and could either represent a crusty covering of iron oxides with minor aluminiumo silicates, or iron-rich chlorite (chamosite) with a reduced aluminium peak. Though Y appears to be a similar crusty covering, large sulfur and iron peaks are consistent with pyrite, while the presence of chlorine complicates this interpretation. The most likely explanation for such a large chlorine peak is the presence of salts or as a hydroxyl substitution in clay. However, the lack of sodium or other typical cations (e.g. calcium, potassium, magnesium) and aluminium is problematic. These cations and/or an aluminium peak may be obscured by the broad silicon peak near 2 keV.

KDS-2 Image 8

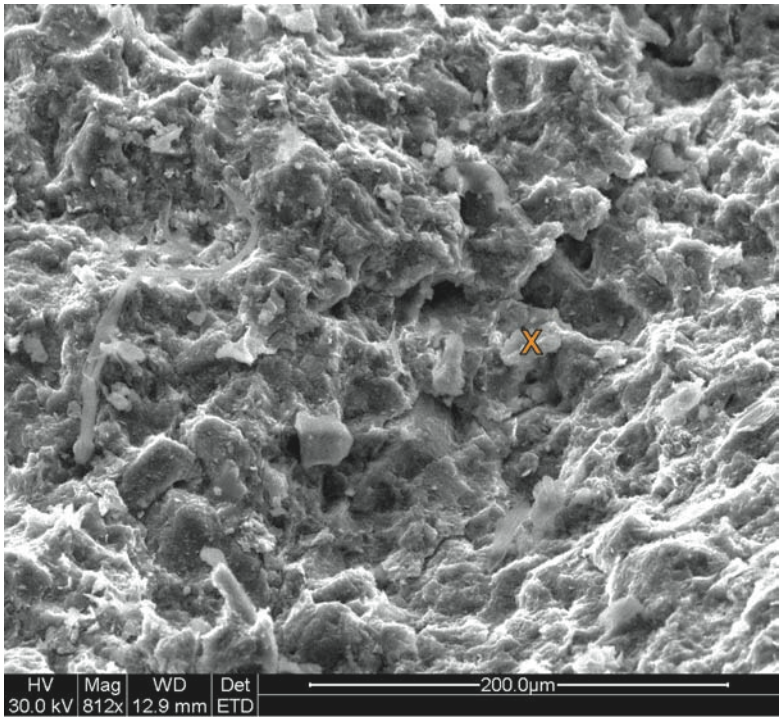

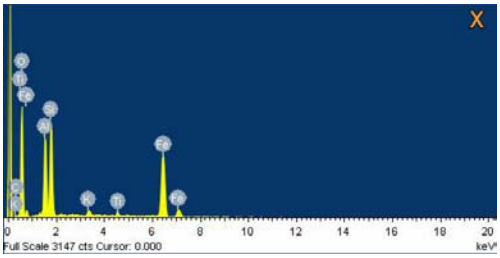

Spectrum X appears to represent iron-rich chlorite, or chamosite with minor potassium and titanium peaks either representing adsorbed cations or additional clay. The spectrum is taken from an apparent, rounded grain, however the morphology does not resemble detrital chlorite grains. It is likely a clayey covering of some other mineral grain.

KDS-2 Image 9

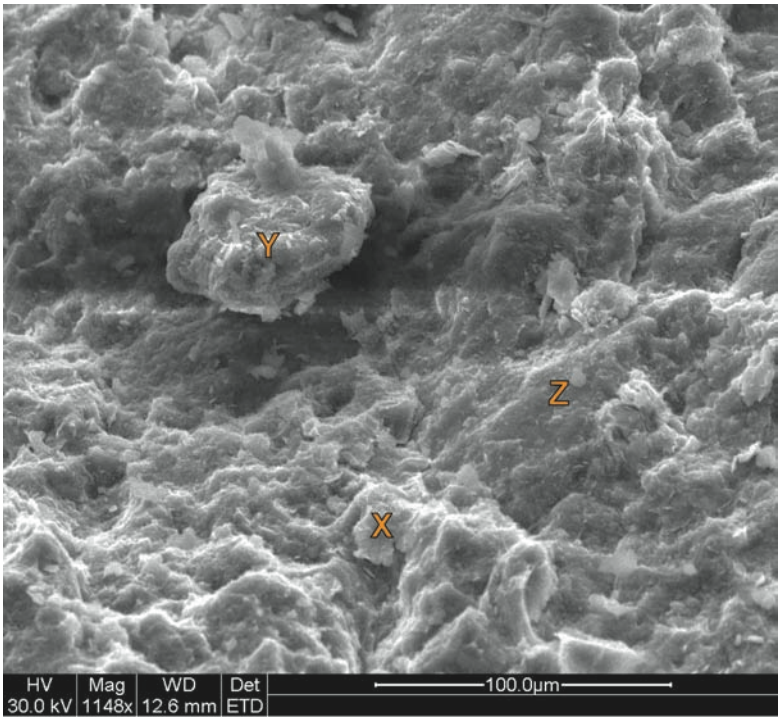

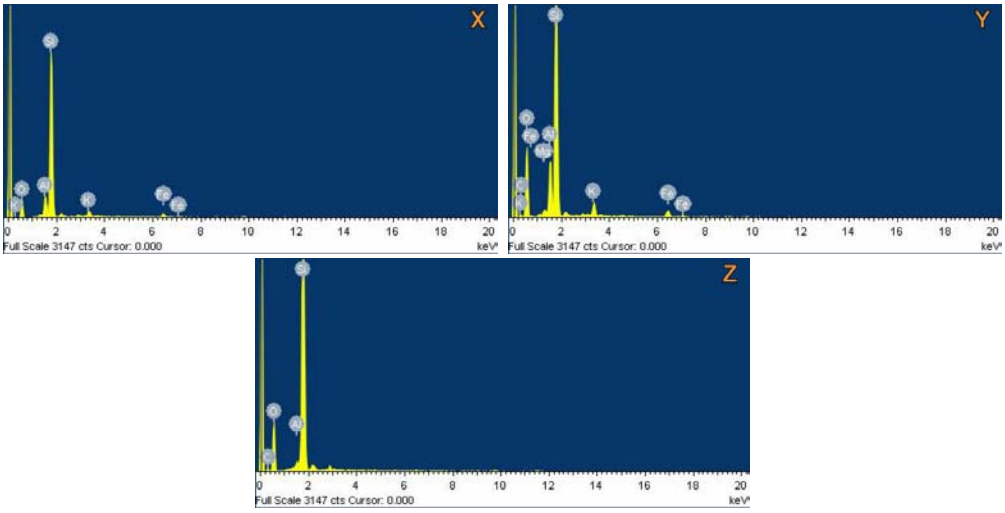

Spectrum X appears to be mica (biotite) which is consistent with its sub-rounded appearance, though the webby covering indicates the presence of clays. Spectrum Y appears to be illite with iron oxides. The clay mass appears to be a detrital grain. Spectrum Z is most consistent with quartz, with the minor aluminium shoulder likely contributed by nearby clay.

KDS-2 Image 10

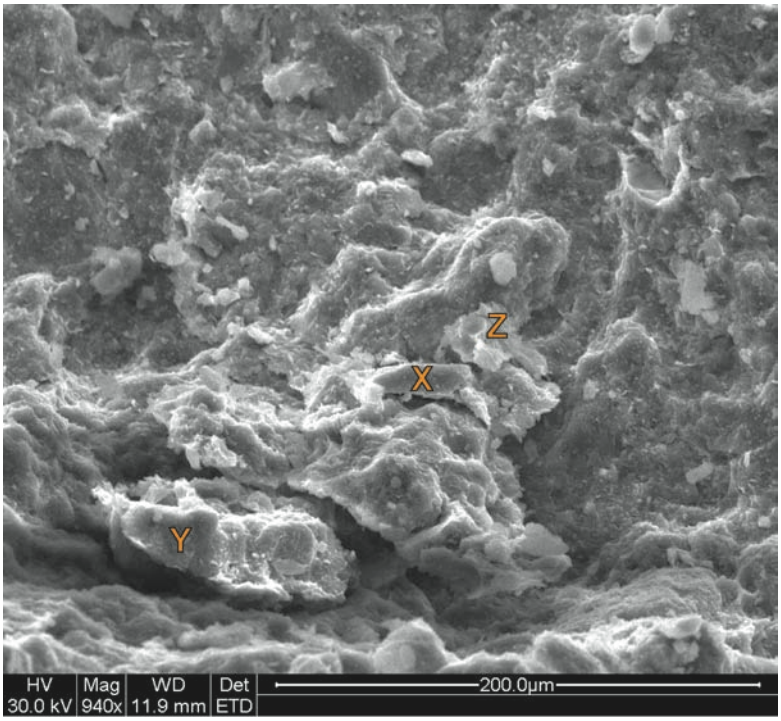

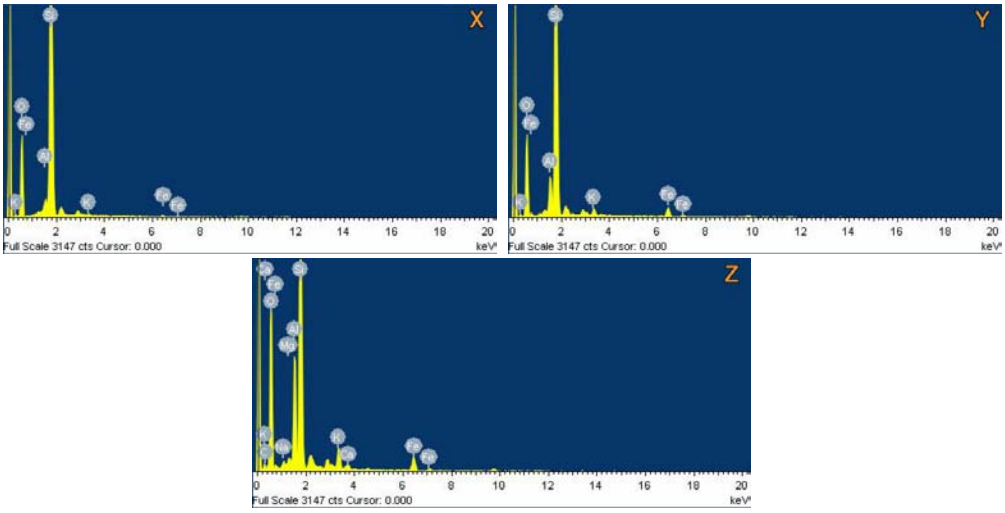

Square and blocky grain X is potassium feldspar, and the small iron peaks in Spectrum X are likely contributed by iron oxides such as hematite, or goethite which were identified in the XRD analysis. The large, slightly flaky grain Y likely represents mica (biotite), though it could be illite with iron replacing magnesium. Spectrum Z is consistent with illite and smectite clay, as is the grains' webby appearance.

KDS-3B Image 1

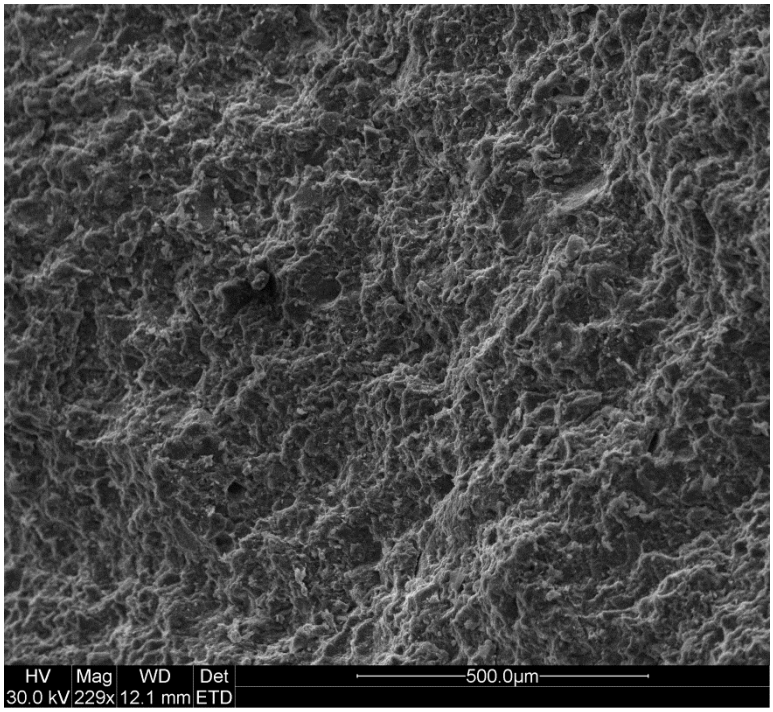

Sample KDS-3B was collected from Palaeosol A 4.5 meters from the base of the outcrop and 34 meters east of the large dolerite dike. The partner sample (KDS3-A) appeared to be an altered, greenish contact aureole of this sample and some other, indurated potential dike. XRF results show an enrichment of calcium (0.94 wt%) compared to others from Palaeosol A (0.07-0.50 wt%), and quartz (84.51 wt%) to stratigraphically bracketing samples KDS2 (65.15 wt%) and KDS4 (68.27 wt%). Proportionately less aluminium is present in this sample (6.05%) to KDS2 (16.11%) and KDS4 (14.76%), which indicate this sample is clay-poor. Trace amounts of ankerite/iron-rich dolomite were detected in the XRD spectrum. These data indicate diagenetic processes have affected this sample. This sample's XRD spectrum has strong peaks for quartz and sodium plagioclase, and minor peaks for mixed layer illite/smectite, chlorite, and kaolinite. Trace amounts of potassium feldspar, ankerite/Fe-dolomite, barite, maghemite, hematite and mica are also present.

KDS-3 XRD Spectrum

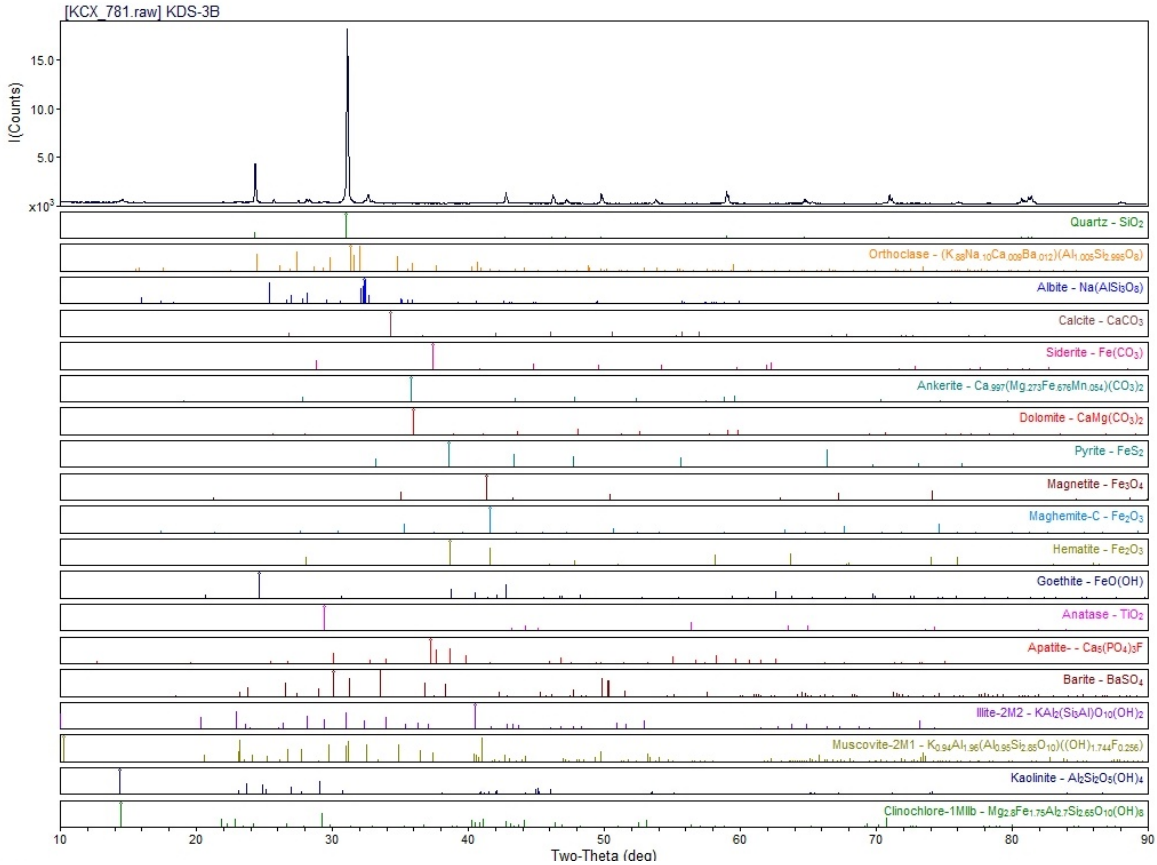

KDS-3B Image 5

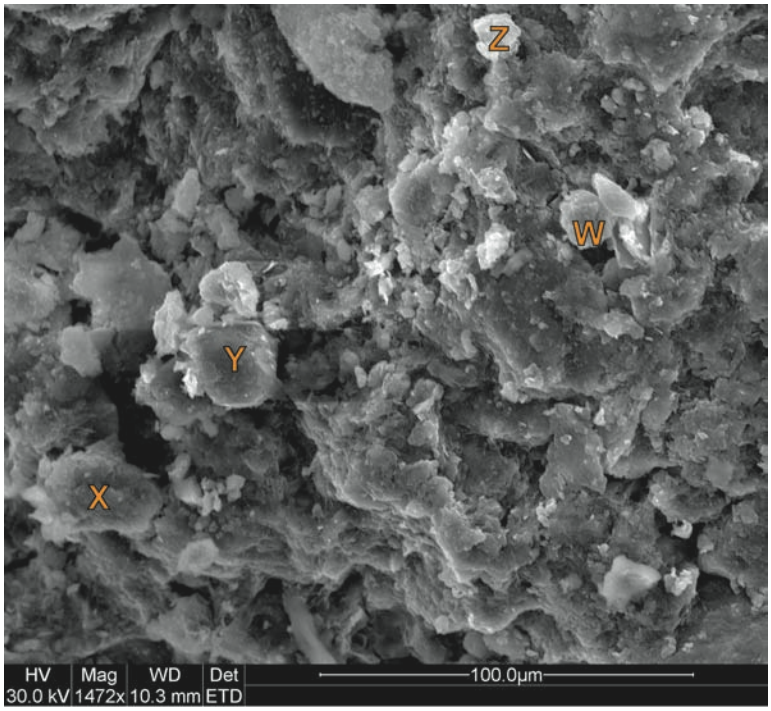

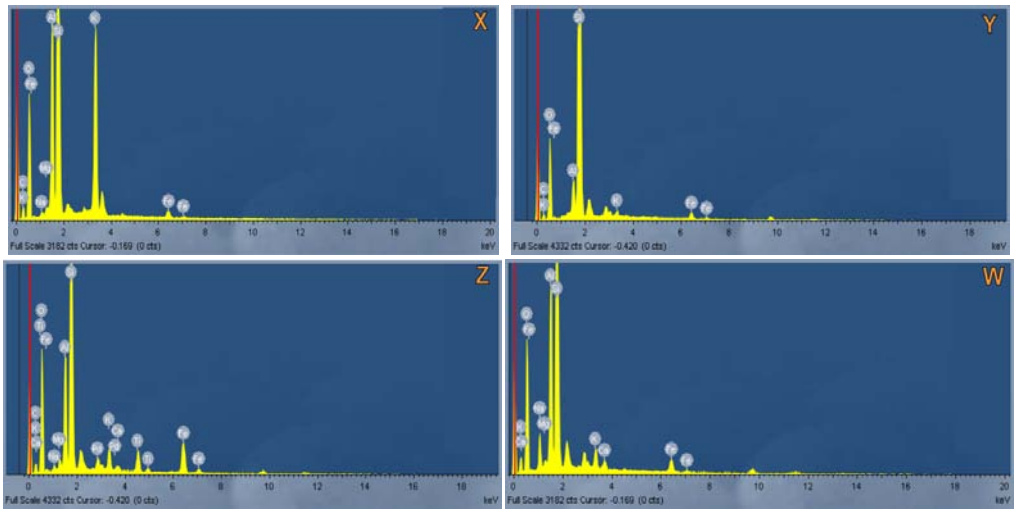

Spectrum X is particularly enriched in aluminium and potassium, consistent with kalsilite. However, as this mineral primarily occurs in igneous rocks (www.webmineral.com), this similarity is likely superficial. Sodium, magnesium, iron and potassium are all characteristic of mixed layer smectite/illite clay, while the enrichment of aluminium may represent additional kaolinite. Potassium enrichment may further indicate diagenetic processes apparent in the sample. The grain is similar to other described detrital illite/smectites from previous samples. Spectrum Y is consistent with potassium feldspar while, the relatively large oxygen peak and iron peaks may indicate the presence of additional iron oxides such as hematite or maghemite, which were detected by XRD analysis. The webby morphology of grains Z and W is typical of illite/smectite clay, and these spectra contain smectite components including calcium, sodium, magnesium, iron, and potassium. The large oxygen peak may indicate that some of the iron and titanium (Z) may be present in oxides. Palladium peaks are from the sample coating.

KDS-3B Image 6

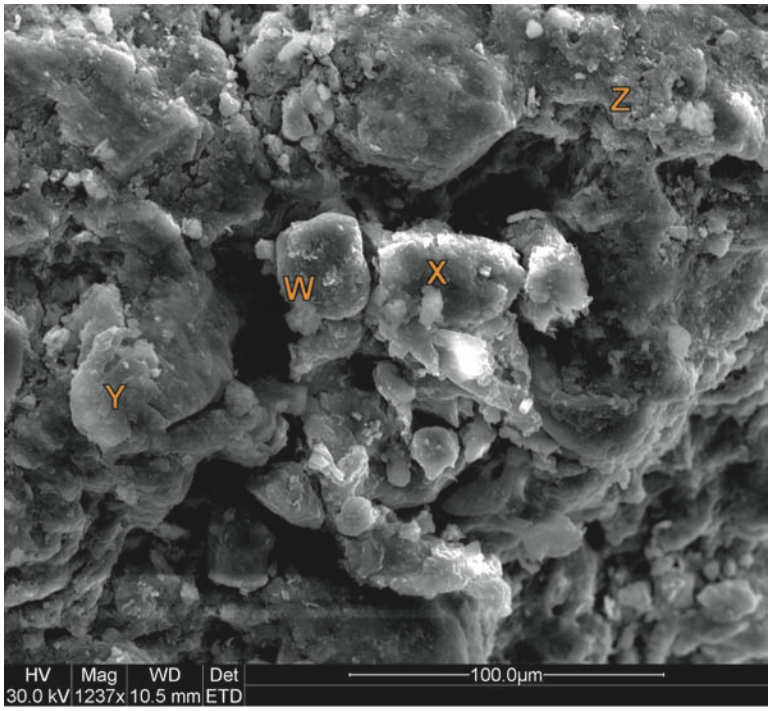

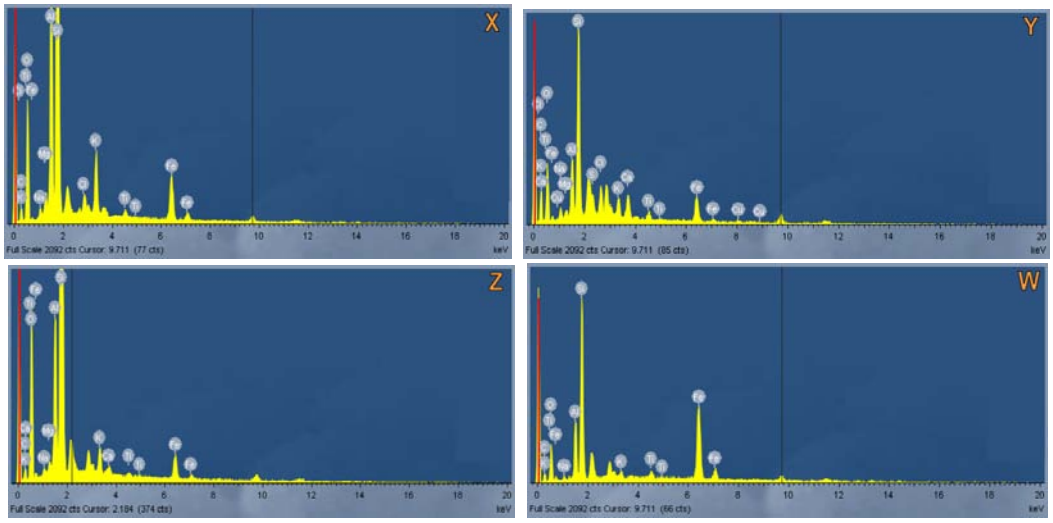

Spectra X, Z and W are consistent with mixed layer smectite and illite, though the enrichment of aluminium relative to silicon in X is not typical of these clay groups and may indicate the additional presence of kaolinite. Chlorine is likely substituting in the hydroxyl groups. The morphology of grain X indicates this webby mass of clay is detrital, while Z appears to be a clay crust that is likely authigenic. Grain W is most atypical of webby clay, and may be another mineral grain covered by a fine, authigenic covering of clay, indicated by the small flakes. Calcium in Spectrum Z may therefore represent diagenetic cation adsorption by smectitic clays, and indicate that calcium enrichment of the sample was related to fluid flow after burial. Spectrum Y appears to be very complex smectite clay with typical cations (potassium, sodium, calcium) in addition to cation replacement by iron, titanium, and copper. Sulfur and chlorine are likely substituting in the hydroxyl group, while copper may be a substitute for the Al-Mg-Fe atoms in octahedral sheets of smectite

(Mosser et al., 1990). While the grain shows some texture consistent with clay, it is far less webby in appearance than grains X or W, and may represent a microcrystalline, authigenic crust.

KDS-4 Image 1

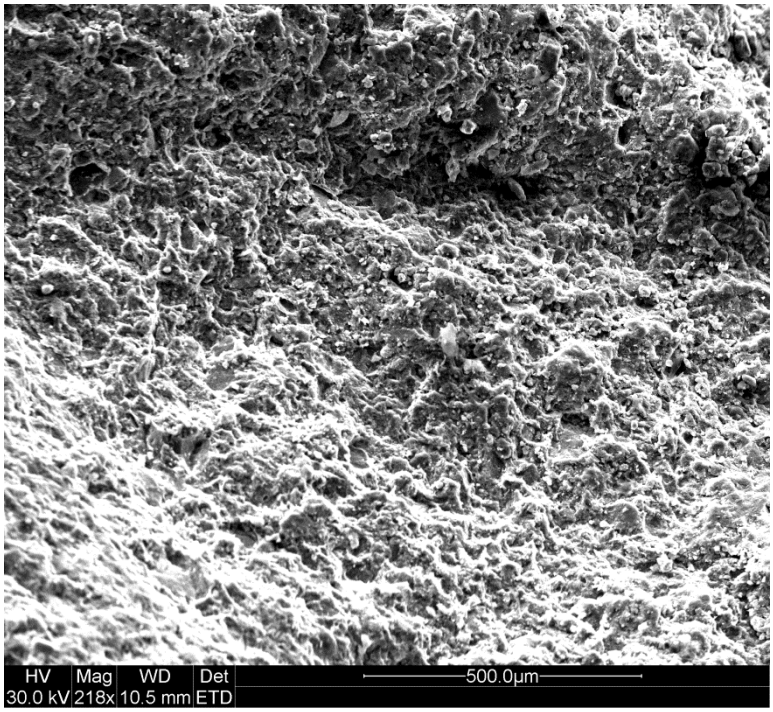

Sample KDS-4 was collected from Palaeosol A approximately 4.5 meters above the base of the outcrop and less than a meter (0.3 m) east of the large dolerite dike. The sample is dark purple (Munsell code) in color. The sample's XRD spectrum has strong peaks for quartz, mixed layer illite/smectite, and mica, and minor peaks for sodic plagioclase, kaolinite and chlorite. Trace peaks for potassium feldspar, maghemite, hematite and goethite are also present.

KDS-4 XRD Spectrum

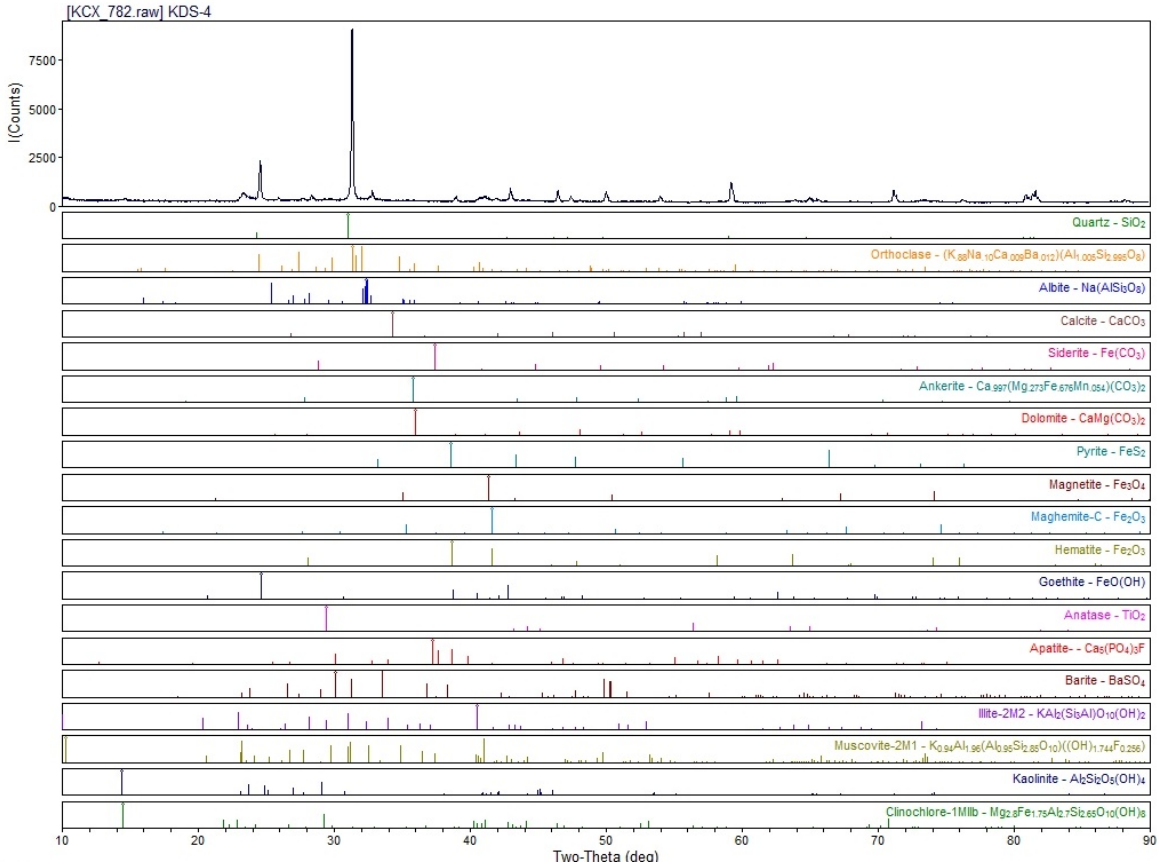

KDS-4 Image 2

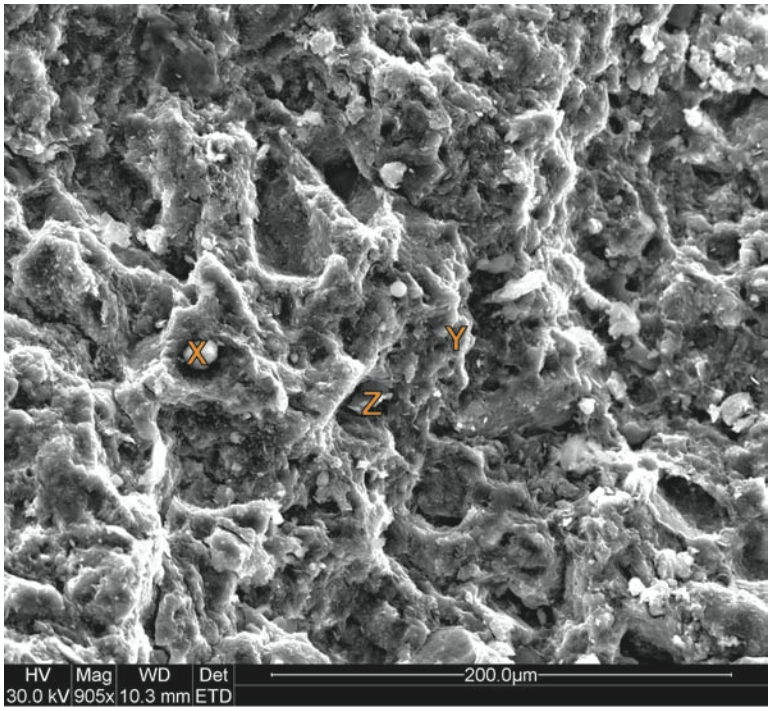

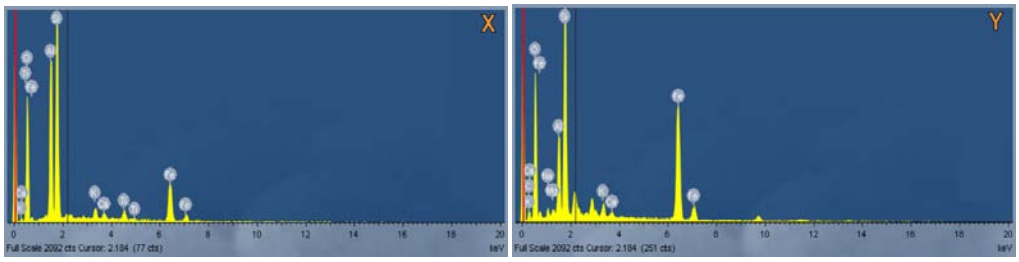

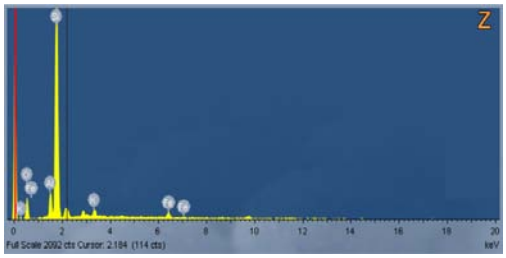

Spectrum X has a large proportion of aluminium to silicon and a large iron peak, consistent with mica (biotite), though the potassium peak is relatively small. Additional calcium and titanium may represent smectitic clay flakes or detrital titanite, though this was not detected in the XRD spectrum. The grain (X) appears to be rounded and detrital. Spectrum Y is fairly complex; the aluminium peak is smaller than associated iron peaks, which is consistent with chlorite (chamosite), though the additional sodium, magnesium, potassium and calcium peaks more closely resemble smectite. Y likely represents mixed chlorite and smectite which forms a fine, authigenic matrix. Alternately, this could be mica covered with iron oxides and smectite clay. Spectrum Z is consistent with potassium feldspar, while associated minor iron peaks may represent iron oxides.

KDS-4 Image 4

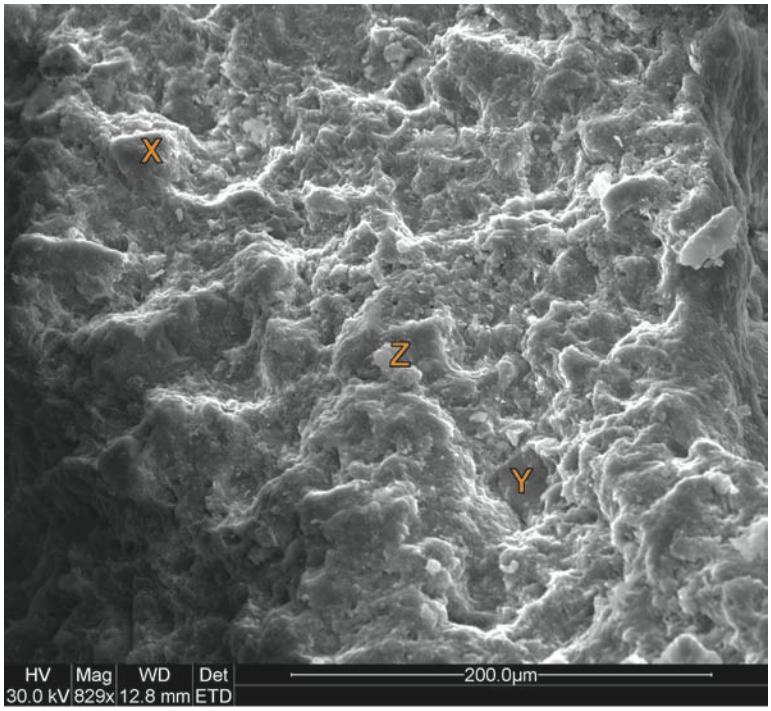

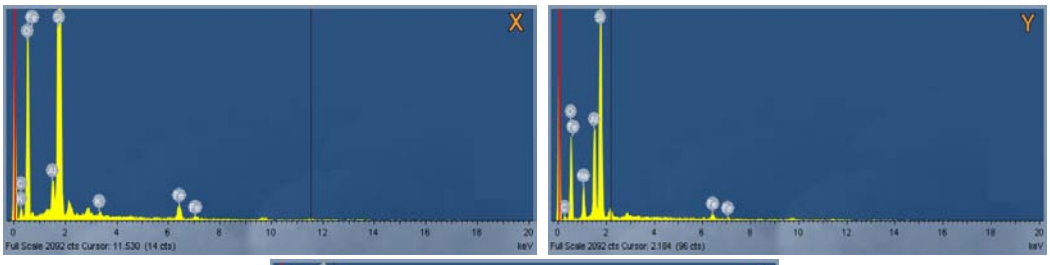

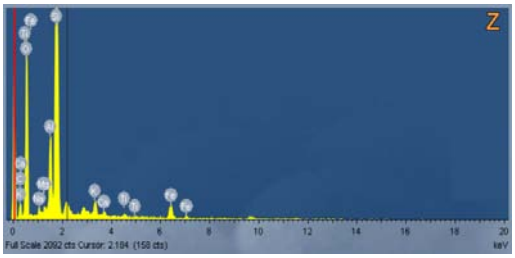

Spectrum X is consistent with potassium feldspar. The large oxygen peak and smaller iron peaks likely represent iron oxides coating the grain. The large silicon peak and relatively smaller aluminium and sodium peaks in spectrum Y are consistent with sodium feldspar, while the persistent presence of minor iron peaks are likely iron oxides present in the surrounding crust. Spectrum Z is typical of mixed illite/smectite; the webby mass of clay (Z) appears to be detrital rather than authigenic.

KDS-5 Image 1

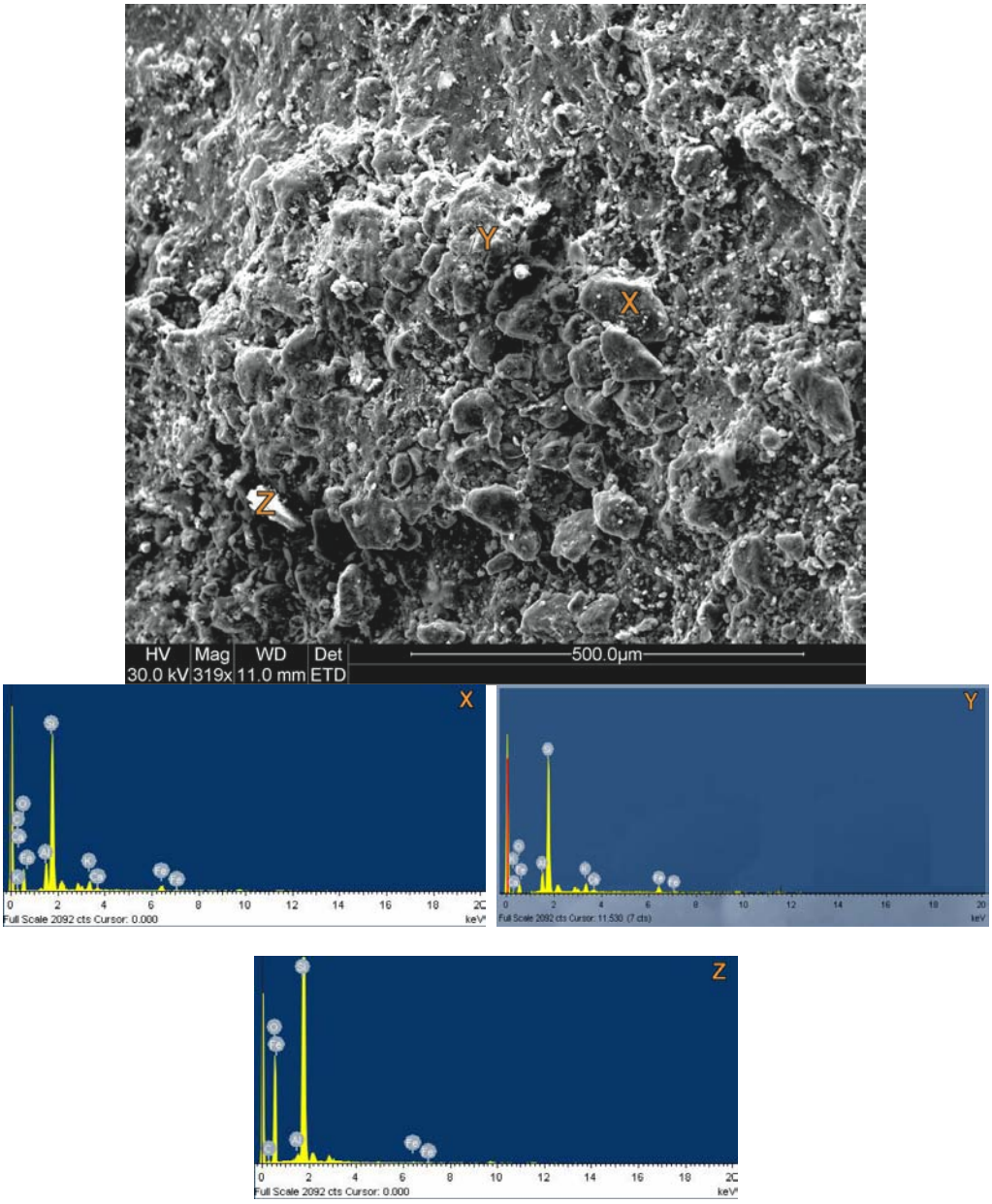

Spectrum X and Y are consistent with potassium feldspar. Minor iron and calcium peaks may represent smectitic clay surrounding and covering the large grains. Grain Y appears to have a crusty, iron oxide covering, though the iron peaks from both grains do not differ in intensity in the EDX spectra. The strong silicon peak in Spectrum Z shows quartz with traces of iron oxides evidenced by the small iron peaks.

KDS-5 a gray (Munsell code), clay sample collected from Palaeosol A approximately 0.8 meters from the top of the outcrop, and 34 meters east of the intrusive dolerite dike. The sample has the lowest amount of aluminium (4.1% by weight) of samples taken from this palaeosol (5.76 – 16.11% by weight; see Table 6); this is likely due to a smaller amount of clay relative to other samples. The above overview image shows relatively large quartz

and feldspar grains, some of which are encrusted with iron oxide and authigenic clay. The sample's XRD spectrum has major quartz, sodium plagioclase, mixed layer illite/smectite, and mica peaks, and minor kaolinite. Trace peaks for potassium feldspar, hematite, goethite, anatase and chlorite are also present.

KDS-5 XRD Spectrum

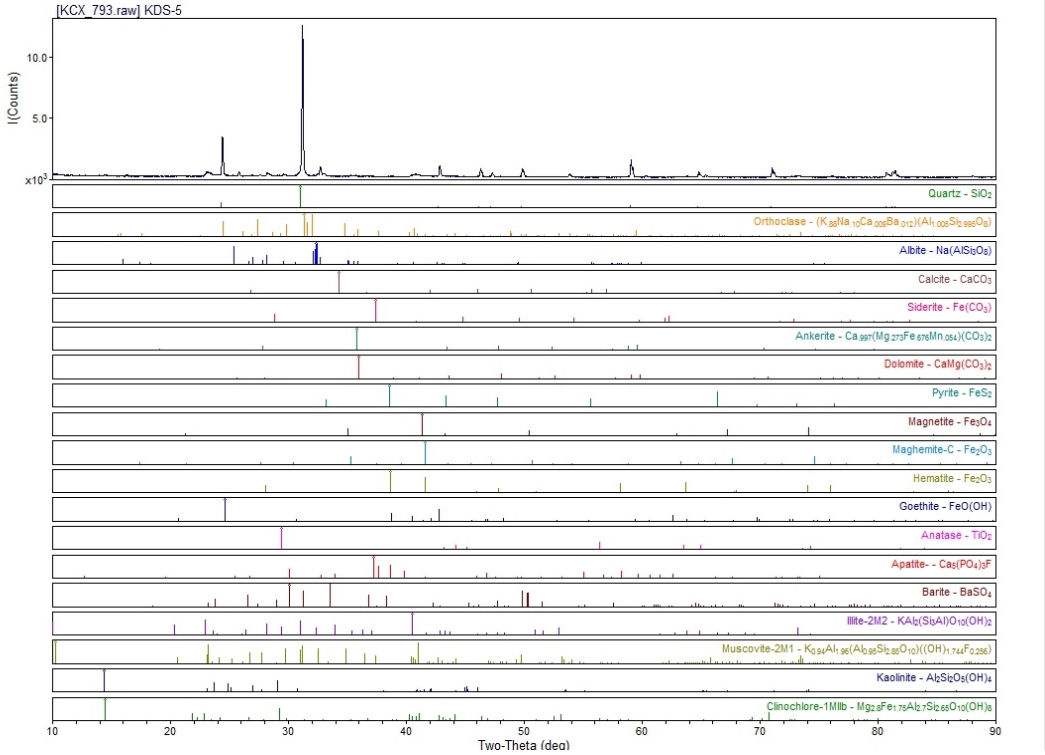

KDS-5 Picture 3

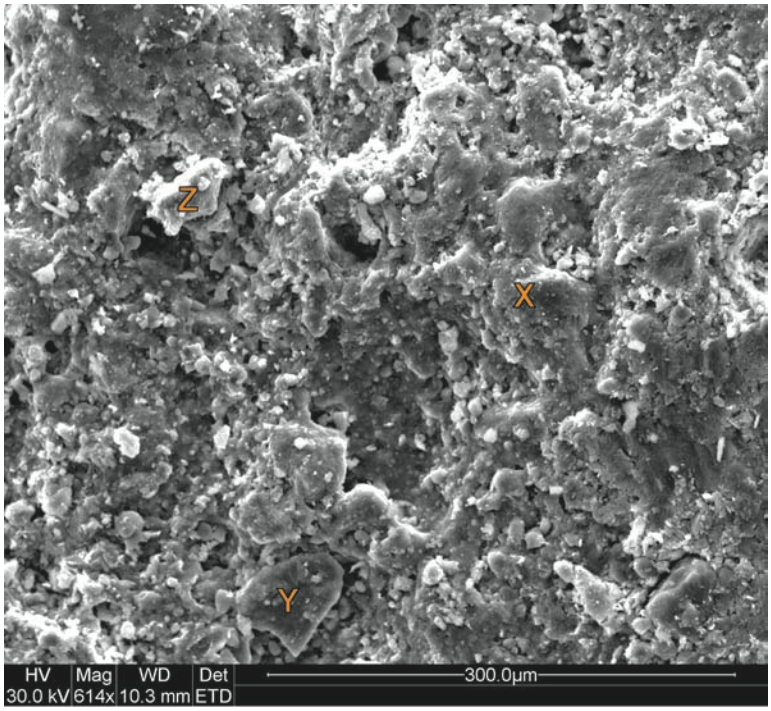

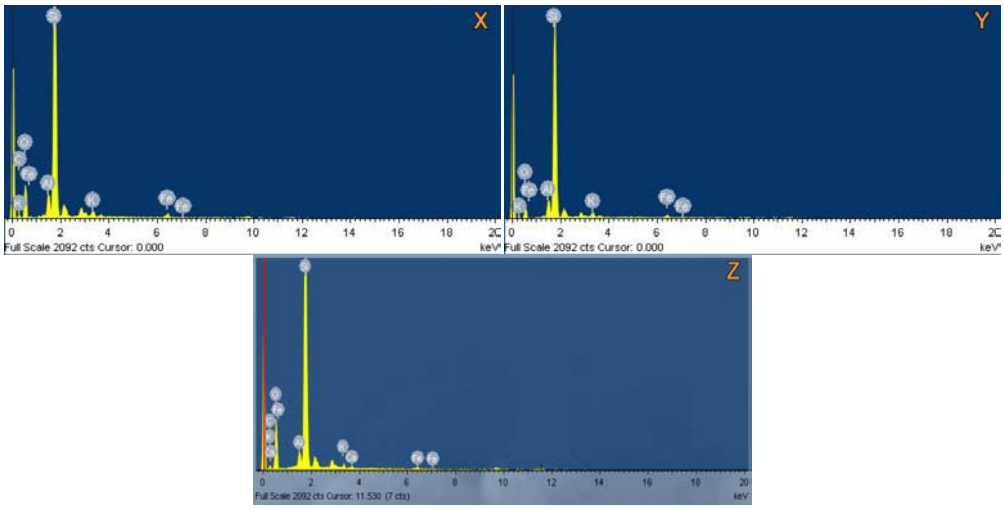

Spectra X, Y and Z are all consistent with mica (biotite) with minor impurities. Iron and calcium (Spectrum Z) can substitute for magnesium in mica. The varying morphologies of these grains may represent varying states of diagenesis or clay covering. The flakes and crusts are likewise variable in morphology; The small flakes on grain Y are barely noticable, whereas grain Z has an almost webby appearance from the authigenic clay covering it. While X is large and roughly polygonal, the thick-appearing encrustation, however the spectra of all three grains are nearly identical.

KDS-5 Picture 4

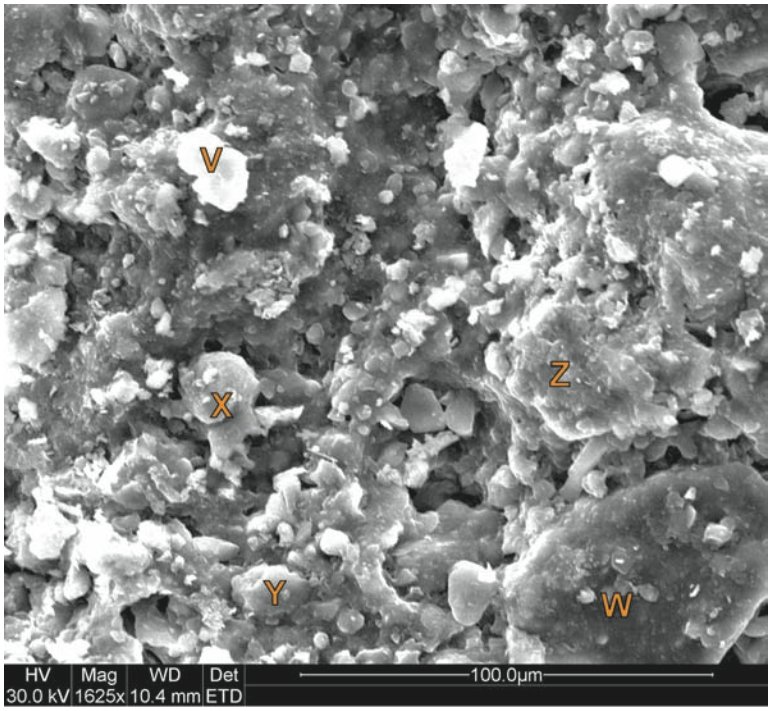

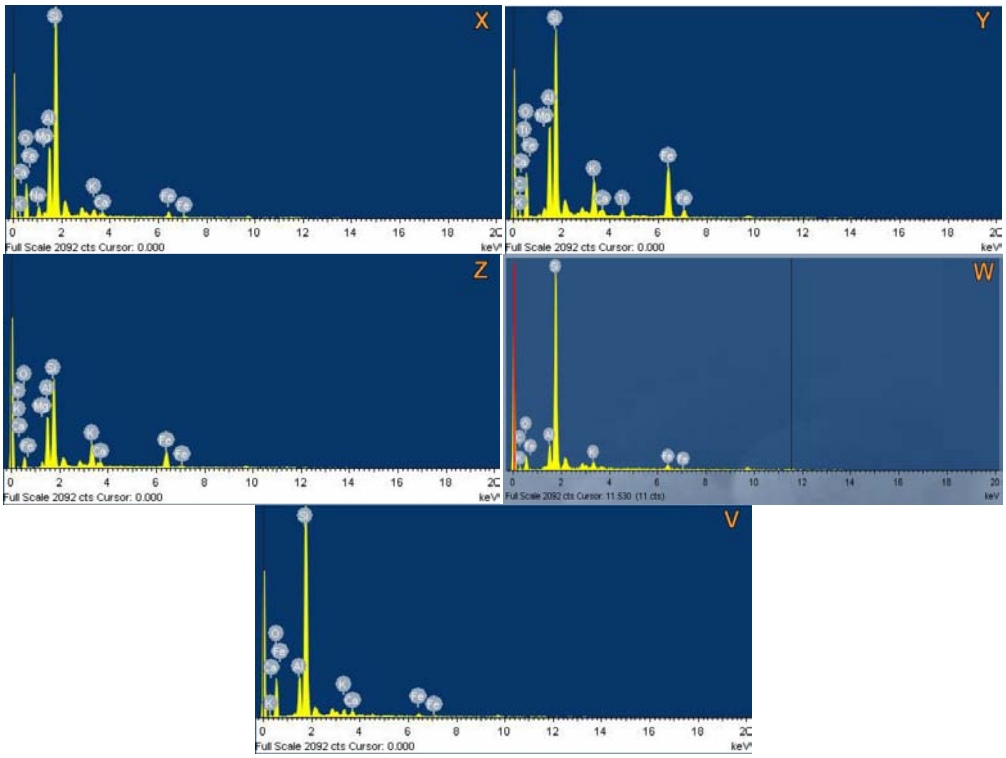

Spectrum X represents mixed illite/smectite, with calcium substituing for sodium or magnesium, and iron substituting for magnesium. Grain X is very large and polygonal, not webby and flaky as is typical of clay. The EDX spectrum may represent microcrystalline clay coverings of another, larger grain. Spectrum Y has subequal aluminium and iron peaks typical of chlorite (chamosite), but the larger silicon peak and relatively large potassium peak indicate the presence of illite. This platy morphology may represent illite

with chlorite films, or mixed layer illite and chlorite. Spectrum Z likely represents illite with calcium impurities, while the associated iron peaks indicate iron oxides in the fine crust covering Z. V is a small, webby appearing grain, while W is a large, polygonal grain with thin flakes on the surface, however their spectra are nearly identical. They both are consistent with smectite clay with calcium, iron and potassium substituting for magnesium. Grain V appears to be detrital while W's spectrum is likely derived from flaky, authigenic coverings.

KDS-5 Picture 5

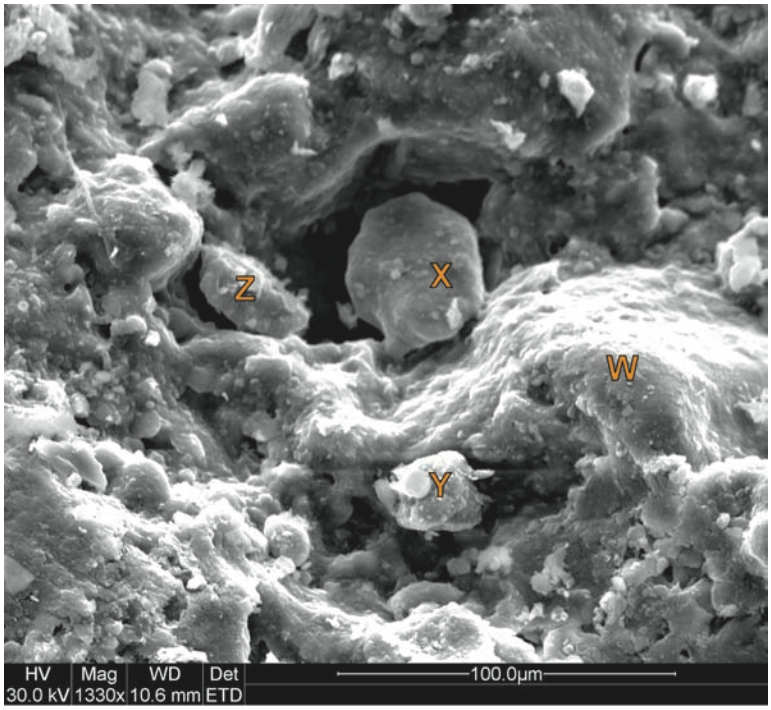

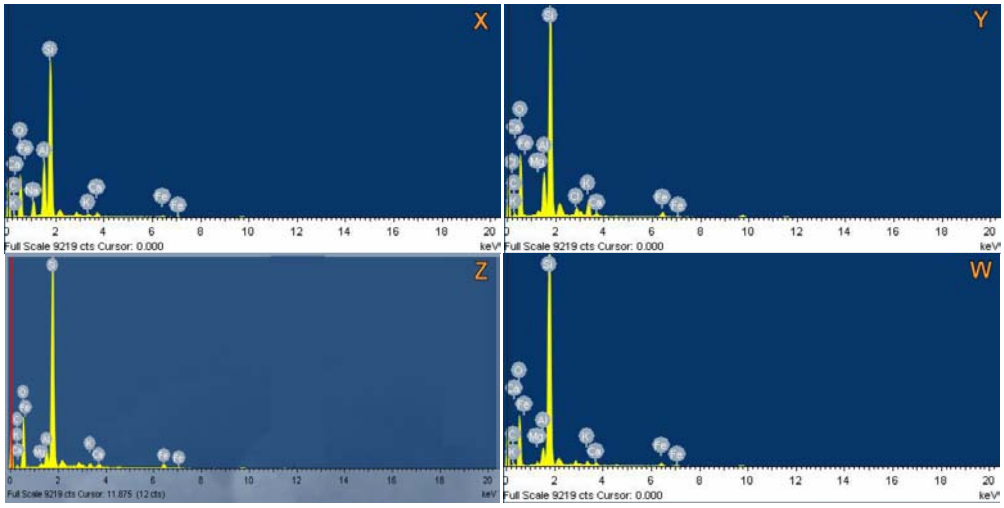

Though X appears to be a large, polygonal grain, the EDX spectrum is consistent with smectite-rich mixed illite/smectite clay with magnsium substituted by calcium and iron. Y is flakier in appearance, and contains magnsium more typical to smectite, with chlorine

substituting in the hydroxyl group. Spectra Z and W have a very small aluminium peak relative to silicon, consistent with mica. Iron may be present in an iron oxide coating.

KDS-5 Picture 6

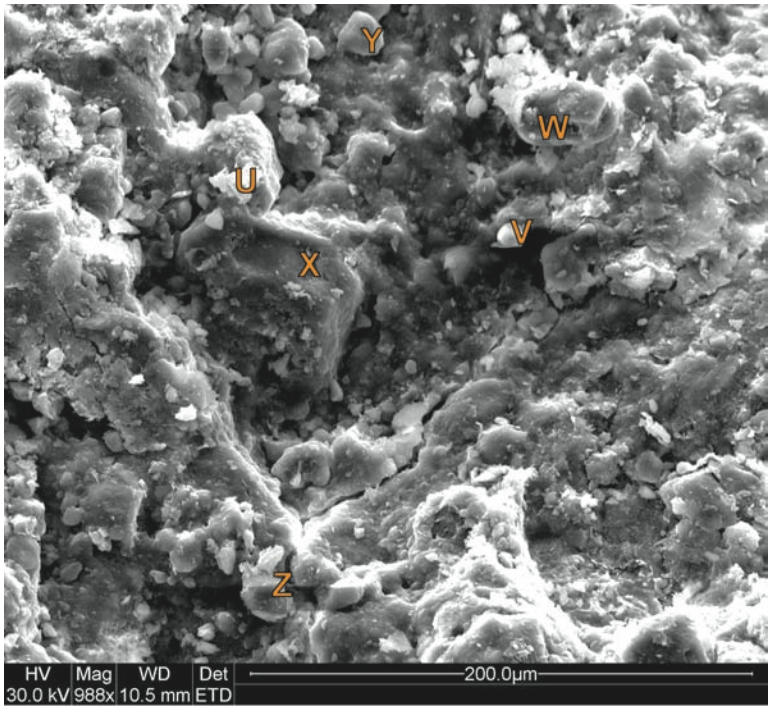

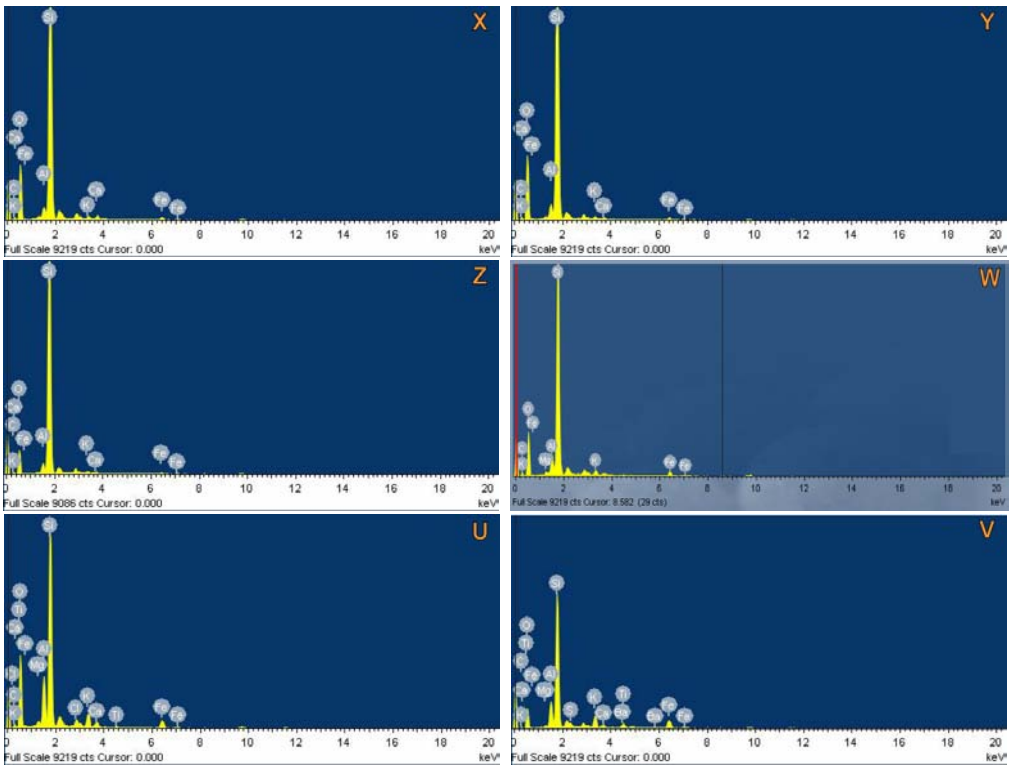

X is a very large, polygonal grain with an EDX spectrum similar to mica. Y and Z have nearly identical EDX spectra to X, despite their different morphologies. W likewise indicates mica (biotite), which is an intermediate size between the largest X, and smaller Y and Z. White, small, webby grains V and U are smectite clay; barium peaks present in Spectrum V likely represent titanium, not barium which has an overlapping pattern. The sulfur and chlorine peaks indicate these elements are susbstituting in the hydroxyl group of the clay. V is rounded and likely detrital, while U is flaky and appears to be forming authigenically on top of mica grains.

KDS-6 Image 2

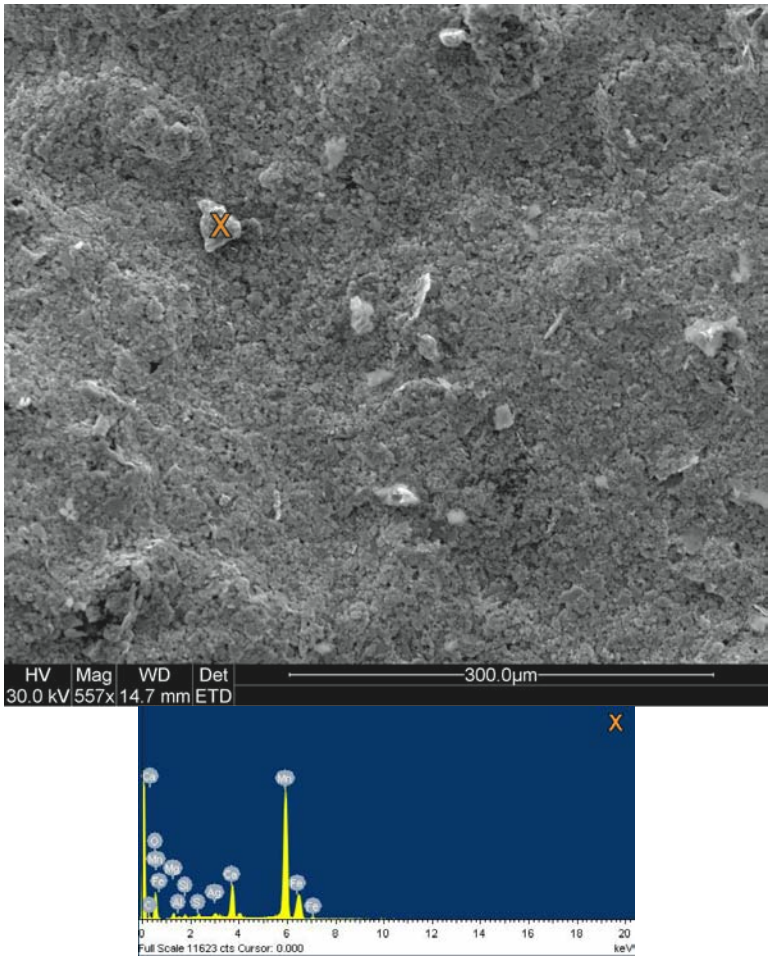

KDS-6 was collected from Palaeosol C, approximately 20 meters above Palaesol A. Like Palaeosol C, Palaesol B is orange and yellow-green (Munsell Code) in color. The sample's XRD spectrum has strong peaks for quartz, plagioclase, mixed illite/smectite, and mica, and trace peaks for potassium feldspar, and chlorite. The above overview image shows a heterogeneous mix of angular grain morphologies and a crusty covering that may represent iron oxides. Grain X has a very strong peak of manganese and a difficult spectrum to interpret. X may be covered by iron oxides with manganese impurities, or manganese oxides.

KDS-6 XRD Spectrum

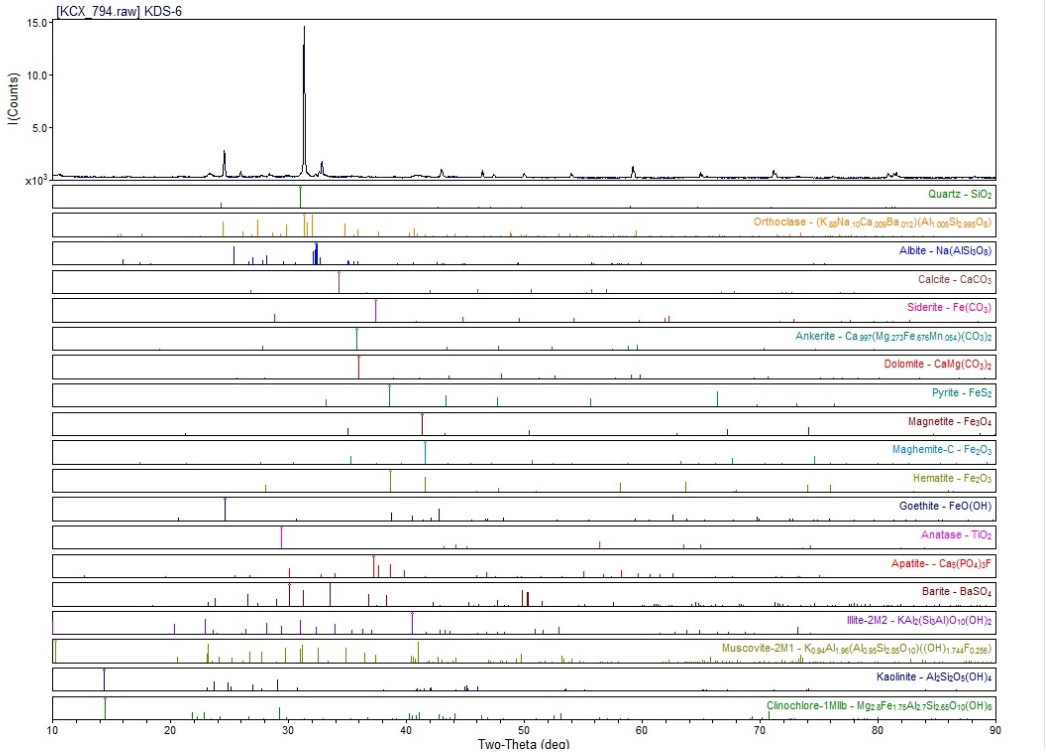

KDS-6 Image 1

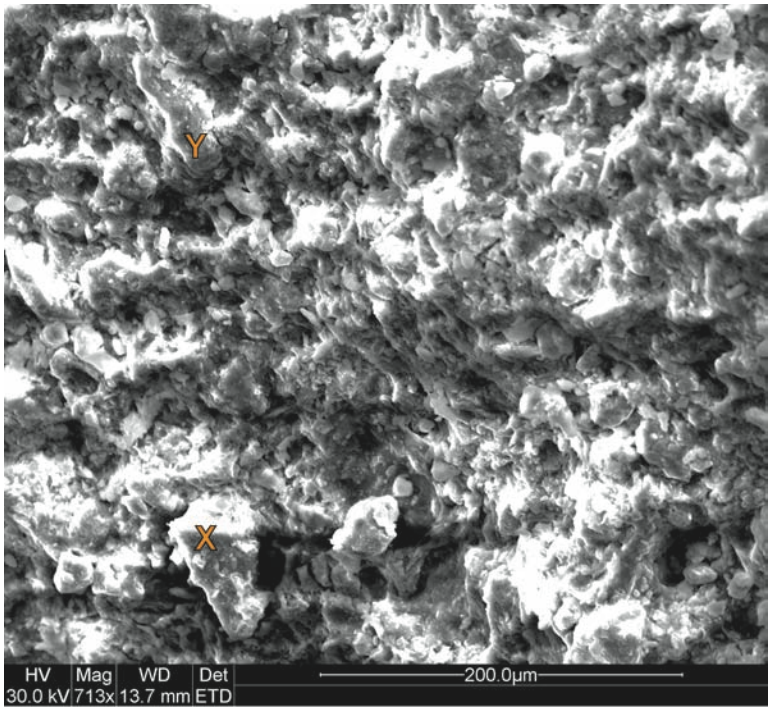

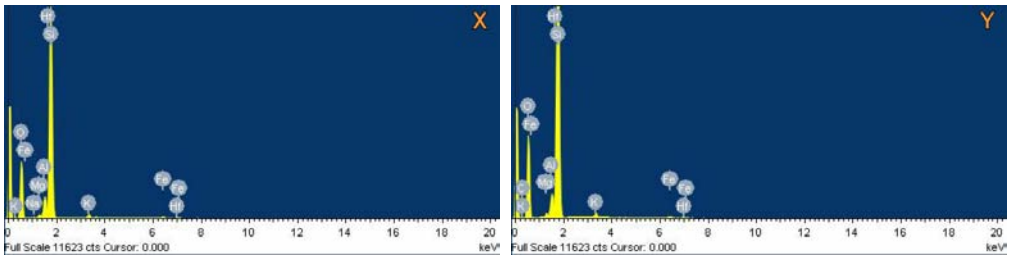

Grains X and Y have similar spectra which both likely represent mica (biotite) with impurities. Sodium peaks in X may come from surrounding clay. Halfnium peaks identified in the spectra are likely erroneous as Halfnium's pattern overlaps with silicon and iron.

KDS-6 Image 3

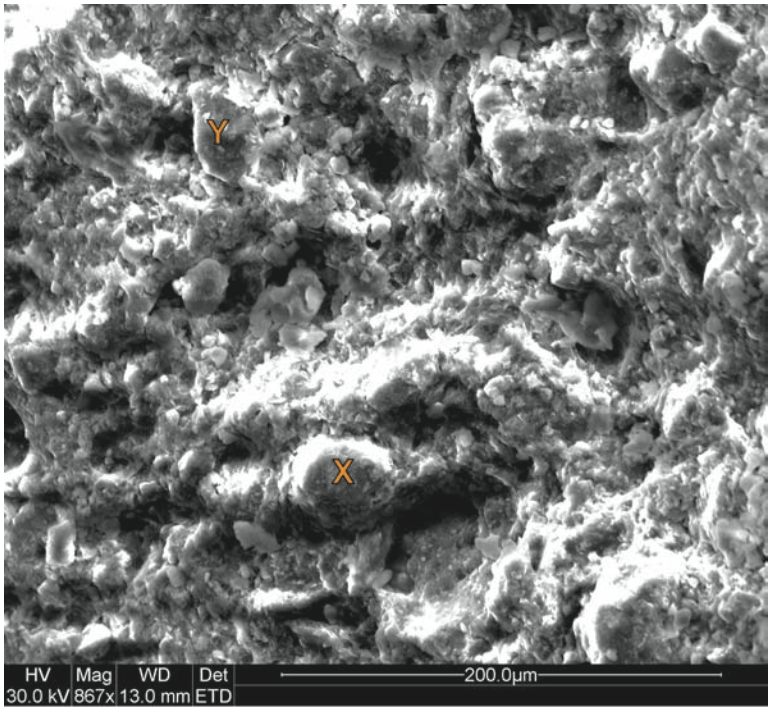

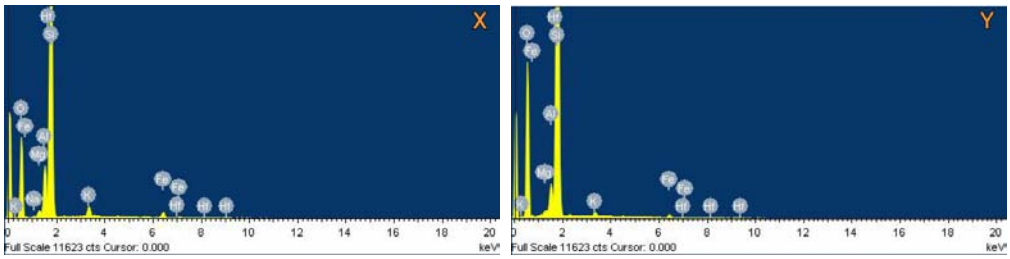

The webby, clayey covering of grain X has a complicated spectrum which likely represents mixed layer illite/smectite. The image is dominated by webby clay surrounding grains and dissolution pockets. The clay forms matrix as well as authigenic coverings on other grains. Spectrum Y represents a mica (biotite). Halfnium peaks may have been erroneously detected as an overlap with silicon and iron.

KDS-6 Image 4

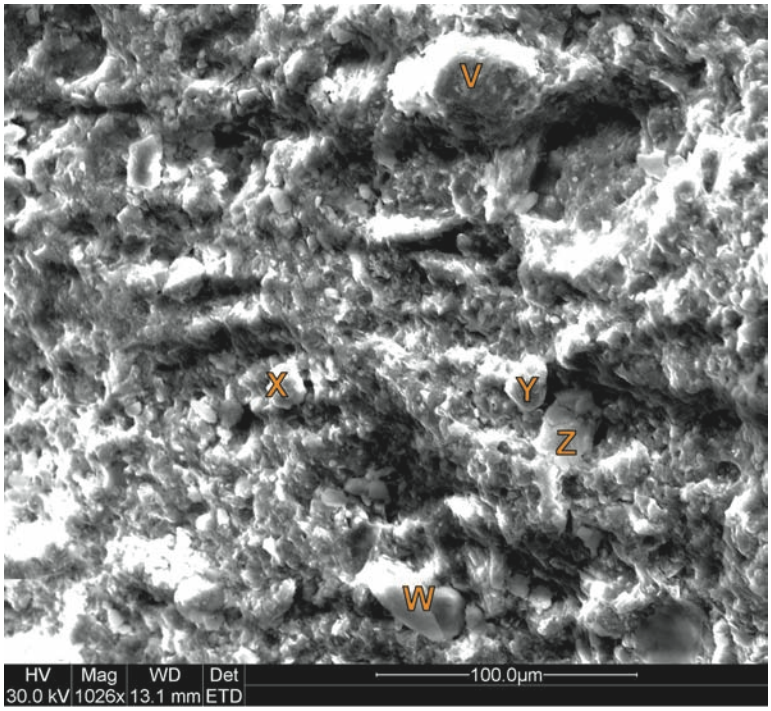

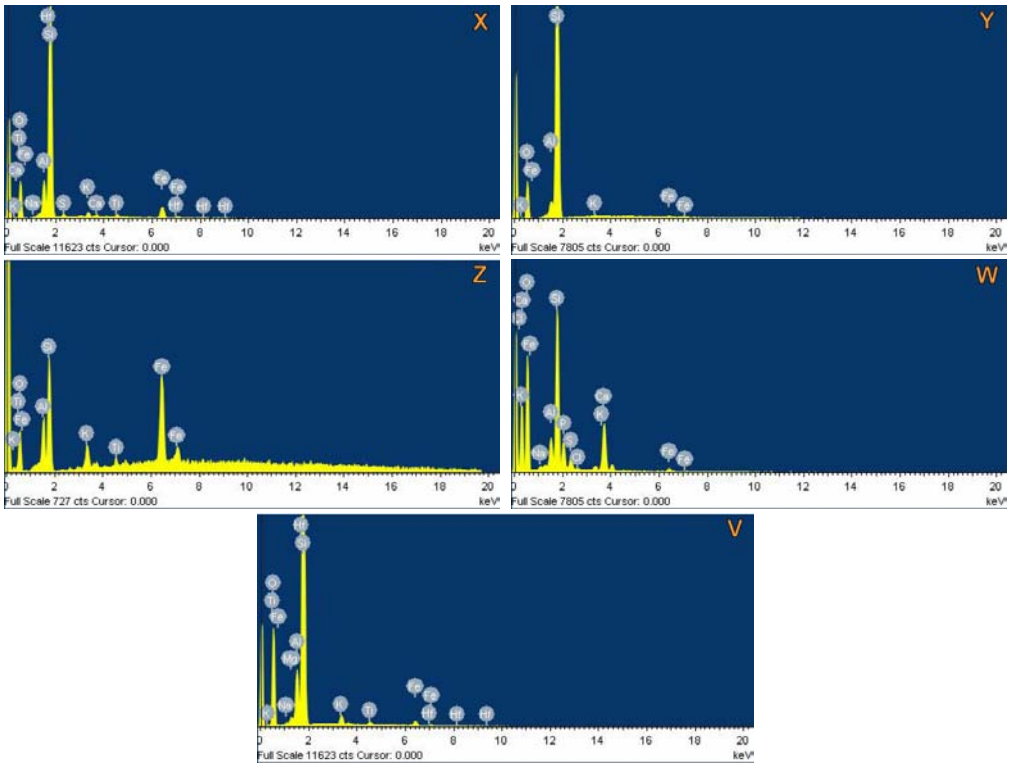

Grain X has a spectrum consistent with quartz and minor smectite/illite clay with sulfur substituting in the hydroxyl group. This grain likely has a thin, clay covering. Spectrum Y also has a much stronger silicon peak, indicating this is also a quartz grain and that EDX has picked up smaller aluminum, potassium and iron from nearby clay and/or iron oxides. Spectrum Z has very large iron peaks and the spectrum is consistent with mixed illite and chlorite. The grain (Z) appears to be platey and smooth, it is likely detrital. V marks a

large, webby mass, but has a spectrum lower in aluminum than clay, and is more consistent with mica (biotite) with some impurities (titanium, sodium). Alternatively, these minor peaks may represent authigenic clay growth on the decaying mica grain. Spectrum W is consistent with mixed illite and smectite clay, though the strong potassium peak indicates more illite than smectite. Sulfur and chlorine are likely substitutes for hyrodoxyls in clay. The morphology of the grain is smooth and polygonal, and appears to be a detrital grain.

KDS-7 Image 1

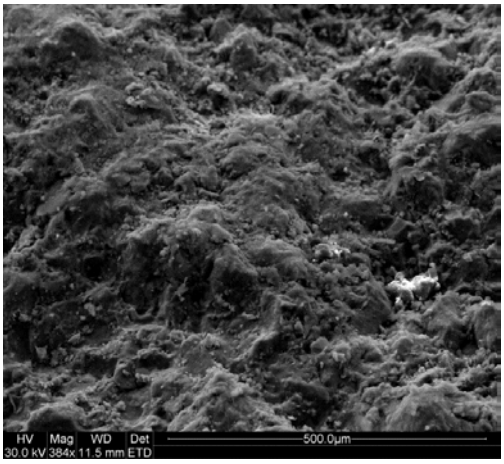

KDS-7 Image 5

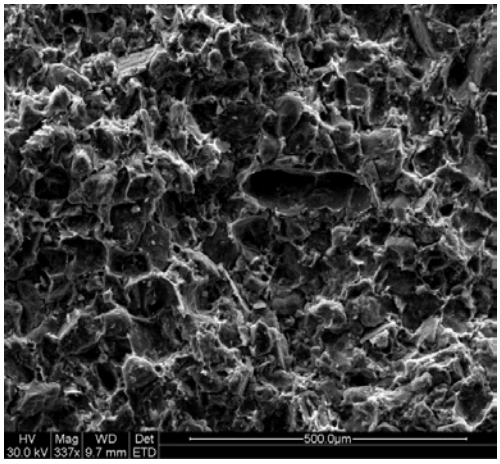

Sample KDS-7 was collected from Palaeosol C approximately 40 meters above Palaeosol A. The sample is orange, and yellow-green (Munsell codes) in color. The sample's XRD spectrum has strong peaks for quartz, plagioclase, mixed layer illite/smectite, mica and kaolinite, and minor peaks for potassium plagioclase, calcite, barite and anatase. Trace peaks for hematite are also present. The overview (left) image shows authigenic clay crusts, and white spots (lower right) likely indicate iron oxides. Another overview image views the surface perpendicular to the loose bedding planes (above right), and shows the clay matrix still present around dissolved grains.

KDS-7 XRD Spectrum

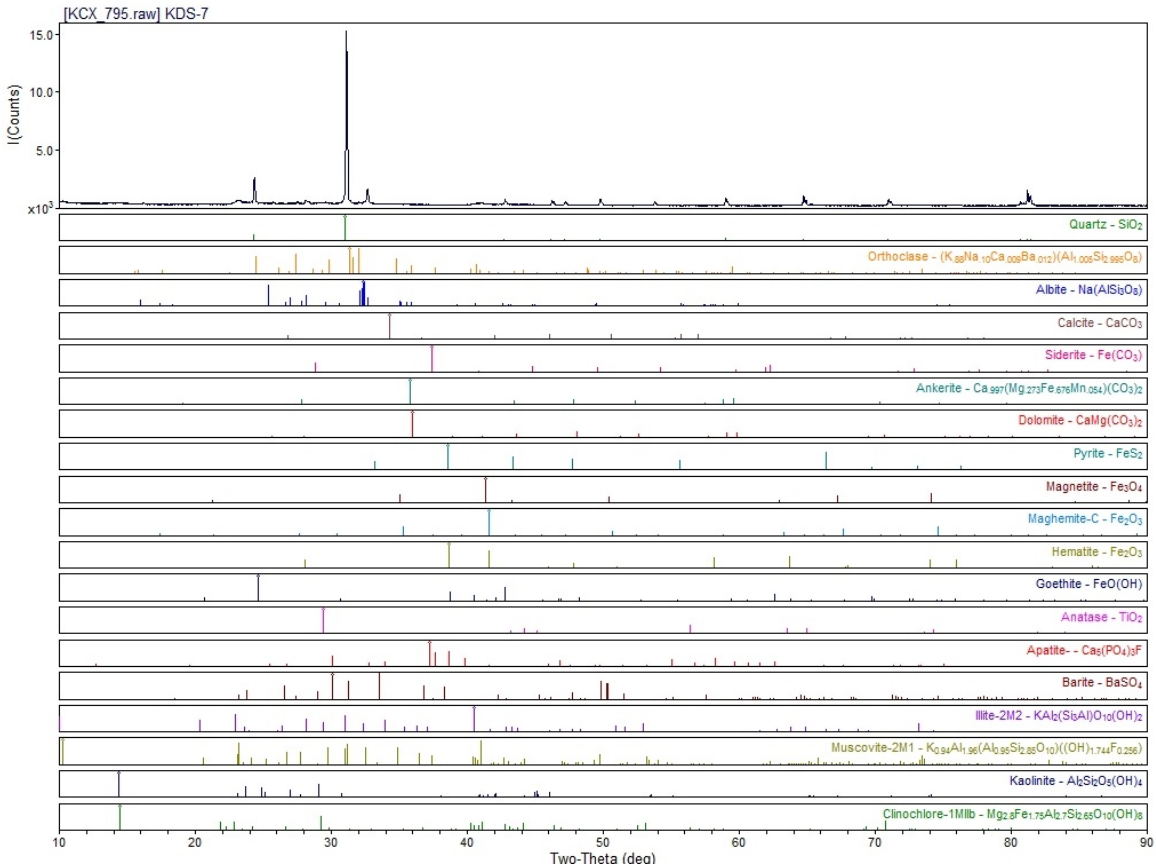

KDS-7 Image 2

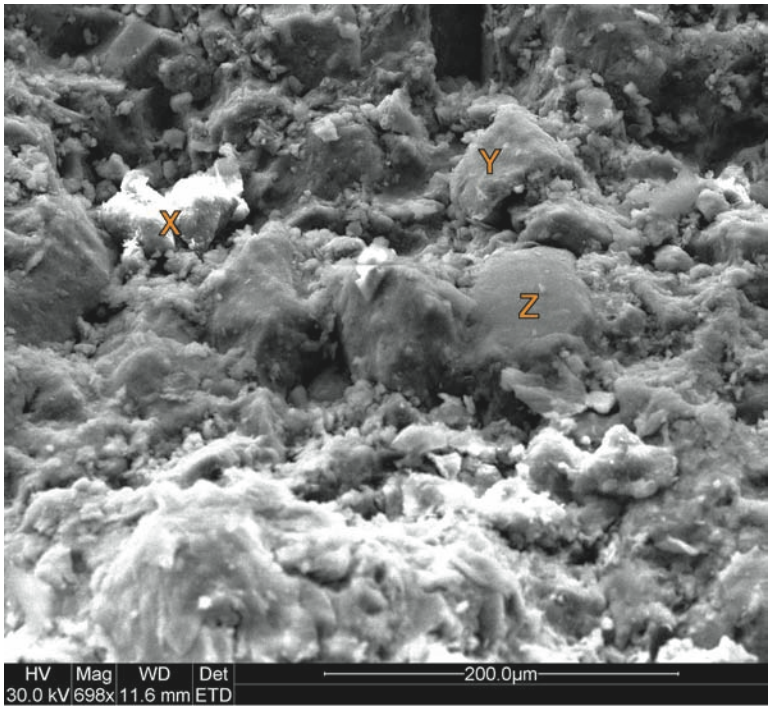

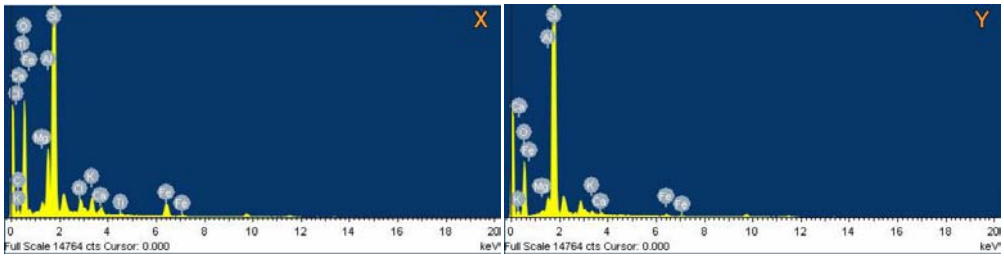

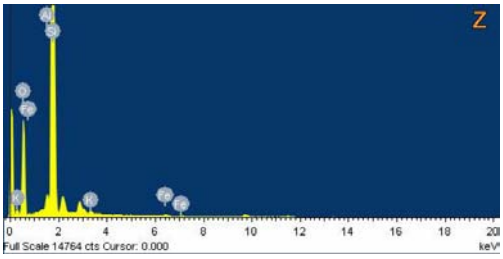

Grains marked by X have a fine, flaky covering which appear to be reacting with the electron beam. The spectrum (X) is consistent with smectite clay, with chlorine substituting in the hydroxyl group, and calcium substituting for sodium. The small aluminum, potassium, iron, calcium and magnesium peaks in Spectrum Y likely represent mica (biotite) with impurities. Large, flat grain Z has a spectrum consistent with potassium feldspar, while minor iron peaks represent iron oxides.

KDS-7 Image 3

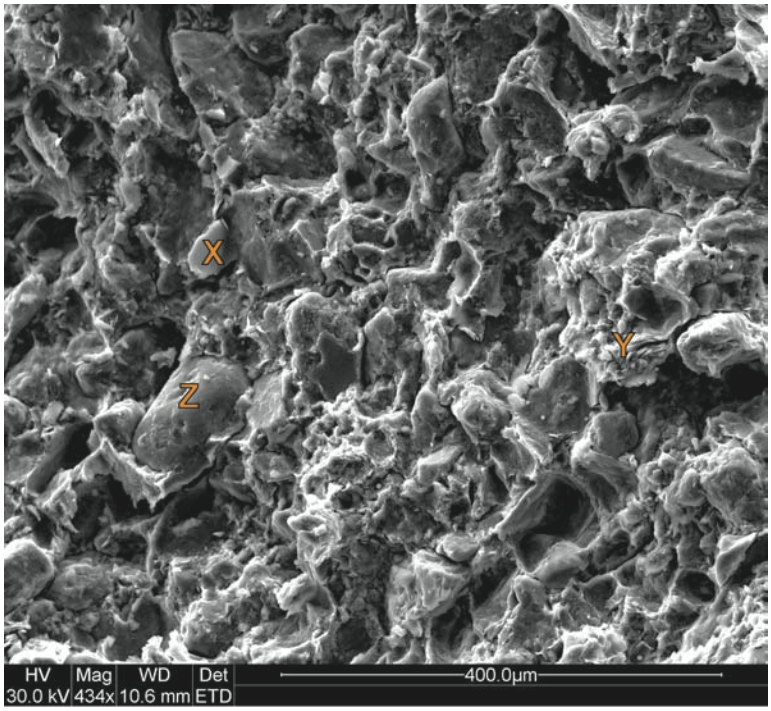

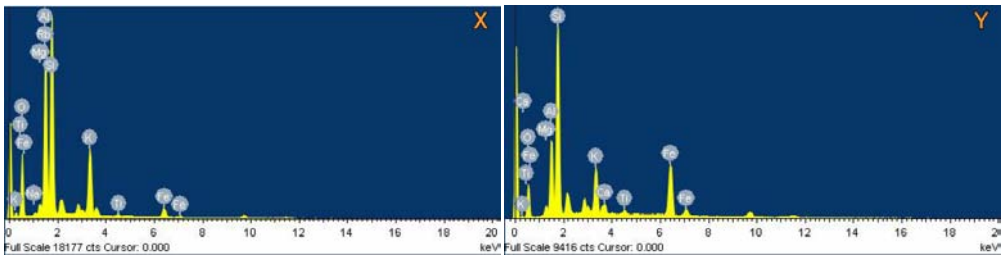

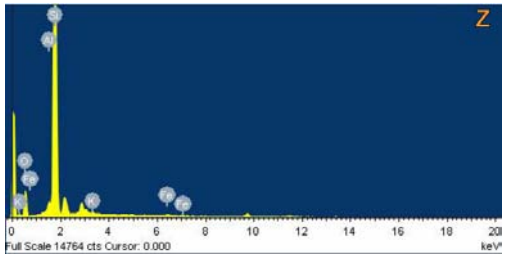

The fresh surface of flake X has a spectrum with a strong aluminum peak consistent with mica (muscovite). Sodium and titanium peaks represent impurities. The folded layers marked by Y appear to be mixed illite and smectite clay. The clay matrix completely envelops grains and dissolution pockets, and appears to be authigenic. The pitted, round grain Z could either be quartz with minor peaks representing traces of clay, or potassium feldspar with associated iron oxides.

KDS-7 Image 4

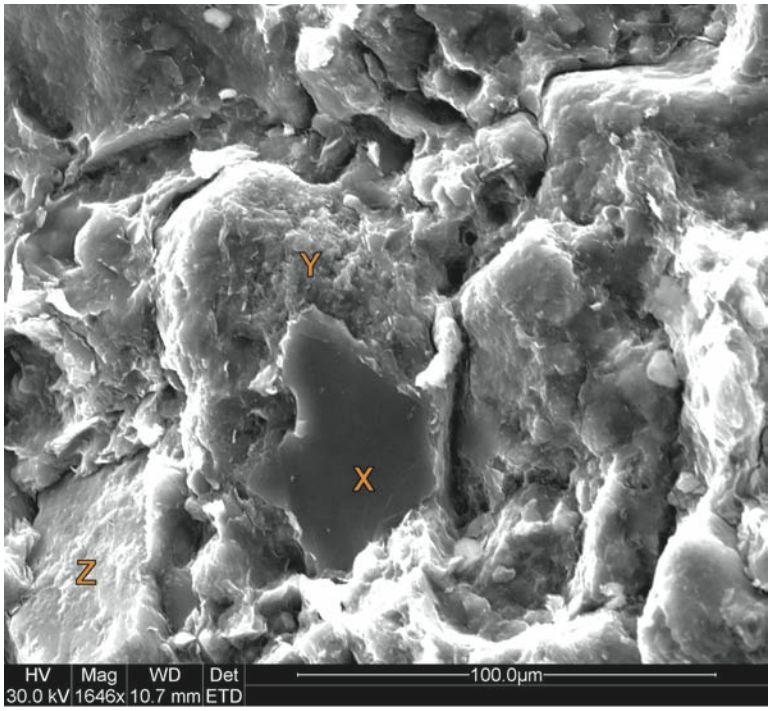

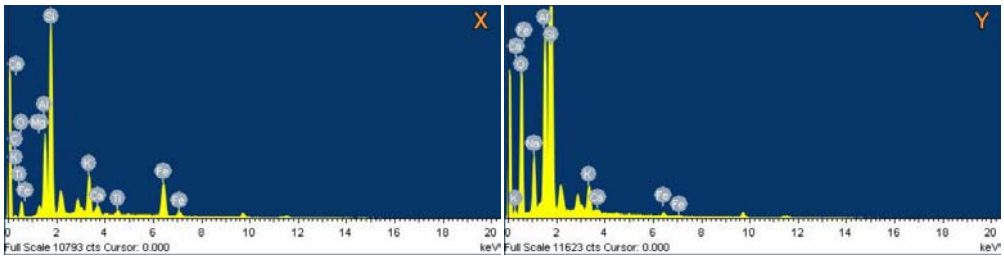

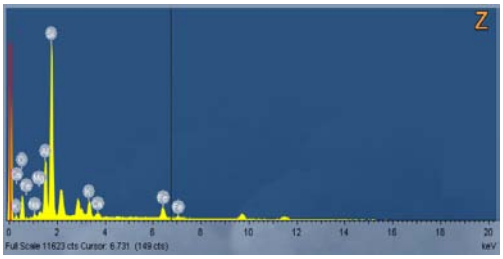

Image 4 is a higher magnification image (1646x) of grains from Image 3. The smooth surface marked by X has a spectrum consistent with mixed layer illite and smectite. The curved appearance of the flake indicates authigenic growth in pore spaces between detrital grains. The webby, clumped morphology of Y is similar to smectite clays, though the strong aluminum and sodium peaks may represent some sort of zeolite (sodium-rich thomsonite?) or other alteration products. This webby authigenic covering is forming on top of a clay-encrusted grain behind X. Though Z marks a flat surface that appears like a grain, the spectrum (Z) is similar to X and also likely represents mixed layer illite and smectite (though it is more sodium-rich, perhaps containing more smectite).